Engineering Probiotic Bacteria as Living Therapeutic Agents

Dissertation
zur Erlangung des Grades
des **Doktors der Naturwissenschaften**
der Naturwissenschaftlich-Technischen Fakultät
der Universität des Saarlandes

von

Sourik Dey

Saarbrücken, July 2024

Tag des Kolloquiums: 20.12.2024

Dekan: Univ.-Prof. Dr.-Ing. Dirk Bähre

Berichterstatter: Prof. Dr. Aránzazu del Campo Bécares

Prof. Dr. Tobias A.M. Gulder

Akad. Mitarbeiter: Dr. Sara Trujillo Muñoz

Vorsitz: Prof. Dr. Tsing-Young Dora Tang

Summary

Living bacterial therapeutics represent an exciting frontier for achieving controlled drug release within the body. However, genetic modules require improvement to control the production and release of therapeutic biomolecules in medically relevant strains. Model probiotic strains like *E. coli* Nissle 1917 have extensive genetic toolkits but still lack rapidly responsive and stringent genetic switches to regulate drug release. On the other hand, probiotic bacteria from the Lactobacilli family have broader applicability in the body but remain as non-model strains with restrictive genetic programmability. This thesis addresses both these limitations. Firstly, I developed a strategy to achieve strict control over the release of an enzymatically synthesized antibiotic (darobactin) from *E. coli* Nissle 1917. By combining parts from pre-established genetic switches, I created a thermo-amplifier circuit that released darobactin at pathogen-inhibitory levels within a few hours. Secondly, I expanded the genetic toolbox of the probiotic *Lactiplantibacillus plantarum* WCFS1 strain with two genetic parts - a strong constitutive promoter (P_{tlpA}) and several type II toxin-antitoxin (TA)-based plasmid retention systems. The performance of these genetic modules in recombinant plasmids was verified using reporter proteins such as mCherry and Staphylococcal nuclease without the need for antibiotic-based selection pressure.

Kurzzusammenfassung

Lebende bakterielle Therapeutika stellen eine spannsende Möglichkeit dar, um eine kontrollierte Freisetzung von Medikamenten im Körper zu erreichen. Die genetischen Module müssen jedoch verbessert werden, um die Produktion und Freisetzung therapeutischer Biomoleküle in medizinisch relevanten Stämmen zu kontrollieren. Probiotische Modellstämme wie *E. coli* Nissle 1917 verfügen zwar über ein umfangreiches genetisches Instrumentarium, doch fehlt es ihnen noch an schnell reagierenden und stringenten genetischen Schaltern zur Steuerung der Wirkstofffreisetzung. Andererseits sind probiotische Bakterien aus der Familie der Laktobazillen zwar breiter im Körper einsetzbar, bleiben aber als Nicht-Modellstämme mit restriktiver genetischer Programmierbarkeit bestehen. Die vorliegende Arbeit befasst sich mit diesen beiden Einschränkungen. Erstens habe ich eine Strategie entwickelt, um die Freisetzung eines enzymatisch synthetisierten Antibiotikums (Darobactin) aus *E. coli* Nissle 1917 streng zu kontrollieren. Durch die Kombination von Teilen bereits etablierter genetischer Schalter schuf ich einen Thermo-Verstärker-Schaltkreis, der Darobactin innerhalb weniger Stunden in pathogenhemmenden Mengen freisetzt. Zweitens habe ich den genetischen Werkzeugkasten des probiotischen *Lactiplantibacillus plantarum* WCFS1-Stammes um zwei genetische Teile erweitert - einen starken konstitutiven Promotor (P_{tlpA}) und mehrere Plasmider haltung systeme auf der Basis von Typ-II-Toxin-Antitoxin (TA). Die Leistungsfähigkeit dieser genetischen Module in rekombinanten Plasmiden wurde mit Reporterproteinen wie mCherry und Staphylokokken-Nuklease ohne antibiotischen Selektionsdruck überprüft.

Acknowledgements

The research for this thesis was conducted at the INM – Leibniz Institute for New Materials in the Bioprogrammable Materials group under the scientific guidance of Dr. Shrikrishnan Sankaran. I want to express my deepest gratitude to my supervisor, Dr. Shrikrishnan Sankaran (Shirish), for allowing me to work in the fascinating field of bacterial therapeutics. I am grateful to him for waiting for me to join the group while navigating the challenges of obtaining a visa amidst the COVID-19 restrictions. Since then, he has consistently supported my research efforts, encouraged my entrepreneurial spirit, and aided my growth as a researcher over the past four years. I am also grateful to Prof. Dr. Aránzazu del Campo for her unwavering support and continuous interest in my research throughout my doctoral journey.

I come from a pure biology background, and at first, I was unsure how my research would be relevant in a materials science institute. However, being part of the Leibniz Science Campus – Living Therapeutic Materials (LSC-LifeMat) Consortium quickly put me at ease and helped me realize the relevance of my research for multiple projects. Through this consortium, I had the opportunity to collaborate with individuals from diverse scientific backgrounds, such as material science, optogenetics, and nanotechnology. Although the interdisciplinary nature of the LSC Consortium was both exciting and challenging, I quickly learned how to collaborate and make meaningful contributions to many projects. I am sincerely grateful to my doctoral colleagues, Carsten E. Seyfert, Selim Basaran, and Shardul Bhusari, for allowing me to contribute a small part to their research endeavors. I am also grateful to Prof. Dr. Tobias Kraus and Prof. Dr. Rolf Müller for all their suggestions and the resources they shared with me to complete my work.

I want to thank my two hardworking colleagues at INM, Marc Blanch-Asensio and Varun Sai Tadimarri, who have become my closest friends in Germany. In addition to our scientific achievements, I will always cherish our conference and retreat trips, joint presentations of our work, and, most importantly, all the lively conversations we shared. I wish you both happiness and success in your lives.

I want to thank Sanjana Balaji Kuttae for her help with the countless plasmid extractions, agarose, and SDS-PAGE gels she prepared for me. Hopefully, I have done justice to all your efforts by assisting you with your Master's thesis project. I also thank Dr. Claudia Fink-Straube for her fantastic help with the ESI-MS analysis of darobactin samples. Chapter 3 could not have been completed without your expertise. I would also like to thank Dr. Andreas M. Kany (HIPS) for his help in validating our ESI-MS results for Chapter 3. I want to thank Christina Muth and Sandiego Himawan for their consistent support in troubleshooting technical issues in the lab and for teaching me practical problem-solving skills. I want to thank Dr. Samuel Pearson and Dr. Hans Smola for inspiring me with their humble and charismatic personality despite their unique scientific insight on many different topics.

I want to thank my amazing officemates, Hanuman Chowdary Kalari and Mokhamad Khamdan, for their stimulating and thought-provoking discussions on various topics that have made my work experience more enjoyable. I also want to thank my colleagues, Dr. Priyanka Dhakane and Kristela Shehu, for their support and positive energy at the workplace. I want to express my gratitude to Martina Bonnard, Sabine Müller, and Bernd Rus for their assistance in facilitating the smooth completion of my doctoral degree in Germany and relieving me of the complex administrative details.

I want to express my gratitude to my dear friend Yogiraj Deepak Jakkal (IIT Roorkee) and my excellent peers Piyush Nanda (Harvard University) and Surjyendu Bhattacharjee (Caltech) for inspiring me to believe in myself and teaching me how to practice impactful science for society.

I want to thank my mother for always being interested in my work, providing valuable insights on how my research could have a positive impact, and being my biggest supporter. I want to thank my elder sister for her constant love and support in every aspect of my life. Lastly, I want to pay tribute to my father and his selfless love and support, without which I would not have achieved anything. I feel incredibly blessed to have all of you in my life.

“Nothing in life is to be feared, it is only to be understood. Now is the time to understand more, so that we may fear less”

-Marie Curie

TABLE OF CONTENTS

Sourik Dey
ORCID: 0000-0001-9619-3959

Parts of this chapter have been used to construct a review article titled **"Engineered bacterial therapeutics with material solutions"** and has been submitted for publication in the *Trends in Biotechnology* journal (Elsevier Publishing Group). Some sections of the chapter are identical to parts of that review, while other sections are substantively similar to parts of the review article but expressed in different words. To avoid self-plagiarism and excessive citation, I am providing this note as a general citation without further citation in the body of the chapter.

Citation - Sourik Dey[1], Shrikrishnan Sankaran[1] (2024) **Engineered bacterial therapeutics with material solutions.**

(Manuscript accepted for publication in *Trends in Biotechnology*)

Contribution Report - Shrikrishnan Sankaran conceived the idea of the review. Sourik Dey and Shrikrishnan Sankaran jointly wrote the manuscript.

Chapter 1

ENGINEERED BACTERIAL AGENTS FOR THERAPEUTIC INTERVENTION

1.1. Biological Platforms for Therapeutic Production

Throughout history, humans have had to combat diseases and invent novel therapies to treat them. No societal development can take place in a community plagued with diseases and limited access to healthcare options for timely recovery. Therefore, humanity has pursued effective solutions for curing diseases, including highly challenging and persistent chronic diseases. For a long time, these solutions have been in the form of drugs either isolated from natural sources or chemically synthesized. The **active pharmaceutical ingredient** (API) of these drugs could then mediate a significant effect toward resolving complex disease conditions. The discovery of these drugs from natural sources can be traced back to the well-known molecule "quinine," which was used for malaria treatment after being isolated from its natural source (cinchona tree bark) in 1820 by Pierre Joseph Pelletier and Joseph Caventou (Achan et al., 2011). Apart from natural sources, one of the first chemically synthesized drugs was ***para*-hydroxyacetanilide**, invented by Harmon Northrop Morse in 1877, which is still consumed globally for its effectiveness as an antipyretic agent under the commonly known generic name "**paracetamol**" (Prescott., 2000). In the last few centuries, extensive efforts towards drug development have allowed the scientific and medical community to treat numerous diseases. Most of these drugs belonged to the conventional "**small molecules**" category with a low molecular weight that can bind to specific biological macromolecules and alter their function (Southey and Brunavs., 2023). Although such drugs have revolutionized human health and progress, several disease conditions require more complex and advanced therapeutic solutions. For instance, an appreciable proportion of the human population suffers from a dysfunctional immune system or severely impacted metabolism due to various factors ranging from **genetic disorders** to **lifestyle-associated habits** (Thorburn et al., 2014). To treat such challenging diseases for which no viable treatment option was previously available, the scientific community and pharmaceutical industry explored a new category of drugs known as "**biological**

therapeutics" (Makurvet., 2021; Singh et al., 2023). According to the **World Health Organization** (WHO), "**biological therapeutics**" or "**biologicals**" are medicinal drugs that are harnessed directly from living cell cultures (both natural and recombinant) in contrast to the chemical synthesis pathways adopted for small molecule-based drug synthesis (Klein et al., 2023). This category of drugs includes **vaccines, antibodies, growth factors, cytokines, anti-infectives** and **therapeutic proteins** that can prevent or treat a specific disease condition (Morrow and Felcone., 2004). One of the classic examples of these "biologics" is the production of the peptide hormone insulin in *Escherichia coli* using recombinant DNA technology for treating patients suffering from the most common metabolic disease, **diabetes** (Falcetta et al., 2022). According to WHO estimates, **422 million people** get globally affected by **diabetes mellitus**, where the patient either develops **insulin resistance (Type I)** or produces **insufficient amounts of insulin (Type II)**, an essential peptide hormone produced in the β cells (islets of Langerhans) in the pancreas (WHO Diabetes Report., 2023). Although there is no preventive strategy currently available for Type I diabetes, the progression of the more commonly occurring Type II diabetes could be kept in check by subcutaneous administration of recombinant insulin at regular intervals to regulate the blood sugar level (ADA Report., 2021). The intermediate-acting insulin, **HUMULIN-N®** and long-acting recombinant insulin, **LANTUS®** are prominent examples of medically prescribed insulin used to treat patients (both children and adults) suffering from diabetes.

In addition to hormones, considerable efforts are also made towards developing "biologics" like **recombinant enzymes and cytokines** that enable proper functioning of the host metabolism and immunity. The external supplementation of these proteins helps compensate for the low levels of critical proteins that are not present in sufficient amounts or are functioning at non-optimal rates in the host system. Multiple metabolic disorders can be directly linked to genetic mutations in critical enzyme-encoding genes, leading to altered metabolism in the host. **Phenylketonuria** is one such rare metabolic disorder where the **Phenylalanine hydroxylase** (PAH) enzyme gets mutated, rendering the host incapable of converting the amino acid phenylalanine to tyrosine (van Spronsen et al., 2021). The excessive accumulation of phenylalanine in the blood can then lead to impaired neurological functions and lead to fatal illnesses, and even death. The current treatment approach for phenylketonuria involves subcutaneous administration of the **recombinant enzyme phenylalanine ammonia-lyase** (PAL), for metabolizing phenylalanine and decreasing its levels

in the blood with minimal adverse side effects. This approach of externally supplementing recombinant hormones and enzymes has shown effectiveness in compensating for the natural deficiency and providing a better lifestyle to the patient (Pavlou, A.K. and Reichert., 2004). However, diseases where no single causal reason has been determined and are generally attributed to multiple genetic markers make it extremely difficult to develop a treatment. This condition applies mainly to debilitating autoimmune disorders, where the immune cells gradually start attacking the healthy tissues of the host, leading to diseases like **multiple sclerosis** (MS). In cases of progressive multiple sclerosis, the protective myelin sheath of the nerve fibers in the central nervous system (sheath) deteriorates, leading to decreased motor skills (Leocani et al., 2007). Although no known cure for MS exists, specific cytokines are known to play an active role in balancing the threshold of inflammatory macromolecules in the brain and promoting neuronal survival (Centonze et al., 2010). **Interferon beta-1b** is one cytokine that has shown remarkable efficiency in decreasing the clinical risk of developing MS and reducing the number of incidents related to relapsing-remitting MS in adults (Zettl et al., 2023).

Besides metabolic and autoimmune disorders, many contagious **bacterial and fungal pathogen-based infections** also affect a large population annually. **Antimicrobials**, which include various candidates like antibiotics and antifungals, exhibit clinical efficacy in eliminating these infectious agents in animals and humans. Microorganisms generally produce these antimicrobial agents as secondary metabolites in their natural environment to reduce the competition for limited nutrients. These secondary metabolites can then reduce competitor species to mediate a survival benefit to the production strain. Although these molecules generally belong to the "small-molecule" category, there is a growing class of antibiotics that fall somewhere between the category of "biologics" and "small-molecules," termed **peptide therapeutics** (Mahlapuu et al., 2016; Fernández de Ullivarri et al., 2020). In nature, these candidates can exist either as "**non-ribosomal peptides**" or "**Ribosomally synthesized and post-translationally modified peptides** (RiPPs)" and can exhibit a myriad of functions (Sieber and Marahiel, et al., 2003; Zhong et al., 2022). In both cases, the peptides can have unconventional compositional features and unique structural modifications unobserved for most linear peptide candidates. One of the most prominent examples is the bactericidal glycopeptide antibiotic, **vancomycin**, which can inhibit pathogenic strains of *Staphylococcus aureus* that causes sepsis and meningitis (Hawley and Gump., 1973). Because

of the superior performance of vancomycin in treating severe, life-threatening infections, it has been classified as a medicine of crucial importance on the WHO's List of Essential Medicines. In the last few decades, the discovery of such peptide therapeutics has gained significant attention due to the ever-increasing number of **antimicrobial resistance** (AMR) cases in pathogenic bacteria. AMR is attributed to genetic mutations and phenotypic evolution in pathogens, making them unresponsive to standard antibiotics used for infectious disease treatment. According to WHO estimates, AMR poses a global threat to public health and contributes to **4.95 million deaths** in the year 2019 (Murray et al., 2022). The increasing infection and mortality rate due to AMR also contributes to additional healthcare costs, predicted to surpass **1 trillion USD** by 2050 (WHO AMR Report., 2023). However, a significant lack of innovation and financial incentives exists in the development pipeline of "small molecule"-based antibiotics to target AMR effectively (Anderson et al., 2023). Therefore, alternative strategies based on the discovery and upscaling of peptide therapeutics can increase the repertoire of antimicrobial agents and tackle the global AMR incidence rate.

"Biologics" also represent a unique class of antibodies - **monoclonal antibodies** (mAbs) that are generated explicitly against protein epitopes (antigens) and are responsible for neutralizing antigen activity and stimulating the immune system. mAbs like **Adalimumab (Humira®)** and **Pembrolizumab (Keytruda®)** can block both soluble cytokines like **Tumor Necrosis Factor-alpha** (TNF alpha) or membrane-bound **programmed cell death protein-1** (PD-1) receptors to prevent disease progression of **rheumatoid arthritis** and **non-small cell lung cancer** (NSCLC) respectively (Navarro-Sarabia et al., 2006; Garon et al., 2015). mAbs are generally produced from mammalian cell cultures to facilitate post-translational modification and N-glycosylation for proper structural folding and functional activity. The robust clinical evidence supporting the efficacy of biologics rose to a record high in the past few years, setting a landmark in the year 2022, where the proportion of biologics approved by the **Food and Drug Administration** (FDA), USA surpassed the approval rate of small molecules-based drugs for the first time (Senior., 2023). Among all these candidates, monoclonal antibodies dominate the global biologics market, with an expected revenue reaching up to **300 billion United States Dollars** (USD) by 2025 (Lu et al., 2020). Although the market potential for monoclonal antibodies is optimistic, specific attributes of mAbs can decrease their overall clinical efficacy. The reason for this reduced effectiveness is

the large size and high antigen-binding affinity of mAbs, which reduces bioavailability and increases cross-reactivity towards healthy tissues, generating adverse side effects in the host (Chames et al., 2009). Additionally, monoclonal antibodies are generally produced from mammalian cell cultures, which require a stringently controlled set of conditions to ensure consistent quality and prevent batch variability. In addition, the vast production cost and cold chain supply associated with these processes make mAbs extremely expensive for the patient population to access. Therefore, considerable efforts are underway to expand the current biologics portfolio beyond conventional options and develop **next-generation biologics** that are more affordable for the patient population. Extensive screening protocols like phage display and peptide library analysis allowed the identification of biological entities that could bind to the target protein of interest. These macromolecules are the basis for developing next-generation biologics in alternate production hosts for rapid scalability and cost-effectiveness. These **next-generation biologics** can range **from synthetic peptides** (Wang et al., 2022; Sharma et al., 2023) **to camelid single-domain antibodies (nanobody)** (De Pauw et al., 2023) and **single-chain variable fragments** (scFv) (Keri et al., 2023), demonstrating favorable pharmacokinetic properties without compromising their effectiveness in targeting the disease condition. These candidates have been shown to target solid tumors, block cell surface receptors, alleviate inflammation, and neutralize antigenic epitopes with great precision. The emergence of next-generation biologics has allowed for a significant shift from conventional mammalian cell lines as a production host to other simpler and cost-effective hosts such as **bacteria and yeast** (Spadiut et al., 2014). Due to their smaller size and simpler structural attributes, these biologics are less susceptible to misfolding, degradation, and aggregate formation in the microbial production hosts. These molecules require almost minimal post-translational modification and glycosylation which simplifies the purification process involved in large scale "biologics" production pipeline. The FDA has recently approved several next-generation biologics to treat various medical conditions. For example, synthetic peptides such as **Dulaglutide** and **Semaglutide** are glucagon-like peptide-1 (GLP-1) receptor agonists used to manage Type II diabetes (Wang et al., 2022). The nanobody **Caplacizumab** targets the von Willebrand factor to treat the rare blood disorder, acquired thrombotic thrombocytopenic purpura (aTTP) (Hollifield et al., 2020). Finally, the scFv **Blinatumomab** can simultaneously target the T-cell-specific antigen (CD3) and tumor-specific antigen (CD19) to achieve effective remission of acute lymphoblastic leukemia (ALL) (De Pauw et al., 2023).

While the efficacy of next-generation biologics has been established, upscaling their production and addressing the global distribution bottlenecks in several **low and middle-income countries** (LMIC) still remains a challenge (Olivieri et al., 2024; Goshua et al., 2021; Caillon et al., 2023). Therefore, more efficient strategies for producing and delivering these next-generation biologics must be developed to increase their availability and affordability worldwide.

1.2. Live Biotherapeutic Products (LBPs)

To cope with the increasing demand for the availability and accessibility of such therapeutic agents for patients, a new emerging field of **"live biotherapeutic products (LBPs)"** has gained immense traction in the last two decades (Cordaillat-Simmons et al., 2020). According to the FDA definition, LBPs are "*a biological product that: i) contains live organisms; ii) applies to the prevention, treatment, or cure of a disease/condition of human beings; and iii) is not a vaccine*" (FDA LBP Report, 2012). LBPs can either be naturally occurring microbe/microbial consortia or genetically enhanced versions of safe microbial chassis (termed “recombinant LBPs”) that are well-tolerated and demonstrate a distinct therapeutic effect towards a disease condition in the host. This capability of LBPs has allowed its rapid expansion in the global market and has achieved promising milestones in recent years. Apart from *in-vitro* and preclinical testing in animal models, several clinical trials for these LBPs are currently active (Rutter et al., 2022). Although adequate information for filling an **Investigational New Drug** (IND) application is needed before it can enter clinical trials, the increasing number **(>10)** of IND applications indicates that the regulatory authorities have an optimistic outlook toward their treatment potential (Brennan., 2022). The strategically planned safety portfolio of the tested LBPs helps prevent adverse side effects among the patient cohort to circumvent any obstacles in its future application. Depending on the conclusive success rate in a statistically significant patient sample size, there is an appreciable chance that some of the LBP candidates could get FDA approval for clinical use (Rouanet et al., 2020). Although many LBP candidates in clinical trials are bacterial species that have not been genetically engineered, a significant interest is ongoing in developing recombinant LBPs, coined as **engineered LBPs (eLBPs)** by the scientific community. The following section will highlight the advancements in eLBP development, where microbial chassis were genetically altered and employed for biotherapeutic production and release into the host environment. The FDA

recommendation guidelines regarding recombinant LBPs have catapulted the field with intense momentum since 2012. A rising number of research groups have used this opportunity to genetically engineer microbes for generating potential eLBP candidates (Charbonneau et al., 2020). This growing interest in eLBPs can be attributed to the following benefits: -

1. eLBPs can act as "**miniature bioreactors**" for producing biotherapeutics in the host.
2. eLBPs can enable **targeted biotherapeutic delivery** without requiring systemic administration.
3. eLBPs can potentially **lower the overall production cost** incurred to purify expensive "biologics".

The rapid advancement in the field of synthetic biology has allowed scientists to genetically modify a diverse range of microbial strains. These can range from simple, minimalistic models, like *Mycoplasma pneumoniae*, to moderately complex prokaryotes like *Escherichia coli*, *Lactococcus lactis* and *Bacteroides thetaiotaomicron* to eukaryotic yeasts like *Saccharomyces boulardii.* Most of these microbial strains belong to the **"Generally recognized as safe (GRAS)"** status (except for *M. pneumoniae*), which suggests that careful use of such microbes should not cause any harm to the host. Apart from that, many of these microbes are also classified as "**probiotics**" which, according to the **International Scientific Association for Probiotics and Prebiotics** (ISAPP) definition, refers to "live microorganisms that, when administered in adequate amounts, confer a health benefit on the host" (Hill et al., 2014). In addition, many of these microbes can colonize and proliferate in a niche-specific manner in the host microenvironment (Han et al., 2021). The safety profile and target-specific nature of these microbes make them ideal candidates for targeting clinically relevant diseases like **diabetes, obesity, ulcerative colitis, cancer, pathogenic infections, and inflammatory conditions** (**Figure 1A**). Depending on the therapeutic effect, eLBPs can alleviate the disease symptoms or prevent disease progression by producing secondary metabolites, expressing recombinant enzymes, or releasing synthetic peptides and oncolytic proteins (**Figure 1B;** Kelly et al., 2020). The most promising examples of such eLBPs that have shown significant success in preclinical animal models and, in some instances, even in human clinical trials, are described below along with the disease conditions treated.

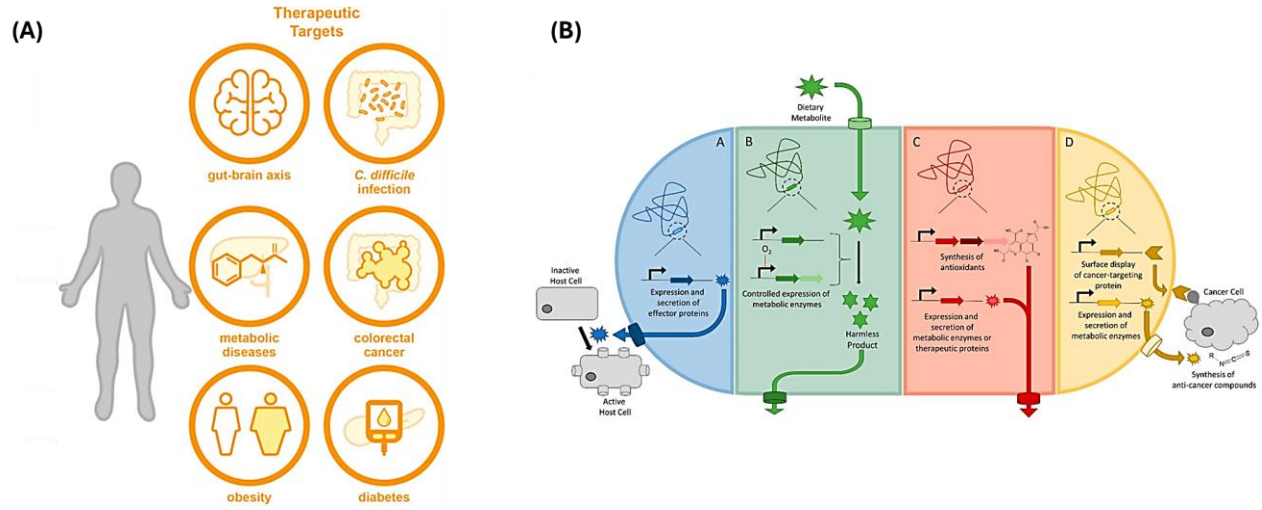

Figure 1. (A) Scheme of different clinically relevant diseases that could be targeted by eLBPs. The diseases range from neurodegenerative disorders, pathogenic infections, metabolic disorders, cancer, obesity and diabetes (Reprinted with permission, Rutter et al., 2022, Copyright © Frontiers Publishing Group) (B) Strategies employed by eLBPs for treating diseases include the production of secondary metabolites, the expression of recombinant enzymes to metabolize toxic molecules, and the secretion of synthetic peptides and oncolytic proteins (Reprinted with permission, Kelly et al., 2020, Copyright © American Chemical Society)

1.2.1. Diabetes and Obesity

The contemporary method to control diabetes in the patient is to undergo repeated administration of the insulin hormone. However, this not only imposes a burden on the patient's lifestyle but leads them to incur substantial medical expenditures, indicated by the global spending on insulin, accounting for 22 billion USD in the year 2022 (Parker et al., 2022). Researchers in recent years have, therefore, started exploring the potential of eLBPs in regulating the blood sugar levels in diabetic patients. One of the very first eLBPs constructed in this direction was a genetically modified strain of *L. lactis* that could secrete the human proinsulin and the **human cytokine interleukin-10** (hIL-10) in **non-obese diabetic** (NOD) mice models (Takiishi et al., 2012). The eLBP and anti-CD3 immune modulator treatment combination (via oral administration) showed the blood sugar levels to revert to their normal levels in ~59% of the tested NOD mice. This reversal showed that preventing onset of autoimmune Type I diabetes (T1D) is possible. In the case of T1D, the patient fails to recognize insulin as a self-antigen, leading to a loss in antigen tolerance and expansion of pancreatic β-cell targeting immune cells. To prevent this self-destructive pathway, the researchers modified the *L. lactis* eLBP to secrete the glutamic acid

decarboxylase (GAD65, 370-575 amino acid residues) autoantigen in combination with the hIL-10 cytokine (Robert et al., 2014). Although the treatment did not eliminate the β-cell–targeting immune cells, it increased the population of CD4+Foxp3+CD25+ regulatory T (Treg) cells. Follow-up studies proved that the Foxp3+ Treg cells played an essential role in maintaining tolerance towards the pancreatic β-cells and enriching their levels using the eLBP administration strategy could prevent T1D onset in preclinical mice models, demonstrating their therapeutic efficacy (Takiishi et al., 2017). Apart from T1D, **462 million individuals** are currently suffering from Type II diabetes (T2D) (Khan et al., 2020), making it a prominent disease category for eLBP development. To prevent T2D based disease progression, strategies involving the active production of the **peptide hormone GLP-1** or sustained release of **GLP-1 receptor agonists** are being investigated. Generally, the biologically active GLP-1 (1-37 amino acid residue) isoform is produced by proteolytic cleavage of the proglucagon peptide hormone in the small intestine. Duan et al., engineered a probiotic *E. coli* Nissle 1917 strain to secrete GLP-1, and the secreted protein stimulated insulin production in epithelial cells (Duan et al., 2008). Following that, the authors incorporated the GLP-1 protein-encoding gene into the commensal strain *Lactobacillus gasseri* genome and fed the eLBP to diabetic rats. They observed that the secreted GLP-1 could stimulate the epithelial cells of the small intestine to secrete insulin, which accounted for ~30% of the average insulin levels typically observed in healthy rats (Duan et al., 2015). In another independent study, the *Lactiplantibacillus plantarum* MH-301 (originally isolated from healthy patients in China) strain was engineered to allow stable expression and release of GLP-1 in transgenic T2D mice models (Hu et al., 2023). The high-fat diet-fed mice were able to revert their diabetic symptoms once the eLBP was administered and showed significant reduction of proinflammatory cytokine expression in the gut. This engineered strain also positively impacted the modulation of the intestinal microflora and altered the fecal metabolic profile in T2D monkey models (Luo et al., 2021). In addition to targeting T2D, these GLP-1-secreting eLBP strains have shown significant effectiveness in reducing the overall body weight of obese mice and improving their gut microbiome (Ma et al., 2020; Wang et al., 2021). Apart from modulating obesity, engineered *L. lactis* strains producing GLP-1 have also shown protective effects against neuroinflammatory conditions in **Alzheimer's disease** (AD) and **Parkinson's disease** (PD) mouse models (Fang et al., 2020). The eLBP prevented cognitive decline by suppressing amyloid plaques (Aβ) and downregulating inflammatory signaling cascades in AD mice (Chen et al., 2018). For the

PD mice model treated with the neurotoxin 1-methyl-4-phenyl-1, 2, 3, 6-tetrahydropyridine (MPTP), the GLP-1-producing *L. lactis* showed a significant reduction in locomotory impairment, diminished astrocyte activation, and increase in the probiotic bacteria population in the gut (Fang et al., 2019). These studies show that eLBPs can positively impact lifestyle-related disorders associated with diabetes and obesity and may also offer protection against neurodegenerative diseases.

1.2.2. Metabolic Disorders

Chronic metabolic disorders are related to the absence or underperformance of enzymes that maintain the metabolism of the complex human diet and the excretion of toxic by-products. These genetically inherited diseases are sporadic in the human population, so the financial incentive to develop **"orphan drugs"** for them is relatively low in the pharmaceutical sector (Fellows and Hollis., 2013). However, these diseases impose a lifetime burden on the affected people and severely impact their everyday lifestyle. Phenylketonuria, homocystinuria, maple syrup urine disease, hyperammonemia, and enteric hyperoxaluria are rare metabolic diseases that have responded to eLBP based treatment in the past decade (Hwang., 2023). Although different research groups have developed a handful of microbial strains to treat such conditions, the foremost player that has changed the eLBP-based treatment landscape for metabolic diseases is the US-based startup **"Synlogic".** Their eLBP portfolio has expanded rapidly using the engineered *E. coli* Nissle 1917 strain as their model microbial chassis. Their engineered strain **SYNB1934 (labafenogene marselecobac)** was genetically modified to allow rapid degradation of excess phenylalanine that accumulated in the gastrointestinal tract of the patients enrolled in their Phase II- trial (Vockley et al., 2023). The strain enables fast import of the **phenylalanine** amino acid (PheP transporter) and conversion to the non-toxic metabolites, **trans-cinnamic acid** [by a **modified PAL** enzyme] and phenylpyruvate [by **L-amino acid deaminase** (LAAD) enzyme] (**Figure 2A**). The strain showed a high response rate (~60%) and reduced levels of phenylalanine accumulation (blood plasma) for patients who responded to the treatment. These positive results helped labafenogene marselecobac to gain fast-track approval from the FDA for entering the **Phase III** clinical trials. Alternate gut symbiont bacteria are also being explored for treating phenylketonuria-associated symptoms by preventing excessive accumulation of phenylalanine. The common gut probiotic bacterium,

Limosilactobacillus reuteri, was engineered to allow constitutive intracellular expression of the PAL enzyme (obtained from *Anabaena variabilis*), which significantly reduced the blood phenylalanine level of mice models fed with a complex diet (Durrer et al., 2017). Apart from intracellular enzyme production, strategies to actively secrete recombinant enzymes like **phenylalanine hydroxylase** (PAH) fused with gastrointestinal signal peptide GI1 have also been investigated in the *Lactiplantibacillus plantarum* CM_PUJ411 strain (Ramírez et al., 2017). Although no animal studies were reported, *in-vitro* studies confirmed that the secreted enzyme was functionally active, allowing active conversion of phenylalanine to tyrosine, and could cross the Caco-2 cell monolayer, a representative cellular model of the **gastrointestinal tract** (GI).

Homocystinuria patients lack the **cystathionine β-synthase** (CBS) enzyme responsible for converting homocysteine (a byproduct of methionine metabolism) to the non-toxic metabolite cystathionine (Kumar et al., 2016). To prevent homocysteine accumulation, patients must follow a stringent diet plan devoid of the methionine amino acid. Synlogic developed an engineered *E. coli* Nissle 1917 strain, **SYNB1353**, that could be potentially beneficial in regulating methionine metabolism in the affected patients (Fishbein et al., 2024). The strain, SYNB1353, was genetically engineered to allow the intracellular import of **methionine** (MetP importer) and conversion to **3-methylthiopropylamine** (3-MTP) by **methionine decarboxylase** (MetDC enzyme) (**Figure 2B**). The bioactive strain reduced the blood plasma levels of homocysteine in mice models and cynomolgus monkeys fed with a methionine-enriched diet. Following preclinical efficacy tests, SYNB1353 progressed to a Phase I clinical trial where the enrolled volunteers safely tolerated the eLBP and reduced the methionine levels (blood plasma) by 26% post-consumption of a methionine-based diet compared to the placebo (Perreault et al., 2024). However, due to financial constraints, Synlogic decided not to proceed with the Phase II clinical trial for the SYNB1353 strain.

Maple syrup urine disease is another rare inherited genetic disorder in which the patients suffer from an excessive accumulation of branched-chain amino acids like isoleucine, leucine, and valine due to the absence of the **branched-chain alpha-keto acid dehydrogenase enzyme complex** (BCKAD) (Blackburn et al., 2017). Synlogic used a high-throughput strain selection strategy to optimize the rapid metabolism of the leucine amino acid using the engineered *E. coli* Nissle 1917

strain, **SYN5941** (Li et al., 2021). The engineered strain could import **leucine** into the intracellular milieu (BrnQ importer) and convert it to the non-toxic metabolite **isopentanol** using the **leucine dehydrogenase** (leuDH), **ketoacid decarboxylase** (KivD) and **alcohol dehydrogenase** (Adh) enzymes (**Figure 2C**). SYN5941 showed a significant decrease in the plasma leucine levels as well as increased levels of **UDP-glucuronosyltransferase** (UGT, the excreted form of isopentanol) in the urine of non-human primates fed with 7 g of peptone. Efforts are underway to progress the SYN5941 strain into Phase I clinical trials and study their tolerability in healthy volunteers.

Hyperammonemia is another metabolic disorder characterized by **elevated ammonia levels** in the blood plasma either due to a deficiency of ammonia metabolism enzymes (like **ornithine transcarbamylase**) (Lichter-Konecki et al., 2022) or by **hepatotoxin-induced liver injury** (Lima et al., 2019). Excessive accumulation of ammonia can lead to the development of **hepatic encephalopathy** and urea cycle dysfunction, increasing the chances of **brain injury and death**. Synlogic developed an *E. coli* Nissle 1917 strain, **SYNB1020**, that could convert **ammonia** to a non-toxic metabolite, **L-arginine**, by deletion of the corresponding negative regulator (ArgR repressor) and intracellular expression of the robust L-arginine biosynthesis enzyme (**N-acetylglutamate synthase**, ArgAY19C) (**Figure 2D**, Kurtz et al., 2019). SYNB1020 significantly reduced the serum ammonia levels in both genetically linked and chemically induced hyperammonemia mice models. The SYNB1020 was tested in healthy volunteers in a Phase I clinical trial, was well-tolerated, generated no serious adverse effects, and cleared from the host system after two weeks of last dosage administration. These positive results allowed the entry of SYNB1020 in a randomized, placebo-controlled Phase Ib/IIa clinical trial to test its effectiveness in reducing serum ammonia levels in patients suffering from liver cirrhosis (Kurtz et al., 2019). However, despite increased urinary nitrate activity, no reduction of serum ammonia levels was noticeably observed in the patient cohort treated with SYNB1020 compared to the placebo, halting further strain testing in additional patients. In an independent study, another natural human commensal strain, *Lactiplantibacillus plantarum* NCIMB8826, was genetically engineered to delete the **L-lactate dehydrogenase** and **D-lactate dehydrogenase** encoding genes and overexpress the **alanine dehydrogenase** enzyme to create the **ammonia hyper consumer strain** (Nicaise et al., 2008). This engineered strain quenched the ammonia produced in the gut, decreased

the blood ammonia levels, and increased the survivability of the rats suffering from fulminant hepatic failure. This study suggests that engineering alternative microbial strains besides *E. coli* Nissle 1917 may also enhance the likelihood of reducing serum ammonia levels in patients suffering from hyperammonemia.

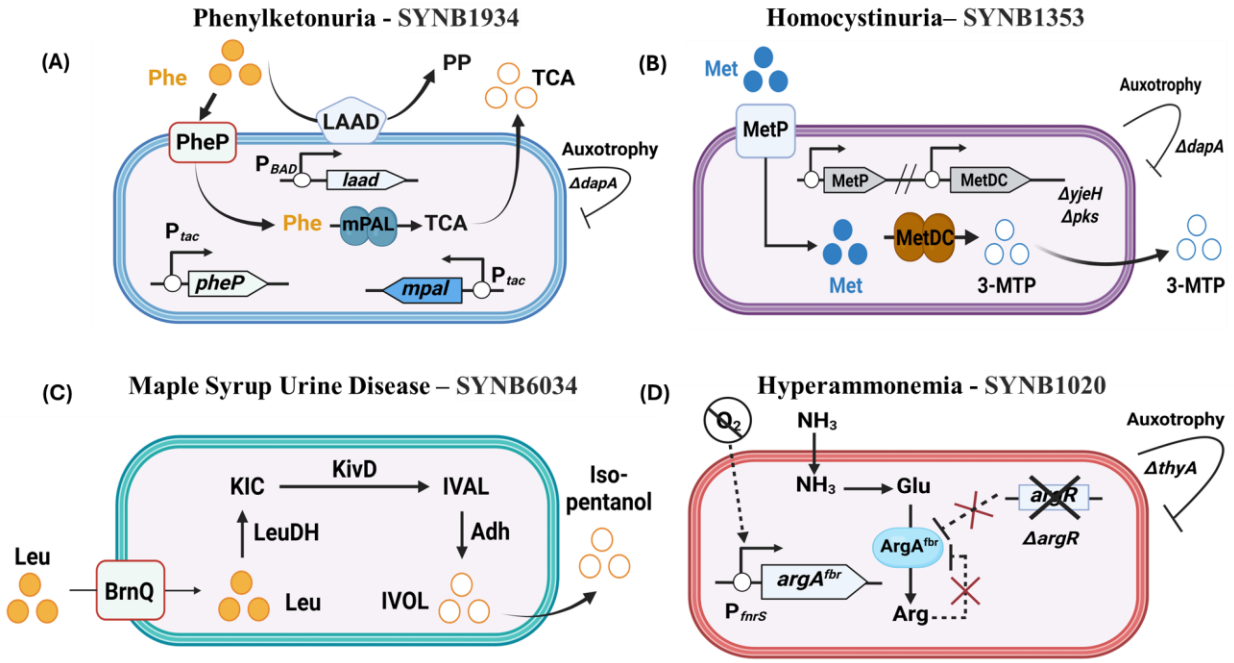

Figure 2. (A) Schematic of the phenylalanine metabolizing *E. coli* Nissle 1917 prototype strain, SYNB1934 (Readapted from Vockley et al., 2023; Copyright © Springer-Nature) (B) Schematic of the methionine-homocysteine metabolizing *E. coli* Nissle 1917 strain, SYNB1353 (Readapted from Perreault et al., Copyright © Elsevier Inc.) (C) Schematic of the leucine metabolizing *E. coli* Nissle 1917 strain, SYNB6034 (Readapted from Li et al., Copyright © Research-Square, Springer-Nature) (D) Schematic of the ammonia metabolizing *E. coli* Nissle 1917 strain, SYNB1020 (Readapted from Kurtz et al., 2019; Copyright © AAAS)

Enteric hyperoxaluria is a metabolic disease characterized by enhanced absorption of **dietary oxalate** and its gradual progression toward kidney stone formation and renal failure (Witting et al., 2021). Synlogic developed the *E. coli* Nissle 1917 - based **SYNB8802** strain that utilizes the oxalate-formate cyclic regeneration pathway to **import oxalate** from the extracellular environment and **export formate** in exchange (Lubkowicz et al., 2022). The imported oxalate is degraded by the **oxalate decarboxylase** (OxdC) enzyme and converted to formate and carbon dioxide by the **formyl-CoA transferase** (Frc) enzyme. SYNB8802 significantly decreased the urinary excretion of oxalate in mice models and non-human primates due to the activated consumption of oxalate directly in the gut. ***In-silico* simulations** (ISS) conducted with these data for determining their

efficacy in the human gastrointestinal tract could predict clinically relevant decreases in oxalate levels in diseased patients (Lubkowicz et al., 2022). Another USA-based startup, **Novome Biotechnologies**, has engineered the commensal bacteria, *Bacteroides,* that degrade oxalate in rat models fed with an oxalate-enriched diet and daily administration of **porphyrin** for stable bacterial colonization (Novome Biotechnologies Inc., 2022). The eLBP mediated a 30% - 50% decrease in urinary oxalate levels, which motivated them to enroll healthy volunteers for a Phase I clinical trial. Although the strain had good tolerability in the healthy volunteers, the strain exhibited no distinct advantage in a randomized Phase IIa study involving patients suffering from hyperoxaluria, leading to a halt in the program (Novome Biotechnologies Inc., 2022). The OxdC enzyme also showed superior performance in oxalate metabolism compared to its counterpart enzyme, **oxalate oxidase** (OxO), when recombinantly expressed in *L. lactis* MG1363 (Zhao et al., 2018). When fed to hyperoxaluria rat models, the recombinant strain significantly reduced urinary oxalate levels and inhibited the formation of kidney stones (calcium oxalate crystals). Another commensal strain, *Lactiplantibacillus plantarum* WCFS1 was also engineered to mediate extracellular secretion of the OxdC enzyme to metabolize the excess oxalate present in the intestine of the rat models (Sasikumar et al., 2014; Paul et al., 2018). The recombinant strain decreased the overall urea, creatinine, and urinary oxalate levels and prevented **calcium oxalate crystal deposition** in rat kidneys. All this evidence suggests that eLBPs can potentially treat multiple metabolic disorders and play an essential role in future healthcare.

1.2.3. Inflammatory Disorders

Inflammatory disorders are characterized by the malfunctioning of the host immune response, during which the immune cells get overstimulated and attack the healthy cells/tissues mediated by molecular markers, leading to disease development. The most common ones that affect a vast global population are **inflammatory bowel disease, diabetic foot ulcers, acne, alcoholic liver disease, gout** and **rheumatoid arthritis**. The past two decades have seen massive progress toward developing eLBPs to target such inflammatory disorders. Some of these eLBPs have been tested in animal models with significant success, with some candidates even progressing towards human clinical trials.

Inflammatory bowel disease (IBD) pertains to inflammatory conditions of the small intestine and colon, including commonly occurring **ulcerative colitis (UC)** and rare **Crohn's disease** (Baumgart and Carding., 2007). According to epidemiological evidence, there were **6.8 million** cases of IBD recorded globally in 2017 (**Figure 3A**), and very few medically approved treatment solutions currently exist for them (Alatab et al., 2020). Although the exact reason for IBD development is poorly understood, IBD progression is related to the imbalanced activation of the Type 1 and Type 2 T helper cell population (Th1 and Th2), typically activated in response to pathogenic bacteria and nematodes. The anti-inflammatory cytokine **Interleukin-10** (IL-10) effectively suppresses the proinflammatory reactions triggered by the Th1 and Th2 immune cells (Taylor et al., 2006). To determine the role of IL-10 in IBD treatment, *L. lactis* was genetically modified to drive its constitutive secretion (murine IL-10) in **dextran sulfate sodium (DSS) induced colitis** IL-10−/− mice models (Steidler et al., 2000). The eLBP was fed daily for 14 days, followed by another 14 days of recovery, and it showed a drastic reduction (~50%) in pathological symptoms compared to the non-engineered control strain. In addition, the eLBP was also able to prevent adenocarcinoma development in the treated mice, a commonly associated adverse reaction linked to DSS-induced colitis. To assess the safety of the eLBP, *L. lactis*, engineered to secrete human IL-10 (hIL-10), was administered into cynomolgus monkeys for four consecutive weeks, followed by a four-week recovery period (Steidler et al., 2009). The eLBP was safely tolerated and did not develop adverse side effects in the primates. Following this success, **ActoBiotics™** then progressed the eLBP candidate into a Phase I, placebo uncontrolled study, with ten enrolled patients suffering from CD (Braat et al., 2006). The patients consumed the hIL-10 secreting *L. lactis* strain for seven days and were regularly monitored for one month. Significant clinical benefit was observed for ~80% of the enrolled patients, with 50% undergoing complete remission and ~30% exhibiting a clinical response indicated by decreased **Crohn's disease activity index** (CDAI) and serum **C-reactive protein** (CRP) levels. Although the strain was supposed to progress into Phase II clinical trial in 2010, no further information about the clinical trials is currently available (Steidler et al., 2009). Another strategy to prevent IBD progression involves neutralizing proinflammatory cytokine **TNF alpha,** which is responsible for mediating severe damage to the intestinal mucosal layer (Tatiya-Aphiradee et al., 2018). *L. lactis* was engineered to secrete single-domain, **anti-TNF alpha nanobodies** and orally administered into DSS-induced colitis IL-10−/− mice models (Vandenbroucke et al., 2010). The eLBP was able to actively deliver the nanobody

at the damaged mucosal layer, leading to reduced levels of inflammatory biomarkers and preventing systemic circulation of the nanobody. Recently, the type III secretion system from *Shigella flexneri* was adapted for *E. coli* Nissle to develop the **PROT$_3$EcT-4** strain that could secrete high yields of the anti-TNF alpha nanobodies (**Figure 3B,** Lynch et al., 2023). A single dose of the eLBP (oral and rectal administration) sufficiently reduced the proinflammatory TNF alpha cytokine concentration in chemically induced colitis mice models, thus preventing damage to the intestinal epithelium. Apart from cytokines and nanobodies, alternative **cytoprotective proteins** can also play an essential role in mitigating the progression of IBD (Nguyen et al., 2015). *L. lactis* was therefore engineered to deliver **trefoil factor proteins** (TFF), responsible for restoring mucosal homeostasis in the intestinal tract of DSS-induced colitis IL-10−/− mice, and was observed to promote epithelial wound healing and alleviate colitis-associated symptoms (Vandenbroucke et al., 2004). To enhance intestinal wound healing, *E. coli* Nissle was engineered to produce a chimeric protein where TFF was fused to the extracellular matrix-forming curli fiber monomer (csgA), creating a mucosal protective layer, termed the **PATCH (probiotic-associated therapeutic curli hybrids)** (**Figure 3C,** Praveschotinunt et al., 2019). The PATCH layer was shown to reinforce the epithelial layer and reduce proinflammatory cytokine levels when rectally administered to DSS-induced colitis mice models. In addition to bacterial species, the eukaryotic yeast *Saccharomyces boulardi* was engineered to deliver the IL-10 cytokine and TNF-alpha inhibitor in mice colitis models (Liu et al., 2020). Although neither IL-10 nor TNF-alpha inhibitor secretion provided any therapeutic benefit, the atrial natriuretic peptide hormone secreting strain was able to decrease the overall proinflammatory cytokine levels of TNF-α, and IL-1β linked to colitis progression, eventually improving the mice's survival rate. Lastly, modulation of a critical metabolite, **(R)-3-hydroxybutyrate** (3HB), in the gut has shown a significant impact in reducing colitis-related symptoms in mice models (Suzuki et al., 2023). *E. coli* Nissle engineered to express 3HB in the gut environment was able to restore the natural gut microbiota, reduce mucosal inflammation, and prevent disease progression in DSS-induced colitis mice models.

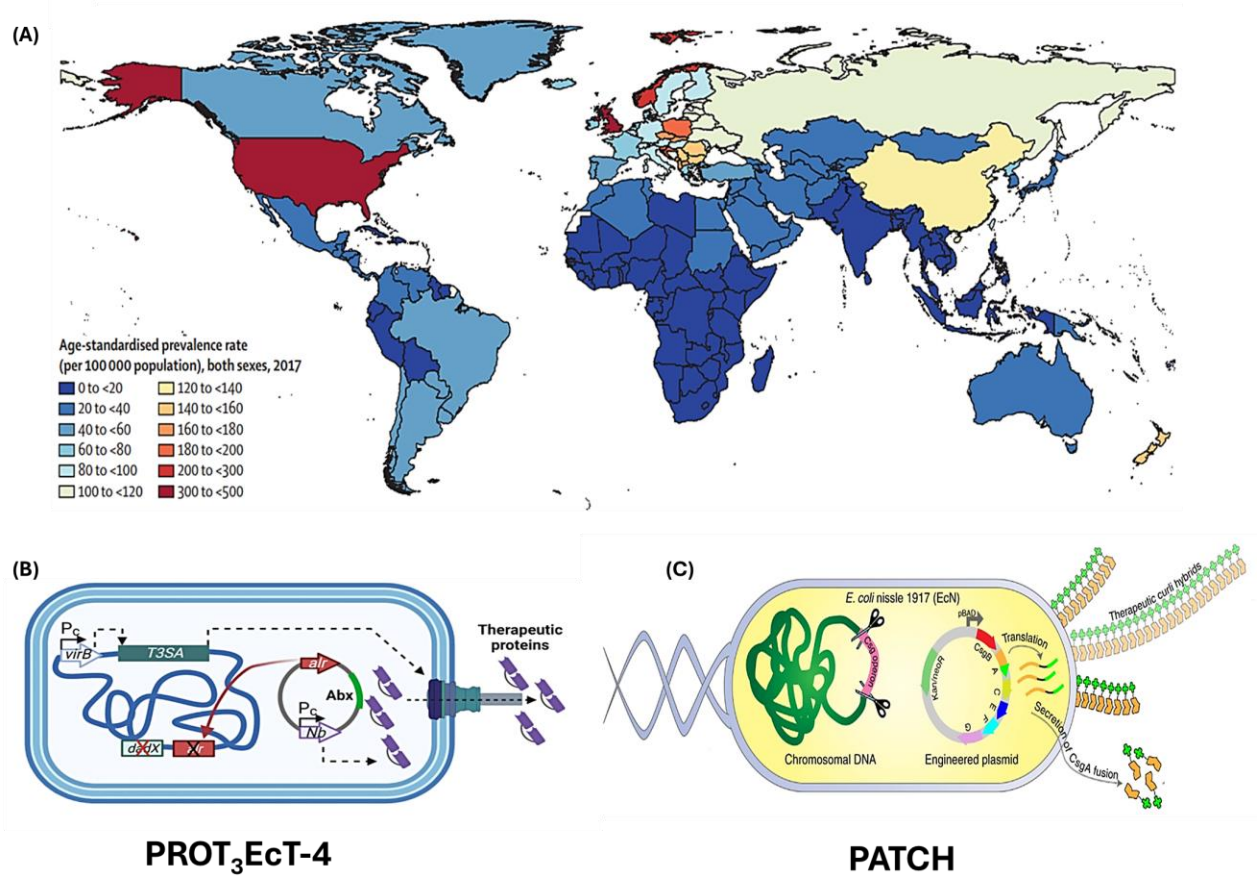

Figure 3. (A) Age-standardised prevalence rate of Inflammatory Bowel Disease (IBD) per 100,000 population of both sexes, in 195 countries and territories surveyed in the year 2017 (Reprinted with permission from GBD 2017 Inflammatory Bowel Disease Collaborators, Alatab et al., 2020; Copyright © Elsevier Inc.) (B) Schematic of the tumor necrosis factor-alpha (TNF-α)-neutralizing Nanobody (Nb) secreting *E. coli* Nissle 1917 strain (PROT3EcT-4) (Reprinted with permission from Lynch et al., 2023; Copyright © Elsevier Inc.) (C) Schematic of the curli fiber monomer (csgA) producing *E. coli* Nissle 1917 strain (PATCH) (Reprinted with permission from Praveschotinunt et al., 2019; Copyright © Springer-Nature)

Besides gastrointestinal inflammation, eLBPs can also play an essential role in skin repair, wound healing, and prevention of skin diseases. Chronic cases like diabetic foot ulcers can initiate an inflammatory cascade and prevent skin repair (Roslan et al., 2023). *L. lactis* was engineered to secrete a pro-angiogenic protein, **vascular endothelial growth factor** (VEGF), to trigger wound healing, and its metabolic byproduct, lactic acid, on the other hand, could induce M1 macrophages, to reverse the inflammatory signals associated with diabetic wounds (Lu et al., 2021). The engineered strain encapsulated in a heparin-poloxamer hydrogel was able to enrich the blood

vessel density in the wounds of diabetic mice up to ~5.5 times in comparison to the control. Besides growth factor proteins, wound healing is also positively influenced by the **chemokine CXCL12** (Stromal cell-derived Factor 1α). The probiotic *Limosilactobacillus reuteri,* engineered to secrete high levels of the beneficial CXCL12 chemokine in the wound microenvironment, showed accelerated wound healing in healthy and diabetic mouse models (**Figure 4A**, Vågesjö et al., 2018). The lactic acid produced by bacterial metabolism helped reduce the local pH and prevented proteolytic degradation of the CXCL12 chemokine in the wound site. The modified *Limosilactobacillus reuteri* strain (**ILP100**) recently progressed into a placebo-controlled Phase I clinical trial designed by **ILYA Pharma**, where its safety profile and efficacy were tested in healthy patients with induced wounds (Öhnstedt et al., 2023). The eLBP was well tolerated, had no adverse effects, and significantly shortened the overall wound healing time for the highest dosage from the 19th day onwards. This finding is highly significant in that a minimum improvement of ~10%-15% in the wound healing period of diabetic patients is seen as a **clinically meaningful result** (FDA Report Ulcer and Burn Wound., 2006). Studies have shown that CXCL12 delivery mediated from engineered *L. lactis*, in conjunction with yellow LED light, was not only able to trigger wound healing but also reduce proinflammatory cytokine levels and reduce the population of pathogenic bacteria *Ralstonia* and *Acinetobacter* at the wound site of mice models (Zhao et al., 2021). Generally, the skin is a **nutrient-deficient environment**, leading to a reduced growth profile of the eLBP. To increase the functional stability, engineered CXCL12 secreting *L. lactis* was encapsulated in a biocompatible Polyethylene Glycol Diacrylate (PEGDA) hydrogel along with the **autotrophic** S*ynechococcus elongatus* PCC7942 strain that could naturally synthesize **sucrose** (Li et al., 2023). The heterotrophic *L. lactis* could utilize this carbon source for better growth and therapeutic secretion profile and promote healing in rat wound models. Instead of secreting a single chemokine (CXCL12), the clinical-stage synthetic biology company **Aurealis Therapeutics** has engineered a *L. lactis* strain (AUP1602-C) to secrete multiple therapeutic proteins, including the human fibroblast growth factor 2 (hFGF-2), human interleukin-4 (hIL-4) and human colony-stimulating factor 1 (hCSF-1) (Kurkipuro et al., 2022). These therapeutic proteins stimulate fibroblast proliferation, promote angiogenesis and immune cell activation, respectively. The eLBP promoted healing in diabetic mouse wound models by angiogenesis stimulation and accelerated wound contraction (**Figure 4B**). Preclinical efficacy made the strain progress into Phase I human clinical trials, where the eLBP was tested on diabetic

foot ulcer patients to assess the safety and efficacy profile (Aurealis Clinical Trial Report., 2024). The eLBP was well-tolerated, showed no dosage-related adverse effect, and 83% of patients achieved complete wound healing without additional ulcer recurrence after a 12-month follow-up period. The strain has now progressed into a multi-country, placebo-controlled Phase II human clinical trial towards treating non-healing ulcers of diabetic foot ulcer patients. **Acne vulgaris** is another chronic inflammatory condition that affects more than a million people annually and is mainly associated with **altered sebum production** and **damaged pilosebaceous follicles** (Cruz et al., 2023). Recently, a natural human skin commensal, *Cutibacterium acnes*, was engineered to secrete the **neutrophil gelatinase-associated lipocalin** (NGAL) protein that can induce apoptosis in the sebum-producing cells (sebocytes) and reduce the overall sebum concentration to mitigate the acne associated symptoms (Knödlseder, et al., 2024). The eLBP successfully engrafted on the mouse skin, mainly colonizing the mice's hair follicles. In addition, the eLBP was also able to secrete NGAL even after four days of engraftment, suggesting that it could be a suitable option for treating skin-related inflammatory disorders.

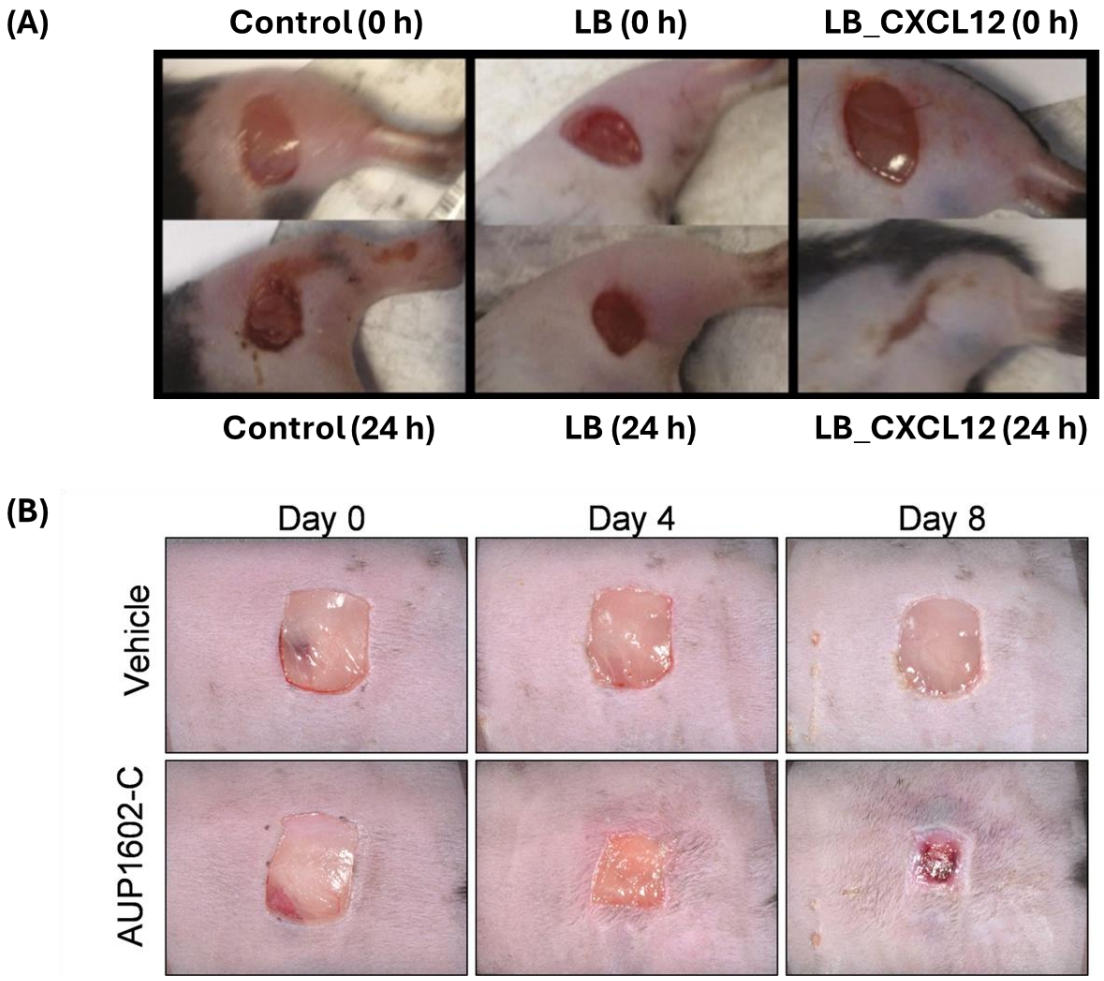

Figure 4. (A) Healing of hind-limb wounds in mice within a 24 h period. The treatment regimen were classified as control (no treatment), LB (treated with control *Limosilactobacillus reuteri* strain) and LB_CXCL12 (treated with CXCL12 chemokine secreting *Limosilactobacillus reuteri* strain) and imaged at the start (0 h) and end (24 h) of the experimental period (Reprinted and slightly modified with permission from Vågesjö et al., 2018; Copyright © PNAS) (B) Healing of left-flank wounds in mice within an 8-day period. The treatment regimen were classified as vehicle (unmodified *L. lactis* strain) and AUP1602-C (*L. lactis* strain engineered to secrete hFGF-2. hIL-4 and hCSF-1) and imaged at the start (Day 0), middle (Day 4) and end (Day 8) of the experimental period (Reprinted with permission from Kurkipuro et al., 2022; Copyright © PLOS)

eLBP can also be a promising alternative for treating lifestyle-associated inflammatory diseases, the most prominent one of them being **alcohol-related liver disease** (ARLD) (Fuenzalida et al., 2021). Excessive alcohol intake can lead to a significant decrease in the regenerative capacity of the liver, causing permanent damage in the form of hepatitis and cirrhosis. Alcohol intake can reduce cytokine expression levels, **Interleukin 22** (IL-22), and antimicrobial **regenerating islet-**

derived 3 gamma (REG3G) protein in the small intestine. The reduced levels of these proteins can cause severe liver damage and inflammation (Hartmann et al., 2013). *Limosilactobacillus reuteri* was therefore engineered to produce and secrete the murine Interleukin 22 (mIL-22) and orally administered to chronic-binge ethanol-fed mice models to restore the REG3G protein levels in the intestine (Hendrikx et al., 2013). The upregulated REG3G protein effectively reduced bacterial translocation from the intestine to the liver and prevented ethanol-induced hepatitis. Instead of modulating the immunoprotective protein levels, strategies to metabolize the excessive alcohol consumed by eLBPs in the gastrointestinal tract could be a viable option to prevent hepatic inflammation. The enzymes **alcohol dehydrogenase** (ADH) and **aldehyde dehydrogenase** (ALDH) are responsible for the sequential oxidation of ethanol to **acetaldehyde** and **acetate**, respectively (Haber et al., 2003). As a first attempt, an engineered *L. lactis* NZ3900 strain capable of expressing both ADH and ALDH enzymes was orally administered to ethanol-fed mice for 15 consecutive days (Lyu et al., 2018). The eLBP maintained the serum lipid level stably and protected against oxidative stress-induced damage to the mice's liver. Another probiotic strain, *Bacillus subtilis* BS001, engineered to co-express the yeast ADH and ALDH enzymes, was able to successfully reduce the overall blood alcohol content in ethanol-fed mice and downregulate serum biomarker levels of **alanine aminotransferase** (ALT) and **aspartate aminotransferase** (AST), and reduce intestinal pathogenic bacteria (Lu et al., 2018). However, the catalytic efficiency of the recombinant ADH and ALDH enzymes was relatively low in both cases, so modified enzymes scADH and istALDH were chromosomally integrated into the probiotic *B. subtilis* fmb8 strain (Lu et al., 2020). The modified strain showed superior performance not only in reducing blood alcohol content in ethanol-fed mice but also in increasing the overall antioxidative enzyme levels of the mouse liver.

Inflammatory connective tissue disorders, like **gout** and **rheumatoid arthritis** (RA), have an overwhelming global burden, with an estimated **55.8 million** and **17.6 million** adults suffering from them, respectively (Cross et al., 2021; Black et al., 2021). Gout is caused by an abnormal increase of **uric acid** in the blood serum, known as **hyperuricemia** (Wortmann., 2002). The increased uric acid production due to a purine-rich diet and its low excretion levels leads to uric acid crystal deposition in the limb joints, causing severe **joint inflammation, swelling,** and **extreme pain**. Rheumatoid arthritis (RA), on the other hand, is an **autoimmune disorder** where the immune cells target the healthy cells, mainly the joints, to cause **inflammation** and **painful**

swelling (Firestein., 2003). eLBPs can be viable options for resolving painful disease-associated symptoms and providing patients with a better quality of life. Metabolizing the excess uric acid accumulated in the small intestine by eLBPs can be an exciting alternative to prevent gout development and progression. The gut probiotic, *E. coli* Nissle, was engineered to express the **uric acid importer enzyme**, YgfU, to increase the intracellular urate concentration so that the additional **recombinant enzymes**, PucL and PucM, could metabolize it into a soluble, non-toxic metabolite **allantoin** (Zhao et al., 2022). The eLBP, when orally administered for seven days in hyperuricemia-induced mice, could actively metabolize the excess uric acid in hypoxic gut conditions to cause a significant reduction in serum uric acid levels (Zhao et al., 2022). To improve the uric acid metabolizing capacity of the eLBP, *E. coli* Nissle was genetically modified to mediate periplasmic (surface) expression of the uricase enzyme isolated from the fungi *Cyberlindnera jadinii* to facilitate uric acid conversion into allantoin (He et al., 2022). The improved uric acid degradation efficiency of the eLBP significantly decreased the serum uric acid levels of diet-induced (purine-rich food) and genetically prone (urate oxidase enzyme deficient) hyperuricemic mice models. The engineered strain also modulated and restored the gut microbial composition appreciably. However, the catalytic performance of uricase was generally superior in the presence of oxygen (aerobic conditions) and drastically dropped under anaerobic conditions. A recent investigation into the **purinolytic** metabolic pathway of anaerobic bacteria led to the discovery of four hydrolases and one decarboxylase enzyme that could directly degrade purines and bypass the formation of the metabolic intermediate, uric acid (Tong et al., 2023). The two main hydrolases of this purine degradation cascade, XnhA, and XnhB, were recombinantly expressed in *E. coli* Nissle and orally administered to hyperuricemic *Drosophila melanogaster* fly models for 14 days (Tong et al., 2023). After administration, the eLBP significantly reduced uric acid concentration in the hindgut and Malpighian tubules (MTs) of the flies and ultimately abolished the formation of uric acid stones compared to the control strain. Rheumatoid arthritis is generally treated by cytokine-modulating biologics (**anti-IL6R, anti-TNF alpha, and anti-IL-1β)** (Colmegna et al., 2012). However, the disease progression is predominantly linked to the irregular activation of the T-lymphocytes in the **synovial cavity** of RA patients (VanderBorght et al., 2001). The T-lymphocyte activation depends on the upregulation of the potassium (K+) channel, **Kv1.3**, making it an attractive therapeutic target for treating RA (Wulff and Zhorov., 2008). Peptidomimetic analysis has helped select a peptide, ShK-186, that could allow efficient and specific blocking of the Kv1.3

channel in both *in-vitro* and *in-vivo* studies. To improve the peptide delivery in the patient population, the probiotic strain *Limosilactobacillus reuteri* ATCC PTA 6475 was engineered to secrete the peptide analog, **ShK-235**, in the gut lumen and have enhanced bioavailability in RA rat models (Wang et al., 2023). The eLBP was well tolerated without eliciting any immunogenicity and significantly reduced joint inflammation, bone deterioration, and cartilage damage.

1.2.4. Cancer

Malignant cells are also prone to developing **drug resistance** and **immune evasion** strategies, thereby facilitating disease relapse, and decreasing the overall chances for disease remission and cure. These reasons have motivated researchers to explore eLBPs as complementary agents for enhancing the curative efficacy of the existing therapeutic portfolio (**Figure 5A,** Zhou et al., 2023). In the past two decades, significant efforts have been made towards engineering several microbes for **targeted colonization** of solid tumors and subsequent release of cytotoxic payloads for inducing cellular death (**apoptosis**). Certain bacterial species can naturally colonize the heavily vascularized solid tumors due to their nutrient-rich and immunoprotective microenvironment, conducive for bacterial survival and proliferation. Although certain microbial strains can act as natural anticancer agents to a certain extent, the significantly enhanced therapeutic ability of eLBPs can increase their overall success rate as potent anticancer agents.

One of the earliest microbial chassis subjected to genetic modification for targeting the cancer microenvironment was the facultative anaerobe, ***Salmonella typhimurium*** (Guo et al., 2020). Although *S. typhimurium* is generally considered a human pathogen, attenuated variants of the bacterial strain have the potential to significantly alter the tumor microenvironment and induce direct tumor cell death. Researchers engineered attenuated *S. typhimurium* strains to release apoptosis-inducing cytokines in the tumor microenvironment post-bacterial colonization. Loeffler and coworkers developed two *S. typhimurium*-based eLBPs to facilitate the secretion of the **tumor necrosis factor superfamily member 14** (TNFSF14) and **Chemokine (C-C motif) ligand 21** (CCL21) cytokines, respectively (Loeffler et al., 2007; Loeffler et al., 2009). As confirmed by luminescence imaging, *S. typhimurium* could colonize solid tumors post-intravenous administration in mice models without eliciting systemic toxicity. The TNFSF14 secreting strain facilitated

lymphotoxin-β receptor-mediated binding to the tumor cells and recruited lymphocytes (CD4+ and CD8+ T cells) to mediate antitumor activity. In addition to lymphocyte recruitment, the CCL21-secreting strain could also significantly elevate the levels of **proinflammatory cytokines** (CXCL9 and CXCL10) in the tumor microenvironment. The elevated cytokines stimulated neutrophil infiltration into the tumor sites to facilitate necrosis and prevent metastasis. **Interferon-gamma** (INF-γ) is another potent immunomodulator protein known to activate cytotoxic CD8+ T cells and natural killer (NK) cells to exhibit antitumor activity and prevent tumor growth. Studies have shown that direct accumulation of INF-γ and its indirect upregulation by **Interleukin-18** (IL-18) cytokine in the tumor microenvironment can mediate cellular apoptosis in melanoma and carcinoma tumor models, respectively (Loeffler et al., 2008). The IL-18-secreting eLBP could colonize both subcutaneous and pulmonary tumors, elevate the intratumoral INF-γ level, and drive chemotactic migration of cytolytic immune cells toward the tumor site. The decreased tumor growth restored the average lung weight (~0.15 gram) and reduced the overall metastasis scores compared to the control strain. Yoon and colleagues engineered the attenuated *S. typhimurium* BRD509 strain to colonize and secrete INF-γ in the mouse melanoma tumor models (Yoon et al., 2017). As anticipated, the intratumoral increase of INF-γ increased NK cell infiltration in the melanoma tumors, significantly reducing tumor volumes and drastically improving mice survival compared to the unmodified strains. These studies further highlight that *S. typhimurium* eLBPs might have the potential to be optimized for treating cancer in humans.

However, even though engineered *S. typhimurium* strains showed anticancer effects in animal models, it could not demonstrate significant efficacy as a monotherapy in human clinical trials (Liang et al., 2019). Therefore, the need for engineering alternate bacterial strains that can specifically accumulate in malignant tumors without producing systemic toxicity has risen in the past decade. The probiotic *E. coli* Nissle 1917 strain is an ideal candidate that satisfies both these requirements and has shown high efficacy towards cancer prevention in multiple studies (Chen et al., 2023). Engineered *E. coli* Nissle has been used to deliver anti-angiogenic agents, tumor blocker proteins, receptor agonists, immune checkpoint inhibitors, cytokines, and organic acids in malignant tumor models to mediate significant tumor regression. He et al. engineered *E. coli* Nissle to release a potent angiogenesis inhibitor protein, **Tumstatin** (Tum-5), in a melanoma mice model to restrict the vasculature spread in the tumor microenvironment (He et al., 2017). Regardless of

the administration route (intravenous, intraperitoneal, or intratumoral), the eLBP was able to colonize the tumor mass selectively, causing reduced vasculature and immune cell recruitment at the tumor site (**Figure 5B**). The anti-angiogenic effect displayed by the eLBP restricted nutrient availability to the tumors, leading to a drastic decrease in tumor mass without eliciting any systemic toxicity in other healthy organs. To enhance tumor suppression, *E. coli* Nissle was engineered to produce a bifunctional protein, where the **Tum-5** was fused to the **tumor-suppressor protein, p53**, using a **matrix-metalloproteinase** (MMP) cleavage site (He et al., 2019). The MMPs overexpressed in the tumor microenvironment would cleave this bifunctional protein to reduce tumor vasculature (Tum-5) and induce cellular apoptosis (p53) in hepatocellular carcinoma mice models. Regarding the tumor mass and volume reduction parameters, the bifunctional protein expressing eLBP displayed superior tumor inhibition compared to the strains expressing the Tum-5 or p53 proteins alone. Elevated levels of the apoptosis signaling biomarker **caspase-3** in the tumor mass confirmed the chemotherapeutic effect of the eLBP without any detectable *in-vivo* toxicity effect. Ji and coworkers recently demonstrated that eLBP-mediated glucose depletion in the tumor microenvironment could induce cellular apoptosis and tumor regression (Ji et al., 2023). *E. coli* MG1655 was engineered to constitutively express the heterologous **glucose dehydrogenase** (GDH) enzyme sourced from *B. subtilis* to facilitate rapid glucose consumption and reduce nutrient availability to the cancer cells. The intravenous administration of the eLBP in a colorectal carcinoma mice model showed gradual tumor colonization and glycolytic-flux alteration, inducing **cellular starvation** and **pro-death autophagic response** in the tumors. The relative tumor inhibition (RTI) ratio measured in terms of the tumor dimension was significantly high for the eLBP (~80%) compared to the control (~42%) even after 15 days post-treatment. Additional evidence highlighting the upregulation of blood coagulation factors and autophagic biomarkers confirmed the eLBP-directed antitumor effect in the resected tumors.

In addition to targeting conventional tumor inhibition pathways, researchers are developing eLBPs that release immunotherapeutic modulators targeting tumor surface receptors to activate antitumor immune responses. One prominent immunomodulation factor is **cyclic di-AMP** (CDA), a receptor agonist responsible for the specific activation of the **Stimulator of Interferon Genes** (STING) (Diner et al., 2013). Synlogic developed an *E. coli* Nissle strain (**SYNB1891**) that could produce

high titers of CDA due to the enzymatic activity of **Diadenylate cyclase** (DacA, sourced from *Listeria monocytogenes*) under hypoxic conditions in melanoma mice tumor models (**Figure 5C,** Leventhal et al., 2020). Intratumoral administration of the eLBP showed effective tumor colonization, CDA-dependent upregulation of Type I Interferons, and active phagocytosis to trigger a robust antitumor activation response. SYNB1891 significantly delayed tumor growth and increased the overall survival rate (~40%) in the treated mice compared to synthetic STING agonist administration. The preclinical success rate of SYNB1891 allowed its progression to a Phase I human clinical trial to assess its safety and antitumor response profile (Luke et al., 2023). The eLBP did not elicit any adverse side effects, showed no off-target localization, and significantly upregulated the expression of interferons, proinflammatory cytokines, and immune cells in the tumor microenvironment post intratumoral administration. However, due to financial constraints, Synlogic decided not to proceed with the Phase II clinical trial for the SYNB1891 strain.

Another popular method currently being adopted for cancer treatment involves the targeted neutralization of immune checkpoint inhibitors to facilitate tumor regression and prevent metastatic lesion development in the host by providing systemic immunity. Gurbatri and coworkers genetically engineered *E. coli* Nissle to allow the synchronized release of the neutralizing nanobodies targeting **cytotoxic T lymphocyte-associated protein-4** (CTLA-4) and **programmed cell death-ligand 1** (PD-L1) receptors in the tumor microenvironment (Gurbatri et al., 2020). The intravenous administration of the eLBP (**SLIC-2**) showed no systemic toxicity (in comparison to monoclonal antibody therapy), and the synergistic blocking of CTLA-4 and PD-L1 showed significant tumor regression, localized immune cell infiltration, and increase in memory T cell population preventing metastatic tumor growth in colorectal tumor mice models. The combinatorial release of the cytokine **granulocyte-macrophage colony-stimulating factor** (GM-CSF) stimulated the active recruitment of T cells even in immunologically "cold" tumors, highlighting the potential of the eLBP (**SLIC-3**) to target a broad range of cancer types (**Figure 5D**). The researchers further assessed whether oral administration of the chassis strain could lead to selective tumor colonization in colorectal cancer patients. qPCR analysis of resected tumor tissues confirmed the presence of *E. coli* Nissle after two weeks of treatment, providing evidence for the logical transition of the eLBP (SLIC-3) into further human clinical trials for efficacy assessment (Gurbatri et al., 2024). **Interleukin-2** (IL-2) cytokine is another key

immunomodulatory cytokine demonstrating potent antitumor activity against multiple cancer types mediated by CD8+ T cell and NK cell activation. However, IL-2 administration causes systemic toxicity in humans, making it difficult to be directly used for cancer immunotherapy. Tumas and coworkers optimized *E. coli* Nissle to sustain IL-2 secretion in cell culture media and confirmed its potential to stimulate INF-γ production in colorectal tumor spheroids and peripheral blood mononuclear cell (PBMC) cocultures (Tumas et al., 2023). Although the eLBP failed to show significant antitumor activity in colorectal tumor mice models due to compromised colonization ability, elevated IL-2 levels in the tumors were detected, confirming the therapeutic potential of such strategies.

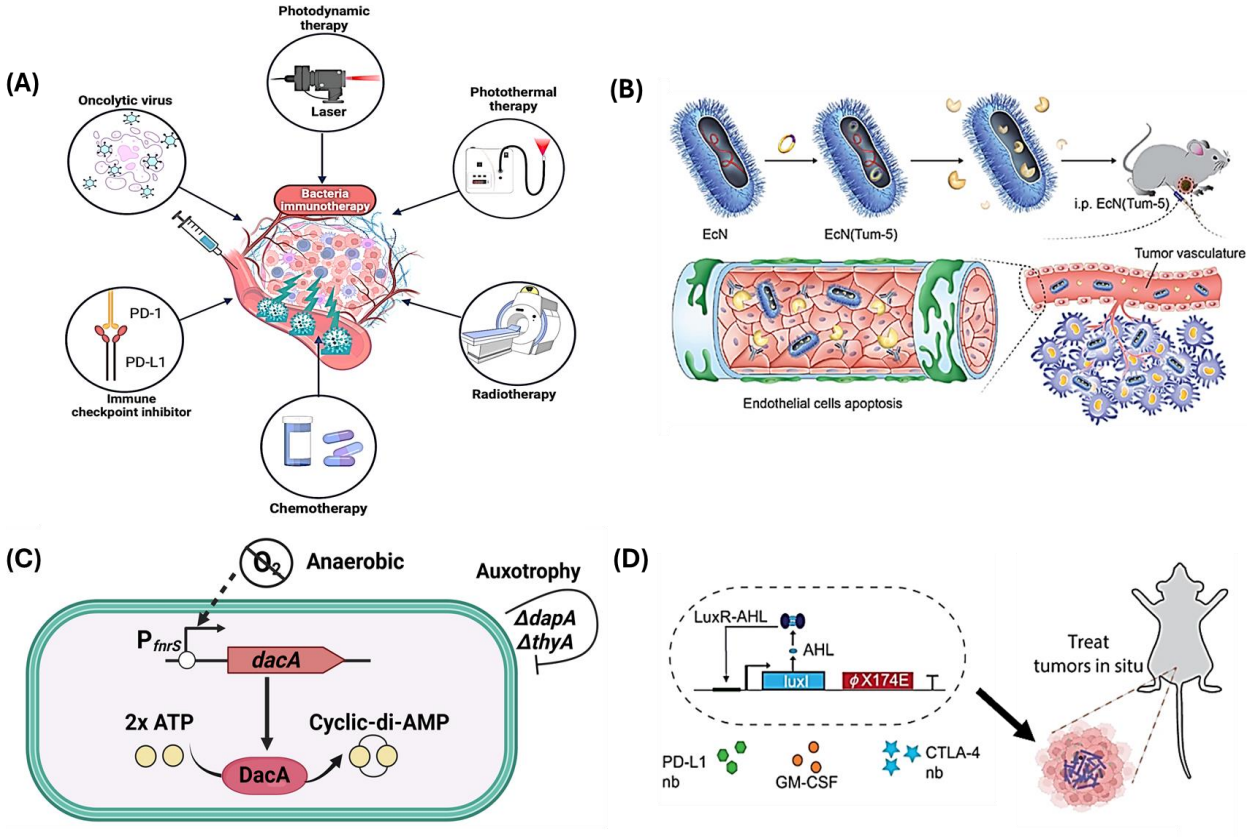

Figure 5. (A) Bacteria-based antitumor immunotherapy in combination with standard cancer treatment modules (Reprinted with permission from Zhou et al., 2023; Copyright © Frontiers Publishing Group) (B) Schematic of the tumstatin (Tum-5) secreting *E. coli* Nissle 1917 strain, that induces endothelial cell apoptosis and suppresses tumor growth (Reprinted with permission from He et al., 2017; Copyright © LLC) (C) Schematic of the anti-tumor immunity providing *E. coli* Nissle 1917 strain, SYNB1891 (Readapted from Leventhal et al., 2020; Copyright © Springer-Nature) (D) Schematic of the *E. coli* Nissle 1917 strain (SLIC-3) engineered to release GM-CSF and (PD-L1 + CTLA-4) neutralizing nanobodies post bacterial lysis at the tumor site in mice models (Reprinted and slightly modified with permission from Gurbatri et al., 2024; Copyright © Springer-Nature)

Lastly, specific metabolites like **butyrate** have shown bioactivity toward cancer treatment by activating the **mitochondrial apoptosis pathway** and arresting cell growth in the tumor microenvironment. Jen Chiang and Hong-Hong altered the metabolic pathway of *E. coli* Nissle to facilitate the conversion of **acetyl-CoA** into **butyrate** under hypoxic conditions (Chiang et al., 2021). Butyrate concentrations higher than ~5 mM downregulated the levels of the anti-apoptotic protein Bcl-2 in colorectal cancer cell lines and significantly reduced the cellular viability in *in-vitro* experiments. Intratumoral administration of the eLBP in colorectal tumor mice models showed efficient tumor colonization, significant tumor volume reduction (~70%), and enhanced rate of tumor apoptosis without eliciting systemic damage to other healthy organs. Altogether, these studies show that eLBPs can soon play an essential role in revolutionizing cancer treatment in patients.

1.2.5. Pathogenic Infections

The ever-increasing incidence of AMR in opportunistic microbes has given rise to several **Multidrug-resistant** (MDR) and **extremely drug-resistant** (XDR) pathogenic strains. In clinical environments, a shortage of effective antimicrobials to treat these infectious pathogens has significantly increased the overall patient mortality rate, becoming a grave concern for the public, medical fraternity, and health departments globally (EU Report., 2023). Predictive analysis has indicated that by the year 2050, ~10 million people will be succumbing to death due to AMR, significantly higher than the global mortality rate expected for diabetes (1.5 million) and cancer (8.2 million) (Dadgostar., 2019). In 2008, Louis Rice coined the acronym **ESKAPE** to represent the six infectious bacterial pathogens, mainly *Enterococcus faecium, Staphylococcus aureus, Klebsiella pneumoniae, Acinetobacter baumannii, Pseudomonas aeruginosa*, and *Enterobacter spp.*, that are resistant to a broad group of antibiotics and are responsible for many nosocomial infections (Rice., 2008). AMR development in these ESKAPE pathogens can be due to acquiring antibiotic resistance genes by **horizontal gene transfer** (HGT). HGT promotes active export and inactivation of antibiotics by upregulating the expression of efflux pumps and antibiotic modifying enzymes, respectively. In addition to HGT, excessive biofilm formation by the ESKAPE pathogens can reduce antibiotic accessibility to the target pathogens and, therefore, facilitate their survival. Although novel antimicrobials can bypass these pathogen resistance mechanisms, ineffective

delivery of such compounds to the infection sites can still hinder pathogen clearance and eventually lead to AMR development. Therefore, eLBPs can act as potential vectors for sustainable production and release of antimicrobial compounds at the target sites to mediate pathogen removal (**Figure 6A**).

P. aeruginosa is an **opportunistic pathogen** responsible for a significant number **of nosocomial infection-based mortality** in hospitalized patients (~2,700 deaths in the USA, 2017) (CDC Report., 2019). *P. aeruginosa* can pose a significant threat to patients, especially those suffering from burn wounds, diarrhea, and chronic lung diseases. At the same time, patients on life support systems, like ventilators and catheters, can act as ideal scaffolds for promoting **bacterial biofilm** development and facilitating *P. aeruginosa* infections. Disruption of *P. aeruginosa* biofilms on abiotic surfaces is therefore crucial to preventing the development of **ventilator-associated pneumonia** in hospitalized patients. To combat this, a human-lung bacterium, *Mycoplasma pneumoniae*, was engineered to secrete the biofilm-disrupting **glycoside hydrolase enzymes** (PelAh and PslGh), and **alginate lyase** (A1-II′), along with the **pyocin L1** that could eliminate *P. aeruginosa* PAO1 (Mazzolini et al., 2023). This engineered Mycoplasma strain (CV2_HA_P1) was able to disrupt the *P. aeruginosa*-associated biofilm in endotracheal tubes of patients receiving mechanical ventilation, restore the **synergistic activity** of routinely used antibiotics (avibactam and tazobactam) and mediate *P. aeruginosa* PAO1 based infection clearance in an *in-vivo* mouse model post-26-hour of eLBP inoculation. Apart from pyocins, eLBPs could also be engineered to produce promising alternatives like the **Siderophore antimicrobial peptides** (sAMPs) for treating bacterial infections. Mortzfeld and coworkers engineered *E. coli* Nissle to constitutively express and secrete the sAMP, **Microcin I47** (MccI47), that could significantly inhibit the growth of carbapenem-resistant (CR) *K. pneumoniae* under *in-vitro* conditions (**Figure 6B,** Mortzfeld et al., 2022). Owing to its potent *in-vitro* activity, mice infected with CR *K. pneumoniae* were then fed with the eLBP for seven consecutive days, which significantly declined the pathogenic bacterial population without affecting the native gut microbiota. sAMPs can also eradicate foodborne pathogens like *Salmonella*, which are responsible for causing **95 million** cases of non-typhoidal *Salmonella* infections globally. Poultry being the primary source of such infections, *E. coli* Nissle, engineered to secrete **Microcin J25** (MccJ25), was fed to a large cohort of turkeys previously infected with *Salmonella enteritidis* (Forkus et al., 2017). The eLBP was able to transiently colonize, secrete MccJ25, and significantly reduce the *Salmonella* bacterial load in the treated

cohort compared to the control (by ~97%). In addition to foodborne diseases, polluted water bodies are the prominent source of the pathogenic bacteria *Vibrio cholerae*, which causes **~4 million cholera** cases globally. *E. coli* Nissle was engineered to overexpress the quorum-sensing molecule **cholera autoinducer 1** (CAI-1), which, in association with the **autoinducer 2 molecule** (AI-2), could downregulate the expression of virulent genes in *V. cholerae* (Duan and March., 2010). Mice fed with the eLBP both before and with *V. cholerae* could increase the overall survival rate by 77% and 27%, respectively. The eLBP could also reduce the *V. cholerae* bacterial load in the mice intestines (69%) and inhibit cholera toxin binding to the intestinal epithelium to prevent diarrhea-related symptoms.

Although Gram-negative bacterial infections are more widespread and challenging to treat due to high cases of AMR, sufficient efforts to eliminate infections caused by several Gram-positive bacteria have also been made. One such bacterium is *Clostridioides difficile*, responsible for **severe diarrhea** and **toxin-induced colitis** that causes significant mortality worldwide (Rineh et al., 2014). In general, *C. difficile* cannot effectively colonize the gastrointestinal tract due to competition by the resident gut microbiota. However, indiscriminate usage of antibiotics can reduce the native bacterial population (**dysbiosis**) and provide a competitive advantage to *C. difficile* to proliferate and colonize the intestine (Becattini et al., 2016). To prevent this, Cubillos-Ruiz and coworkers engineered the *L. lactis* strain to synthesize a **split β-lactamase enzyme system** (spTEM1), where the enzyme subunits could reconstitute to yield a functional enzyme post extracellular secretion (Cubillos-Ruiz et al., 2022). This system would not confer any antibiotic resistance properties to the eLBP, thereby reducing the probability of HGT in the intestine. The active enzyme secreted by the eLBP could hydrolyze the intraperitoneally administered β-lactam antibiotic (200 mg/kg ampicillin for three consecutive days) and prevent antibiotic-induced gut dysbiosis in the mice models. The eLBP not only inactivated the antibiotic (ampicillin) but could also prevent *C. difficile* colonization in the gut, as demonstrated by the fecal bacterial load. *C. difficile* exotoxins, **toxin A** (TcdA), and **toxin B** (TcdB) are potent virulence factors responsible for inducing **colonic inflammation** (colitis). To counter the harmful effects of these toxins, researchers engineered probiotic Lactobacilli strains to either display neutralizing nanobodies on the cell surface or to release immunoprotective lipids. The probiotic *Lacticaseibacillus paracasei* BL23 strain was modified to surface display two different **TcdB neutralizing nanobodies** (VHH-

B2 and VHH-G3) because of their high *in-vitro* toxin binding and neutralization activity (Andersen et al., 2016). The eLBPs were orally administered (equimolar ratio) to hamsters previously colonized with the TcdB-producing *C. difficile* strain. The toxin-neutralizing effect of the nanobodies helped limit the intensity of inflammation in the colonic mucosa, delayed the disease progression in some cases, and showed a disease-protective impact on most of the tested animals. In addition to toxin neutralization, *in-vivo* delivery of immunomodulatory factors, like lipids and cytokines, have also played an essential role in mitigating *C. difficile* infection-induced colitis. *Lacticaseibacillus paracasei* was genetically modified to express the human **N-acyl-phosphatidylethanolamine-specific phospholipase D** (NAPE-PLD) enzyme, responsible for the conversion of **palmitate** (fatty acid) into a fatty acid amide, **palmitoylethanolamide** (PEA) known to have an immunoprotective role (Esposito et al., 2021). The eLBP was then orally administered to mice fed with a palmitate-rich diet one week before toxin A (TcdA) - producing *C. difficile* infection (rectal administration). The PEA-producing eLBP significantly decreased inflammatory biomarker levels, improved the mucosal integrity of the colon, and prevented the progression of TcdA-induced colitis in the treated animals compared to the control. Two other classes of MDR Gram-positive bacteria, **Vancomycin-resistant *Enterococcus*** (VRE) and **Methicillin-resistant *Staphylococcus aureus*** (MRSA) are responsible for causing severe intestinal and wound infections in patients worldwide (Amberpet et al., 2018; Thimmappa et al., 2021). Geldart and coworkers engineered *E. coli* Nissle to facilitate the simultaneous secretion of three potent antimicrobial peptides (**Enterocin A**, **Emterocin B**, and **Hiracin JM79**) that could specifically eliminate the VRE candidates, *Enterococcus faecium* 8E9 and *Enterococcus faecalis* V583R (**Figure 6C**, Geldart et al., 2018). Due to the high *in-vitro* inhibition activity of the antimicrobial peptides, male Balb/cJ mice previously colonized with VRE were fed with the eLBPs (via water intake). Post-treatment fecal matter analysis showed a significantly reduced VRE population in the mice cohort fed with the eLBP compared to the control, suggesting active elimination of VRE strains in the gut. In addition to AMR pathways, the pathogenicity of MRSA strains is significantly enhanced by their ability to form biofilms on skin wounds and medical support devices, like catheters. Guan and coworkers genetically modified a skin commensal, *Staphylococcus epidermidis*, to detect the quorum sensing autoinducer peptide (AIP) produced by the *S. aureus* bacterial community and to release the biofilm eradicating enzyme, **lysostaphin**, to mitigate MRSA strains under *in-vitro* conditions (**Figure 6D**, Guan et al., 2022). To further assess its anti-

MRSA activity, the eLBP was swabbed on the ears of germ-free C57BL6/J mice in conjunction with the pathogenic *S. aureus* strain. Although no direct correlation could be established between the eLBP activation and MRSA colonization in the mice models, the study did provide significant insights into engineering skin commensals as protective agents for MRSA eradication. *M. pneumoniae* is another interesting chassis that has recently gained traction for MRSA eradication owing to its minimal genome, lack of cell wall, and overall reduced immunogenicity. Garrido and coworkers engineered an attenuated *M. pneumoniae* strain (CV2) to simultaneously secrete the **anti-biofilm enzymes, dispersin B** and **lysostaphin**, in subcutaneously **implanted catheters** in mice (Garrido et al., 2021). The eLBP was able to efficiently disrupt the *S. aureus* biofilms and reduce the overall bacterial load of *S. aureus* in the colonized catheters, as confirmed by positron tomography (PET) imaging.

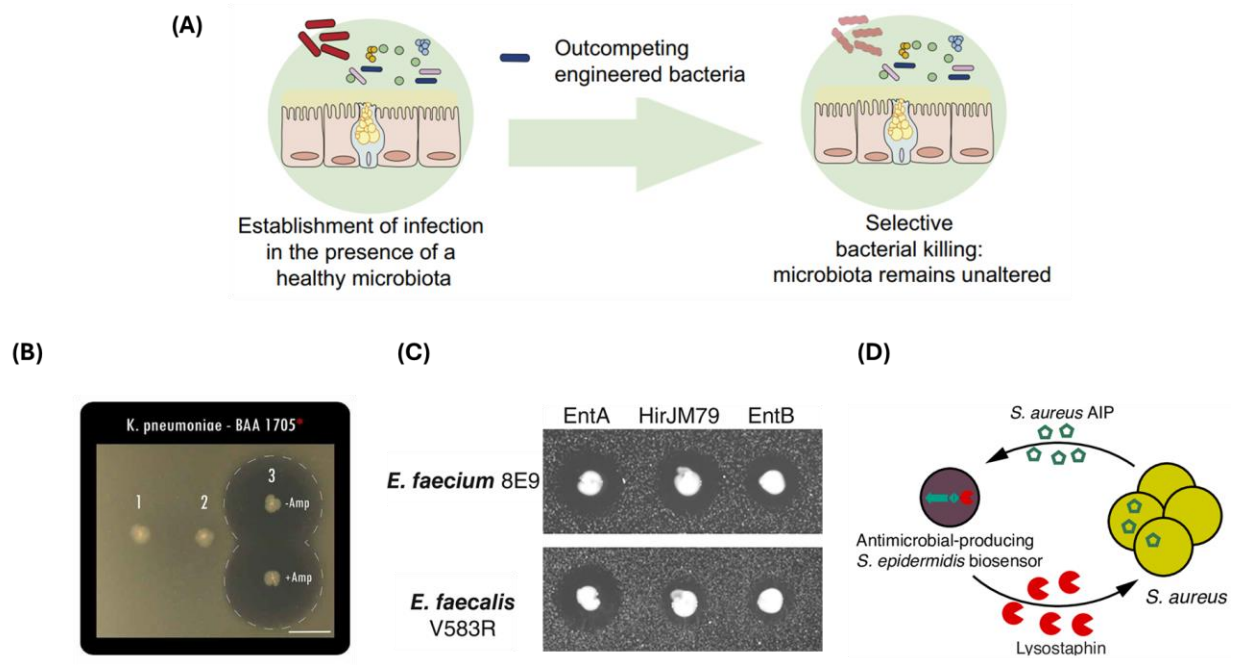

Figure 6. (A) Novel approach to facilitate selective killing of pathogenic bacteria (without disturbing the natural host microbiota) using outcompeting engineered bacteria producing potent antimicrobial compounds (Reprinted and slightly modified with permission from Becattini et al., 2016; Copyright © Elsevier Inc.) (B) Static inhibition assay comparing inhibitory activity of engineered *E. coli* Nissle 1917 strain producing Microcin I47 (MccI47) against carbapenem-resistant *Klebsiella pneumoniae* - BAA 1705, independent of ampicillin supplementation (Reprinted with permission from Mortzfeld et al., 2022; Copyright © Taylor and Francis Group) (C) Agar diffusion assay comparing inhibitory activity of engineered *E. coli* Nissle 1917 strains producing Enterocin A (EntA), Hiracin JM79 (HirJM79), and

Enterocin B (EntB) against *E. faecium* 8E9 and *E. faecalis* V583R (Reprinted and slightly modified with permission from Geldart et al., 2018; Copyright © Wiley) (D) Schematic representation of the engineered *S. epidermidis* strain that allows the production of lysostaphin in response to a quorum signaling molecule (AIP) to inhibit the growth of methicillin-resistant *Staphylococcus aureus* (MRSA) strain (Reprinted with permission from Guan et al., 2022; Copyright © PLOS)

1.3. Stimuli Responsive eLBPs

As highlighted in the previous sections, eLBPs have been used successfully for treating multiple genetic disorders and lifestyle-associated diseases. Conventional genetic engineering approaches have facilitated the eLBP mediated release of therapeutic enzymes, cytokines, growth factors, and antimicrobial agents for treating different disease conditions. However, despite several advantages, the off-target activity and insufficient drug production capability of eLBPs at the host target sites have led to the failure of multiple clinical trials (Amrofell et al., 2020). To improve upon the poor performance of several first-generation eLBPs, researchers are currently focusing on developing a new class of "**stimuli-responsive**" eLBPs. This new category of eLBPs can show responsiveness toward specific stimuli (**Figure 7**), ranging from chemical ligands (physical proximity) to externally applied light and temperature pulses (physically distant). These "**stimuli-responsive**" eLBPs can facilitate a more precise and regulated therapeutic response under both *in-vitro and in-vivo* conditions. The following section highlights examples of different categories of "**stimuli-responsive**" eLBPs that have demonstrated preclinical efficacy, sorted according to their respective induction mechanisms.

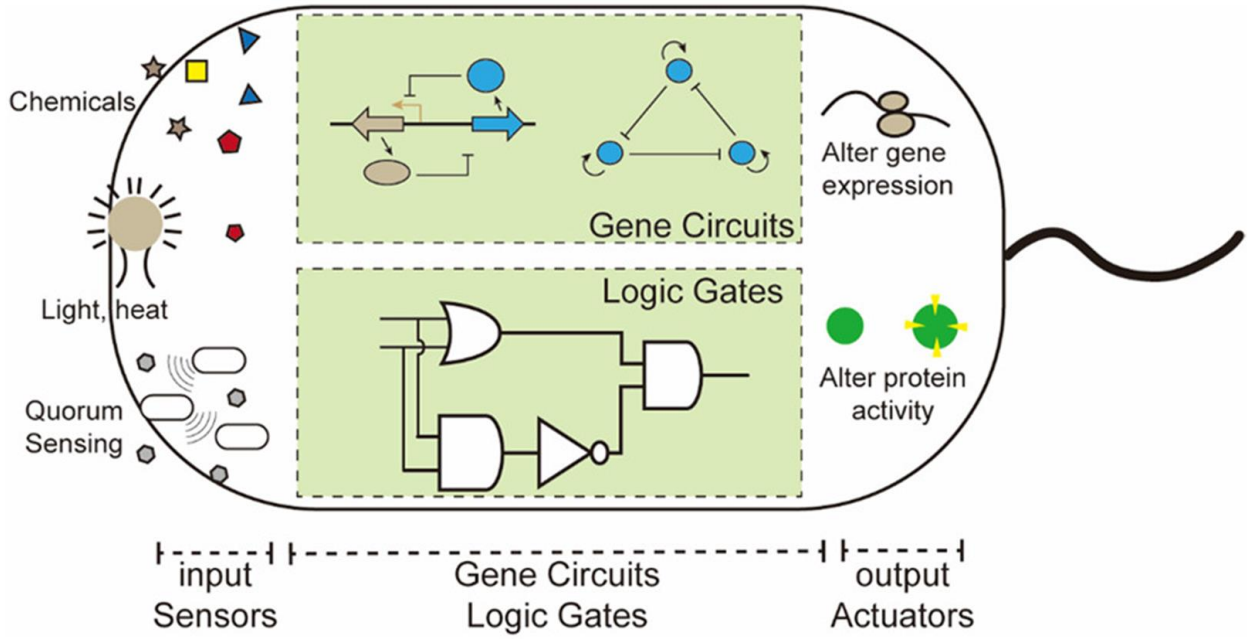

Figure 7. Stimuli-responsive eLBPs can react to specific stimuli, such as chemical ligands, quorum sensing molecules (in physical proximity), or externally applied light and temperature pulses (when physically distant). They can then modulate downstream gene expression and protein activity through multilayered genetic circuits (Reprinted with permission from Cui et al., 2021; Copyright © American Chemical Society)

1.3.1. Chemically inducible eLBPs

Chemical inducers have been essential in understanding gene expression dynamics and implementing feedback loops to build multifunctional logic gates in microbial species. Interaction of the chemical ligand with its cognate transcription factor influences its conformational stability and regulates its binding to a particular stretch of DNA known as the "**operator**" region. A large proportion of the transcription factors used in genetic circuit construction belong to the family of **repressor** proteins, which bind to "**operator**" regions and prevent the expression of the gene of interest (Browning and Busby., 2016). In the presence of the ligand, the repressor protein becomes inactive, and the derepression of the "operator" allows for active gene expression. The most prominent ligand-repressor combinations are **Isopropyl-ß-D-thiogalactopyranoside (IPTG)-lacI** and **anhydrotetracycline (aTc)-tetR** systems, which helped establish the foundational "**toggle-switch**" and "**repressilator**" circuits (Gardner et al., 2000; Elowitz and Leibler., 2000). In addition to repressors, specific transcription factors, known as **activators**, can also bind to the "operator" region only in the presence of the ligand and show positive regulation in gene

expression levels. The **arabinose-AraC** and **acyl homoserine lactone (AHL)-luxR** systems are the most prominent ligand-activator combinations (Cui et al., 2021). The ligand-specificity and orthogonal response regulation of chemically inducible genetic circuits make them suitable for developing "**stimuli-responsive**" eLBPs. Recent studies have shown that chemically inducible eLBPs allow disease alleviation by regulated release of therapeutic macromolecules (nucleic acids and proteins) in the host environment.

Gao and Sun demonstrated that chemical inducer-regulated RNA production by *E. coli* could silence gene expression and mediate physiology modulation in a *Caenorhabditis elegans* model (**Figure 8A,** Gao and Sun., 2021). The authors developed an IPTG inducible system for delivering single-stranded RNA (ssRNA) targeting green fluorescent protein (GFP) expression within *C. elegans*. The efficiency of gene silencing was maximized by tuning the dynamic range of the genetic circuit based on both inducer concentration and ssRNA length. To incorporate a multi-variable response, an eLBP-based "**OR**" and "**AND**" logic gate was constructed to regulate the "**twitching**" phenotype and **fat storage** within *C. elegans* in response to **arabinose** and **aTc**. The activation of the genetic circuits led to significant "twitching" activation and fat storage reduction across the treated *C. elegans* model, with a success rate of 100% and 60%, respectively. Hwang and coworkers further engineered *E. coli* Nissle to detect the *P. aeruginosa* specific quorum sensing molecule **N-acyl homoserine lactone** (AHL) and release antimicrobial agents to tackle the infection-causing bacteria. Upon AHL induction, the eLBP could undergo self-lysis to release the enzyme **dispersin B** (DspB) to disrupt the bacterial biofilm and increase accessibility for the *P. aeruginosa* specific toxin, **pyocin S5**, for ensuring pathogen clearance (**Figure 8B,** Hwang et al., 2017). The eLBP detected pre-established *P. aeruginosa* infections in the gut of *Caenorhabditis elegans* and mice and significantly reduced the pathogenic bacterial load without generating any adverse side effects. Besides standard inducers, disease-related biomarkers can also regulate genetic circuits of "**stimuli-responsive**" eLBPs under *in-vivo* conditions. Koh and coworkers engineered *E. coli* Nissle to show responsiveness towards **sialic acid** (a marker for gut dysbiosis) and activate intracellular expression of the **bile salt hydrolase** (Cbh) enzyme, sourced from *Clostridium perfringens* (Koh et al., 2022*).* Recombinant Cbh facilitated deconjugation of the bile salts, **taurocholate** and **glycocholate** into **cholate**, allowing active **inhibition of endospore germination**, decreased viability of vegetative cells, and reduced toxin production by

the pathogenic *C. difficile* strain in *in-vitro* assays. To assess its *in-vivo* efficiency, the eLBP was orally administered to mice, followed by the virulent *C. difficile* VPI10463 strain, with the disease progression measured over nine days. The treatment showed reduced *C. difficile* burden (confirmed by 16S RNA metagenomic sequencing), alleviated colonic inflammation and tissue damage, and significantly increased the mice survival rate (100%) compared to the control group. Fecal matter analysis revealed that in the initial days of infection, sialic acid levels increased, followed by elevated levels of cholate and reduced levels of taurocholate and glycocholate in the eLBP-fed mice. The results highlighted the critical role of chemical signals in controlling and boosting the overall therapeutic response of eLBPs.

Recent studies have demonstrated that chemical inducers can potentially increase the antitumoral response and tumor-specificity of eLBPs in the tumor microenvironment. Chiang and Huang deleted the **arabinose metabolism** and **glucose-mediated catabolite repression** pathways in *E. coli* Nissle to facilitate the rapid, sensitive, arabinose-induced expression of the cytotoxic **hemolysin E** (HlyE) protein (Chiang and Huang., 2021). HlyE demonstrated an apoptotic response towards tumor cells, significantly reducing their cellular viability in *in-vitro* assays. Intratumoral and intraperitoneal administration of the eLBP and **arabinose-spiked** drinking water achieved significant tumor necrosis and volume reduction in colorectal cancer mice models without eliciting systemic toxicity. Harimoto and coworkers devised an unique strategy to enhance tumor-directed eLBP delivery by mediating transient regulation over the **capsular polysaccharide** formation in Δ*kfic E. coli* Nissle strain (**Figure 8C,** Harimoto et al., 2022). The *kfic* gene (responsible for heparosan production) expression was regulated by the IPTG-lacI repressor system, where IPTG induction led to increased bacterial capsular thickness to facilitate immune evasion and increased viability in human whole blood samples. Higher capsular polysaccharide expression enhanced bacterial tolerance at high dosages and showed better bioavailability across **distal tumors** in colorectal cancer mice models. After IPTG withdrawal, *kfic* gene expression dropped significantly, decreasing capsular synthesis, facilitating immune clearance, and preventing long-term bacterial persistence. The eLBP was further modified to release the antitumoral **theta toxin** (TT) protein in response to AHL after tumor colonization, leading to a drastic decrease in tumor volume compared to the control. Chowdhury and coworkers established another acylhomoserine lactone (AHL) based self-lysis circuit in *E. coli* Nissle to facilitate the cumulative release of the antagonist (nanobody) of the **CD47 anti-phagocytic receptor** in tumor models (Chowdhury et al., 2019).

Post intratumoral administration of the eLBP, the nanobody triggered tumor cell phagocytosis to allow significant tumor regression. The eLBP also mediated an antitumor T cell priming response to facilitate the regression of untreated tumors in the mice model, which was not observed with the monoclonal antibody therapy alone.

Researchers are also actively investigating alternate inducible systems that can autonomously sense tumor-specific biomarkers and initiate a therapeutic response towards them. Zhou and coworkers recently developed three independent *E. coli* Nissle strains that showed responsiveness to lactate, acidic pH, and hypoxic conditions within the tumor microenvironment (Zhou et al., 2024). The strains further encoded for the **serine integrase protein** (TP901) regulating the XOR switch to allow **autolysis** (**φX174E lysis protein**) and subsequent release of HlyE for mediating antitumoral response in subcutaneous tumors in mice models. Intratumoral administration of the eLBPs showed significant tumor regression without decreasing the overall body weight compared to the strains constitutively expressing HlyE (~90%). A synthetic bacterial consortium (**SynCon3**) of all these three strains was then orally administered to colitis-induced colorectal cancer mice models to assess its *in-vivo* efficacy (**Figure 8D**). **SynCon3** reduced the number and volume of colon polypoid tumors by inducing tumor apoptosis, significantly improved the intestinal barrier integrity, and increased the overall colon length compared to the control. **SynCon3** also helped restore the gut microbiota, with significant changes in the population of *Lachnospiraceae* (increase) and *Bacteroides* (decrease) species, which are known to have negative and positive associations with colorectal cancer progression, respectively. Although these studies demonstrate the therapeutic potential of chemically induced eLBPs, further research is needed to evaluate their suitability for human clinical trials.

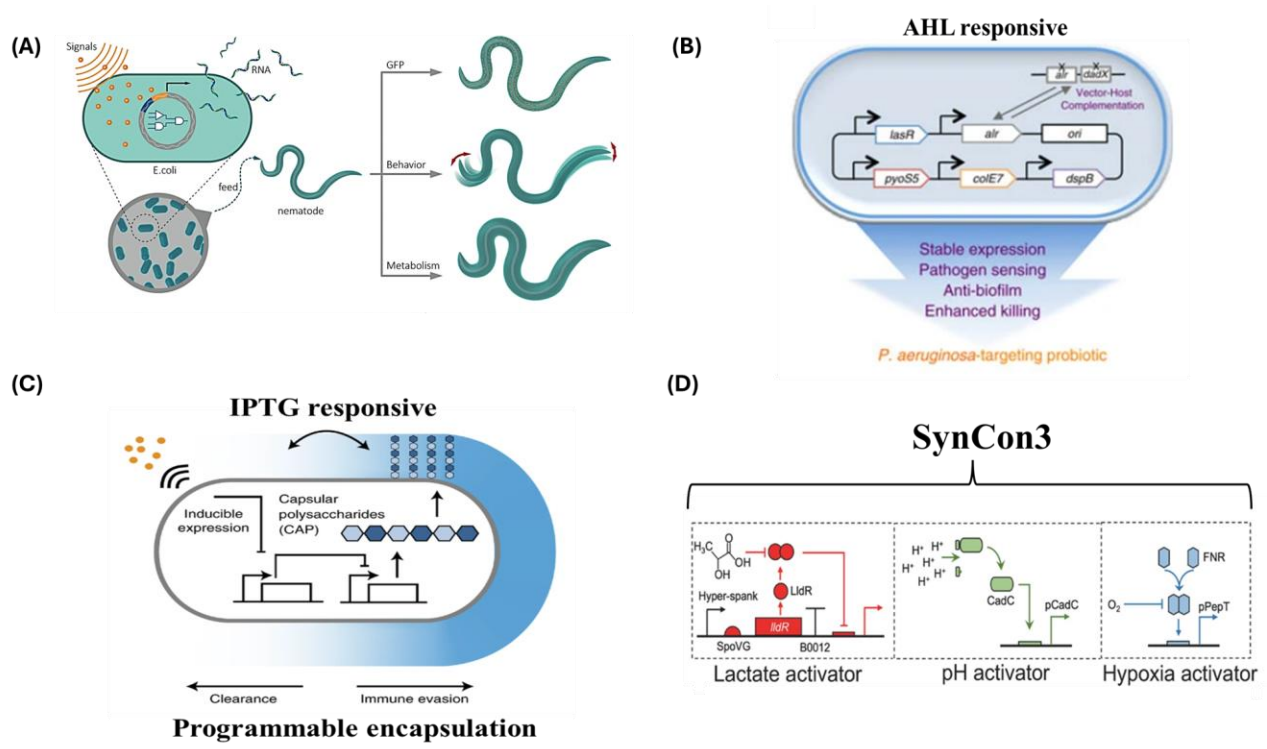

Figure 8. (A) Chemical inducer-regulated RNA expression in *E. coli* enables the control of protein expression (GFP) and phenotypic changes such as fat storage and twitching behavior in *C. elegans* (Reprinted with permission from Gao and Sun., 2021; Copyright © Springer-Nature) (B) Schematic representation of the AHL-responsive *E. coli* Nissle 1917 strain, enabling the production of S5 pyocin and Dispersin B to exert inhibitory and anti-biofilm effects against the opportunistic pathogenic strain of *P. aeruginosa* PAO1 (Reprinted and slightly modified with permission from Hwang et al., 2017; Copyright © Springer-Nature) (C) Schematic representation of the IPTG-inducible *E. coli* Nissle 1917 strain, enabling tunable and dynamic modulation of the capsular polysaccharide layer to facilitate immune evasion and clearance in the host system (Reprinted and slightly modified with permission from Harimoto et al., 2022; Copyright © Springer-Nature) (D) Schematic representation of *E. coli* Nissle 1917 strain-based bacterial consortia (SynCon3) engineered to sense lactate, pH, and hypoxic conditions unique to tumor microenvironments. Once activated, these bacteria release the therapeutic payload in the tumor microenvironment, thus promoting tumor regression. (Reprinted and slightly modified with permission from Zhou et al., 2024; Copyright © Springer-Nature)

1.3.2. Optogenetically inducible eLBPs

The ability to use light as an external trigger to control a biological process through cognate genetic parts is termed "**optogenetics**". The field gained immense momentum because it allowed researchers to better understand the biological functions of complex cells like **neurons** and **cardiomyocytes** (Entcheva and Kay., 2021). However, the spatiotemporal control mediated by light made it an exciting choice for developing "**light-responsive**" genetic circuits within the

microbial chassis (Hoffman et al., 2022). Levskaya and coworkers demonstrated for the first time that gene expression could be regulated in *E. coli* by light application (Levskaya et al., 2005). They created a two-component system based on the **cyanobacterial phytochrome** (Cph) – **histidine kinase** (EnvZ) fusion protein complex that prevented β-galactosidase (LacZ) gene expression in the presence of **red light**. Inspired by the results, the authors modified the optogenetic circuit to render responsiveness to a multichromatic optical spectrum (red and green light) for controlling LacZ gene expression (Tabor et al., 2011). The orthogonal nature of the Cph-EnvZ protein complex and the CcaS histidine kinase-CcaR response regulator combination facilitated reversible activation of the reporter gene in the presence of **red light** and **green light,** respectively. However, these light-activated systems (red and green light) showed high basal level expression and a low dynamic range post-light activation.

Therefore, further investigation towards creating alternative optogenetically activated genetic circuits in microbial species was necessary. Ohlendorf and coworkers combined the photosensory **Light-Oxygen-Voltage** (LOV) module with the **YF1 histidine kinase - FixJ response regulator** domains to construct two modular, blue-light responsive plasmids, **pDusk** and **pDawn** (Ohlendorf et al., 2012). pDusk and pDawn allowed fluorescent protein (dsRed) production within *E. coli* in the absence and presence of blue light, respectively. Compared to the previous systems, these genetic circuits showed minimal basal level expression and displayed a high dynamic range, especially for the pDawn system (~460 fold, **Figure 9A**).

Cui and coworkers developed a pDawn circuit-based *E. coli* Nissle strain modified to release mIL-10 in the intestinal tract of DSS-induced colitis mice models (Cui et al., 2021). The eLBP and **upconversion rods** (UCRs) were encapsulated in **calcium alginate-chitosan scaffolds** to create **upconversion microgels** (UCMs) that would disintegrate and release the eLBP-UCR mixture in the gut lumen. The UCRs then converted the externally applied **near-infrared light** (NIR) to **blue light** (475 nm), activating the pDawn-mediated mIL-10 release in the inflamed colon of colitis mice. This therapeutic intervention significantly reduced neutrophil infiltration and proinflammatory cytokine levels in the gut and increased intestinal epithelium integrity compared to the control group. The authors also demonstrated that the pDawn circuit could show light-responsive gene expression in other microbes, like *L. lactis* (Cui et al., 2023). They incorporated

the pDawn-regulated mIL-10 (fused to a renal-targeting peptide) secreting plasmid in *L. lactis* and encapsulated the eLBP in calcium alginate-chitosan-based microparticles (without UCRs). The microparticles protected the bacteria from the harsh gastric environment and disintegrated in the intestine to facilitate eLBP release. The released eLBP was activated using a wearable optical device (emitting blue light pulses) to secrete mIL-10, and the renal-targeting peptide moiety allowed its accumulation within the kidneys of mice suffering from renal fibrosis. Histopathological analysis confirmed that the treatment reduced inflammatory cell infiltration and proinflammatory cytokine levels in the renal tubules, thus causing significant alleviation of renal fibrosis-associated symptoms.

However, the low tissue penetrability of blue light could lead to insufficient eLBP activation and render a sub-optimal therapeutic response in the host. Wu and coworkers developed **NIR-activated upconversion nanoparticles** (UCNPs) to absorb and convert the incident NIR light into blue light to tackle this issue (Wu et al., 2022). The blue light would then activate the pDawn circuit in *L. lactis* to facilitate the **INF-γ** secretion and enable metastatic tumor regression (**Figure 9B**). The eLBP and UCNPs were encapsulated in an alginate-chitosan scaffold and orally administered to melanoma tumor mice models. Upon reaching the intestine (4 hours), the mice were irradiated with NIR to activate the eLBP and allow the secreted INF-γ to diffuse from the pH-responsive hydrogel (pore formation triggered by intestinal pH). The strategy realized a significant reduction in distal tumor growth, upregulation in immune markers, and systemic prevention of tumor development in metastasis-prone organs (lungs and liver) in the treated mice compared to the control group. This evidence highlighted that eLBPs could systemically elicit therapeutic benefits, utilizing their passage through the gut as a transient drug release source. Pan and coworkers further demonstrated that the eLBPs could exploit the gut-brain axis to prevent psychological stress and neurodegenerative disease progression (Pan et al., 2022). At first, the authors encapsulated pDawn-mediated **gamma-aminobutyric acid** (GABA) secreting *L. lactis* and UCNPs in **proton-dependent transporter 1** (PepT1) antibody-tagged chitosan microgels for small intestine targeted eLBP release. Once released, UCNP-mediated NIR to blue light conversion facilitated GABA secretion and increased bioabsorption in the intestinal tract (**Figure 9C**). Post NIR illumination (60 minutes), the treated and control mice groups were subjected to the **elevated plus maze** (EPM) and **open field test** (OPT) to assess their anxiety behavior. The

eLBPs significantly relieved anxiety behavior and reduced the proinflammatory cytokine levels (IL-6 and TNF-alpha) in the treated mice compared to the control. Next, the authors used a similar design to facilitate the light-responsive release of the neuroprotective protein, **granulocyte-colony stimulating factor** (GCSF), within the gut to prevent PD progression (**Figure 9C**). PD model mice were fed with eLBP-loaded microgels for ten days, followed by NIR light illumination for another seven days before assessing their spatial cognitive ability using the Y-maze test. The treated mice showed better spatial cognition, decreased neuroinflammatory markers, and upregulation in the **protein kinase C alpha** (*Prkca*) level correlated to the neuronal survival pathway. Lastly, the authors designed a light-activated GLP-1 secreting *L. lactis* strain to demonstrate that eLBPs could regulate stimulatory activation of the vagal nerve via the gut (**Figure 9C**). Electrophysiological analysis of the treated mice post NIR illumination showed increased spike frequency, highlighting increased neuronal activity compared to the control.

However, efforts are underway to develop genetic circuits that are directly responsive to red light, thus avoiding the incorporation of UCNPs. Although no NIR-light-activated *L. lactis* strain has been reported yet, Zhang and coworkers successfully constructed an *E. coli* Nissle strain to undergo **red-light-activated autolysis** and **therapeutic drug release** under *in-vivo* conditions (Zhang et al., 2023). Post-red-light illumination, the Cph-EnvZ photoresponsive module activated the lysis protein (ΦX174E) production, allowing the release of **Exendin-4** (constitutively produced) (**Figure 9D**). Alginate microspheres let the targeted release of the encapsulated eLBPs in the alkaline intestinal environment. To assess whether the red-light-activated Exendin-4 release could exhibit neuroprotective effects, the authors orally administered the eLBP-loaded microspheres to PD model mice. The treated mice showed reduced movement disorder (pole test), improved spatial memory (Y-maze), significant dopaminergic neuron recovery, and reduced neuronal inflammation compared to the control (**Figure 9D**). The lab that developed the pDawn system, further demonstrated that exchanging the LOV photosensory module with the **Bacteriophytochrome** (Bphp) sourced from *Deinococcus radiodurans* could switch the responsiveness of the genetic circuits towards red light (Multamäki et al., 2022). The superior tissue penetrability of red light and the high dynamic range of the **pREDusk** and **pREDawn** plasmids could provide significant advantages for developing enhanced "light-responsive" eLBP

candidates. These studies therefore highlight that optogenetically regulated eLBPs could be optimized for developing suitable disease intervention strategies.

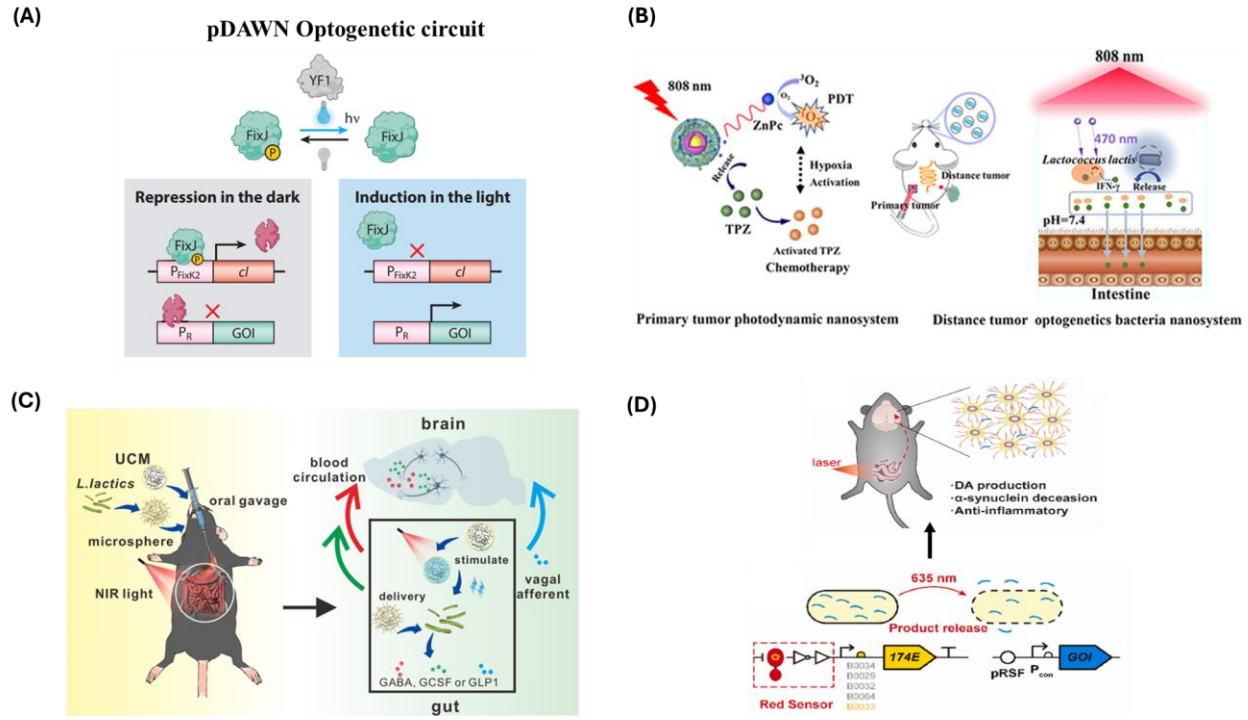

Figure 9. (A) Schematic representation of the blue-light activated pDawn optogenetic circuit. The two-component system (TCS) uses a light-responsive kinase (YF1) and response regulator (FixJ) to express another transcriptional regulator (cI), that regulates the expression of the gene of interest (GOI) (Reprinted and slightly modified with permission from Hoffman et al., 2022; Copyright © Annual Reviews) (B) Schematic representation of a two-step synergistic method for treating cancer. The first step involves using photodynamic therapy to generate reactive oxygen species (ROS) in primary tumors. The second step consists of converting near-infrared (NIR) light into blue light using upconversion nanoparticles (UCNPs) to activate the release of INF-γ from *L. lactis* in the intestine, thereby inhibiting the growth of secondary tumors (Reprinted with permission from Wu et al., 2022; Copyright © American Chemical Society) (C) Schematic representation of three *L. lactis* strains that respond to blue light (converted from incident NIR light by UCNPs) to regulate the production of GABA, GCSF, and GLP-1. These substances help alleviate anxiety, treat Parkinson's disease, and act as a vagal afferent, respectively, by utilizing the gut-brain axis route (Reprinted with permission from Pan et al., 2022; ; Copyright © American Chemical Society) (D) Schematic representation of the *E. coli* Nissle 1917 strain engineered to release Exendin-4 upon bacterial autolysis, aiding in dopaminergic neuron recovery and reducing neuronal inflammation in response to red light induction (Reprinted with permission from Zhang et al., 2023; Copyright © Elsevier Inc.)

1.3.3. Thermally inducible eLBPs

The ability to use temperature changes to regulate biological processes through genetic circuits is called **thermogenetics**. In line with optogenetics, thermogenetics development allowed

researchers to elucidate neurological processes in **poikilothermal** model organisms like *Drosophila melanogaster* (Bernstein et al., 2012). Although thermal stimulation lacks the temporal resolution provided by optogenetics, the ambient temperature modulation approach could achieve homogeneous activation of biological activity control in the poikilothermal model organism (Hamada et al., 2008). Unlike poikilotherms, **higher-order animals**, including humans, can regulate their body temperature irrespective of the ambient temperature through **homeostasis** (Benzinger., 1969; Gomes da Silva et al., 2013). The hypothalamic region of the brain controls thermal homeostasis by the neuronal feedback loops and ensures the organism's survival. However, the core body temperature can significantly increase in cases like **fever**, **hyperpyrexia**, and **hyperthermia** in response to infection and excessive heat exposure. Although prolonged temperature elevation is unfavorable for the host, it can effectively regulate the activation of "**temperature-responsive**" genetic circuits encoded within the microbial chassis. Earlier studies have reported that transcription factors, like the **lacIts** and **cI857** repressors (created by site-directed mutagenesis of lacI and cI repressor), could undergo temperature-dependent conformational changes to regulate reporter gene expression (Chao et al., 2002; Villaverde et al., 1993). In addition, certain promoter elements in microbes could significantly upregulate their transcriptional rate under thermal stress. Recombinant expression of fluorescent reporter proteins encoded under these heat shock promoters occurring specifically at higher incubation temperatures highlighted their temperature-dependent activity (Rodrigues et al., 2014). However, these genetic tools generally have poor fold change and high transition temperature requirements, restricting their use in eLBP development. In search of suitable thermoresponsive genetic elements, Piraner and colleagues compared the temperature-dependent gene expression strength of several transcription factors and heat shock promoters in *E. coli* (Piraner et al., 2017). The authors observed that the transcriptional repressors, **cI857** (sourced initially from bacteriophage λ) and **TlpA** (sourced from *S. typhimurium*), showed low basal level activity, orthogonal activation, and higher gene expression levels at 40° and 45°C respectively. Inspired by their robust performance, the authors created several variants of the repressors (by error-prone mutation) to develop genetic switches that could be explicitly activated beyond certain temperature thresholds. Several repressors, like the **TlpA$_{36}$**, **TlpA$_{39}$**, and **TcI$_{42}$**, were constructed, which repressed reporter gene expression (**"OFF" state**) below the threshold temperatures of 36°C, 39°C, and 42°C respectively. Beyond their respective temperature thresholds, the conformational stability of the repressors

decreased significantly, thus allowing the reporter gene expression to occur **("ON" state**). Apart from their efficient *in-vitro* activity, the authors also assessed the performance of these genetic switches under *in-vivo* conditions. For this, the authors subcutaneously injected the engineered bacteria in the flank (hindlimbs) of nude mice models and subjected them to both Magnetic Resonance Imaging (MRI) - guided focused ultrasound exposure (45 minutes) and hyperthermic incubation (2 hours) conditions. Both methods activated the bacterial genetic circuits and allowed significant fluorescence production at the target site. The spatial activation of the genetic switches within the host environment confirmed their robust ability to develop "**temperature-responsive**" eLBPs.

As highlighted in the previous sections, achieving malignant tumor remission has been the key focus of researchers and clinicians in developing a cancer treatment regimen. Modern adjuvant methods like photothermal therapy and hyperthermia have significantly benefited cancer treatment in synergy with conventional therapeutic strategies (Chang et al., 2021). In both techniques, localized heat application elevates the tumor temperature and induces cellular apoptosis without affecting the surrounding healthy tissues. The protocols can use **focused ultrasound** (FUS) or **magnetic fields** and **NIR light** (in conjunction with metallic nanoparticles) to deliver heat at the target site effectively. Abedi and colleagues demonstrated that heat application could further activate thermoresponsive eLBPs within the tumor microenvironment to elicit an antitumoral response (**Figure 10A,** Abedi et al., 2022). At first, the authors constructed an *E. coli* Nissle-based thermally activated circuit (>42 °C, TcI42) to control the expression of the **serine integrase** (Bxb1) responsible for the inversion of the attP/attB DNA recognition elements. Post-temperature-induced gene inversion, the eLBP facilitated the constitutive production and secretion of the immune checkpoint inhibitors, **αCTLA-4** and **αPD-L1** nanobodies, into the extracellular environment. The intravenous administration of the eLBPs (1:1) into tumor-bearing mice models allowed their effective colonization within two days, followed by FUS pulse application at the tumor sites (1-hour exposure). An elevated tumor core temperature (43 °C) triggered sustained nanobody secretion for two weeks, leading to significantly decreased tumor volume and reduced systemic toxicity compared to the non-activated controls. However, immune cell-mediated bacterial clearance can reduce the overall therapeutic efficacy, requiring a higher eLBP dosage administration. Li and colleagues addressed this issue by surface coating the bacteria (*E. coli* Nissle) with chitosan (2 mg/mL) before intravenous administration to 4T1 tumor-bearing mice

models (Li et al., 2022). The chitosan-coated bacteria showed reduced clearance, decreased immune cell activation during systemic circulation, and better tumor colonization than the uncoated control. The authors then constructed a cI857 repressor-regulated genetic circuit in *E. coli* Nissle to facilitate **TNF-alpha** secretion only at elevated temperatures (42 °C, **Figure 10B**). The chitosan-coated thermoresponsive eLBPs colonized the tumor microenvironment (3 days since intravenous injection), followed by heat induction (thermal heating pad, 30 minutes exposure) at regular intervals (every three days) till the 11th day. The mice safely tolerated the treatment regimen, which resulted in significant reduction of the tumor volume compared to the uninduced controls (**Figure 10B**). Chen and coworkers developed an *E. coli* MG1655-based eLBP where the cI857 repressor inhibited the production of **INF-γ** at physiological temperature (37 °C) and triggered its release specifically at elevated temperature (45 °C) (**Figure 10C**, Chen et al., 2022). Systematic characterization of FUS parameters revealed that an acoustic pressure of 4.93 MPa sustained the hyperthermic temperature (45°C) for prolonged periods under both *in-vitro* and *in-vivo* conditions. Intravenous administration of the non-viable (dead) eLBP showed higher localization in the liver and spleen, in contrast to the viable (live) eLBP, which preferentially colonized the tumors of mice models (4T1). FUS pulse-mediated hyperthermia further activated the genetic circuit to release INF-γ within the tumor microenvironment, leading to reduced tumor volume (<250 mm^3), increased tumor apoptosis, and a longer survival rate than the controls. The FUS pulse-based eLBP activation triggered lung tumor regression in mice models, highlighting its capability to eliminate even deep-seated tumors within the host. The treatment regimen also allowed systemic upregulation of the host **memory (CD4+)** and **cytotoxic (CD8+)** T-cell population, significantly inhibiting metastasis and distal tumor growth.

In addition to FUS application, **photothermal therapy** and **magnetic hyperthermia** can elevate core tumor temperature to activate thermoresponsive eLBPs to elicit an antitumoral response. However, unlike FUS, these strategies require additional synergistic components, like gold nanoparticles (photothermal therapy) and magnetite nanoparticles (magnetic hyperthermia). Fan and colleagues demonstrated that bacterial nitrate reductase could reduce $\mathbf{Au^{3+}}$ (gold ions) to $\mathbf{Au^{0}}$ (metallic gold) and allow its deposition on the bacterial surface (Fan et al., 2018). The authors utilized this strategy to deposit gold nanoparticles on the cI857 repressor-regulated, TNF-alpha-secreting *E. coli* MG1655 strain to develop photothermic eLBPs. Post-oral administration, the photothermic eLBPs demonstrated superior stability in the gastrointestinal tract, negligible

systemic toxicity, and eventual tumor colonization in mice models. **Localized NIR-laser exposure** (808 nm, 24 hours) increased the core tumor temperature (42°C), triggering TNF-alpha release and stimulating INF-γ production within the tumor microenvironment. The elevated proinflammatory cytokine levels drove significant cellular apoptosis and tumor volume reduction (>200 mm^3) in the treated mice compared to the control. Ma and coworkers have discovered a way to control the activation of thermoresponsive eLBP in tumors using magnetic hyperthermia (**Figure 10D**, Ma et al., 2023). They achieved this through two methods: Firstly, they expressed **Histone-like protein A** (HlpA) on the *E. coli* BL21 strain, which allowed them to bind to the **heparan sulfate proteoglycans** (HSPG) of colon tumors. Secondly, via a site-specific labeling technique, they decorated the eLBP lipid bilayer with **magnetite** (Fe_3O_4) lipid nanocomposites linked to **dibenzocyclooctyne** (-DBCO). Post administration, the HlpA domain of the eLBP allowed it to colonize within the CT-26 tumor model in mice. In addition, when exposed to an **alternating magnetic field** (AMF), the surface-bound magnetite nanoparticles could mediate a magnetic-to-heat signal conversion and increase the core tumor temperature to 42°C. The elevated temperature would derepress the cI857-regulated lysis protein production, leading to bacterial lysis and release of the CD47 targeting nanobody within the tumors. The combination of bacterial lysates and **CD47 blockade** synergistically increased immune cell populations (M1 macrophages, neutrophils, and natural killer cells) in the tumor microenvironment, significantly reducing tumor volume and increasing mice survival rate (**Figure 10D**). The treatment increased plasma cytokine levels (IFN-γ, IFN-α1, TNF-alpha, and IL-6) and CD8+ T cell population in mice, thereby enhancing systemic immunity against metastatic tumor development (**Figure 10D**). These studies demonstrate that localized hyperthermia effectively regulates drug release from thermoresponsive eLBP, improving tumor elimination *in-vivo*.

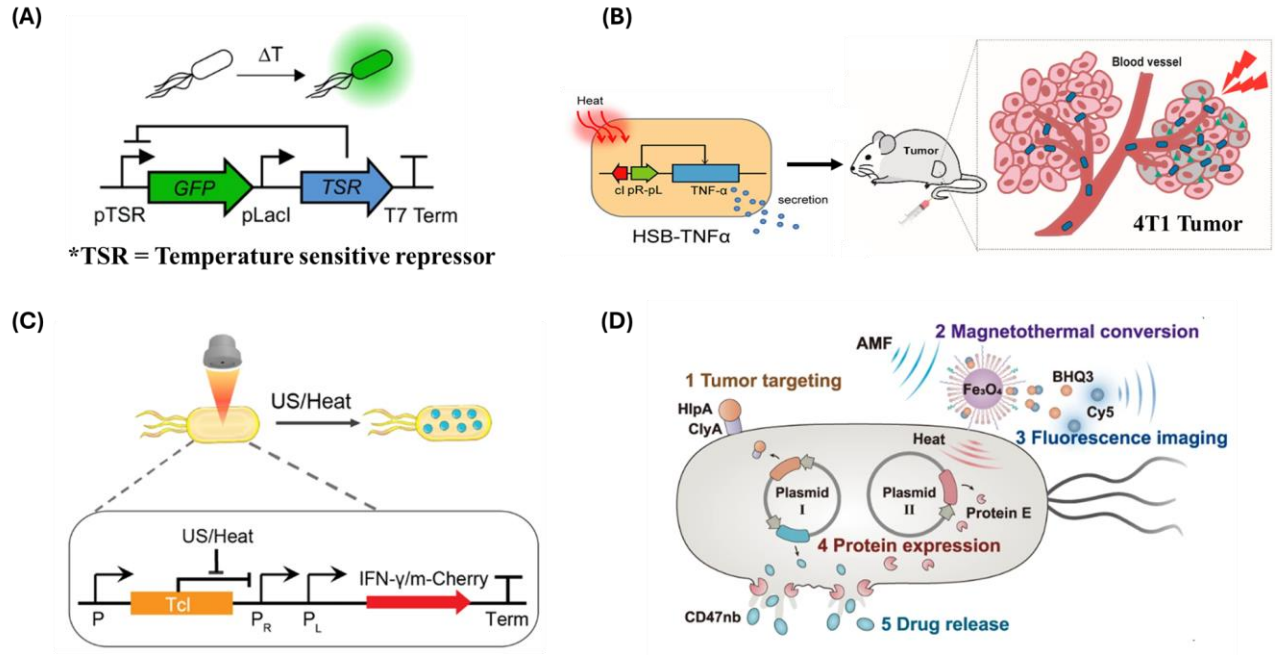

Figure 10. (A) Schematic representation of the temperature-regulated expression of the gene of interest (GOI, shown here as GFP), controlled by the temperature-sensitive repressor (TSR) in the *E. coli* Nissle 1917 strain (Reprinted and slightly modified with permission from Abedi et al., 2022; Copyright © Springer-Nature) (B) Schematic representation of temperature-regulated expression and secretion of TNF-alpha from the *E. coli* Nissle 1917 strain leads to regression of 4T1 tumors in mouse models (Reprinted and slightly modified with permission from Li et al., 2022; Copyright © American Chemical Society) (C) Schematic representation of temperature-regulated mCherry/IFN-γ expression from the *E. coli* Nissle 1917 strain prevents tumor growth and metastasis in mouse models (Reprinted with permission from Chen et al., 2022; Copyright © Springer-Nature) (D) Schematic representation of magnetic hyperthermia-based temperature elevation in the tumor core to activate *E. coli* Nissle 1917 strain engineered to release CD47-targeting nanobody post bacterial autolysis, facilitating tumor regression and preventing metastatic spread of cancer in mouse models (Reprinted and slightly modified with permission from Ma et al., 2023; ; Copyright © Springer-Nature)

1.4. References

1. Achan, J., Talisuna, A.O., Erhart, A., Yeka, A., Tibenderana, J.K., Baliraine, F.N., Rosenthal, P.J. and D'Alessandro, U., 2011. Quinine, an old anti-malarial drug in a modern world: role in the treatment of malaria. *Malaria journal*, *10*(1), pp.1-12.
2. Prescott, L.F., 2000. Paracetamol: past, present, and future. *American journal of therapeutics*, *7*(2), pp.143-148.
3. Southey, M.W. and Brunavs, M., 2023. Introduction to small molecule drug discovery and preclinical development. *Frontiers in Drug Discovery*, *3*, p.1314077.
4. Thorburn, A.N., Macia, L. and Mackay, C.R., 2014. Diet, metabolites, and "western-lifestyle" inflammatory diseases. *Immunity*, *40*(6), pp.833-842.

5. Makurvet, F.D., 2021. Biologics vs. small molecules: Drug costs and patient access. *Medicine in Drug Discovery*, *9*, p.100075.
6. Singh, N., Vayer, P., Tanwar, S., Poyet, J.L., Tsaioun, K. and Villoutreix, B.O., 2023. Drug discovery and development: introduction to the general public and patient groups. *Frontiers in Drug Discovery*, *3*, p.1201419.
7. Klein, K., Gencoglu, M., Heisterberg, J., Acha, V. and Stolk, P., 2023. The global landscape of manufacturers of follow-on biologics: an overview of five major biosimilar markets and 15 countries. *BioDrugs*, *37*(2), pp.235-245.
8. Morrow, T. and Felcone, L.H., 2004. Defining the difference: what makes biologics unique. *Biotechnology healthcare*, *1*(4), p.24.
9. Falcetta, P., Aragona, M., Bertolotto, A., Bianchi, C., Campi, F., Garofolo, M. and Del Prato, S., 2022. Insulin discovery: a pivotal point in medical history. *Metabolism*, *127*, p.154941.
10. https://www.who.int/news-room/fact-sheets/detail/diabetes (Indexed on 05th April, 2023)
11. American Diabetes Association, 2021. 9. Pharmacologic approaches to glycemic treatment: Standards of Medical Care in Diabetes—2021. *Diabetes care*, *44*(Supplement_1), pp.S111-S124.
12. van Spronsen, F.J., Blau, N., Harding, C., Burlina, A., Longo, N. and Bosch, A.M., 2021. Phenylketonuria. *Nature reviews Disease primers*, *7*(1), p.36.
13. Pavlou, A.K. and Reichert, J.M., 2004. Recombinant protein therapeutics—success rates, market trends and values to 2010. *Nature biotechnology*, *22*(12), pp.1513-1519.
14. Leocani, L., Comi, E., Annovazzi, P., Rovaris, M., Rossi, P., Cursi, M., Comola, M., Martinelli, V. and Comi, G., 2007. Impaired short-term motor learning in multiple sclerosis: evidence from virtual reality. *Neurorehabilitation and neural repair*, *21*(3), pp.273-278.
15. Centonze, D., Muzio, L., Rossi, S., Furlan, R., Bernardi, G. and Martino, G., 2010. The link between inflammation, synaptic transmission and neurodegeneration in multiple sclerosis. *Cell Death & Differentiation*, *17*(7), pp.1083-1091.
16. Zettl, U.K., Rommer, P.S., Aktas, O., Wagner, T., Richter, J., Oschmann, P., Cepek, L., Elias-Hamp, B., Gehring, K., Chan, A. and Hecker, M., 2023. Interferon beta-1a sc at 25 years: a mainstay in the treatment of multiple sclerosis over the period of one generation. *Expert review of clinical immunology*, *19*(11), pp.1343-1359.
17. Mahlapuu, M., Håkansson, J., Ringstad, L. and Björn, C., 2016. Antimicrobial peptides: an emerging category of therapeutic agents. *Frontiers in cellular and infection microbiology*, p.194.
18. Fernández de Ullivarri, M., Arbulu, S., Garcia-Gutierrez, E. and Cotter, P.D., 2020. Antifungal peptides as therapeutic agents. *Frontiers in Cellular and Infection Microbiology*, *10*, p.105.
19. Sieber, S.A. and Marahiel, M.A., 2003. Learning from Nature's Drug Factories: Nonribosomal Synthesisof MacrocyclicPeptides. *Journal of bacteriology*, *185*(24), pp.7036-7043.
20. Zhong, G., Wang, Z.J., Yan, F., Zhang, Y. and Huo, L., 2022. Recent Advances in Discovery, Bioengineering, and Bioactivity-Evaluation of Ribosomally Synthesized and Post-translationally Modified Peptides. *ACS bio & med Chem Au*, *3*(1), pp.1-31.
21. Hawley, H.B. and Gump, D.W., 1973. Vancomycin therapy of bacterial meningitis. *American journal of diseases of children*, *126*(2), pp.261-264.

22. Murray, C.J., Ikuta, K.S., Sharara, F., Swetschinski, L., Aguilar, G.R., Gray, A., Han, C., Bisignano, C., Rao, P., Wool, E. and Johnson, S.C., 2022. Global burden of bacterial antimicrobial resistance in 2019: a systematic analysis. *The Lancet*, *399*(10325), pp.629-655.
23. https://apps.who.int/gb/ebwha/pdf_files/EB154/B154_13-en.pdf (Indexed on 21st December, 2023)
24. Anderson, M., Panteli, D., Van Kessel, R., Ljungqvist, G., Colombo, F. and Mossialos, E., 2023. Challenges and opportunities for incentivising antibiotic research and development in Europe. *The Lancet Regional Health–Europe*, *33*.
25. Navarro-Sarabia, F., Ariza-Ariza, R., Hernández-Cruz, B. and Villanueva, I., 2006. Adalimumab for treating rheumatoid arthritis. *The Journal of rheumatology*, *33*(6), pp.1075-1081.
26. Garon, E.B., Rizvi, N.A., Hui, R., Leighl, N., Balmanoukian, A.S., Eder, J.P., Patnaik, A., Aggarwal, C., Gubens, M., Horn, L. and Carcereny, E., 2015. Pembrolizumab for the treatment of non–small-cell lung cancer. *New England Journal of Medicine*, *372*(21), pp.2018-2028.
27. Senior, M., 2023. Fresh from the biotech pipeline: fewer approvals, but biologics gain share. *Nature Biotechnology*, p.1.
28. Lu, R.M., Hwang, Y.C., Liu, I.J., Lee, C.C., Tsai, H.Z., Li, H.J. and Wu, H.C., 2020. Development of therapeutic antibodies for the treatment of diseases. *Journal of biomedical science*, *27*(1), pp.1-30.
29. Chames, P., Van Regenmortel, M., Weiss, E. and Baty, D., 2009. Therapeutic antibodies: successes, limitations and hopes for the future. *British journal of pharmacology*, *157*(2), pp.220-233.
30. Wang, L., Wang, N., Zhang, W., Cheng, X., Yan, Z., Shao, G., Wang, X., Wang, R. and Fu, C., 2022. Therapeutic peptides: Current applications and future directions. *Signal Transduction and Targeted Therapy*, *7*(1), p.48.
31. Sharma, K., Sharma, K.K., Sharma, A. and Jain, R., 2023. Peptide-based drug discovery: Current status and recent advances. *Drug Discovery Today*, *28*(2), p.103464.
32. De Pauw, T., De Mey, L., Debacker, J.M., Raes, G., Van Ginderachter, J.A., De Groof, T.W. and Devoogdt, N., 2023. Current status and future expectations of nanobodies in oncology trials. *Expert Opinion on Investigational Drugs*, *32*(8), pp.705-721.
33. Keri, D., Walker, M., Singh, I., Nishikawa, K. and Garces, F., 2023. Next generation of multispecific antibody engineering. *Antibody Therapeutics*, p.tbad027.
34. Spadiut, O., Capone, S., Krainer, F., Glieder, A. and Herwig, C., 2014. Microbials for the production of monoclonal antibodies and antibody fragments. *Trends in biotechnology*, *32*(1), pp.54-60.
35. Wang, L., Wang, N., Zhang, W., Cheng, X., Yan, Z., Shao, G., Wang, X., Wang, R. and Fu, C., 2022. Therapeutic peptides: current applications and future directions. *Signal Transduction and Targeted Therapy*, *7*(1), p.48.
36. Hollifield, A.L., Arnall, J.R. and Moore, D.C., 2020. Caplacizumab: an anti–von Willebrand factor antibody for the treatment of thrombotic thrombocytopenic purpura. *American Journal of Health-System Pharmacy*, *77*(15), pp.1201-1207.

37. Olivieri, A.V., Muratov, S., Larsen, S., Luckevich, M., Chan, K., Lamotte, M. and Lau, D.C., 2024. Cost-effectiveness of weight-management pharmacotherapies in Canada: a societal perspective. *International Journal of Obesity*, pp.1-11.
38. Goshua, G., Sinha, P., Hendrickson, J.E., Tormey, C., Bendapudi, P.K. and Lee, A.I., 2021. Cost effectiveness of caplacizumab in acquired thrombotic thrombocytopenic purpura. *Blood, The Journal of the American Society of Hematology*, *137*(7), pp.969-976.
39. Caillon, M., Brethon, B., van Beurden-Tan, C., Supiot, R., Le Mezo, A., Chauny, J.V., Majer, I. and Petit, A., 2023. Cost-Effectiveness of Blinatumomab in Pediatric Patients with High-Risk First-Relapse B-Cell Precursor Acute Lymphoblastic Leukemia in France. *PharmacoEconomics-Open*, *7*(4), pp.639-653.
40. Cordaillat-Simmons, M., Rouanet, A. and Pot, B., 2020. Live biotherapeutic products: the importance of a defined regulatory framework. *Experimental & molecular medicine*, *52*(9), pp.1397-1406.
41. FDA. *Early Clinical Trials with Live Biotherapeutic Products: Chemistry, Manufacturing, and Control Information* (FDA, Released on February 2012; Updated on June 2016).
42. Rutter, J.W., Dekker, L., Owen, K.A. and Barnes, C.P., 2022. Microbiome engineering: engineered live biotherapeutic products for treating human disease. *Frontiers in Bioengineering and Biotechnology*, *10*, p.1000873.
43. Brennan, A.M., 2022. Development of synthetic biotics as treatment for human diseases. *Synthetic Biology*, *7*(1), p.ysac001.
44. Rouanet, A., Bolca, S., Bru, A., Claes, I., Cvejic, H., Girgis, H., Harper, A., Lavergne, S.N., Mathys, S., Pane, M. and Pot, B., 2020. Live biotherapeutic products, a road map for safety assessment. *Frontiers in Medicine*, p.237.
45. Charbonneau, M.R., Isabella, V.M., Li, N. and Kurtz, C.B., 2020. Developing a new class of engineered live bacterial therapeutics to treat human diseases. *Nature Communications*, *11*(1), p.1738.
46. Hill, C., Guarner, F., Reid, G., Gibson, G.R., Merenstein, D.J., Pot, B., Morelli, L., Canani, R.B., Flint, H.J., Salminen, S. and Calder, P.C., 2014. The International Scientific Association for Probiotics and Prebiotics consensus statement on the scope and appropriate use of the term probiotic. *Nature reviews Gastroenterology & hepatology*, *11*(8), pp.506-514.
47. Han, S., Lu, Y., Xie, J., Fei, Y., Zheng, G., Wang, Z., Liu, J., Lv, L., Ling, Z., Berglund, B. and Yao, M., 2021. Probiotic gastrointestinal transit and colonization after oral administration: A long journey. *Frontiers in cellular and infection microbiology*, *11*, p.609722.
48. Kelly, V.W., Liang, B.K. and Sirk, S.J., 2020. Living therapeutics: the next frontier of precision medicine. *ACS synthetic biology*, *9*(12), pp.3184-3201.
49. Parker, E.D., Lin, J., Mahoney, T., Ume, N., Yang, G., Gabbay, R.A., ElSayed, N.A. and Bannuru, R.R., 2024. Economic costs of diabetes in the US in 2022. *Diabetes Care*, *47*(1), pp.26-43.
50. Takiishi, T., Korf, H., Van Belle, T.L., Robert, S., Grieco, F.A., Caluwaerts, S., Galleri, L., Spagnuolo, I., Steidler, L., Van Huynegem, K. and Demetter, P., 2012. Reversal of autoimmune

diabetes by restoration of antigen-specific tolerance using genetically modified Lactococcus lactis in mice. *The Journal of clinical investigation*, *122*(5), pp.1717-1725.

51. Robert, S., Gysemans, C., Takiishi, T., Korf, H., Spagnuolo, I., Sebastiani, G., Van Huynegem, K., Steidler, L., Caluwaerts, S., Demetter, P. and Wasserfall, C.H., 2014. Oral delivery of glutamic acid decarboxylase (GAD)-65 and IL10 by Lactococcus lactis reverses diabetes in recent-onset NOD mice. *Diabetes*, *63*(8), pp.2876-2887.
52. Takiishi, T., Cook, D.P., Korf, H., Sebastiani, G., Mancarella, F., Cunha, J.P.M.C.M., Wasserfall, C., Casares, N., Lasarte, J.J., Steidler, L. and Rottiers, P., 2017. Reversal of diabetes in NOD mice by clinical-grade proinsulin and IL-10–secreting lactococcus lactis in combination with low-dose anti-CD3 depends on the induction of Foxp3-positive T cells. *Diabetes*, *66*(2), pp.448-459.
53. Abdul Basith Khan, M., Hashim, M.J., King, J.K., Govender, R.D., Mustafa, H. and Al Kaabi, J., 2020. Epidemiology of type 2 diabetes—global burden of disease and forecasted trends. *Journal of epidemiology and global health*, *10*(1), pp.107-111.
54. Duan, F., Curtis, K.L. and March, J.C., 2008. Secretion of insulinotropic proteins by commensal bacteria: rewiring the gut to treat diabetes. *Applied and environmental microbiology*, *74*(23), pp.7437-7438.
55. Duan, F.F., Liu, J.H. and March, J.C., 2015. Engineered commensal bacteria reprogram intestinal cells into glucose-responsive insulin-secreting cells for the treatment of diabetes. Diabetes, 64(5), pp.1794-1803.
56. Hu, H., Luo, J., Liu, Y., Li, H., Jin, R., Li, S., Wei, J., Wei, H. and Chen, T., 2023. Improvement effect of a next-generation probiotic L. plantarum-pMG36e-GLP-1 on type 2 diabetes mellitus via the gut–pancreas–liver axis. *Food & Function*, *14*(7), pp.3179-3195.
57. Luo, J., Zhang, H., Lu, J., Ma, C. and Chen, T., 2021. Antidiabetic effect of an engineered bacterium Lactobacillus plantarum-pMG36e-GLP-1 in monkey model. *Synthetic and Systems Biotechnology*, *6*(4), pp.272-282.
58. Ma, J., Li, C., Wang, J. and Gu, J., 2020. Genetically Engineered Escherichia coli Nissle 1917 Secreting GLP-1 Analog Exhibits Potential Antiobesity Effect in High-Fat Diet-Induced Obesity Mice. *Obesity*, *28*(2), pp.315-322.
59. Wang, L., Chen, T., Wang, H., Wu, X., Cao, Q., Wen, K., Deng, K.Y. and Xin, H., 2021. Engineered bacteria of MG1363-pMG36e-GLP-1 attenuated obesity-induced by high fat diet in mice. *Frontiers in Cellular and Infection Microbiology*, *11*, p.595575.
60. Fang, X., Zhou, X., Miao, Y., Han, Y., Wei, J. and Chen, T., 2020. Therapeutic effect of GLP-1 engineered strain on mice model of Alzheimer's disease and Parkinson's disease. *Amb Express*, *10*(1), pp.1-13.
61. Chen, T., Tian, P., Huang, Z., Zhao, X., Wang, H., Xia, C., Wang, L. and Wei, H., 2018. Engineered commensal bacteria prevent systemic inflammation-induced memory impairment and amyloidogenesis via producing GLP-1. *Applied Microbiology and Biotechnology*, *102*, pp.7565-7575.
62. Fang, X., Tian, P., Zhao, X., Jiang, C. and Chen, T., 2019. Neuroprotective effects of an engineered commensal bacterium in the 1-methyl-4-phenyl-1, 2, 3, 6-tetrahydropyridine Parkinson disease

mouse model via producing glucagon-like peptide-1. *Journal of Neurochemistry*, *150*(4), pp.441-452.
63. Fellows, G.K. and Hollis, A., 2013. Funding innovation for treatment for rare diseases: adopting a cost-based yardstick approach. *Orphanet journal of rare diseases*, *8*, pp.1-9.
64. Hwang, I.Y., 2023. Engineering live bacterial therapeutics to treat human diseases. *Current Opinion in Systems Biology*, p.100492.
65. Vockley, J., Sondheimer, N., Puurunen, M., Diaz, G.A., Ginevic, I., Grange, D.K., Harding, C., Northrup, H., Phillips III, J.A., Searle, S. and Thomas, J.A., 2023. Efficacy and safety of a synthetic biotic for treatment of phenylketonuria: a phase 2 clinical trial. *Nature Metabolism*, *5*(10), pp.1685-1690.
66. Durrer, K.E., Allen, M.S. and Hunt von Herbing, I., 2017. Genetically engineered probiotic for the treatment of phenylketonuria (PKU); assessment of a novel treatment in vitro and in the PAHenu2 mouse model of PKU. *PloS one*, *12*(5), p.e0176286.
67. Ramírez, A.M., Rodriguez-López, A., Ardila, A., Beltran, L., Patarroyo, C.A., Melendez, A.D.P., Sánchez, O.F. and Alméciga-Díaz, C.J., 2017. Production of human recombinant phenylalanine hydroxylase in Lactobacillus plantarum for gastrointestinal delivery. *European Journal of Pharmaceutical Sciences*, *109*, pp.48-55.
68. Kumar, T., Sharma, G.S. and Singh, L.R., 2016. Homocystinuria: therapeutic approach. *Clinica Chimica Acta*, *458*, pp.55-62.
69. Fishbein, S.R., Evbuomwan, E.M. and Dantas, G., 2024. Conquering homocystinuria with engineered probiotics. *Cell Host & Microbe*, *32*(3), pp.298-300.
70. Perreault, M., Means, J., Gerson, E., James, M., Cotton, S., Bergeron, C.G., Simon, M., Carlin, D.A., Schmidt, N., Moore, T.C. and Blasbalg, J., 2024. The live biotherapeutic SYNB1353 decreases plasma methionine via directed degradation in animal models and healthy volunteers. *Cell Host & Microbe*.
71. Blackburn, P.R., Gass, J.M., Vairo, F.P.E., Farnham, K.M., Atwal, H.K., Macklin, S., Klee, E.W. and Atwal, P.S., 2017. Maple syrup urine disease: mechanisms and management. *The application of clinical genetics*, pp.57-66.
72. Li, N., Tucker, A., Gao, J.R., Renaud, L., James, M., Castillo, M., Galvan, S., Jain, R., Putman, R., Marr, S. and Carlin, D., 2021. Development of an engineered probiotic for the treatment of branched chain amino acid related metabolic diseases.
73. Lichter-Konecki, U., Caldovic, L., Morizono, H., Simpson, K., Mew, A. and MacLeod, E., 2022. Ornithine transcarbamylase deficiency.
74. Lima, L.C.D., Miranda, A.S., Ferreira, R.N., Rachid, M.A. and e Silva, A.C.S., 2019. Hepatic encephalopathy: Lessons from preclinical studies. *World Journal of Hepatology*, *11*(2), p.173.
75. Kurtz, C.B., Millet, Y.A., Puurunen, M.K., Perreault, M., Charbonneau, M.R., Isabella, V.M., Kotula, J.W., Antipov, E., Dagon, Y., Denney, W.S. and Wagner, D.A., 2019. An engineered E. coli Nissle improves hyperammonemia and survival in mice and shows dose-dependent exposure in healthy humans. *Science Translational Medicine*, *11*(475), p.eaau7975.

76. Nicaise, C., Prozzi, D., Viaene, E., Moreno, C., Gustot, T., Quertinmont, E., Demetter, P., Suain, V., Goffin, P., Deviere, J. and Hols, P., 2008. Control of acute, chronic, and constitutive hyperammonemia by wild-type and genetically engineered Lactobacillus plantarum in rodents. *Hepatology*, *48*(4), pp.1184-1192.
77. Witting, C., Langman, C.B., Assimos, D., Baum, M.A., Kausz, A., Milliner, D., Tasian, G., Worcester, E., Allain, M., West, M. and Knauf, F., 2021. Pathophysiology and treatment of enteric hyperoxaluria. *Clinical Journal of the American Society of Nephrology*, *16*(3), pp.487-495.
78. Lubkowicz, D., Horvath, N.G., James, M.J., Cantarella, P., Renaud, L., Bergeron, C.G., Shmueli, R.B., Anderson, C., Gao, J.R., Kurtz, C.B. and Perreault, M., 2022. An engineered bacterial therapeutic lowers urinary oxalate in preclinical models and in silico simulations of enteric hyperoxaluria. *Molecular systems biology*, *18*(3), p.e10539.
79. Novome Biotechnologies Inc. 2022. Phase 1-2a safety, tolerability, and pharmacodynamics controlled study of NOV-001 in healthy volunteers and patients with enteric hyperoxaluria. NCT04909723. clinicaltrials.gov.
80. Zhao, C., Yang, H., Zhu, X., Li, Y., Wang, N., Han, S., Xu, H., Chen, Z. and Ye, Z., 2018. Oxalate-degrading enzyme recombined lactic acid bacteria strains reduce hyperoxaluria. *Urology*, *113*, pp.253-e1.
81. Sasikumar, P., Gomathi, S., Anbazhagan, K., Abhishek, A., Paul, E., Vasudevan, V., Sasikumar, S. and Selvam, G.S., 2014. Recombinant Lactobacillus plantarum expressing and secreting heterologous oxalate decarboxylase prevents renal calcium oxalate stone deposition in experimental rats. *Journal of biomedical science*, *21*(1), pp.1-13.
82. Paul, E., Albert, A., Ponnusamy, S., Mishra, S.R., Vignesh, A.G., Sivakumar, S.M., Sivasamy, G. and Sadasivam, S.G., 2018. Designer probiotic Lactobacillus plantarum expressing oxalate decarboxylase developed using group II intron degrades intestinal oxalate in hyperoxaluric rats. *Microbiological Research*, *215*, pp.65-75.
83. Baumgart, D.C. and Carding, S.R., 2007. Inflammatory bowel disease: cause and immunobiology. *The Lancet*, *369*(9573), pp.1627-1640.
84. Alatab, S., Sepanlou, S.G., Ikuta, K., Vahedi, H., Bisignano, C., Safiri, S., Sadeghi, A., Nixon, M.R., Abdoli, A., Abolhassani, H. and Alipour, V., 2020. The global, regional, and national burden of inflammatory bowel disease in 195 countries and territories, 1990–2017: a systematic analysis for the Global Burden of Disease Study 2017. *The Lancet gastroenterology & hepatology*, *5*(1), pp.17-30.
85. Taylor, A., Verhagen, J., Blaser, K., Akdis, M. and Akdis, C.A., 2006. Mechanisms of immune suppression by interleukin-10 and transforming growth factor-β: the role of T regulatory cells. *Immunology*, *117*(4), pp.433-442.
86. Steidler, L., Hans, W., Schotte, L., Neirynck, S., Obermeier, F., Falk, W., Fiers, W. and Remaut, E., 2000. Treatment of murine colitis by Lactococcus lactis secreting interleukin-10. *Science*, *289*(5483), pp.1352-1355.

87. Braat, H., Rottiers, P., Huyghebaert, N., Remaut, E., Remon, J.P., van Deventer, S., Neirynck, S., Peppelenbosch, M.P., Steidler, L.S. and Hommes, D.W., 2006. IL-10 Producing Lactococcus lactis for the Treatment of Crohn's Disease. *Inflammatory Bowel Diseases*, *12*(suppl_2), pp.S26-S27.
88. Steidler, L., Rottiers, P. and Coulie, B., 2009. Actobiotics™ as a Novel Method for Cytokine Delivery: The Interleukin-10 Case. *Annals of the New York Academy of Sciences*, *1182*(1), pp.135-145.
89. Tatiya-Aphiradee, N., Chatuphonprasert, W. and Jarukamjorn, K., 2018. Immune response and inflammatory pathway of ulcerative colitis. *Journal of basic and clinical physiology and pharmacology*, *30*(1), pp.1-10.
90. Vandenbroucke, K., De Haard, H., Beirnaert, E., Dreier, T., Lauwereys, M., Huyck, L., Van Huysse, J., Demetter, P., Steidler, L., Remaut, E. and Cuvelier, C., 2010. Orally administered L. lactis secreting an anti-TNF Nanobody demonstrate efficacy in chronic colitis. *Mucosal immunology*, *3*(1), pp.49-56.
91. Lynch, J.P., González-Prieto, C., Reeves, A.Z., Bae, S., Powale, U., Godbole, N.P., Tremblay, J.M., Schmidt, F.I., Ploegh, H.L., Kansra, V. and Glickman, J.N., 2023. Engineered Escherichia coli for the in situ secretion of therapeutic nanobodies in the gut. *Cell Host & Microbe*, *31*(4), pp.634-649.
92. Nguyen, P.M., Putoczki, T.L. and Ernst, M., 2015. STAT3-activating cytokines: a therapeutic opportunity for inflammatory bowel disease?. *Journal of interferon & cytokine research*, *35*(5), pp.340-350.
93. Vandenbroucke, K., Hans, W., Van Huysse, J., Neirynck, S., Demetter, P., Remaut, E., Rottiers, P. and Steidler, L., 2004. Active delivery of trefoil factors by genetically modified Lactococcus lactis prevents and heals acute colitis in mice. *Gastroenterology*, *127*(2), pp.502-513.
94. Praveschotinunt, P., Duraj-Thatte, A.M., Gelfat, I., Bahl, F., Chou, D.B. and Joshi, N.S., 2019. Engineered E. coli Nissle 1917 for the delivery of matrix-tethered therapeutic domains to the gut. *Nature communications*, *10*(1), p.5580.
95. Liu, C.H., Chang, J.H., Chang, Y.C. and Mou, K.Y., 2020. Treatment of murine colitis by Saccharomyces boulardii secreting atrial natriuretic peptide. *Journal of Molecular Medicine*, *98*, pp.1675-1687.
96. Suzuki, R., Mishima, M., Nagane, M., Mizugaki, H., Suzuki, T., Komuro, M., Shimizu, T., Fukuyama, T., Takeda, S., Ogata, M. and Miyamoto, T., 2023. The novel sustained 3-hydroxybutyrate donor poly-D-3-hydroxybutyric acid prevents inflammatory bowel disease through upregulation of regulatory T-cells. *The FASEB Journal*, *37*(1), p.e22708.
97. Yan, X., Liu, X.Y., Zhang, D., Zhang, Y.D., Li, Z.H., Liu, X., Wu, F. and Chen, G.Q., 2021. Construction of a sustainable 3-hydroxybutyrate-producing probiotic Escherichia coli for treatment of colitis. *Cellular & Molecular Immunology*, *18*(10), pp.2344-2357.
98. Roslan, M.A.M., Omar, M.N., Sharif, N.A.M., Raston, N.H.A., Arzmi, M.H., Neoh, H.M. and Ramzi, A.B., 2023. Recent advances in single-cell engineered live biotherapeutic products research for skin repair and disease treatment. *npj Biofilms and Microbiomes*, *9*(1), p.95.

99. Lu, Y., Li, H., Wang, J., Yao, M., Peng, Y., Liu, T., Li, Z., Luo, G. and Deng, J., 2021. Engineering bacteria-activated multifunctionalized hydrogel for promoting diabetic wound healing. *Advanced Functional Materials*, *31*(48), p.2105749.
100. Vågesjö, E., Öhnstedt, E., Mortier, A., Lofton, H., Huss, F., Proost, P., Roos, S. and Phillipson, M., 2018. Accelerated wound healing in mice by on-site production and delivery of CXCL12 by transformed lactic acid bacteria. *Proceedings of the National Academy of Sciences*, *115*(8), pp.1895-1900.
101. Öhnstedt, E., Vågesjö, E., Fasth, A., Tomenius, H.L., Dahg, P., Jönsson, S., Tyagi, N., Åström, M., Myktybekova, Z., Ringstad, L. and Jorvid, M., 2023. Engineered bacteria to accelerate wound healing: an adaptive, randomised, double-blind, placebo-controlled, first-in-human phase 1 trial. *Eclinicalmedicine*, *60*.
102. Guidance for industry chronic cutaneous ulcer and burn wounds — developing products for treatment. https://www.fda.gov/media/71278/download. Date: 2006 Date accessed: May, 2024
103. Zhao, X., Li, S., Ding, J., Wei, J., Tian, P., Wei, H. and Chen, T., 2021. Combination of an engineered Lactococcus lactis expressing CXCL12 with light-emitting diode yellow light as a treatment for scalded skin in mice. *Microbial Biotechnology*, *14*(5), pp.2090-2100.
104. Li, L., Yang, C., Ma, B., Lu, S., Liu, J., Pan, Y., Wang, X., Zhang, Y., Wang, H., Sun, T. and Liu, D., 2023. Hydrogel-encapsulated engineered microbial consortium as a photoautotrophic "living material" for promoting skin wound healing. *ACS Applied Materials & Interfaces*, *15*(5), pp.6536-6547.
105. Kurkipuro, J., Mierau, I., Wirth, T., Samaranayake, H., Smith, W., Kärkkäinen, H.R., Tikkanen, M. and Yrjänheikki, J., 2022. Four in one—Combination therapy using live Lactococcus lactis expressing three therapeutic proteins for the treatment of chronic non-healing wounds. *PLoS One*, *17*(2), p.e0264775.
106. Aurealis Clinical Trial Report:- https://aurealistherapeutics.com/chronic-wounds/#clinical-trials-aup-16, Accessed on May, 2024
107. Cruz, S., Vecerek, N. and Elbuluk, N., 2023. Targeting Inflammation in Acne: Current Treatments and Future Prospects. *American Journal of Clinical Dermatology*, pp.1-14.
108. Knödlseder, N., Fábrega, M.J., Santos-Moreno, J., Manils, J., Toloza, L., Marín Vilar, M., Fernández, C., Broadbent, K., Maruotti, J., Lemenager, H. and Carolis, C., 2024. Delivery of a sebum modulator by an engineered skin microbe in mice. *Nature Biotechnology*, pp.1-6.
109. Fuenzalida, C., Dufeu, M.S., Poniachik, J., Roblero, J.P., Valenzuela-Pérez, L. and Beltrán, C.J., 2021. Probiotics-based treatment as an integral approach for alcohol use disorder in alcoholic liver disease. *Frontiers in pharmacology*, *12*, p.729950.
110. Hartmann, P., Chen, P., Wang, H.J., Wang, L., McCole, D.F., Brandl, K., Stärkel, P., Belzer, C., Hellerbrand, C., Tsukamoto, H. and Ho, S.B., 2013. Deficiency of intestinal mucin-2 ameliorates experimental alcoholic liver disease in mice. *Hepatology*, *58*(1), pp.108-119.
111. Hendrikx, T., Duan, Y.I., Wang, Y., Oh, J.H., Alexander, L.M., Huang, W., Stärkel, P., Ho, S.B., Gao, B., Fiehn, O. and Emond, P., 2019. Bacteria engineered to produce IL-22 in intestine induce expression of REG3G to reduce ethanol-induced liver disease in mice. *Gut*, *68*(8), pp.1504-1515.

112. Haber, P.S., Warner, R., Seth, D., Gorrell, M.D. and McCaughan, G.W., 2003. Pathogenesis and management of alcoholic hepatitis. *Journal of gastroenterology and hepatology*, *18*(12), pp.1332-1344.
113. Lyu, Y., Zhong, L., Liu, Y., Lu, J., LaPointe, G., Lu, F. and Lu, Z., 2018. Protective effects of Lactococcus lactis expressing alcohol dehydrogenase and acetaldehyde dehydrogenase on acute alcoholic liver injury in mice. *Journal of Chemical Technology & Biotechnology*, *93*(5), pp.1502-1510.
114. Lu, J., Lyu, Y., Li, M., Sun, J., Huang, Z., Lu, F. and Lu, Z., 2018. Alleviating acute alcoholic liver injury in mice with Bacillus subtilis co-expressing alcohol dehydrogenase and acetaldehyde dehydrogenase. *Journal of Functional Foods*, *49*, pp.342-350.
115. Lu, J., Zhu, X., Zhang, C., Lu, F., Lu, Z. and Lu, Y., 2020. Co-expression of alcohol dehydrogenase and aldehyde dehydrogenase in Bacillus subtilis for alcohol detoxification. *Food and Chemical Toxicology*, *135*, p.110890.
116. Cross, M., Culbreth, G., Steinmetz, J., Kopec, J., Haile, L., Brooks, P., Rhinehart, P.A., Hagins, H., Ong, L., Kopansky-Giles, D. and Dreinhoefer, K., Global, Regional, and National Burden of Gout, 1990–2020, and Projections to 2050: A Systematic Analysis of the Global Burden of Disease Study 2021.
117. Black, R.J., Cross, M., Haile, L.M., Culbreth, G.T., Steinmetz, J.D., Hagins, H., Kopec, J.A., Brooks, P.M., Woolf, A.D., Ong, K.L. and Kopansky-Giles, D.R., 2023. Global, regional, and national burden of rheumatoid arthritis, 1990–2020, and projections to 2050: a systematic analysis of the Global Burden of Disease Study 2021. *The Lancet Rheumatology*, *5*(10), pp.e594-e610.
118. Wortmann, R.L., 2002. Gout and hyperuricemia. *Current opinion in rheumatology*, *14*(3), pp.281-286.
119. Firestein, G.S., 2003. Evolving concepts of rheumatoid arthritis. *Nature*, *423*(6937), pp.356-361.
120. Zhao, R., Li, Z., Sun, Y., Ge, W., Wang, M., Liu, H., Xun, L. and Xia, Y., 2022. Engineered Escherichia coli Nissle 1917 with urate oxidase and an oxygen-recycling system for hyperuricemia treatment. *Gut microbes*, *14*(1), p.2070391.
121. He, L., Tang, W., Huang, L., Zhou, W., Huang, S., Zou, L., Yuan, L., Men, D., Chen, S. and Hu, Y., 2022. Insulated expression of periplasmic uricase in E. coli Nissle 1917 for the treatment of hyperuricemia. *bioRxiv*, pp.2022-04.
122. Tong, Y., Wei, Y., Ju, Y., Li, P., Zhang, Y., Li, L., Gao, L., Liu, S., Liu, D., Hu, Y. and Li, Z., 2023. Anaerobic purinolytic enzymes enable dietary purine clearance by engineered gut bacteria. *Cell Chemical Biology*.
123. Colmegna, I., Ohata, B.R. and Menard, H.A., 2012. Current understanding of rheumatoid arthritis therapy. *Clinical Pharmacology & Therapeutics*, *91*(4), pp.607-620.
124. VanderBorght, A., Geusens, P., Raus, J. and Stinissen, P., 2001, December. The autoimmune pathogenesis of rheumatoid arthritis: role of autoreactive T cells and new immunotherapies. In *Seminars in arthritis and rheumatism* (Vol. 31, No. 3, pp. 160-175). WB Saunders.
125. Wulff, H. and Zhorov, B.S., 2008. K+ channel modulators for the treatment of neurological disorders and autoimmune diseases. *Chemical reviews*, *108*(5), pp.1744-1773.

126. Wang, Y., Zhu, D., Ortiz-Velez, L.C., Perry, J.L., Pennington, M.W., Hyser, J.M., Britton, R.A. and Beeton, C., 2023. A bioengineered probiotic for the oral delivery of a peptide Kv1. 3 channel blocker to treat rheumatoid arthritis. *Proceedings of the National Academy of Sciences*, *120*(2), p.e2211977120.
127. Zhou, M., Tang, Y., Xu, W., Hao, X., Li, Y., Huang, S., Xiang, D. and Wu, J., 2023. Bacteria-based immunotherapy for cancer: a systematic review of preclinical studies. *Frontiers in Immunology*, *14*, p.1140463.
128. Guo, Y., Chen, Y., Liu, X., Min, J.J., Tan, W. and Zheng, J.H., 2020. Targeted cancer immunotherapy with genetically engineered oncolytic Salmonella typhimurium. *Cancer letters*, *469*, pp.102-110.
129. Loeffler, M., Le'Negrate, G., Krajewska, M. and Reed, J.C., 2007. Attenuated Salmonella engineered to produce human cytokine LIGHT inhibit tumor growth. *Proceedings of the National Academy of Sciences*, *104*(31), pp.12879-12883.
130. Loeffler, M., Le'Negrate, G., Krajewska, M. and Reed, J.C., 2009. Salmonella typhimurium engineered to produce CCL21 inhibit tumor growth. *Cancer immunology, immunotherapy*, *58*, pp.769-775.
131. Loeffler, M., Le'Negrate, G., Krajewska, M. and Reed, J.C., 2008. IL-18-producing Salmonella inhibit tumor growth. *Cancer gene therapy*, *15*(12), pp.787-794.
132. Yoon, W., Park, Y.C., Kim, J., Chae, Y.S., Byeon, J.H., Min, S.H., Park, S., Yoo, Y., Park, Y.K. and Kim, B.M., 2017. Application of genetically engineered Salmonella typhimurium for interferon-gamma–induced therapy against melanoma. *European Journal of Cancer*, *70*, pp.48-61.
133. Liang, K., Liu, Q., Li, P., Luo, H., Wang, H. and Kong, Q., 2019. Genetically engineered Salmonella Typhimurium: Recent advances in cancer therapy. *Cancer letters*, *448*, pp.168-181.
134. Chen, H., Lei, P., Ji, H., Yang, Q., Peng, B., Ma, J., Fang, Y., Qu, L., Li, H., Wu, W. and Jin, L., 2023. Advances in Escherichia coli Nissle 1917 as a customizable drug delivery system for disease treatment and diagnosis strategies. *Materials Today Bio*, *18*, p.100543.
135. He, L., Yang, H., Liu, F., Chen, Y., Tang, S., Ji, W., Tang, J., Liu, Z., Sun, Y., Hu, S. and Zhang, Y., 2017. Escherichia coli Nissle 1917 engineered to express Tum-5 can restrain murine melanoma growth. *Oncotarget*, *8*(49), p.85772.
136. He, L., Yang, H., Tang, J., Liu, Z., Chen, Y., Lu, B., He, H., Tang, S., Sun, Y., Liu, F. and Ding, X., 2019. Intestinal probiotics E. coli Nissle 1917 as a targeted vehicle for delivery of p53 and Tum-5 to solid tumors for cancer therapy. *Journal of biological engineering*, *13*, pp.1-13.
137. Ji, P., An, B., Jie, Z., Wang, L., Qiu, S., Ge, C., Wu, Q., Shi, J. and Huo, M., 2023. Genetically engineered probiotics as catalytic glucose depriver for tumor starvation therapy. *Materials Today Bio*, *18*, p.100515.
138. Diner, E.J., Burdette, D.L., Wilson, S.C., Monroe, K.M., Kellenberger, C.A., Hyodo, M., Hayakawa, Y., Hammond, M.C. and Vance, R.E., 2013. The innate immune DNA sensor cGAS produces a noncanonical cyclic dinucleotide that activates human STING. *Cell reports*, *3*(5), pp.1355-1361.

139. Leventhal, D.S., Sokolovska, A., Li, N., Plescia, C., Kolodziej, S.A., Gallant, C.W., Christmas, R., Gao, J.R., James, M.J., Abin-Fuentes, A. and Momin, M., 2020. Immunotherapy with engineered bacteria by targeting the STING pathway for anti-tumor immunity. *Nature communications*, *11*(1), p.2739.
140. Luke, J.J., Piha-Paul, S.A., Medina, T., Verschraegen, C.F., Varterasian, M., Brennan, A.M., Riese, R.J., Sokolovska, A., Strauss, J., Hava, D.L. and Janku, F., 2023. Phase I Study of SYNB1891, an Engineered E. coli Nissle Strain Expressing STING Agonist, with and without Atezolizumab in Advanced Malignancies. *Clinical Cancer Research*, pp.OF1-OF10.
141. Gurbatri, C.R., Lia, I., Vincent, R., Coker, C., Castro, S., Treuting, P.M., Hinchliffe, T.E., Arpaia, N. and Danino, T., 2020. Engineered probiotics for local tumor delivery of checkpoint blockade nanobodies. *Science translational medicine*, *12*(530), p.eaax0876.
142. Gurbatri, C.R., Radford, G.A., Vrbanac, L., Im, J., Thomas, E.M., Coker, C., Taylor, S.R., Jang, Y., Sivan, A., Rhee, K. and Saleh, A.A., 2024. Engineering tumor-colonizing E. coli Nissle 1917 for detection and treatment of colorectal neoplasia. *Nature Communications*, *15*(1), p.646.
143. Tumas, S., Meldgaard, T.S., Vaaben, T.H., Suarez Hernandez, S., Rasmussen, A.T., Vazquez-Uribe, R., Hadrup, S.R. and Sommer, M.O., 2023. Engineered E. coli Nissle 1917 for delivery of bioactive IL-2 for cancer immunotherapy. *Scientific Reports*, *13*(1), p.12506.
144. Chiang, C.J. and Hong, Y.H., In situ delivery of biobutyrate by probiotic Escherichia coli for cancer therapy, Sci. Rep. 11 (2021), 18172.
145. https://ec.europa.eu/commission/presscorner/detail/en/ip_23_3890 (Released on July 2023, Accessed on May 2024)
146. Dadgostar, P., 2019. Antimicrobial resistance: implications and costs. *Infection and drug resistance*, pp.3903-3910.
147. Rice, L.B., 2008. Federal funding for the study of antimicrobial resistance in nosocomial pathogens: no ESKAPE. *The Journal of infectious diseases*, *197*(8), pp.1079-1081.
148. https://www.cdc.gov/drugresistance/pdf/threats-report/pseudomonas-aeruginosa-508.pdf (Released on December 2019, Accessed on May, 2024)
149. Mazzolini, R., Rodríguez-Arce, I., Fernández-Barat, L., Piñero-Lambea, C., Garrido, V., Rebollada-Merino, A., Motos, A., Torres, A., Grilló, M.J., Serrano, L. and Lluch-Senar, M., 2023. Engineered live bacteria suppress Pseudomonas aeruginosa infection in mouse lung and dissolve endotracheal-tube biofilms. *Nature Biotechnology*, pp.1-10.
150. Mortzfeld, B.M., Palmer, J.D., Bhattarai, S.K., Dupre, H.L., Mercado-Lubio, R., Silby, M.W., Bang, C., McCormick, B.A. and Bucci, V., 2022. Microcin MccI47 selectively inhibits enteric bacteria and reduces carbapenem-resistant Klebsiella pneumoniae colonization in vivo when administered via an engineered live biotherapeutic. *Gut Microbes*, *14*(1), p.2127633.
151. Forkus, B., Ritter, S., Vlysidis, M., Geldart, K. and Kaznessis, Y.N., 2017. Antimicrobial probiotics reduce Salmonella enterica in turkey gastrointestinal tracts. *Scientific reports*, *7*(1), p.40695.
152. Duan, F. and March, J.C., 2010. Engineered bacterial communication prevents Vibrio cholerae virulence in an infant mouse model. *Proceedings of the National Academy of Sciences*, *107*(25), pp.11260-11264.

153. Rineh, A., Kelso, M.J., Vatansever, F., Tegos, G.P. and Hamblin, M.R., 2014. Clostridium difficile infection: molecular pathogenesis and novel therapeutics. *Expert review of anti-infective therapy*, *12*(1), pp.131-150.
154. Becattini, S., Taur, Y. and Pamer, E.G., 2016. Antibiotic-induced changes in the intestinal microbiota and disease. *Trends in molecular medicine*, *22*(6), pp.458-478.
155. Cubillos-Ruiz, A., Alcantar, M.A., Donghia, N.M., Cárdenas, P., Avila-Pacheco, J. and Collins, J.J., 2022. An engineered live biotherapeutic for the prevention of antibiotic-induced dysbiosis. *Nature biomedical engineering*, *6*(7), pp.910-921.
156. Andersen, K.K., Strokappe, N.M., Hultberg, A., Truusalu, K., Smidt, I., Mikelsaar, R.H., Mikelsaar, M., Verrips, T., Hammarström, L. and Marcotte, H., 2016. Neutralization of Clostridium difficile toxin B mediated by engineered lactobacilli that produce single-domain antibodies. *Infection and immunity*, *84*(2), pp.395-406.
157. Esposito, G., Corpetti, C., Pesce, M., Seguella, L., Annunziata, G., Del Re, A., Vincenzi, M., Lattanzi, R., Lu, J., Sanseverino, W. and Sarnelli, G., 2021. A palmitoylethanolamide producing lactobacillus paracasei improves clostridium difficile toxin A-induced colitis. *Frontiers in Pharmacology*, *12*, p.639728.
158. Amberpet, R., Sistla, S., Parija, S.C. and Rameshkumar, R., 2018. Risk factors for intestinal colonization with vancomycin resistant enterococci'A prospective study in a level III pediatric intensive care unit. *Journal of Laboratory Physicians*, *10*(01), pp.089-094.
159. Thimmappa, L., Bhat, A., Hande, M., Mukhopadhyay, C., Devi, E., Nayak, B. and George, A., 2021. Risk factors for wound infection caused by Methicillin Resistant Staphylococcus aureus among hospitalized patients: a case control study from a tertiary care hospital in India. *African health sciences*, *21*(1), pp.286-94.
160. Geldart, K.G., Kommineni, S., Forbes, M., Hayward, M., Dunny, G.M., Salzman, N.H. and Kaznessis, Y.N., 2018. Engineered E. coli Nissle 1917 for the reduction of vancomycin-resistant Enterococcus in the intestinal tract. *Bioengineering & translational medicine*, *3*(3), pp.197-208.
161. Guan, C., Larson, P.J., Fleming, E., Tikhonov, A.P., Mootien, S., Grossman, T.H., Golino, C. and Oh, J., 2022. Engineering a "detect and destroy" skin probiotic to combat methicillin-resistant Staphylococcus aureus. *Plos one*, *17*(12), p.e0276795.
162. Garrido, V., Piñero-Lambea, C., Rodriguez-Arce, I., Paetzold, B., Ferrar, T., Weber, M., Garcia-Ramallo, E., Gallo, C., Collantes, M., Peñuelas, I. and Serrano, L., 2021. Engineering a genome-reduced bacterium to eliminate Staphylococcus aureus biofilms in vivo. Molecular Systems Biology, 17(10), p.e10145.
163. Amrofell, M.B., Rottinghaus, A.G. and Moon, T.S., 2020. Engineering microbial diagnostics and therapeutics with smart control. *Current opinion in biotechnology*, *66*, pp.11-17.
164. Browning, D.F. and Busby, S.J., 2016. Local and global regulation of transcription initiation in bacteria. *Nature Reviews Microbiology*, *14*(10), pp.638-650.
165. Gardner, T.S., Cantor, C.R. and Collins, J.J., 2000. Construction of a genetic toggle switch in Escherichia coli. *Nature*, *403*(6767), pp.339-342.

166. Elowitz, M.B. and Leibler, S., 2000. A synthetic oscillatory network of transcriptional regulators. *Nature*, *403*(6767), pp.335-338.
167. Cui, S., Lv, X., Xu, X., Chen, T., Zhang, H., Liu, Y., Li, J., Du, G., Ledesma-Amaro, R. and Liu, L., 2021. Multilayer genetic circuits for dynamic regulation of metabolic pathways. *ACS Synthetic Biology*, *10*(7), pp.1587-1597.
168. Gao, B. and Sun, Q., 2021. Programming gene expression in multicellular organisms for physiology modulation through engineered bacteria. *Nature Communications*, *12*(1), p.2689.
169. Hwang, I.Y., Koh, E., Wong, A., March, J.C., Bentley, W.E., Lee, Y.S. and Chang, M.W., 2017. Engineered probiotic Escherichia coli can eliminate and prevent Pseudomonas aeruginosa gut infection in animal models. *Nature communications*, *8*(1), p.15028.
170. Koh, E., Hwang, I.Y., Lee, H.L., De Sotto, R., Lee, J.W.J., Lee, Y.S., March, J.C. and Chang, M.W., 2022. Engineering probiotics to inhibit Clostridioides difficile infection by dynamic regulation of intestinal metabolism. *Nature Communications*, *13*(1), p.3834.
171. Chiang, C.J. and Huang, P.H., 2021. Metabolic engineering of probiotic Escherichia coli for cytolytic therapy of tumors. *Scientific reports*, *11*(1), p.5853.
172. Harimoto, T., Hahn, J., Chen, Y.Y., Im, J., Zhang, J., Hou, N., Li, F., Coker, C., Gray, K., Harr, N. and Chowdhury, S., 2022. A programmable encapsulation system improves delivery of therapeutic bacteria in mice. *Nature Biotechnology*, *40*(8), pp.1259-1269.
173. Chowdhury, S., Castro, S., Coker, C., Hinchliffe, T.E., Arpaia, N. and Danino, T., 2019. Programmable bacteria induce durable tumor regression and systemic antitumor immunity. *Nature medicine*, *25*(7), pp.1057-1063.
174. Zhou, T., Wu, J., Tang, H., Liu, D., Jeon, B.H., Jin, W., Wang, Y., Zheng, Y., Khan, A., Han, H. and Li, X., 2024. Enhancing tumor-specific recognition of programmable synthetic bacterial consortium for precision therapy of colorectal cancer. *npj Biofilms and Microbiomes*, *10*(1), p.6.
175. Entcheva, E. and Kay, M.W., 2021. Cardiac optogenetics: a decade of enlightenment. *Nature Reviews Cardiology*, *18*(5), pp.349-367.
176. Hoffman, S.M., Tang, A.Y. and Avalos, J.L., 2022. Optogenetics illuminates applications in microbial engineering. *Annual Review of Chemical and Biomolecular Engineering*, *13*, pp.373-403.
177. Levskaya, A., Chevalier, A.A., Tabor, J.J., Simpson, Z.B., Lavery, L.A., Levy, M., Davidson, E.A., Scouras, A., Ellington, A.D., Marcotte, E.M. and Voigt, C.A., 2005. Engineering Escherichia coli to see light. *Nature*, *438*(7067), pp.441-442.
178. Tabor, J.J., Levskaya, A. and Voigt, C.A., 2011. Multichromatic control of gene expression in Escherichia coli. *Journal of molecular biology*, *405*(2), pp.315-324.
179. Ohlendorf, R., Vidavski, R.R., Eldar, A., Moffat, K. and Möglich, A., 2012. From dusk till dawn: one-plasmid systems for light-regulated gene expression. *Journal of molecular biology*, *416*(4), pp.534-542.
180. Cui, M., Pang, G., Zhang, T., Sun, T., Zhang, L., Kang, R., Xue, X., Pan, H., Yang, C., Zhang, X. and Chang, J., 2021. Optotheranostic nanosystem with phone visual diagnosis and optogenetic microbial therapy for ulcerative colitis at-home care. *ACS nano*, *15*(4), pp.7040-7052.

181. Cui, M., Ling, W., Zhang, L., Li, Y., Liu, J., Sun, T., Ma, B., Lu, S., Pan, H., Pang, G. and Zhang, Y., 2023. Smartphone bioelectronic drug with visual colorimetric sensor and bulk nanoencapsulation optogenetic bacteria for chronic kidney disease theragnostics. *Chemical Engineering Journal*, *451*, p.138812.
182. Wu, C., Cui, M., Cai, L., Chen, C., Zhu, X., Wu, Y., Liu, J., Wang, H. and Zhang, Y., 2022. NIR-responsive photodynamic nanosystem combined with antitumor immune optogenetics bacteria for precise synergetic therapy. *ACS Applied Materials & Interfaces*, *14*(11), pp.13094-13106.
183. Pan, H., Sun, T., Cui, M., Ma, N., Yang, C., Liu, J., Pang, G., Liu, B., Li, L., Zhang, X. and Zhang, W., 2022. Light-sensitive Lactococcus lactis for microbe–gut–brain Axis regulating via upconversion optogenetic micro-nano system. *ACS nano*, *16*(4), pp.6049-6063.
184. Zhang, X., Pang, G., Sun, T., Liu, X., Pan, H., Zhang, Y., Liu, J., Chang, J., Wang, H. and Liu, D., 2023. A red light-controlled probiotic bio-system for in-situ gut-brain axis regulation. *Biomaterials*, *294*, p.122005.
185. Multamäki, E., García de Fuentes, A., Sieryi, O., Bykov, A., Gerken, U., Ranzani, A.T., Köhler, J., Meglinski, I., Möglich, A. and Takala, H., 2022. Optogenetic control of bacterial expression by red light. *ACS Synthetic Biology*, *11*(10), pp.3354-3367.
186. Bernstein, J.G., Garrity, P.A. and Boyden, E.S., 2012. Optogenetics and thermogenetics: technologies for controlling the activity of targeted cells within intact neural circuits. *Current opinion in neurobiology*, *22*(1), pp.61-71.
187. Hamada, F.N., Rosenzweig, M., Kang, K., Pulver, S.R., Ghezzi, A., Jegla, T.J. and Garrity, P.A., 2008. An internal thermal sensor controlling temperature preference in Drosophila. *Nature*, *454*(7201), pp.217-220.
188. Benzinger, T.H., 1969. Heat regulation: homeostasis of central temperature in man. *Physiological reviews*, *49*(4), pp.671-759.
189. Gomes da Silva, R., Campos Maia, A.S., da Silva, R.G. and Maia, A.S.C., 2013. Thermal balance and thermoregulation. *Principles of Animal Biometeorology*, pp.75-106.
190. Chao, Y.P., Chern, J.T., Wen, C.S. and Fu, H., 2002. Construction and characterization of thermo-inducible vectors derived from heat-sensitive lacI genes in combination with the T7 A1 promoter. *Biotechnology and bioengineering*, *79*(1), pp.1-8.
191. Villaverde, A., Benito, A., Viaplana, E. and Cubarsi, R., 1993. Fine regulation of cI857-controlled gene expression in continuous culture of recombinant Escherichia coli by temperature. *Applied and Environmental Microbiology*, *59*(10), pp.3485-3487.
192. Rodrigues, J.L., Sousa, M., Prather, K.L., Kluskens, L.D. and Rodrigues, L.R., 2014. Selection of Escherichia coli heat shock promoters toward their application as stress probes. *Journal of Biotechnology*, *188*, pp.61-71.
193. Piraner, D.I., Abedi, M.H., Moser, B.A., Lee-Gosselin, A. and Shapiro, M.G., 2017. Tunable thermal bioswitches for in vivo control of microbial therapeutics. *Nature chemical biology*, *13*(1), pp.75-80.
194. Chang, M., Hou, Z., Wang, M., Li, C. and Lin, J., 2021. Recent advances in hyperthermia therapy-based synergistic immunotherapy. *Advanced Materials*, *33*(4), p.2004788.

195. Abedi, M.H., Yao, M.S., Mittelstein, D.R., Bar-Zion, A., Swift, M.B., Lee-Gosselin, A., Barturen-Larrea, P., Buss, M.T. and Shapiro, M.G., 2022. Ultrasound-controllable engineered bacteria for cancer immunotherapy. *Nature Communications*, *13*(1), p.1585.
196. Li, L., Pan, H., Pang, G., Lang, H., Shen, Y., Sun, T., Zhang, Y., Liu, J., Chang, J., Kang, J. and Zheng, H., 2022. Precise thermal regulation of engineered bacteria secretion for breast cancer treatment in vivo. *ACS Synthetic Biology*, *11*(3), pp.1167-1177.
197. Chen, Y., Du, M., Yuan, Z., Chen, Z. and Yan, F., 2022. Spatiotemporal control of engineered bacteria to express interferon-γ by focused ultrasound for tumor immunotherapy. *Nature Communications*, *13*(1), p.4468.
198. Fan, J.X., Li, Z.H., Liu, X.H., Zheng, D.W., Chen, Y. and Zhang, X.Z., 2018. Bacteria-mediated tumor therapy utilizing photothermally-controlled TNF-α expression via oral administration. *Nano letters*, *18*(4), pp.2373-2380.
199. Ma, X., Liang, X., Li, Y., Feng, Q., Cheng, K., Ma, N., Zhu, F., Guo, X., Yue, Y., Liu, G. and Zhang, T., 2023. Modular-designed engineered bacteria for precision tumor immunotherapy via spatiotemporal manipulation by magnetic field. *Nature Communications*, *14*(1), p.1606.

Chapter 2

MOTIVATION AND OUTLINE

2.1. Challenges associated with eLBP development

All the examples mentioned in the previous chapter demonstrate that eLBPs offer the possibility to produce complex therapeutic molecules directly at the host target site to treat several disease conditions. However, despite the success of several eLBP candidates in both preclinical animal models and human Phase I clinical trials, most **have failed to demonstrate efficacy** at the Phase II/III stage of clinical trials (Sahoo and Mishra., 2022). Although clinical efficacy depends on multiple factors, ensuring that the therapeutic payload is available at the necessary **concentration** at the target site is a vital factor. The limited success of most eLBP candidates indicates that their design needs further improvement to reach efficacy endpoints in late-stage clinical trials. One approach has involved using engineered therapeutic biomolecules with enhanced stability and bioactivity (Li et al., 2021). Although these biomolecular variants offer superior therapeutic capabilities, their heterologous expression can cause a significant metabolic burden on the microbial chassis (Glick., 1995; Zhang et al., 2016). Therefore, to achieve optimal efficiency without compromising the performance of eLBPs, **better control** of therapeutic production and release kinetics is necessary.

Advanced genetic switches responsive to specific triggers (chemical, light, heat) can sustain the regulated production of therapeutic molecules, as reported previously (Refer to Sections 1.3.1 - 1.3.3). Although these "**stimuli-responsive**" eLBP candidates have shown promising results in regulating the production of therapeutic cytokines, nanobodies and antimicrobial proteins, there has been limited research to investigate their performance for therapeutic proteins/peptides that require post-translational modification to be effective. Genetic designs that regulate the production of therapeutic compounds/macromolecules produced through enzymatic cascades have previously been prone to **high basal expression** (Sankaran et al., 2019) or have resulted in **reduced output yield** (Macek et al., 2019). In addition, the expression of such complex macromolecules needs to strike a balance between achieving sufficient concentrations and preventing excessive intracellular

toxicity. Therefore, developing a genetic design that could offer **stringent control** over the therapeutic macromolecule production would be a significant step forward in creating **better "stimuli-responsive" eLBP candidates**.

Another critical factor for the success of an eLBP candidate is its intrinsic capability to colonize the host target site and deliver therapeutic molecules. Due to their genetic tractability, eLBP development has relied on a **limited number** of microbial candidates, such as *E. coli* and *L. lactis* (Rutter et al., 2022). These strains typically have low colonization ability and are only suitable for a few host target sites, with the gut environment being widely tested for therapeutic applications. The limited selection of microbial strains suitable for genetic manipulation restricts their clinical application, and **alternate microbial candidates** are needed to diversify the current eLBP portfolio (Cruz et al., 2022). **Commensal** bacterial strains, such as *Bacteroides thetaiotaomicron* and *Bifidobacterium longum*, have garnered interest in the last decade due to their innate capacity to inhabit and colonize the human gut (Mishra and Imlay., 2013; Zhang et al., 2019). Extensive research efforts have expanded the genetic toolbox for these bacterial strains, paving the way for developing superior eLBP candidates (Lai et al., 2022; Zuo et al., 2020). However, as **obligate-anaerobes**, these strains require specialized growth chambers for cultivation and genetic modification, making the process **cost-intensive** and **cumbersome** (Hong et al., 2021). Hence, there is a need for **alternative human commensal strains** that can **colonize** the targeted host site but would **not have specialized requirements** regarding their **propagation** and **genetic modification**. Expanding the **genetic toolbox** of such bacterial strains would streamline the entire eLBP development process, making its therapeutic landscape expansion more cost-effective.

2.2. Outline of this thesis

This thesis aims to tackle two challenges associated with eLBP development: (i) Developing genetic design to attain strict control over post-translationally modified therapeutic production and (ii) Identifying genetic parts for recombinant protein expression in commensal bacteria.

The first part of this thesis (**Chapter 3**) describes the development of a "stimuli-responsive" bacterial strain that can regulate the production of a ribosomally synthesized and post-translationally modified peptide (RiPP), darobactin. Darobactin is a promising RiPP candidate

with a small molecular weight (<1 kDa) that has shown antimicrobial activity against several Gram-negative pathogens, leading to a reduction in the overall bacterial load in animal infection models (Imai et al., 2019). Although previous attempts at heterologous expression of darobactin in *E. coli* have been successful, it exhibited high basal expression when regulated using chemical inducers like IPTG (Groß et al., 2021). The "leakiness" of chemical-inducible systems can lead to imbalanced gene expression, inducing spontaneous mutations in the recombinant genetic modules (Inda and Lu, 2020) and compromising the overall fitness of the microbial strain (Tanna et al., 2021). In addition, the basal gene expression level could be further amplified in the host, as many well-studied chemical inducers are structurally similar to sugars commonly consumed in the diet and could lead to significant cross-reactivity (Durmusoglu et al., 2023). The ineffective regulation of darobactin production could expose the pathogenic strains to sub-inhibitory darobactin concentration, thereby making them prone to develop resistance against darobactin. Therefore, gene expression designs that undergo minimal cross-talk with host-associated factors would be ideal for regulating therapeutic delivery. Such a "genetically orthogonal" system would be capable of repressing gene expression in the absence of stimuli without compromising the overall gene expression level in its presence (Brooks and Alper., 2021). The genetically orthogonal circuit-based drug delivery approach could ensure the production of darobactin in response to infection-related factors, facilitating pathogen clearance and simultaneously preventing antimicrobial resistance with minimal external intervention. Conventional orthogonal systems are generally designed to sense and respond to disease-related chemical biomarkers like quorum sensing molecules (Hwang et al., 2017). However, the responses of these biomarkers can vary widely due to the cross-talk mediated by similar signaling molecules produced by the resident microbiome (Xue et al., 2021). This variable behavior in different patient microbiomes could significantly reduce the effectiveness of treatment and potentially contribute to antimicrobial resistance. In a recent study, regulating antimicrobial production using near-infrared light (NIR) helped eliminate *P. aeruginosa* PAO1 infection from mouse wound healing models (Gao et al., 2023). To eradicate the pathogenic *P. aeruginosa* PAO1 strain, an attenuated strain of *P. aeruginosa* was engineered to undergo lysis and release a chimeric pyocin when exposed to NIR light. Although this approach can effectively treat topical infections, the constant dependence on externally applied stimuli increases the complexity and treatment costs during extended application periods. In addition, the intrinsic virulence of attenuated strains, the narrow target spectrum, and the high molecular weight

(~90 kDa) of the pyocin also significantly restrict the feasibility of such an approach (Paškevičius et al., 2022).

The superior ADMET (absorption, distribution, metabolism, excretion, and toxicity) profile, broad-spectrum activity, and cyclic structure-based proteolytic stability make darobactin a better antimicrobial candidate than pyocins (Fu et al., 2021; Pfeiffer et al., 2024). Therefore, creating a genetically orthogonal circuit design to stimulate darobactin production within a shorter induction period, without external intervention, would make the bacterial infection treatment approach more feasible. The onset of fever is closely linked to bacterial infections and can cause temperatures as high as 42°C in infected adults (Mahadevan and Garmel, 2012). A genetic circuit capable of detecting this increase in ambient temperature could activate the production of darobactin from the engineered strain to then eliminate the bacterial pathogens. A recent report showed that engineered bacteria containing protein-based thermal switches could respond to increased temperature within the host (Piraner et al., 2017). This ability to sense changes in the host's internal temperature can eliminate the need for bacterial activation by an external trigger. Therefore, I used the $TlpA_{39}$-based thermal switch module to enable darobactin production in response to fever-like conditions. In line with previous observations based on fluorescent and matrix proteins (Kan et al., 2020), thermal regulation of darobactin production from the non-endotoxic *E. coli* strain (ClearColi) was possible. However, the production of darobactin decreased compared to the chemically inducible system, indicating insufficient expression of darobactin precursor peptide from the P_{tlpA} promoter.

Therefore, an alternative approach was required to improve darobactin production (signal output) without compromising thermal regulation (signal input). One way to accomplish this would be by creating an "amplifier" circuit (Karig and Weiss., 2005). "Amplifier" genetic circuits consist of two main modules: the sensor, which recognizes the input signal, and the amplifier, which boosts the signal output level as the actuation response. Such an amplifier could also be further fine-tuned at both the transcriptional and translational levels to achieve precise regulation over the signal output production (Wan et al., 2019). Multiple reports have shown that high titers of darobactin can be obtained from *E. coli* using the P_{T7} promoter-based expression vectors (Groß et al., 2021; Wuisan et al., 2021). This is because the T7 RNA polymerase (T7-RNAP) responsible for transcription initiation from the P_{T7} promoter has a rapid RNA elongation rate (~5-fold faster) compared to the native *E. coli* RNA polymerase (Tegel et al., 2011). Considering this, I decided to

create a "thermo-amplifier" circuit that combined the high transcriptional strength of the T7-RNAP/P_{T7} promoter system with the thermal regulation capabilities of the $TlpA_{39}$-P_{tlpA} system. To achieve orthogonal control over darobactin production, the "thermo-amplifier" circuit was incorporated into the probiotic *E. coli* Nissle 1917 (EcN) strain. The lack of chromosomally expressed T7-RNAP would ensure no cross-talk between the "amplifier" module and the microbial chassis and prevent basal level darobactin expression at lower incubation temperature. This approach minimizes the metabolic burden on the microbial chassis and reduces the chances of generating mutant populations (Aggarwal et al., 2020). Darobactin production by the "thermo-amplifier" EcN strain was further assessed at different incubation temperatures and tested for its ability to inhibit the growth of the pathogenic *P. aeruginosa* PAO1 strain. "Amplifier" genetic circuits are generally prone to prolonged response time because of the additional layers of gene regulation (Wang et al., 2013). Therefore, it was essential to determine the minimal time required for sufficient signal output, in this case, the darobactin concentration produced by the "thermo-amplifier" EcN strain. A genetic circuit with rapid activation dynamics reduces the induction period and enhances the therapeutic potential of the engineered strain. Transcript-level analysis by Quantitative reverse transcription polymerase chain reaction (RT-qPCR) confirmed that within ~6 hours, the "thermo-amplifier" circuit could derepress T7-RNAP production and activate darobactin production.

Stabilizing the recombinant vector in the microbial chassis is crucial to ensure optimal therapeutic performance (Murali and Mansell., 2024). Despite being a non-colonizer, the EcN strain can undergo cellular growth and division during its transient passage in the host (Conway et al., 2004). Although an "amplifier" genetic circuit helps prevent stress generation on cellular metabolism, the microbial chassis is prone to plasmid loss from dividing daughter cells without selection pressure (Son et al., 2021). Maintaining external selection pressure to facilitate plasmid retention in the engineered strains is impractical and prone to failure. On the other hand, stabilization systems based on internal selection pressure have shown promising results for retaining plasmids in engineered strains (Peubez et al., 2010). Two plasmid stabilization systems based on nutrient auxotrophy (D-alanine auxotrophy) and toxin-antitoxin (Txe-Axe) modules were tested in *E. coli*. The outcomes of this testing revealed similar efficiency of both plasmid stabilization systems, so I employed the Txe-Axe module to stabilize the "thermo-amplifier" genetic circuits in EcN due to its ease of use across related *E. coli* strains (Fedorec et al., 2019). The orthogonality of the Txe-

Axe module with the darobactin production capacity of the "thermo-amplifier" circuit was further confirmed in EcN to dictate the system's applicability.

Considering that rapid clearance of infection is preferable, it must be ensured that the microbial chassis cannot harm the host. Although EcN is a widely accepted probiotic, it contains a polyketide synthase (pks) cluster that encodes the chemically unstable metabolite known as colibactin (Massip et al., 2019). The genotoxicity of colibactin is a significant concern regarding the use of EcN-based therapeutic intervention agents. Despite an ongoing debate in the scientific community about whether colibactin could have adverse effects on the host, excluding it from the engineered strain is advisable (Kalantari et al., 2023). In accordance with biosafety measures, the "thermo-amplifier" genetic circuit was incorporated into a colibactin-deficient (*Δclb* EcN) strain of EcN. Basal protein expression levels, induction timespan, and post-induction darobactin production were evaluated in the colibactin-deficient EcN strain. In addition to addressing the safety of the engineered strains, it is well known that host-associated exocrine secretions (such as bile) and nutrient concentrations can impact bacterial growth (Adediran et al., 2014) and therapeutic production (Guzmán-Trampe et al., 2017). Therefore, the "thermo-amplifier" *Δclb* EcN strain was cultivated in the presence of bile and reduced nutrient composition to evaluate their influence on darobactin production. Finally, detailed insights about improvements in strain design are discussed as an outlook for further development towards preclinical testing of the engineered "thermo-amplifier" strain.

The second part of the thesis (**Chapters 4 and 5**) addresses the challenge of expanding the limited genetic toolbox of the human commensal and probiotic strain, *Lactiplantibacillus plantarum* WCFS1, by screening for suitable genetic parts. The microbial chassis shows promise for developing bacterial therapeutics due to its ability to colonize different host microbiomes and its amenability to genetic modification (van den Nieuwboer et al., 2016). Previous studies have shown that both natural and engineered *L. plantarum* strains can exhibit certain therapeutic benefits in the oral cavity, respiratory tract, and vaginal environment (Oh et al., 2007; Du et al., 2022; Cappello et al., 2023). These unique features of *L. plantarum* have inspired researchers to use it as a therapeutic platform for treating metabolic disorders (Luo et al., 2021), pathogenic infection (Li et al., 2023) and cancer (Shen et al., 2024). Two essential criteria that dictated the

success of these engineered *L. plantarum* strains involve -1) High gene expression levels and 2) Stable retention of recombinant modules. The genetic components currently available for modifying *L. plantarum* have either been obtained from their own genome or that of related bacterial species. A detailed understanding of these genetic components has been crucial for determining the rational design of recombinant genetic circuits. However, despite these advances, the genetic toolkit for engineering *L. plantarum* is still limited to a few well-characterized genetic parts (Blanch-Asensio et al., 2024).

Although stimuli-responsive genetic circuits are crucial for specialized therapeutic applications, many approaches still rely on constitutive promoters to continuously deliver therapeutic molecules. This straightforward method of expressing recombinant modules is particularly useful in situations where the constitutive promoter needs to express molecules that are:- 1) Not toxic to healthy tissue, 2) Have a limited half-life at the target site, and 3) Do not confer a fitness advantage to the microbial chassis. Finding strong constitutive promoters that can facilitate the expression of therapeutic molecules at adequate levels can help overcome the current constraints of bacterial therapeutic applications (Mugwanda et al., 2023). An ideal constitutive promoter should be able to - 1) Efficiently utilize the intrinsic transcriptional machinery and 2) Not impose a metabolic burden on the microbial chassis. In the past two decades, there has been an increasing emphasis on finding alternative strong constitutive promoters that can meet both conditions (Son and Jeong., 2020). Certain studies have indicated that specific promoters can initiate gene transcription in bacterial species that are phylogenetically distant from each other. For example, the P_R promoter, originally isolated from the lambda (λ) bacteriophage, has been shown to drive gene expression in both *E. coli* (Ohlendorf et al., 2012) and *L. lactis* (Pan et al., 2022). Incidentally, the P_R promoter also drives gene expression from the thermo-responsive TcI-regulated genetic circuit in *E. coli* (as mentioned in Section 1.3.3). Therefore, to assess the transcriptional activity, the promoters of both the TcI- and TlpA-regulated genetic circuits were evaluated in *L. plantarum*. Despite the P_R promoter's poor performance, the P_{tlpA} promoter showed high transcriptional strength in *L. plantarum* for mCherry reporter protein production. In addition to production, it is crucial to facilitate the extracellular delivery of the recombinant protein for most bacterial therapeutic approaches. Protein overexpression can overload the membrane exporters of the microbial chassis, leading to reduced secretion capacity of a recombinant protein (Pedrolli et al., 2019). Therefore,

the P_{tlpA} promoter was further evaluated for its production and secretion capacity of the Staphylococcal nuclease (sNucA) protein.

Expression and secretion of heterologous proteins may reduce the fitness of the engineered strain unless there is selective pressure to maintain the recombinant modules (Russell et al., 2022). Like *E. coli*, stable plasmid retention in Lactobacilli has also mainly depended on auxotrophy-based plasmid stabilization systems. In cases of auxotrophy, deleting an essential protein-encoding gene from the bacterial genome makes the bacterial chassis dependent on external supplementation of the essential metabolite. Reincorporating the essential gene in the recombinant plasmid allows bacteria to survive without external metabolite supplementation and promotes stable plasmid retention. Although this method is effective for short-term therapy, it is highly susceptible to breakdown due to horizontal gene transfer (Hayashi et al., 2024) or the direct presence of metabolites at the host target site (Siguenza et al., 2024). In addition, auxotrophic variants require the creation of genetic knockouts, which is a time-consuming and labor-intensive process (Kim et al., 2023). D-alanine auxotrophy is often utilized to ensure the stable retention of recombinant plasmids in *L. plantarum* (Nguyen et al., 2011; Sak-Ubol et al., 2016). However, recent evidence suggests that D-amino acids occur naturally in the human body (Kimura et al., 2024), which could reduce the auxotrophic efficacy and cause eventual loss of the recombinant plasmid. Therefore, screening for alternative plasmid retention strategies that can overcome the limitations imposed by nutrient auxotrophy is essential. A recent study has highlighted that the type II toxin-antitoxin module, Txe-Axe, could enable plasmid retention in *E. coli* for over 30 days without antibiotic supplementation-based selection pressure (Fedorec et al., 2019). Bioinformatic analysis of bacterial species related to *L. plantarum* could also help identify similar type II toxin-antitoxin (TA) systems, which may have comparable plasmid stabilization efficiency. Optimizing the plasmid retention system based on the toxin-antitoxin module for *L. plantarum* could simplify genetic manipulation and overcome the limitations of auxotrophic systems. An ideal system for plasmid retention should also not disrupt the microbial chassis' protein production and secretion machinery. An independent assessment of these features in nutrient-enriched and nutrient-starved media can help determine the effectiveness of the toxin-antitoxin modules for plasmid retention. Altogether, these insights could help expand the design criteria for engineering *L. plantarum* strains as therapeutic agents to address disease-related clinical conditions.

2.3. References

1. Sahoo, S. and Misra, N., 2022. Affordable Therapeutics Through Engineered Microbes. In *Microbial Engineering for Therapeutics* (pp. 327-343). Singapore: Springer Nature Singapore.
2. Li, N., Tucker, A., Gao, J.R., Renaud, L., James, M., Castillo, M., Galvan, S., Jain, R., Putman, R., Marr, S. and Carlin, D., 2021. Development of an engineered probiotic for the treatment of branched chain amino acid related metabolic diseases.
3. Glick, B.R., 1995. Metabolic load and heterologous gene expression. *Biotechnology advances*, *13*(2), pp.247-261.
4. Zhang, M.M., Wang, Y., Ang, E.L. and Zhao, H., 2016. Engineering microbial hosts for production of bacterial natural products. *Natural product reports*, *33*(8), pp.963-987.
5. Sankaran, S., Becker, J., Wittmann, C. and Del Campo, A., 2019. Optoregulated drug release from an engineered living material: self-replenishing drug depots for long-term, light-regulated delivery. *Small*, *15*(5), p.1804717.
6. Macek, B., Forchhammer, K., Hardouin, J., Weber-Ban, E., Grangeasse, C. and Mijakovic, I., 2019. Protein post-translational modifications in bacteria. *Nature Reviews Microbiology*, *17*(11), pp.651-664.
7. Rutter, J.W., Dekker, L., Owen, K.A. and Barnes, C.P., 2022. Microbiome engineering: engineered live biotherapeutic products for treating human disease. *Frontiers in Bioengineering and Biotechnology*, *10*, p.1000873.
8. Cruz, K.C.P., Enekegho, L.O. and Stuart, D.T., 2022. Bioengineered probiotics: synthetic biology can provide live cell therapeutics for the treatment of foodborne diseases. *Frontiers in Bioengineering and Biotechnology*, *10*, p.890479.
9. Mishra, S. and Imlay, J.A., 2013. An anaerobic bacterium, Bacteroides thetaiotaomicron, uses a consortium of enzymes to scavenge hydrogen peroxide. *Molecular microbiology*, *90*(6), pp.1356-1371.
10. Zhang, C., Yu, Z., Zhao, J., Zhang, H., Zhai, Q. and Chen, W., 2019. Colonization and probiotic function of Bifidobacterium longum. *Journal of Functional Foods*, *53*, pp.157-165.
11. Lai, Y., Hayashi, N. and Lu, T.K., 2022. Engineering the human gut commensal Bacteroides thetaiotaomicron with synthetic biology. *Current Opinion in Chemical Biology*, *70*, p.102178.

12. Zuo, F., Chen, S. and Marcotte, H., 2020. Engineer probiotic bifidobacteria for food and biomedical applications-Current status and future prospective. *Biotechnology Advances*, *45*, p.107654.
13. Hong, W., Rao, F.Q., Zhao, X.X., Guo, Z.Y., Chen, Y.M., Wang, B., Guan, Z.Z. and Qi, X.L., 2021. An inexpensive anaerobic chamber for the genetic manipulation of strictly anaerobic bacteria. *Anaerobe*, *69*, p.102349.
14. Imai Y, Meyer KJ, Iinishi A, Favre-Godal Q, Green R, Manuse S, Caboni M, Mori M, Niles S, Ghiglieri M, Honrao C. A new antibiotic selectively kills Gram-negative pathogens. Nature. 2019 Dec 19;576(7787):459-64.
15. Groß S, Panter F, Pogorevc D, Seyfert CE, Deckarm S, Bader CD, Herrmann J, Müller R. Improved broad-spectrum antibiotics against Gram-negative pathogens via darobactin biosynthetic pathway engineering. Chemical science. 2021;12(35):11882-93.
16. Inda, M.E. and Lu, T.K., 2020. Microbes as biosensors. *Annual Review of Microbiology*, *74*(1), pp.337-359.
17. Tanna, T., Ramachanderan, R. and Platt, R.J., 2021. Engineered bacteria to report gut function: technologies and implementation. *Current opinion in microbiology*, *59*, pp.24-33.
18. Durmusoglu, D., Haller, D.J., Al'Abri, I.S., Day, K., Sands, C., Clark, A., San-Miguel, A., Vazquez-Uribe, R., Sommer, M.O. and Crook, N.C., 2023. Programming Probiotics: Diet-responsive gene expression and colonization control in engineered S. boulardii. *ACS Synthetic Biology*.
19. Brooks, S.M. and Alper, H.S., 2021. Applications, challenges, and needs for employing synthetic biology beyond the lab. *Nature Communications*, *12*(1), p.1390.
20. Hwang, I.Y., Koh, E., Wong, A., March, J.C., Bentley, W.E., Lee, Y.S. and Chang, M.W., 2017. Engineered probiotic Escherichia coli can eliminate and prevent Pseudomonas aeruginosa gut infection in animal models. *Nature communications*, *8*(1), p.15028.
21. Xue, J., Chi, L., Tu, P., Lai, Y., Liu, C.W., Ru, H. and Lu, K., 2021. Detection of gut microbiota and pathogen produced N-acyl homoserine in host circulation and tissues. *npj Biofilms and Microbiomes*, *7*(1), p.53.
22. Gao, Y., Wei, J., Pu, L., Fu, S., Xing, X., Zhang, R. and Jin, F., 2023. Remotely controllable engineered bacteria for targeted therapy of Pseudomonas aeruginosa infection. *ACS Synthetic Biology*, *12*(7), pp.1961-1971.

23. Paškevičius, Š., Dapkutė, V., Misiūnas, A., Balzaris, M., Thommes, P., Sattar, A., Gleba, Y. and Ražanskienė, A., 2022. Chimeric bacteriocin S5-PmnH engineered by domain swapping efficiently controls Pseudomonas aeruginosa infection in murine keratitis and lung models. *Scientific reports*, *12*(1), p.5865.
24. Fu, Y., Jaarsma, A.H. and Kuipers, O.P., 2021. Antiviral activities and applications of ribosomally synthesized and post-translationally modified peptides (RiPPs). *Cellular and Molecular Life Sciences*, *78*(8), pp.3921-3940.
25. Pfeiffer, I.P.M., Schröder, M.P. and Mordhorst, S., 2024. Opportunities and challenges of RiPP-based therapeutics. *Natural Product Reports*.
26. Mahadevan, S.V. and Garmel, G.M. eds., 2012. *An introduction to clinical emergency medicine*. Cambridge university press.
27. Piraner, D.I., Abedi, M.H., Moser, B.A., Lee-Gosselin, A. and Shapiro, M.G., 2017. Tunable thermal bioswitches for in vivo control of microbial therapeutics. *Nature chemical biology*, *13*(1), pp.75-80.
28. Kan, A., Gelfat, I., Emani, S., Praveschotinunt, P. and Joshi, N.S., 2020. Plasmid vectors for in vivo selection-free use with the probiotic E. coli Nissle 1917. *ACS synthetic biology*, *10*(1), pp.94-106.
29. Karig, D. and Weiss, R., 2005. Signal-amplifying genetic circuit enables in vivo observation of weak promoter activation in the Rhl quorum sensing system. *Biotechnology and bioengineering*, *89*(6), pp.709-718.
30. Wan, X., Volpetti, F., Petrova, E., French, C., Maerkl, S.J. and Wang, B., 2019. Cascaded amplifying circuits enable ultrasensitive cellular sensors for toxic metals. *Nature chemical biology*, *15*(5), pp.540-548.
31. Wuisan, Z.G., Kresna, I.D.M., Böhringer, N., Lewis, K. and Schäberle, T.F., 2021. Optimization of heterologous Darobactin A expression and identification of the minimal biosynthetic gene cluster. *Metabolic Engineering*, *66*, pp.123-136.
32. Tegel, H., Ottosson, J. and Hober, S., 2011. Enhancing the protein production levels in Escherichia coli with a strong promoter. *The FEBS journal*, *278*(5), pp.729-739.
33. Aggarwal, N., Breedon, A.M.E., Davis, C.M., Hwang, I.Y. and Chang, M.W., 2020. Engineering probiotics for therapeutic applications: recent examples and translational outlook. *Current opinion in biotechnology*, *65*, pp.171-179.

34. Wang, B., Barahona, M. and Buck, M., 2013. A modular cell-based biosensor using engineered genetic logic circuits to detect and integrate multiple environmental signals. *Biosensors and Bioelectronics*, *40*(1), pp.368-376.
35. Murali, S.K. and Mansell, T.J., 2024. Next generation probiotics: Engineering live biotherapeutics. *Biotechnology Advances*, p.108336.
36. Conway, T., Krogfelt, K.A. and Cohen, P.S., 2004. The life of commensal Escherichia coli in the mammalian intestine. *EcoSal Plus*, *1*(1), pp.10-1128.
37. Son, H.I., Weiss, A. and You, L., 2021. Design patterns for engineering genetic stability. *Current opinion in biomedical engineering*, *19*, p.100297.
38. Peubez, I., Chaudet, N., Mignon, C., Hild, G., Husson, S., Courtois, V., De Luca, K., Speck, D. and Sodoyer, R., 2010. Antibiotic-free selection in E. coli: new considerations for optimal design and improved production. *Microbial cell factories*, *9*, pp.1-10.
39. Fedorec, A.J., Ozdemir, T., Doshi, A., Ho, Y.K., Rosa, L., Rutter, J., Velazquez, O., Pinheiro, V.B., Danino, T. and Barnes, C.P., 2019. Two new plasmid post-segregational killing mechanisms for the implementation of synthetic gene networks in Escherichia coli. *Iscience*, *14*, pp.323-334.
40. Massip, C., Branchu, P., Bossuet-Greif, N., Chagneau, C.V., Gaillard, D., Martin, P., Boury, M., Secher, T., Dubois, D., Nougayrède, J.P. and Oswald, E., 2019. Deciphering the interplay between the genotoxic and probiotic activities of Escherichia coli Nissle 1917. *PLoS pathogens*, *15*(9), p.e1008029.
41. Kalantari, A., James, M.J., Renaud, L.A., Perreault, M., Monahan, C.E., McDonald, M.N., Hava, D.L. and Isabella, V.M., 2023. Robust performance of a live bacterial therapeutic chassis lacking the colibactin gene cluster. *PLoS One*, *18*(2), p.e0280499.
42. Adediran, J., Leatham-Jensen, M.P., Mokszycki, M.E., Frimodt-Møller, J., Krogfelt, K.A., Kazmierczak, K., Kenney, L.J., Conway, T. and Cohen, P.S., 2014. An Escherichia coli Nissle 1917 missense mutant colonizes the streptomycin-treated mouse intestine better than the wild type but is not a better probiotic. *Infection and immunity*, *82*(2), pp.670-682.
43. Guzmán-Trampe, S., Ceapa, C.D., Manzo-Ruiz, M. and Sánchez, S., 2017. Synthetic biology era: Improving antibiotic's world. *Biochemical pharmacology*, *134*, pp.99-113.

44. van den Nieuwboer, M., van Hemert, S., Claassen, E. and de Vos, W.M., 2016. Lactobacillus plantarum WCFS 1 and its host interaction: a dozen years after the genome. *Microbial biotechnology*, *9*(4), pp.452-465.
45. Oh, Y., Varmanen, P., Han, X.Y., Bennett, G., Xu, Z., Lu, T. and Palva, A., 2007. Lactobacillus plantarum for oral peptide delivery. *Oral microbiology and immunology*, *22*(2), pp.140-144.
46. Du, T., Lei, A., Zhang, N. and Zhu, C., 2022. The beneficial role of probiotic Lactobacillus in respiratory diseases. *Frontiers in immunology*, *13*, p.908010.
47. Cappello, C., Acin-Albiac, M., Pinto, D., Polo, A., Filannino, P., Rinaldi, F., Gobbetti, M. and Di Cagno, R., 2023. Do nomadic lactobacilli fit as potential vaginal probiotics? The answer lies in a successful selective multi-step and scoring approach. *Microbial Cell Factories*, *22*(1), p.27.
48. Luo, J., Zhang, H., Lu, J., Ma, C. and Chen, T., 2021. Antidiabetic effect of an engineered bacterium Lactobacillus plantarum-pMG36e-GLP-1 in monkey model. *Synthetic and Systems Biotechnology*, *6*(4), pp.272-282.
49. Li, H., Jia, M., Qi, Q. and Wang, Q., 2023. Engineered probiotic Lactobacillus plantarum WCSF I for monitoring and treatment of Staphylococcus aureus infection. *Microbiology Spectrum*, *11*(6), pp.e01829-23.
50. Shen, H., Zhang, C., Li, S., Liang, Y., Lee, L.T., Aggarwal, N., Wun, K.S., Liu, J., Nadarajan, S.P., Weng, C. and Ling, H., 2024. Prodrug-conjugated tumor-seeking commensals for targeted cancer therapy. *Nature Communications*, *15*(1), p.4343.
51. Blanch-Asensio, M., Dey, S., Tadimarri, V.S. and Sankaran, S., 2024. Expanding the genetic programmability of Lactiplantibacillus plantarum. *Microbial Biotechnology*, *17*(1), p.e14335.
52. Mugwanda, K., Hamese, S., Van Zyl, W.F., Prinsloo, E., Du Plessis, M., Dicks, L.M. and Thimiri Govinda Raj, D.B., 2023. Recent advances in genetic tools for engineering probiotic lactic acid bacteria. *Bioscience Reports*, *43*(1), p.BSR20211299.
53. Son, J. and Jeong, K.J., 2020. Recent advances in synthetic biology for the engineering of lactic acid bacteria. *Biotechnology and Bioprocess Engineering*, *25*, pp.962-973.
54. Ohlendorf, R., Vidavski, R.R., Eldar, A., Moffat, K. and Möglich, A., 2012. From dusk till dawn: one-plasmid systems for light-regulated gene expression. *Journal of molecular biology*, *416*(4), pp.534-542.

55. Pan, H., Sun, T., Cui, M., Ma, N., Yang, C., Liu, J., Pang, G., Liu, B., Li, L., Zhang, X. and Zhang, W., 2022. Light-sensitive Lactococcus lactis for microbe–gut–brain axis regulating via upconversion optogenetic micro-nano system. *ACS nano*, *16*(4), pp.6049-6063.
56. Pedrolli, D.B., Ribeiro, N.V., Squizato, P.N., de Jesus, V.N., Cozetto, D.A., Tuma, R.B., Gracindo, A., Cesar, M.B., Freire, P.J., da Costa, A.F. and Lins, M.R., 2019. Engineering microbial living therapeutics: the synthetic biology toolbox. *Trends in biotechnology*, *37*(1), pp.100-115.
57. Russell, B.J., Brown, S.D., Siguenza, N., Mai, I., Saran, A.R., Lingaraju, A., Maissy, E.S., Machado, A.C.D., Pinto, A.F., Sanchez, C. and Rossitto, L.A., 2022. Intestinal transgene delivery with native E. coli chassis allows persistent physiological changes. *Cell*, *185*(17), pp.3263-3277.
58. Hayashi, N., Lai, Y., Fuerte-Stone, J., Mimee, M. and Lu, T.K., 2024. Cas9-assisted biological containment of a genetically engineered human commensal bacterium and genetic elements. *Nature Communications*, *15*(1), p.2096.
59. Siguenza, N., Brevi, A., Zhang, J.T., Pabani, A., Bhushan, A., Das, M., Ding, Y., Hasty, J., Ghosh, P. and Zarrinpar, A., 2024. Engineered bacterial therapeutics for detecting and treating CRC. *Trends in Cancer*.
60. Kim, K., Kang, M. and Cho, B.K., 2023. Systems and synthetic biology-driven engineering of live bacterial therapeutics. *Frontiers in Bioengineering and Biotechnology*, *11*, p.1267378.
61. Nguyen, T.T., Mathiesen, G., Fredriksen, L., Kittl, R., Nguyen, T.H., Eijsink, V.G., Haltrich, D. and Peterbauer, C.K., 2011. A food-grade system for inducible gene expression in Lactobacillus plantarum using an alanine racemase-encoding selection marker. *Journal of agricultural and food chemistry*, *59*(10), pp.5617-5624.
62. Sak-Ubol, S., Namvijitr, P., Pechsrichuang, P., Haltrich, D., Nguyen, T.H., Mathiesen, G., Eijsink, V.G. and Yamabhai, M., 2016. Secretory production of a beta-mannanase and a chitosanase using a Lactobacillus plantarum expression system. *Microbial Cell Factories*, *15*, pp.1-12.
63. Kimura, T., Sakai, S., Horio, M., Takahara, S., Ishigo, S., Nakane, M., Negishi, E., Imoto, H., Mita, M., Hamase, K. and Higa-Maekawa, Y., 2024. Kinetical analysis of D-alanine upon oral intake. *medRxiv*, pp.2024-05.

This chapter has been adapted from the preprint (Dey et al., 2024). Some sections of the text are identical to parts of that preprint, while other sections are substantively similar to parts of that preprint but expressed in different words. To avoid self-plagiarism and excessive citation, I am providing this note as a general citation without further citation in the body of the chapter.

Citation – Sourik Dey, Carsten E. Seyfert, Claudia Fink-Straube, Andreas M. Kany, Rolf Müller and Shrikrishnan Sankaran (2024) Thermally activated antibiotic production by probiotic bacteria for pathogen elimination. *bioRxiv*, pp.2024-02.

Contribution Report

Sourik Dey designed and constructed the recombinant plasmids, performed all the darobactin production and thermal regulation experiments, and analyzed the data. Carsten E. Seyfert provided the purified darobactin standard. Claudia Fink-Straube and Andreas M. Kany helped in the quantitative estimation of darobactin in the extracellular media. Shrikrishnan Sankaran conceived and oversaw the overall project. Sourik Dey and Shrikrishnan Sankaran wrote the manuscript. Carsten E. Seyfert and Rolf Müller revised the manuscript.

Chapter 3

THERMALLY ACTIVATED ANTIBIOTIC PRODUCTION BY PROBIOTIC BACTERIA FOR PATHOGEN ELIMINATION

3.1. Introduction

According to the Global Burden of Disease (GBD) study conducted in 2019, bacterial infections were identified as the second leading cause of death worldwide (Ikuta et al., 2022). The study showed that bacterial infections caused 7.7 million deaths in 2019, accounting for 13.6% of total deaths and equivalent to one in every eight deaths. Five bacterial strains - *Staphylococcus aureus, Streptococcus pneumoniae*, *Escherichia coli*, *Klebsiella pneumoniae*, and *Pseudomonas aeruginosa* - were responsible for most bacterial infection-related deaths across a broad age group. It has also become increasingly common for these pathogens to become less susceptible to currently available antibiotics, leading to the emergence of multi-drug resistant (MDR) pathogenic strains. The emergence of these MDR strains has become a significant concern for both international governments and the medical community. Unfortunately, due to the lack of financial incentives and several regulatory hurdles, developing new antibiotics has not kept pace with the increasing population of MDR pathogens (Årdal et al., 2020). In late-stage clinical studies, only 25% of newly developed antibiotics have successfully treated MDR pathogenic infections (Payne et al., 2007). One reason for the limited efficacy of these antibiotic candidates may be due to the ability of pathogenic strains to counteract their mechanism of action (MOA) and reduce their antimicrobial activity (Holmes et al., 2016). Therefore, identifying new antibiotic candidates with unique MOA is sought after to increase their efficacy and reduce the likelihood of developing antimicrobial resistance among pathogenic strains. In 2015, Kim Lewis and colleagues isolated a non-ribosomal peptide called teixobactin (molecular weight – 1243 Daltons) from a soil bacterium, *Eleftheria terrae*, that showed significant antimicrobial activity against methicillin-resistant *S. aureus (*MRSA) and *S. pneumoniae* in *in-vivo* mice models (Ling et al., 2015). The MOA involved binding to the conserved lipid motifs of the cell wall and preventing its synthesis in Gram-positive bacteria. In addition, no resistance was detected for teixobactin among the pathogenic strains, making it a promising candidate for further clinical testing. However, as teixobactin proved

ineffective against Gram-negative bacteria, the group started investigating alternate natural sources to find an equally effective antibiotic against those strains. In 2019, they discovered a new antibiotic called darobactin, which was highly effective in preventing infections caused by Gram-negative bacteria like *E. coli, K. pneumoniae*, and *P. aeruginosa* in mouse models (Imai et al., 2019). In addition, darobactin did not exhibit any antimicrobial activity against Gram-positive bacteria, including the human gut symbionts, *Bifidobacterium longum* and *Limosilactobacillus reuteri*. Darobactin is a ribosomally synthesized and post-translationally modified peptide produced by the Gram-negative nematophilic bacteria *Photorhabdus khanii* HGB1456. The darobactin biosynthetic gene cluster (BGC) encodes a linear DarA propeptide of 58 amino acids divided into the leader, core, and tail regions. The DarE enzyme catalyzes macrocyclic cross-linking within the DarA propeptide core, followed by leader and tail trimming to form the mature bicyclic heptapeptide, darobactin (**Figure 1A**). Darobactin has a net molecular weight of 965 Daltons (**Figure 1B**), which surpasses the molecular cutoff threshold (<600 Daltons) for penetrating the outer membrane of Gram-negative bacteria. Therefore, the researchers concluded that darobactin must interfere with the functioning of proteins on the outer membrane to exhibit antimicrobial activity. Cryogenic electron microscopy (cryo-EM) analysis revealed that darobactin could interact with the β-barrel assembly machinery (BAM) complex of Gram-negative bacteria (**Figure 1C**, Kaur et al., 2021). The BAM complex comprises five essential proteins (BamA-BamE), responsible for properly folding and inserting the outer membrane proteins (OMPs) onto the cell surface. The β-strand mimicking structure of darobactin allows it to bind and seal the lateral gate of the BamA protein (**Figure 1D**). By doing so, darobactin blocks the BamA-mediated OMP folding and translocation, crucial in maintaining bacterial cell viability (**Figure 1E**, Knowles et al., 2009). The MOA of darobactin involves targeting a conserved protein complex of Gram-negative bacteria, making it highly robust against resistance development. Owing to its superior antimicrobial properties, medicinal chemists have optimized the chemical synthesis route of darobactin using the Larock-based cyclization methods to produce darobactin on a multigram scale (Nesic et al., 2022; Lin et al., 2022). Besides chemical synthesis, significant progress has also been made to facilitate the heterologous expression of darobactin in alternate microbial chassis (Wuisan et al., 2021; Groß et al., 2021). The biosynthetic route for producing darobactin is not only important for economic upscaling but can also provide a unique opportunity for synthetic biologists to explore its potential for development as a "living therapeutic".

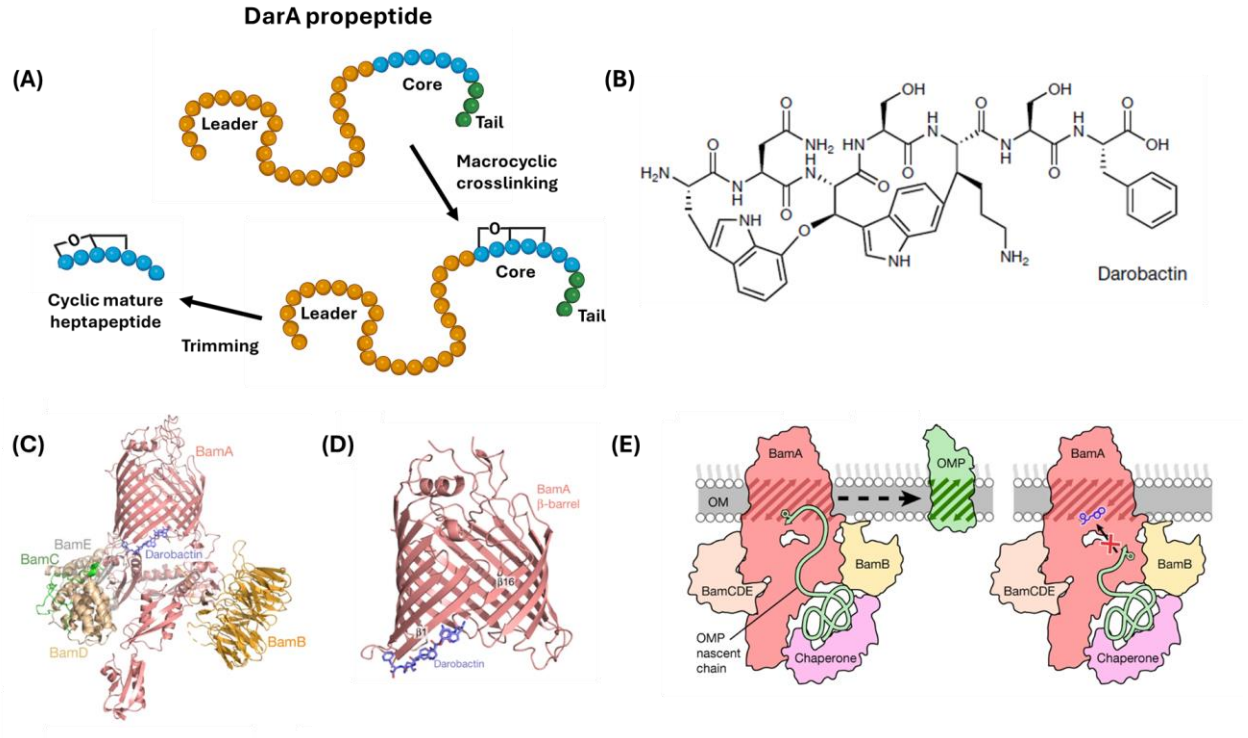

Figure 1. (A) Schematic diagram of the maturation process of the DarA propeptide, highlighted in three segments (leader, core, and tail). The heptapeptide core structure (W^1–N^2–W^3–S^4–K^5–S^6–F^7) undergoes an ether and C–C crosslinking. In the following steps, trimming and cleavage of the adjacent regions take place leading to the formation of the mature darobactin heptapeptide (B) Chemical structure of darobactin (Reprinted with permission, Imai et al., 2019; Copyright© Springer-Nature) (C) Three-dimensional structure of the BAM complex (BamA-BamE proteins) with bound darobactin (blue) resolved by cryo-EM 3.0 Å resolution (Reprinted with permission, Kaur et al., 2021; Copyright© Springer-Nature) (D) Crystal structure of the BamA β-barrel with bound darobactin, resolved to 2.3 Å resolution (Reprinted with permission, Kaur et al., 2021; Copyright© Springer-Nature) (E) In its native function, BamA recognizes the consensus β-signal in OMP nascent chains and folds and inserts them into the membrane (left). Darobactin binds to the dynamic lateral gate of BamA, blocking the β-signal binding site and thus preventing BamA from functioning (right) (Reprinted with permission, Kaur et al., 2021; Copyright© Springer-Nature)

Every year, more than a billion people worldwide suffer from bacterial gastroenteritis from consuming contaminated food and water containing Gram-negative pathogens (Fleckenstein et al., 2021). Most of these infections are mainly associated with bacterial strains like *Salmonella enteritidis* (Hennessy et al., 1996)*, Shigella flexneri* (Khaghani et al., 2014), *and Campylobacter jejuni* (Igwaran and Okoh., 2019). However, some opportunistic pathogens such as *Pseudomonas aeruginosa* (Chuang et al., 2014) and *Acinetobacter lwoffii* (Regalado et al., 2009) have also been reported to contribute to gastroenteritis development. Although most cases of infection resolve

naturally, some can result in severe conditions such as abdominal pain, dehydration, and bloody diarrhea, with rare cases even leading to death (Sattar and Singh, 2024). A recent report, jointly published by the European Food Safety Authority (EFSA) and the European Centre for Disease Prevention and Control (ECDC), has highlighted that *Salmonella* and *Campylobacter* bacterial strains have developed resistance to the carbapenem and fluoroquinolone class of antibiotics, which are commonly used to eliminate these bacterial pathogens. This study has raised concerns among healthcare providers as it indicates that certain antibiotics may no longer be effective in treating infections caused by certain strains of bacteria. Darobactin can therefore be a promising candidate for tackling these increasing number of antibiotic-resistant bacterial gastroenteritis cases. Studies have also demonstrated that strains developing resistance to darobactin through mutations in the BamA sequence generally exhibit reduced metabolic fitness and virulence (Imai et al., 2019; Walker and Black, 2021). However, the reduced essentiality of the BamA protein in MDR pathogens and the generation of darobactin-resistant mutants can render the continuous production of darobactin by a "living therapeutic" ineffective. Therefore, it is desirable to control the production of darobactin with a genetic switch that can be triggered by a stimulus associated with bacterial infections.

Previous research indicates that regulating antimicrobial production by quorum-sensing molecules (Hwang et al., 2017) and chemical biomarkers (Koh et al., 2022) can effectively prevent the growth of pathogenic bacteria. However, the limited specificity of these biomarkers can severely restrict the "living therapeutic" strain from eliminating a wide range of infection-causing pathogenic bacteria. Apart from chemical biomarkers, one of the most common physiological changes associated with bacterial infection is the onset of fever (pyrexia). The normal human body temperature ranges from 37.2°C to 38.3°C (Achaiah et al., 2021), and temperature elevation beyond this range can be classified as fever (Balli et al., 2022). Fever can be caused by infections from microorganisms like viruses, bacteria, or fungi (**Figure 2A**, Cole and Kramer., 2016) or due to over-activation of immune cells, especially in autoimmune disorders (**Figure 2A**, Carsons., 1996). Fever in humans is a natural response to infection and can limit the growth and spread of microbial agents (Casadevall., 2016). Antibiotic-resistant bacteria causing gastroenteritis can also induce the formation of endogenous pyrogens, which can increase the hypothalamic thermoregulation set-point in humans and result in fever (El-Radhi, 2018). Fever can rise as high as 40°C in infected individuals, especially in infants, older adults, and those with weakened immune systems (Dennehy,

2019). Depending on the severity of the infection, an elevated body temperature can last for several days, requiring prompt medical intervention. However, most of these bacteria can grow and tolerate temperatures well beyond 40°C, which means that increased temperature alone is not enough to eliminate them (D'Aoust and Doyle, 1989; Zaika, 1989; Doyle and Roman, 1981). Despite that, fever induction can be a suitable trigger to modulate the performance of thermally regulated "living therapeutic" strains and facilitate antimicrobial production to eliminate the infection-causing microbial agent.

Synthetic riboswitches and RNA thermometers (RNATs) were previously used to achieve temperature-regulated gene expression in microbial species (Wei et al., 2016). However, the high thermal transition range and leaky expression levels of RNATs have significantly restricted their application in "living therapeutics". In recent years, researchers have been exploring alternative transcription factors that could lead to more effective temperature-regulated protein production. One pioneering attempt by Piraner and colleagues led to a prominent understanding of the temperature-sensitive transcriptional repressor protein (TlpA) isolated from *Salmonella typhimurium* (Piraner et al., 2017). Although the original TlpA protein-based temperature regulation could only be observed at higher temperatures (42ºC), the authors could generate several TlpA variants responsive to lower thermal shifts. One variant was the $TlpA_{39}$ repressor protein, which was ideal for regulating protein production at the onset of fever-like conditions. The $TlpA_{39}$ protein (371 amino acids) consists of two parts: a short DNA-binding domain (DBD) and a long coiled-coil corepressor-binding domain (CBD) (**Figure 2B**). When in close proximity, the CBD region of the $TlpA_{39}$ monomer can form a homo-dimeric structure at temperatures lower than 39ºC (**Figure 2B**). The $TlpA_{39}$ repressor can recognize and specifically bind to its cognate operator site in the P_{tlpA} promoter in its homodimer state. This interaction between the $TlpA_{39}$ homodimer and the P_{tlpA} promoter prevents the housekeeping σ70-RNA Polymerase (σ70-RNAP) complex from initiating transcription from the P_{tlpA} promoter (**Figure 2C**). Upon crossing the thermal set-point of 39 ºC, the homodimer $TlpA_{39}$ protein rapidly uncoils in the CBD region and transitions back to its monomeric state in a cooperative manner (**Figure 2C**). The de-repression of the P_{tlpA} promoter then allows the σ70-RNAP complex to initiate gene transcription at the elevated temperature. In this chapter, I will discuss how I used the thermo-regulation capability of the $TlpA_{39}$ repressor protein to facilitate temperature-dependent darobactin production from a probiotic bacterial strain. The engineered strain inhibited darobactin production at 37°C, representing the average human

physiological temperature (**Figure 2D**). In contrast, the strain facilitated the production and extracellular release of darobactin at 40°C, representing a high-grade pyrexia (fever)-like condition to eliminate the opportunistic pathogen, *P. aeruginosa* PAO1, under *in-vitro* conditions (**Figure 2D**).

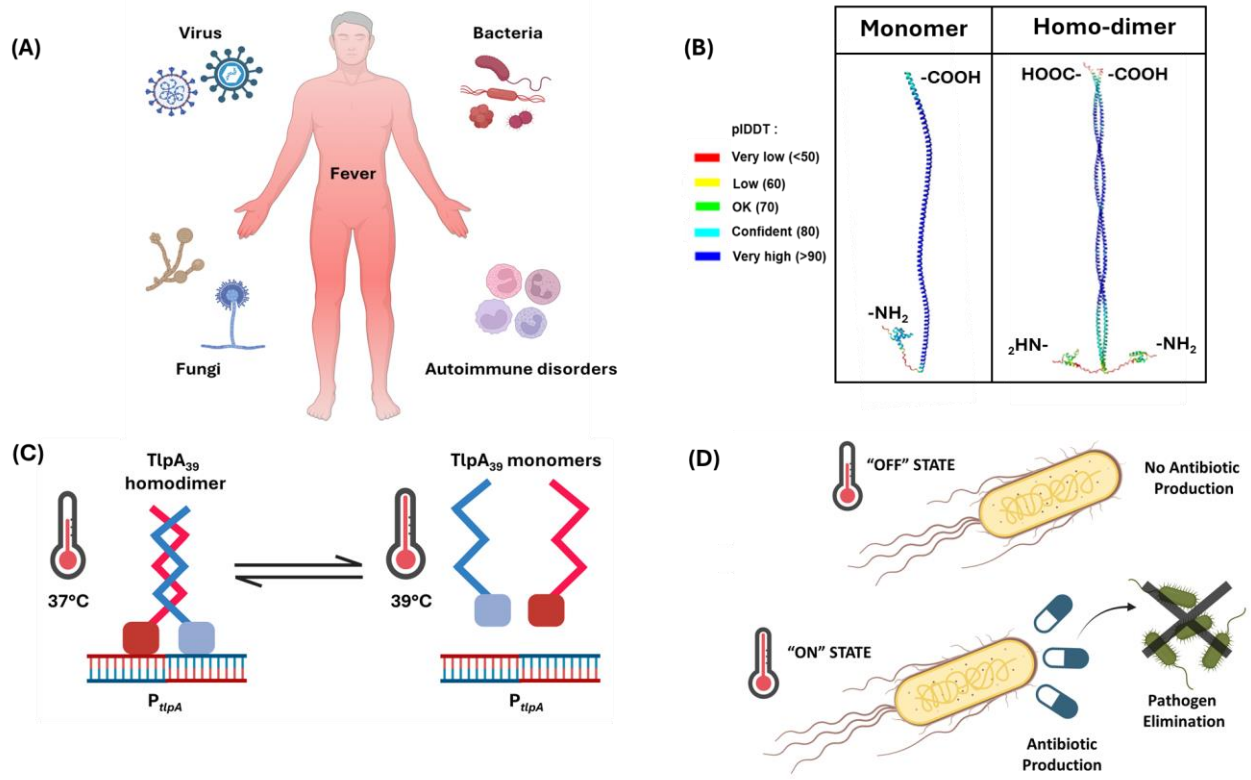

Figure 2. (A) Schematic diagram of the causative agents that lead to fever development in human hosts. The causative agents can range from viruses, bacteria, fungi, and inflammatory autoimmune disorders (B) AlphaFold 3D structure prediction of the $TlpA_{39}$ repressor protein in monomeric and homo-dimeric conformation. The coiled-coil domains help in stabilizing the homo-dimeric interaction of the $TlpA_{39}$ repressor protein. The per-residue confidence metric (pLDDT) highlights the confidence in the predicted structure represented by the respective color codes (C) Schematic diagram of the $TlpA_{39}$ repressor forming a homo-dimeric structure to bind and repress gene transcription from the P_{tlpA} promoter at physiological temperature (37°C). At elevated temperatures (>39°C), the thermodynamic stability of the homo-dimeric structure is compromised, and it reverts to its monomeric form, leading to de-repression of the P_{tlpA} promoter and allowing gene transcription (D) Schematic diagram of the engineered bacteria producing antibiotic in a thermo-responsive manner. In the "OFF" state (physiological temperature), the genetic circuit would repress the production and release of the antibiotic. However, in the "ON" state (elevated temperature), the genetic circuit would be activated, leading to production and release of the antibiotic, that would eventually eliminate the fever inducing pathogenic bacteria.

3.2. Materials and Methods

Media, bacterial strains and growth conditions

Luria-Bertani (LB) and Mueller-Hinton (MHI) bacterial growth media used for this study were procured from Carl-Roth. Unfractionated Bovine Bile (CAS No – 8008-63-7, B3883-25G) was purchased from Merck Millipore GmbH, Germany. NEB® 5-alpha Competent *E. coli* cells (C2987H) were routinely used for recombinant plasmid cloning and maintenance. The thermo-amplifier constructs were assembled in chemically competent ABLE-K cells (200172) procured from Agilent Technologies (USA). ClearColi BL21 DE3 cells were obtained from BioCat GmbH (Heidelberg, Germany) and the alanine auxotrophic *Δalr Δdadx* ClearColi BL21 DE3 strain was created by Gen-H GmbH (Heidelberg, Germany) using Cre-loxP recombination technique. ClearColi were grown in Luria-Bertani (LB) broth supplemented with 2% (w/v) sodium chloride (LB-NaCl), with additional supplementation of 40 µg/mL D-alanine for *Δalr Δdadx* ClearColi. The *E. coli* Nissle 1917 (EcN) strain was isolated from the commercially available Mutaflor® capsule (Ardeypharm GmbH, Germany). The EcN-T7 (DSMZ 115365) strain was provided to us by Nicole Frankenberg-Dinkel. *P. aeruginosa* PAO1 (DSMZ 22644) was procured from the Leibniz Institute DSMZ GmbH (Braunschweig, Germany).

Procured plasmids

The pTlpA$_{39}$-mWasabi (Addgene #86116) plasmid was provided to us by Mikhail Shapiro (Piraner et al., 2017). The pUC-GFP-AT (Addgene #133306) plasmid was provided to us by Chris Barnes (Fedorec et al., 2019). The mBP-T7RNAP (Addgene #74096) plasmid was provided to us by Paul Freemont (Moore et al., 2016). The p3E-FRT-KanR-FRT pA (p3E-KanR) plasmid (Addgene #82601) was provided to us by Kryn Stankunas (Fowler et al., 2016). The pUC19 plasmid was provided to us by New England Biolabs GmbH, Germany.

Molecular biology reagents and oligonucleotides

Q5 DNA Polymerase was used for DNA amplification and colony PCR screening (New England Biolabs, Germany). Gibson Assembly and site-directed mutagenesis was performed using the NEBuilder HiFi DNA Assembly Cloning Kit (E5520S) and KLD Enzyme Mix (M0554S) respectively. Qiagen Plasmid Kit (12125) was used for plasmid extraction and Wizard® SV Gel

and PCR Clean-Up System (A9282) was used for DNA purification. Oligonucleotides used in this study were synthesized from Integrated DNA Technologies (IDT, Belgium) and recombinant plasmids were verified by Sanger Sequencing (Eurofins, Germany). The nucleotide sequences of the genetic modules tested in this study have been listed in Table S1.

Competent cell preparation

Electrocompetent cells of ClearColi and *Δalr Δdadx* ClearColi (alanine auxotroph) were prepared by repeated washing of bacterial pellet harvested at early exponential growth phase with 10% (v/v) glycerol. Plasmids (500 ng) were transformed in the competent cells by electroporation at 1.8 kV, using 0.1 cm electroporation cuvettes (1652083) in the Bio-Rad MicropulserTM Electroporator. To prepare chemically competent EcN and EcN-T7 cells, bacterial cultures were grown overnight in LB broth at 37°C, 250 rpm and subcultured in 100 mL of fresh LB media [1:100 (v/v) dilution]. The cultures were incubated at 37 °C, 250 rpm until an OD_{600} = 0.4 was reached. The bacteria were pelleted down by centrifugation at 4000 rpm (3363 X g), 4 °C for 15 minutes (min) and the supernatant was discarded. The bacterial pellet was then washed twice with ice-cold $CaCl_2$ (200 mM) and once with a 1:1 mixture of $CaCl_2$ (200 mM) and glycerol (10% w/v). After the final wash, the pellet was resuspended in 1 mL of $CaCl_2$+glycerol mixture and stored at -80°C as 100 µL aliquots. For bacterial transformation, 1 µg of the plasmids were added to the competent cells and gently mixed by flicking. The competent cells were then chilled on ice for 30 min and transferred to a 42 °C water bath for 45 seconds (sec), followed by incubation on ice for 2 min. SOC media (900 µL) was added and mixed, and the cell suspension was incubated at 37 °C, 250 rpm for an hour (h) before plating on LB-NaCl or LB agar with appropriate antibiotics.

Cultivation of the darobactin production strains

Recombinant strains were inoculated into LB (for EcN and EcN-T7 variants) and LB-NaCl (for ClearColi BL21 DE3 variants) from the glycerol stocks and cultivated overnight at 30°C, 250 rpm with appropriate antibiotics. The bacterial suspensions were then subcultured in 25 mL of Formulated Media (FM) [Composition - (K_2HPO_4 - 12.54 g/L, KH_2PO_4 – 2.31 g/L, D-Glucose – 4 g/L, NH_4Cl – 1 g/L, Yeast Extract – 12 g/L, NaCl – 5 g/L, $MgSO_4$ – 0.24 g/L)] at a 1:25 (v/v) ratio in a sterile glass conical flask (250 mL). The incubation temperature, time and antibiotic supplementation for the subcultured bacterial samples were chosen according to the experimental

requirements. For IPTG inducible conditions, 0.5 mM (500 µM) IPTG was added to the cultures at OD_{600}=0.4 and further incubated for 24 h at the designated temperature. The bacterial biomass was measured on the Denver Instrument SI-234 analytical balance (Cole-Parmer GmbH, Germany) after discarding the cell-free supernatant.

P. aeruginosa PAO1 survival assay

P. aeruginosa PAO1 was inoculated into 5 mL FM from glycerol stock and subjected to overnight incubation at 37°C with 180 rpm orbital shaking. The following day, *P. aeruginosa* PAO1 was subcultured in fresh FM at 1:50 ratio (v/v) and grown till it reached log phase (OD_{600}=0.4). The log-phase bacteria were further diluted in FM to optimize the bacterial cell number to $55X10^5$ CFU/mL. For antibiotic susceptibility experiments, 10 µL of the diluted bacterial culture were added to 100 µL of fresh FM supplemented with known antibiotic concentrations (kanamycin, ampicillin or darobactin). For determining the antimicrobial activity of the darobactin containing extracellular media, 10 µL of the diluted bacterial culture ($55X10^5$ CFU/mL) was added to 100 µL of filter-sterilized supernatants (0.22 µm filters, Carl Roth GmbH, Germany) in a sterile 96-well U-bottom transparent plate (REF 351177, Corning, USA) to bring the final bacterial cell number to $5X10^5$ CFU/mL. The plates were then incubated under static conditions for 18 h at 37°C and bacterial growth was determined by measuring absorbance at 600 nm in Microplate Reader Infinite 200 Pro (Tecan Deutschland GmbH, Germany). For the recultivation assay, 100 µL of the supernatant treated *P. aeruginosa* PAO1 samples were plated on 20 mL of MHI Agar (without antibiotic supplementation) and incubated at 37°C for 18 h before imaging.

Thermal gradient assay

The thermal gradient protocol was optimized from my previously reported protocol (Basaran et al., 2023). Bacterial cultures ($pTlpA_{39}$-mWasabi, $pTlpA_{39}$-iLOV and $pTlpA_{39}$-mCherry) were incubated overnight in 5 mL of LB-NaCl media (supplemented with 100 µg/mL ampicillin) at 30°C with continuous shaking (250 rpm). The following day, cultures were diluted to 0.1 OD_{600} in 3 mL of antibiotic-supplemented fresh media and regrown at 30°C, 250 rpm. At OD_{600} = 0.3, the cultures were dispensed into Fisherbrand™ 0.2 mL PCR Tube Strips with Flat Caps (Thermo Electron LED GmbH, Germany) and placed in the Biometra Thermocycler (Analytik Jena. GmbH, Germany). The thermal assay was set at a temperature gradient from 31°C to 43°C with regular

increment of 2°C. The lid temperature was set at 50°C to prevent the evaporation of the liquid and maintain a homogeneous temperature in the spatially allocated PCR tubes. Following an 18 h incubation period, the PCR strips were centrifuged in a tabletop minicentrifuge (Biozym GmbH, Germany) to pellet down the cells and discard the supernatant. The cells were then resuspended in 200 µL of 1X PBS and added to the clear bottom 96-well microtiter plate (Corning® 96 well clear bottom black plate, USA). The respective absorbance values of the samples were then measured at 600 nm (OD_{600}) in the Microplate Reader Infinite 200 Pro (Tecan Deutschland GmbH, Germany). mWasabi, iLOV and mCherry fluorescence intensity were measured at Ex_{λ} / Em_{λ} =493 nm/530 nm, Ex_{λ} / Em_{λ} =447 nm/497 nm and Ex_{λ} / Em_{λ} = 587 nm/625 nm respectively. The z-position and gain settings for recording all the fluorescent intensities were set to 19442 µm and 136 respectively. Fluorescence values were then normalized with their respective OD_{600} values to calculate the final Relative Fluorescence Units (RFU) using the formula RFU = Fluorescence/OD_{600}.

Electrospray Ionization - Mass Spectrometry (ESI-MS) based darobactin quantification

For LC/ESI QTOF-MS analysis was performed on a 1260 Infinity LC in combination with a 6545A high-resolution time-of-flight mass analyzer, both from Agilent Technologies (Santa Barbara, CA, USA). Separation of 1 µL of sample was performed using a Poroshell HPH-C18 column (3.0 x 50 mm, 2.7 µm) equipped with the same guard column (3.0 x 5 mm, 2.7 µm) by a linear gradient from (A) ACN + 0.1% formic acid to (B) water + 0.1% formic acid at a flow rate of 500µL/min and a column temperature of 45°C. Gradient conditions were as follows: 0-0.5min, 95% B; 0.5-6min, 95-60.5% B; 6-9.5 min 60.5-20% B at 1500 µL/min (column cleaning), 9.5-13min 95% B down to 500µL/min (equilibrium).

After separation, the LC flow entered the dual AJS ESI source set to 3500 V as capillary voltage, 40 psi nebulizer gas pressure and 7 l/min dry gas flow, and 300 °C dry gas temperature. The TOF parameters used were high resolution mode (4 GHz), 140 V fragmentor and 45 V skimmer voltage. The mass spectra were acquired in the time interval of 2-6 min in full scan mode in the range m/z 150-3000 with a spectra rate of 4/s. For quantification of the Darobactin, the positive charged mass $[M+2H]^{2+}$ at m/z 483.7089 Da were extracted and automatically integrated using Mass Hunter software. Standards were prepared from Darobactin stock solution of 100 µg/mL (purified as mentioned before by Seyfert et al., 2023) in mobile phase (5% A, 95% B) or blank media.

Calibration was done between 0 and 1 µg/mL or 0 and 10 µg/mL with recovery rates 97-105%. For analyzing real samples, the bacterial biomass was removed post-incubation by centrifugation [4000 rpm (3363Xg), 30 min, 4 °C] and the respective supernatants were filter-sterilized with 0.22 µm filters (Carl Roth, Germany) and provided with respective controls.

Further verification of darobactin in the extracellular media was conducted using an associated estimation technique. For that, Darobactin was quantified using a Vanquish Flex UHPLC (Thermo Fisher, Dreieich, Germany), coupled to a TSQ Altis Plus mass spectrometer (Thermo Fisher, Dreieich, Germany). Samples were diluted 1:10 in PBS pH 7.4, followed by addition of 2 volumes 10%MeOH/ACN containing 15 nM diphenhydramine as internal standard. Samples were centrifuged (15 min, 4°C, 4000 rpm) before analysis and darobactin content quantified in SRM mode using a calibration curve up to 5 µM. LC conditions were as follows: column: Hypersil GOLD C-18 (1.9 µm, 100 x 2.1 mm; Thermo Fisher, Dreieich, Germany); temperature 40°C; flow rate 0.700 mL/min; solvent A: water + 0.1% formic acid; solvent B: acetonitrile + 0.1% formic acid; gradient: 0-0.2 min 10% B, 0.2-1.2 min 10-90% B, 1.2-1.6 min 90% B, 1.6-2.0 min 10% B. MS conditions were as follows: vaporizer temperature 350°C, ion transfer tube temperature 380°C, Sheath Gas 30, Aux Gas 10, Sweep Gas 2; spray voltage: 4345 V, mass transition: 483.75 – 475.083 ($[M+2H]^{2+}$), collision energy: 11.0 V; Tube lens offset 55 V.

qPCR analysis for plasmid retention

Bacterial cultures (pTAMP-DarA-AT EcN) were cultivated overnight in 5 mL of LB media (supplemented with 100 µg/mL ampicillin) at 30°C with continuous shaking (120 rpm). Following day, the bacterial suspension was subcultured in 25 mL of FM both with and without antibiotic supplementation (100 µg/mL ampicillin) in a 1:25 (v/v) ratio. Bacterial cultures were immediately kept at 40°C and incubated for 24 h. Post 24 h incubation, the OD_{600} was measured, and fresh FM cultures were inoculated with the respective bacterial cultures at a starting OD_{600} of 0.01. This procedure was repeated over 5 days, resulting in 50 consecutive bacterial generations. For qPCR analysis, 1 mL of the bacterial samples after every 10 generations were normalized to OD_{600} of 0.8 with sterile PBS. The normalized cultures were centrifuged at 13,000 rpm (16200Xg) and washed thrice with sterile Dulbecco's 1× PBS (Phosphate Buffer Saline) solution. 500 µL of the bacterial samples were then kept at 98°C for 15 min to undergo lysis in a static thermomixer (Eppendorf GmbH, Germany) according to the reported protocol (Škulj et al., 2008). The samples were then

stored at -20°C. After collecting bacterial samples for 50 generations, qPCR was performed using the iTaq™ Universal SYBR ® Green Supermix (BioRad GmbH, Germany) in the Bio-Rad CFX96 Real time system C1000 Touch thermal cycler. To prevent sample heterogeneity, qPCR reactions were conducted with primers specific to the pUC replication origin of the recombinant plasmid and the 16S rRNA gene in the bacterial chromosome. The nucleotide sequences of the qPCR primers used are listed in Table S2. The cycle threshold (Ct) values were selected by the regression determination mode and the mean ΔCt for the pUC and 16S rRNA gene was determined by the following formula: - ΔCt= Ct (50^{th} generation) – Ct (10^{th} generation). The relative quantification (RQ) values were then calculated using the Pffafl method ($2^{-\Delta\Delta Ct}$), where ΔΔCt=ΔCt (pUC)−ΔCt (16S rRNA). The final data was represented in the form of fold change (FC), where FC = $2^{-\Delta\Delta Ct}$ of ampicillin supplemented samples/ $2^{-\Delta\Delta Ct}$ of non-ampicillin supplemented samples.

Bacterial growth curve

Bacterial cultures were incubated overnight in 5 mL of LB media (supplemented with 100 µg/mL ampicillin) at 30°C with continuous shaking (250 rpm). The following day, the bacterial strains were subcultured in fresh FM (no antibiotic supplementation) in a 1:25 (v/v) ratio. 200 µL of the subcultured bacteria were then dispensed into UV STAR Flat Bottom 96-well microtitre plates (Greiner BioOne GmbH, Germany) and incubated in the Microplate Reader Infinite 200 Pro (Tecan Deutschland GmbH, Germany) with orbital shaking at an incubation temperature of either 37°C or 40°C. The sample absorbance at 600 nm (OD_{600}) was measured at every 15 min interval for 24 h and the respective bacterial growth kinetics were then plotted.

RT-qPCR analysis for gene expression

Bacterial cultures were cultivated in 5 mL of LB media (supplemented with 100 µg/mL ampicillin) at 30°C with continuous shaking (120 rpm). The following day, the bacterial suspension was subcultured in 25 mL of FM (without antibiotic supplementation) in a 1:25 (v/v) ratio and incubated at either 37°C or 40°C. Post 6 h incubation at the respective temperatures, the OD_{600} was determined using the NanoDrop Microvolume UV–Vis Spectrophotometer (ThermoFisher Scientific GmbH, Germany). All the bacterial cultures were normalized to OD_{600} of 0.8 to maintain an equivalent cell count. The normalized cultures were centrifuged at 13,000 rpm (16200Xg) and washed thrice with sterile Dulbecco's 1× PBS (Phosphate Buffer Saline) solution. The bacterial

pellet was then resuspended in 1X DNA/RNA protection reagent supplied with the Monarch Total RNA Miniprep Kit (NEB #T2010) (New England BioLabs, USA) and subjected to mechanical lysis using the FastPrep-24™ 5G bead beating grinder system (MP Biomedicals Germany GmbH). Total RNA was isolated according to the manufacturer guidelines and measured at 260 nm to determine the net yield and purity. 500 ng of the total RNA from all extracted samples were then immediately converted into cDNA using the Thermo-Scientific Revertaid first strand cDNA synthesis kit (#K1622). Real time qPCR was performed using the iTaq™ Universal SYBR ® Green Supermix (BioRad GmbH, Germany) in the Bio-Rad CFX96 Real time system C1000 Touch thermal cycler to determine the gene expression level of target genes. Bacterial 16S rRNA levels were also measured for all the samples as a control (Smati et al., 2013). The specific sequences of RT-qPCR primers are listed in Table S2. The threshold cycle (Ct) values were selected by the regression determination mode and the mean ΔCt values for the *darA* and *t7-RNAP* genes, along with their 16S rRNA reference gene were determined by the following formula: - ΔCt= Ct (37°C) – Cq (40°C). The relative quantification (RQ) values were then calculated using the Pffafl method ($2^{-\Delta\Delta Ct}$), where ΔΔCt=ΔCt (*darA* or *t7-RNAP*) − ΔCt (16S rRNA), and represented in the form of gene expression fold change at 40°C compared to 37°C.

Bile tolerance assay

Bacterial cultures were cultivated overnight in 5 mL of LB media (supplemented with 100 µg/mL ampicillin) at 30°C with continuous shaking (120 rpm). Following day, the bacterial suspension was subcultured in 25 mL of FM (no antibiotic) supplemented with filter-sterilized 0.3% (w/v) Bovine Bile in a 1:25 (v/v) ratio and incubated at 37°C or 40°C for 24 h. Post incubation, the darobactin concentration in the cell-free media was determined and its antimicrobial activity was analyzed in terms of its ability to inhibit the growth of *P. aeruginosa* PAO1.

Simulating darobactin production in nutrient-limited media

Bacterial cultures were cultivated overnight in 5 mL of LB media (supplemented with 100 µg/mL ampicillin) at 30°C with continuous shaking (120 rpm). The following day, the bacterial suspension was subcultured in 25 mL of FM (without antibiotic supplementation) in a 1:25 (v/v) ratio and incubated at 30°C for 24 h. Post incubation, the bacterial pellet was centrifuged at 4000 rpm (3363Xg), for 30 min, 4 °C and the supernatant was discarded. The bacterial pellet was then

resuspended in 25 mL of M9 Minimal Media [Na_2HPO_4•$7H_2O$ – 12.8 g/L**,** KH_2PO_4 – 3 g/L**,** NH_4Cl – 1 g/L**,** NaCl – 0.5 g/L**,** D-Glucose – 4 g/L**,** $MgSO_4$ – 0.24 g/L**,** $CaCl_2$ – 0.011 g/L] and incubated at 37°C and 40°C for 24 h. Post incubation, the bacterial pellet was discarded and the darobactin concentration in the cell-free media along with its antimicrobial activity against *P. aeruginosa* PAO1 was assessed.

Statistical and bioinformatics analysis

GraphPad Prism 7.0 software was used to plot the graphs. Student t-test was used for estimating significant differences between the mean values of different samples. AlphaFold2 GitHub code (ColabFold v1.5.5) was used to predict the 3D structures of the T7-RNAP protein. All the schematic figures were generated using Biorender.

3.3. Results and Discussions

3.3.1. Determining the antimicrobial activity of Darobactin

Our initial goal was to compare the antimicrobial activity of darobactin with two commonly used bactericidal antibiotics in research environments: ampicillin and kanamycin. Ampicillin belongs to the ß-lactam group of antibiotics, which interfere with bacterial cell wall synthesis. On the other hand, kanamycin is an aminoglycoside that interacts with the bacterial 30S ribosomal subunit to hinder bacterial protein translation. We used high dosages of these antibiotics to assess their effectiveness in inhibiting the growth of the opportunistic pathogen, *P. aeruginosa* PAO1 strain in the enriched media (FM). Although 100 µg/mL and 200 µg/mL of ampicillin partially and completely inhibited *P. aeruginosa* PAO1 growth, respectively (**Figure 3A**), equivalent concentrations of kanamycin failed to demonstrate a similar effect on *P. aeruginosa* PAO1 (**Figure 3B**). In comparison, we found that much lower concentrations of darobactin could inhibit *P. aeruginosa* PAO1 growth under identical test conditions (**Figure 3C**). To revalidate our findings from the growth inhibition assay, I plated the *P. aeruginosa* PAO1 samples treated with different darobactin concentrations on MHI Agar (no antibiotic supplementation) and incubated them at 37°C. A bacterial lawn was observed on MHI Agar for *P. aeruginosa* PAO1 samples treated with 0.5 and 1 µg/mL of darobactin, whereas only a few isolated colonies appeared for the samples

treated with 2 and 4 µg/mL of darobactin (**Figure 3D**). These experiments confirmed that darobactin concentrations as low as 2 µg/mL could inhibit the growth of the opportunistic pathogen, *P. aeruginosa* PAO1 in nutritionally enriched media along with ensuring a lower rate of re-emergence when cultivated on fresh media.

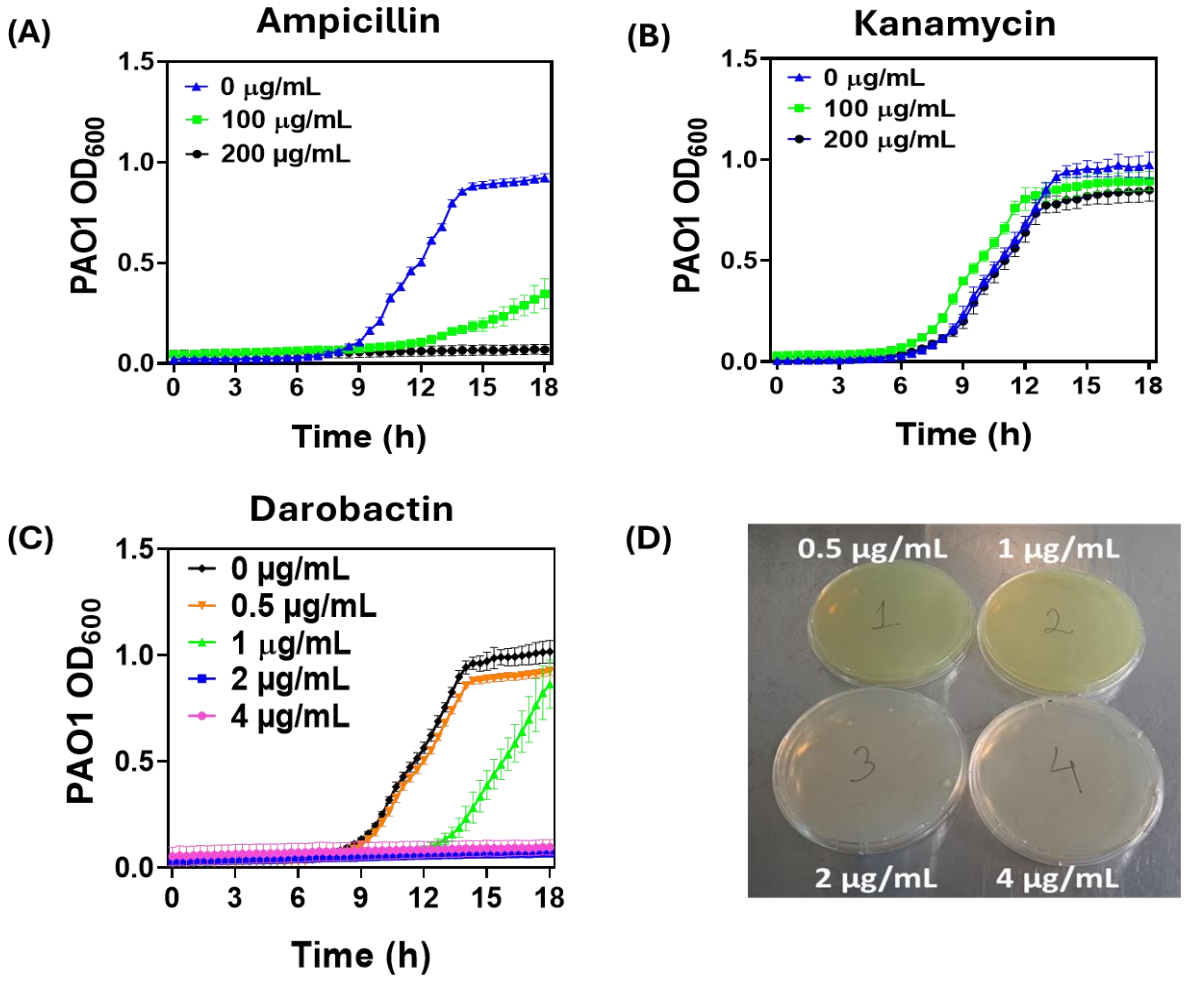

Figure 3. (A) Growth Kinetics of *P. aeruginosa* PAO1 (DSMZ 22644) in FM supplemented with 0, 100 and 200 µg/mL of ampicillin respectively. The samples were shaken continuously with steady incubation at 37°C and their Optical Density (OD_{600}) was measured at equal time intervals. The error bars represent standard deviation based on three independent measurements (B) Growth Kinetics of *P. aeruginosa* PAO1 in FM supplemented with 0, 100 and 200 µg/mL of kanamycin respectively. The samples were shaken continuously with steady incubation at 37°C and their Optical Density (OD_{600}) was measured at equal time intervals. The error bars represent standard deviation based on three independent measurements (C) Growth Kinetics of *P. aeruginosa* PAO1 in FM supplemented with 0, 0.5, 1, 2 and 4 µg/mL of darobactin respectively. The samples were shaken continuously with steady incubation at 37°C and their Optical Density (OD_{600}) was measured at equal time intervals. The error bars represent standard deviation based on three independent measurements (D) *P. aeruginosa* PAO1 cultivated on Mueller-Hinton (MHI) Agar post

treatment with 0.5, 1, 2 and 4 μg/mL of darobactin (Figure 3C). The agar plates were placed in a static incubator at 37°C for 18 h before imaging. The 0.5 and 1 μg/mL darobactin treated samples gave rise to a lawn of *P. aeruginosa* PAO1 bacteria (The plate appears green due to pyoverdine pigment produced naturally by the bacteria). 2 and 4 μg/mL darobactin treated samples only produced a few isolated colonies of *P. aeruginosa* PAO1 (The plate appears yellowish due to the natural color of the MHI Agar devoid of any pigment production). The data was independently verified at least two times.

3.3.2. Functional characterization of inducible darobactin production

First, I compared the darobactin production ability of different genetic circuits reported in the literature. I chose the pNOSO-darABCDE circuit (Groß et al., 2021) and the pZW-ADC7 and pZW-ADC9 circuits (Wuisan et al., 2021) due to their high yields of darobactin production (as claimed in literature). The biosynthetic gene cluster (BGC) arrangement was similar in all these circuits, with the *darA* gene encoded downstream of an IPTG-inducible P_{T7}-lacO (promoter-operator complex) regulated by the constitutively expressed lacI repressor protein. The *darBCD* gene cluster encodes for a permease protein (DarB), membrane fusion protein (DarC), and ATP-binding protein (DarD), which altogether comprise a tripartite efflux pump to export darobactin into the extracellular milieu. The *darE* gene encodes for a radical S-adenosyl-l-methionine (SAM) enzyme (DarE) that catalyzes the formation of the ether and C–C crosslinking in the heptapeptide core (W^1–N^2–W^3–S^4–K^5–S^6–F^7) of the DarA propeptide (Nguyen et al., 2022). The P_{TN5} promoter enabled constitutive transcription of the *darBCDE* gene cluster in the pNOSO-darABCDE genetic circuit (**Figure 4A**), whereas, for the pZW-ADC7 genetic circuit, the *darBCDE* genes were co-transcribed with the *darA* gene by the P_{T7} promoter, regulated by the lacI-lacO repressor-operator complex (**Figure 4B**). The pZW-ADC9 circuit had a similar gene arrangement like pZW-ADC7, except it did not encode for the efflux pump encoding *darBCD* genes (**Figure 4C**). In addition, the pNOSO-darABCDE plasmid contained a medium-copy number replicon (p15A), whereas the pZW-ADC7/pZW-ADC9 plasmids were cloned in a vector backbone with a high-copy number replicon (RSF1030). All three recombinant plasmids were transformed and maintained in an endotoxin-free *E. coli* strain, ClearColi (Mamat et al., 2015). This strain was previously rendered endotoxin-free through the deletion of seven genes namely the *gutQ* and *kdsD* genes (D-arabinose 5-phosphate isomerases), *lpxL* gene (Kdo2-lipid IVA lauroyl-ACP acyltransferase), *lpxM* gene (Kdo2-lauroyl-lipid IVA myristoyl-ACP acyltransferase), *pagP* gene (phospholipid: lipid A palmitoyl transferase), *lpxP* gene (Kdo2-lipid IVA palmitoleoyl-ACP acyltransferase), and *eptA*

gene (lipid A P-EtN transferase) responsible for the glycosylation of the bacterial lipopolysaccharide (LPS) layer from the bacterial genome (**Figure 4D**). Thus, ClearColi is a potentially safer strain for use in the body while supporting overexpression of recombinant proteins, similar to the standard *E. coli* BL21 DE3 strain. The recombinant ClearColi strains were cultivated in FM and induced with 500 µM IPTG to allow darobactin production and release into the extracellular medium at 37 °C following a 24-hour incubation period. The pNOSO-darABCDE construct carrying strain generated ~2.5 µg/mL darobactin in the extracellular medium in 24 h, which was ~6-fold (0.4 µg/mL) and ~25-fold (0.1 µg/mL) higher than the darobactin concentration detected for the pZW-ADC7 and pZW-ADC9 ClearColi strains, respectively (**Figure 4E**). The higher darobactin concentration for the pNOSO-darABCDE construct highlighted that transcriptional decoupling of the *darA* and *darBCDE* genes could allow rapid processing of the DarA propeptide (DarE enzyme) and export of the mature darobactin (DarB, DarC, DarD) into the extracellular environment. In addition to transcriptional decoupling, the absence of the *darBCD* genes from the pZW-ADC9 genetic circuit led to a decreased (~4-fold) darobactin concentration in the extracellular media, highlighting the essential role of the DarBCD efflux pump in boosting darobactin release. From these experiments, I concluded that the pNOSO-darABCDE genetic circuit allowed efficient production and export of darobactin into the extracellular environment compared to its counterparts.

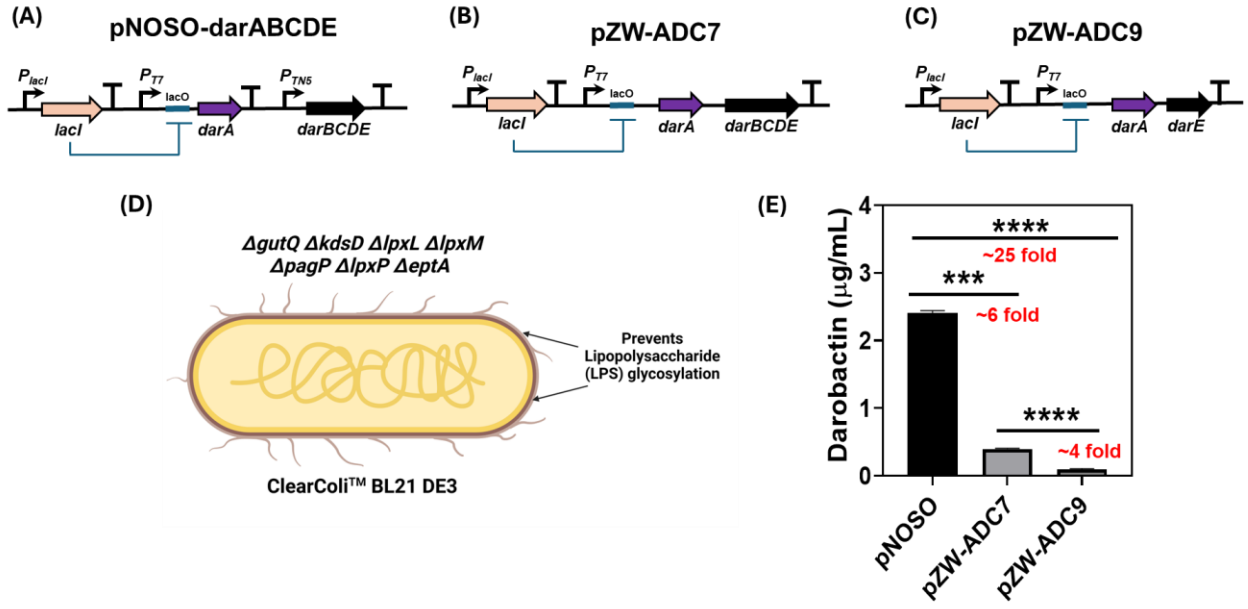

Figure 4. (A) Schematic diagram of pNOSO-darABCDE genetic circuit (Groß et al., 2021) (B) Schematic diagram of pZW-ADC7 genetic circuit (Wuisan et al., 2021) (C) Schematic diagram of pZW-ADC9 genetic circuit (Wuisan et al., 2021) (D) Schematic diagram of the recombinant protein expression microbial chassis, ClearColi™ BL21 (DE3). The deletion of the genes *gutQ*, *kdsD*, *lpxL*, *lpxM*, *pagP*, *lpxP* and *eptA* from the bacterial genome prevents glycosylation of the lipopolysaccharide (LPS) layer of the bacteria. Proteins purified from this chassis prevent endotoxic response in the human cell lines (Mamat et al., 2015) (E) Darobactin concentration in the liquid medium (in µg/mL) for the pNOSO-darABCDE, pZW-ADC7 and pZW-ADC9 constructs in ClearColi BL21 (DE3) strain after 24 h of incubation at 37°C. The bacteria were induced with 500 µM of IPTG at OD_{600} =0.4 in FM supplemented with 50 µg/mL kanamycin. The error bars represent standard deviation based on three independent measurements (***p=0.0001, ****p<0.0001 as calculated by paired t-test).

Although darobactin was detected in the extracellular media, I needed to assess whether it retained antimicrobial activity against *P. aeruginosa* PAO1 as previously demonstrated for the pure compound. To do so, I collected the cell-free extracellular media and tested whether it inhibited the growth of *P. aeruginosa* PAO1 (**Figure 5A**). To confirm that the residual kanamycin present in the media, initially added for plasmid retention, did not inhibit *P. aeruginosa* PAO1 growth, extracellular media (FM) collected post-growth of the wild-type ClearColi strain was supplemented with kanamycin and darobactin to test for their antimicrobial potential towards *P. aeruginosa* PAO1. Although kanamycin (50 µg/mL) did not exhibit any antimicrobial activity, darobactin (2 µg/mL) significantly inhibited the growth of *P. aeruginosa* PAO1 (**Figure 5B**). In addition, no significant synergistic effect for the antibiotic combinations (50 µg/mL kanamycin and 2 µg/mL darobactin) against *P. aeruginosa* PAO1 was observed compared to darobactin supplementation alone. Therefore, any antimicrobial activity exhibited by the extracellular media could be solely attributed to darobactin and not to the residual levels of kanamycin. As expected, only the higher concentration of darobactin in the extracellular media collected from the IPTG-induced pNOSO-darABCDE ClearColi strain demonstrated significant antimicrobial activity against *P. aeruginosa* PAO1 (**Figure 5C**). On the other hand, low darobactin concentration in the extracellular media collected from the pZW-ADC7, pZW-ADC9, and p3E-KanR (control) ClearColi strains did not mediate any antimicrobial activity against *P. aeruginosa* PAO1. These observations indicated that the antimicrobial activity of both pure and microbially-released darobactin could display similar antimicrobial activity against the pathogenic strain.

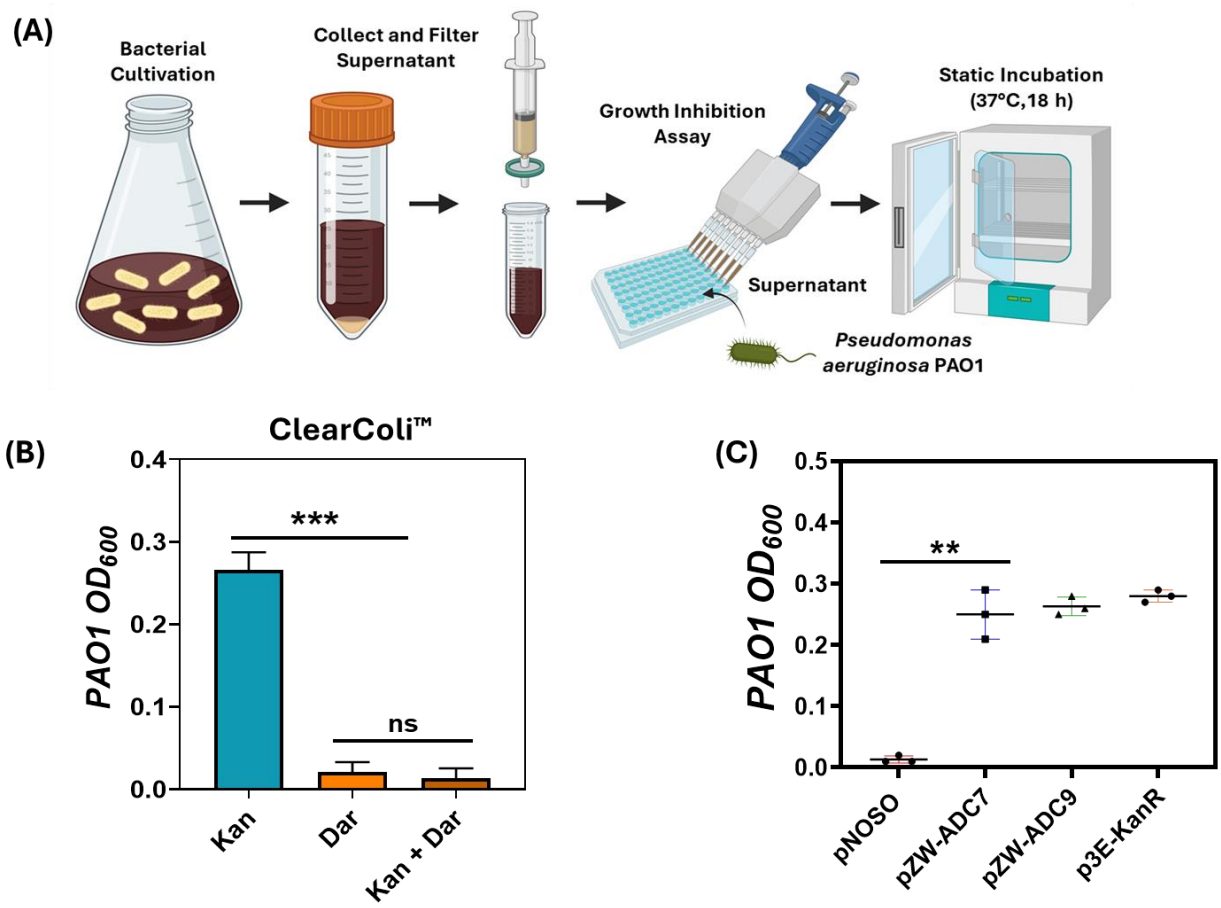

Figure 5. (A) Schematic diagram of the steps taken to test the growth inhibitory effect of the darobactin secreted into the extracellular media on the pathogenic strain *P. aeruginosa* PAO1 (B) End-point absorbance (OD_{600}) of *P. aeruginosa* PAO1 after 18 h incubation at 37°C in filter-sterilized FM sustaining the growth of the wild type ClearColi™ strain. The extracellular media was supplemented with 50 µg/mL kanamycin, 2 µg/mL darobactin or a combination of both (50 µg/mL kanamycin + 2 µg/mL darobactin) before the assay to assess their respective antimicrobial activity. The error bars represent standard deviation based on three independent measurements (***p=0.0005, ^{ns}p=0.3593 as calculated by paired t-test) (C) End-point absorbance (OD_{600}) of *P. aeruginosa* PAO1 after 18 h incubation at 37°C in filter-sterilized FM sustaining the growth of the pNOSO-darABCDE, pZW-ADC7, pZW-ADC9 and p3E-KanR constructs in ClearColi BL21 (DE3) strain. The darobactin production strains were induced with 500 µM of IPTG at OD_{600}=0.4 in FM supplemented with 50 µg/mL kanamycin. The error bars represent standard deviation based on three independent measurements (*p= 0.0096 as calculated by paired t-test).

This preliminary analysis confirmed that the pNOSO-darABCDE ClearColi strain could sustain sufficient darobactin release without compromising its antimicrobial activity at 37°C. Next, I wanted to check whether different incubation temperatures affected the overall concentration and antimicrobial potential of the darobactin accumulated in the extracellular medium. I found that the concentration of darobactin was significantly higher for the pNOSO-darABCDE ClearColi

samples incubated at 34°C compared to those incubated at 37°C - 42°C post-IPTG induction (**Figure 6A**). However, no significant difference in the darobactin concentration was observed between the strains cultivated at either 37°C or 40°C (**Figure 6A**). Despite differences in the overall concentration, sufficient darobactin accumulated in extracellular media at all tested incubation temperatures to inhibit the growth of *P. aeruginosa* PAO1 compared to the control strain (**Figure 6B**). This highlighted that darobactin is relatively thermostable, and its antimicrobial activity is not significantly affected due to the incubation temperatures ranging from 34°C to 42°C. To further evaluate the effectiveness of lacI repressor-based regulation on darobactin production, the pNOSO-darABCDE ClearColi strain was cultivated with and without IPTG supplementation. Even without IPTG induction, I observed a significant basal level expression that sustained the accumulation of approximately 1 µg/mL of darobactin in the medium (FM) (**Figure 6C**). The leakiness of the genetic circuit could be attributed to the inefficient repression by the lacI protein (Singha et al., 2017) or its propensity to undergo de-repression by binding to related auto-inducer molecules such as lactose and galactose present in the growth media (Xu et al., 2012). Therefore, cross-reactivity of the lacI repressor protein to simple carbohydrates can render IPTG-inducible genetic circuits less effective under therapeutically relevant conditions. To study the effects of constitutive darobactin production on the microbial chassis, a pT7-darABCDE plasmid was created and established in ClearColi. The lacI-lacO repressor-operator complex was removed from the genetic circuit to allow the constitutive transcription of the *darA* gene from the P_{T7} promoter (**Figure 6D**). The P_{T7} promoter is recognized explicitly by its cognate T7 RNA Polymerase (T7RNAP) enzyme constitutively expressed from the bacterial genome. After cultivating the pT7-darABCDE and IPTG-induced pNOSO-darABCDE Clearcoli strains at 37°C for 24 hours, I observed that the pT7-darABCDE ClearColi strain had a much lower bacterial biomass (~100 mg for 25 mL of FM) compared to the IPTG-induced pNOSO-darABCDE ClearColi strain (~430 mg for 25 mL of FM) (**Figure 6E**). I hypothesized that the pT7-darABCDE construct caused a significant metabolic burden on the producer strain because of the constitutive expression and extracellular release of darobactin. The reduced biomass also accounted for a substantial decrease in the overall darobactin concentration for the pT7-darABCDE strain (~0.09 µg/mL) compared to the pNOSO-darABCDE construct (~2.5 µg/mL) (**Figure 6F**). Based on these observations, I concluded that inducible expression was necessary to achieve a higher darobactin concentration in the extracellular media without causing an excessive metabolic burden on the microbial chassis.

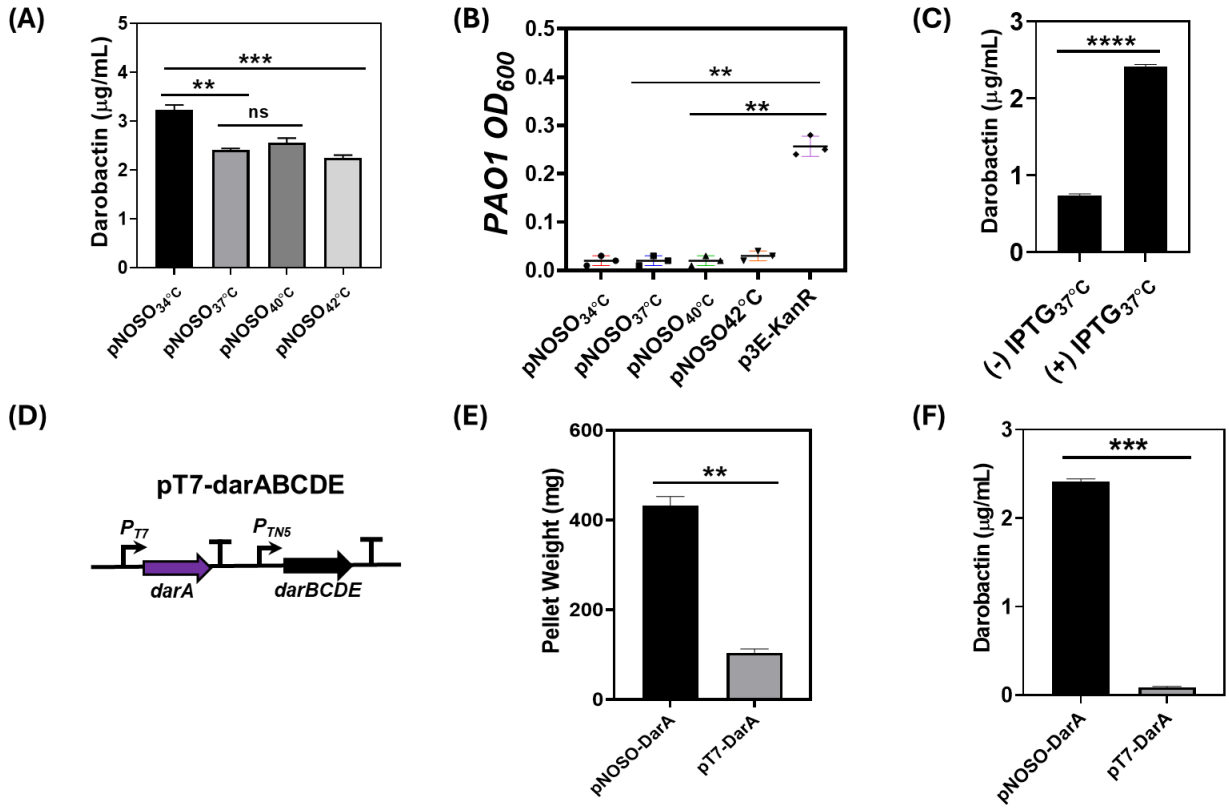

Figure 6. (A) Darobactin concentration in the liquid medium (in µg/mL) for the pNOSO-darABCDE construct in ClearColi BL21 (DE3) strain after 24 h of incubation at 34°C, 37°C, 40°C and 42°C respectively. The bacteria were induced with 500 µM of IPTG at OD_{600} =0.4 in FM supplemented with 50 µg/mL kanamycin. The error bars represent standard deviation based on three independent measurements (^{ns}p= 0.0629,**p=0.0023,***p=0.0007 as calculated by paired t-test) (B) End-point absorbance (OD_{600}) of *P. aeruginosa* PAO1 after 18 h incubation at 37°C in filter-sterilized FM sustaining the growth of the pNOSO-darABCDE ClearColi BL21 (DE3) strain for 24 h at 34°C, 37°C, 40°C and 42°C incubation temperatures respectively. The darobactin production strains were induced with 500 µM of IPTG at OD_{600} =0.4 in FM supplemented with 50 µg/mL kanamycin. The p3E-KanR ClearColi strain was used as a negative control. The error bars represent standard deviation based on three independent measurements (**p= 0.0055 as calculated by paired t-test) (C) Darobactin concentration in the liquid medium (µg/mL) for the pNOSO-darABCDE ClearColi BL21 (DE3) strain after 24 h incubation at 37°C, both in the absence and presence of 500 µM IPTG (added at OD_{600}=0.4) in FM supplemented with 50 µg/mL kanamycin. The error bars represent standard deviation based on three independent measurements (****p<0.0001 as calculated by paired t-test) (D) Schematic diagram of the pT7-darABCDE genetic circuit (E) Biomass comparison in terms of bacterial pellet wet weight (in milligrams (mg)) obtained from a 25 mL culture after 24 h incubation at 37°C. The pNOSO-darABCDE ClearColi BL21 DE3 sample was induced with 500 µM IPTG at log phase (OD_{600}=0.4), whereas the pT7-darABCDE ClearColi BL21 DE3 strain was not subjected to external IPTG supplementation. The error bars represent standard deviation based on three independent measurements (**p=0.0010 as calculated by paired t-test) (F) Darobactin concentration in the liquid medium (in µg/mL) of the IPTG induced pNOSO-darABCDE ClearColi BL21 DE3 strain in comparison to the pT7-darABCDE Clearcoli BL21 DE3 strain after 24 h of incubation at 37°C. The error bars represent standard deviation based on three independent measurements (***p=0.0001 as calculated by paired t-test).

3.3.3. Functional characterization of thermo-responsive darobactin production

As an alternative to chemical inducers, I tested whether external temperature could be utilized to regulate the activation of genetic circuits. Before attempting to produce darobactin, I established the pTlpA$_{39}$-mWasabi plasmid (created by Piraner et al., 2017) in the ClearColi strain (**Figure 7A**). Following that, I assessed mWasabi (green-fluorescent reporter protein) production in ClearColi as a function of incubation temperature (**Figure 7B**). The TlpA$_{39}$ repressor protein tightly regulated the P$_{tlpA}$ promoter and prevented mWasabi production at temperatures below 39°C. On increasing the incubation temperature to 39°C, drastic de-repression of the system was observed in terms of significant intracellular mWasabi accumulation. Maximum mWasabi protein production was observed to peak between 40-41°C, with no substantial increase beyond this range. To validate whether temperature-based regulation could induce the production of other reporter proteins, I replaced the *mWasabi* gene with *iLOV* (anaerobic green fluorescent protein) and *mCherry* (red fluorescent protein) genes to create the pTlpA$_{39}$-iLOV (**Figure 7C**) and pTlpA$_{39}$-mCherry (**Figure 7E**) recombinant plasmids, respectively. Both the genetic circuits were maintained in ClearColi, where they showed a similar trend in iLOV (**Figure 7D**) and mCherry (**Figure 7F**) fluorescent reporter protein production in response to the incubation temperature as previously observed for the pTlpA$_{39}$-mWasabi ClearColi strain. This observation suggested that temperature-based regulation was reliable for inducing the expression of fluorescent reporter proteins.

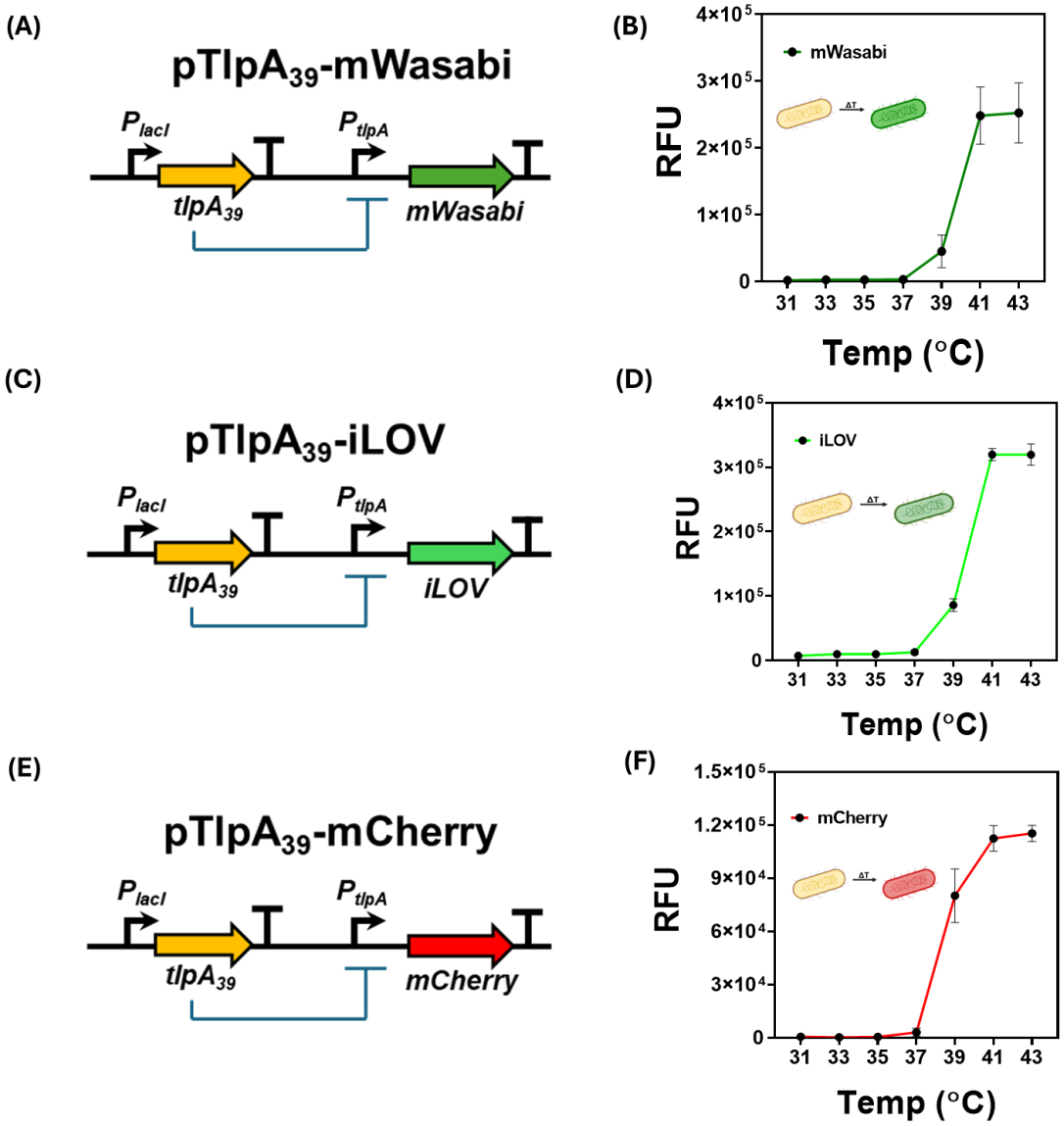

Figure 7. (A) Schematic diagram of pTlpA$_{39}$-mWasabi genetic circuit (B) Relative Fluorescence Units (RFU) of mWasabi fluorescent protein (Ex$_\lambda$ / Em$_\lambda$ =493 nm/530 nm; z-position = 19442 µm; gain = 136) produced by the pTlpA$_{39}$-mWasabi construct in ClearColi BL21 (DE3) strain after 18 h growth at different incubation temperatures. The error bars represent standard deviation based on three independent measurements (C) Schematic diagram of pTlpA$_{39}$-iLOV genetic circuit (D) Relative Fluorescence Units (RFU) of iLOV fluorescent protein (Ex$_\lambda$ / Em$_\lambda$ =447 nm/497 nm; z-position = 19442 µm; gain = 136) produced by the pTlpA$_{39}$-iLOV construct in ClearColi BL21 (DE3) strain after 18 h growth at different incubation temperatures. The error bars represent standard deviation based on three independent measurements (E) Schematic diagram of pTlpA$_{39}$-mCherry genetic circuit (F) Relative Fluorescence Units (RFU) of mCherry fluorescent protein (Ex$_\lambda$ / Em$_\lambda$ =587 nm/625 nm; z-position = 19442 µm; gain = 136) produced by the pTlpA$_{39}$-mCherry construct in ClearColi BL21 (DE3) strain after 18 h growth at different incubation temperatures. The error bars represent standard deviation based on three independent measurements.

To gain further insights into the lacI-IPTG mediated genetic circuit regulation, I replaced the *darA* gene of the pNOSO-darABCDE plasmid with the *mCherry* gene to create the pNOSO-mCherry construct and established it in ClearColi (**Figure 8A**). I also introduced the P_{TN5} promoter driven *darBCDE* gene cluster into the pTlpA$_{39}$-mCherry plasmid to establish the pUC-Tlp-mCherry construct in ClearColi (**Figure 8B**, named after the high-copy number pUC replication origin) to investigate the influence of orthogonally expressed proteins on the thermo-responsive circuit performance. The mCherry protein production observed for the pUC-Tlp-mCherry ClearColi strain at 40°C was twice that of the IPTG-induced pNOSO-mCherry ClearColi strain (**Figure 8C**). In addition, IPTG supplementation only led to a ~2.5-fold increase in mCherry protein production for the pNOSO-mCherry ClearColi strain compared to the non-IPTG-supplemented samples (**Figure 8D**). The poor fold change was primarily due to the leaky expression of mCherry protein, as observed previously for the darobactin-producing pNOSO-darABCDE ClearColi strain. On the other hand, the pUC-Tlp-mCherry ClearColi strain exhibited a ~40-fold increase in mCherry production for the samples incubated at 40°C compared to those incubated at 37°C (**Figure 8D**). The tight regulation mediated by the TlpA$_{39}$ repressor protein ensured negligible mCherry expression at 37°C, making thermal regulation a more feasible option for regulating recombinant protein expression in ClearColi compared to chemical inducers.

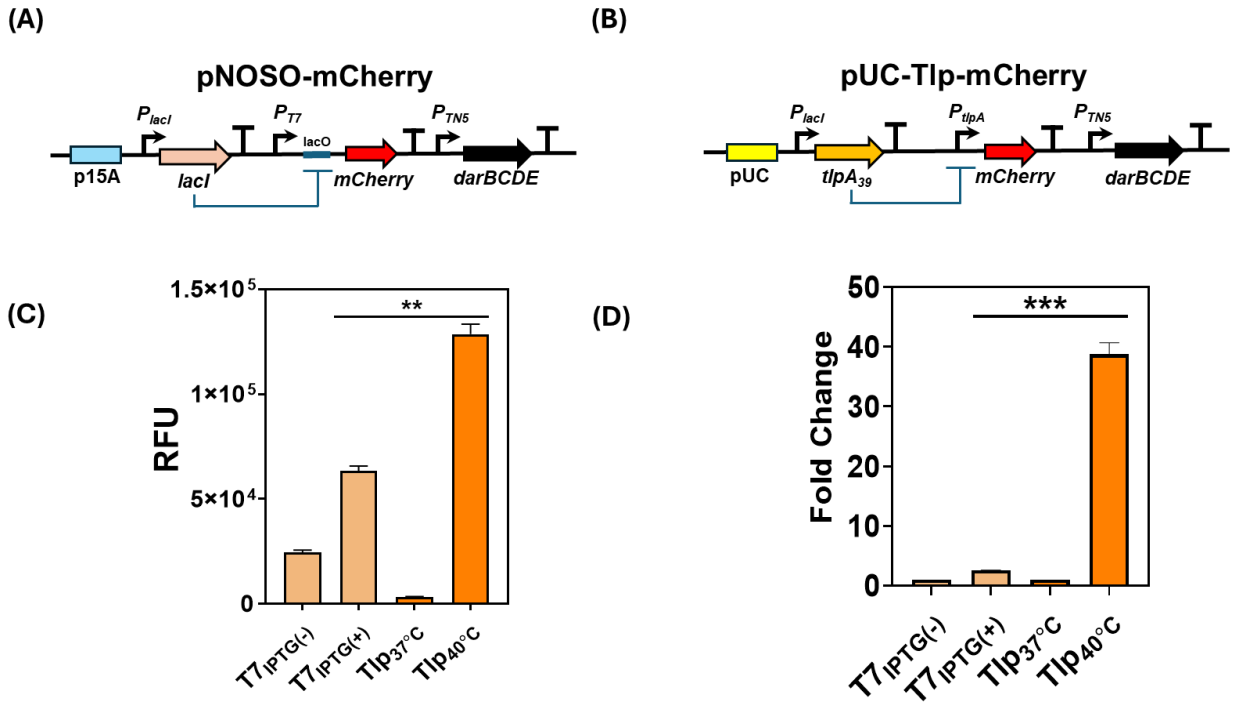

Figure 8. (A) Schematic representation of the pNOSO-mCherry genetic circuit (B) Schematic representation of the pUC-Tlp-mCherry genetic circuit (C) Relative Fluorescence Units (RFU) of mCherry fluorescent protein produced by the pNOSO-mCherry and pUC-Tlp-mCherry ClearColi BL21 (DE3) strain after 24 h incubation. For pNOSO-mCherry circuit, mCherry expression both in the absence [$T7_{IPTG(-)}$] and presence [$T7_{IPTG(+)}$] of IPTG induction (500 µM, 37°C) has been highlighted. For pUC-Tlp-mCherry circuit, mCherry expression both at 37°C ($Tlp_{37°C}$) and 40°C ($Tlp_{40°C}$) incubation temperature has been highlighted. Relative Fluorescence Units (RFU) of the strains were obtained by normalizing the mCherry fluorescence (measured at Ex_{λ} / Em_{λ} =587 nm/625 nm; z-position = 19442 µm; gain = 136) with their respective OD_{600} values. The error bars represent standard deviation based on three independent measurements (**p=0.0016 as calculated by paired t-test) (D) Fold Change in mCherry fluorescent protein production by the pNOSO-mCherry and pUC-Tlp-mCherry ClearColi BL21 (DE3) strain after 24 h incubation. For pNOSO-mCherry circuit, mCherry production fold change both in the absence [$T7_{IPTG(-)}$] and presence [$T7_{IPTG(+)}$] of IPTG induction (500 µM, 37°C) has been highlighted. For pUC-Tlp-mCherry circuit, mCherry production fold change both at 37°C ($Tlp_{37°C}$) and 40°C ($Tlp_{40°C}$) incubation temperature has been highlighted. The error bars represent standard deviation based on three independent measurements (***p=0.0010 as calculated by paired t-test).

Inspired by the performance of the thermo-responsive genetic circuits, I created two thermally regulated darobactin production plasmids (p15A-Tlp-DarA and pUC-Tlp-DarA) and established them in ClearColi. The p15A-Tlp-DarA plasmid had a medium-copy number replicon (p15A) (**Figure 9A**), while the pUC-Tlp-DarA plasmid had a high-copy number replicon (pUC) (**Figure 9B**). In both plasmids, the transcription of the *darA* gene was regulated by the $TlpA_{39}$-P_{tlpA} repressor-promoter complex. To assess their capacity to produce darobactin, the p15A-Tlp-DarA and pUC-Tlp-DarA ClearColi strains were incubated at 37°C and 40°C for 24 hours. At both incubation temperatures, no darobactin was detected in the extracellular media collected from the p15A-Tlp-DarA ClearColi strains (**Figure 9C**). In contrast, the pUC-Tlp-DarA ClearColi strains incubated at 37°C and 40°C allowed the accumulation of ~0.03 µg/mL and ~0.14 µg/mL darobactin in the extracellular media, respectively (**Figure 9C**). Although darobactin concentration was ~5 times higher at 40°C than 37°C for the pUC-Tlp-DarA ClearColi strain, it was still significantly lower than the IPTG-induced pNOSO-darABCDE ClearColi strain. No significant increase in darobactin concentration was observed at incubation temperatures above 40°C for the pUC-Tlp-DarA ClearColi strain (**Figure 9D**). The production levels of mCherry and darobactin from the pUC-Tlp-mCherry and pUC-Tlp-DarA ClearColi strains indicate that the transcriptional rate of the *darA* gene was not comparable to that of the *mCherry* gene. The insufficient *darA* mRNA population may have disrupted the *darA*:*darE* transcript ratio, negatively affecting overall darobactin production from the microbial chassis (Wuisan et al., 2021). Despite the low concentration of darobactin, I wanted to test whether the extracellular media could still exhibit an

antimicrobial activity against *P. aeruginosa* PAO1. To ensure plasmid retention in the ClearColi strains, I had added 100 µg/mL of ampicillin to the growth media. However, I needed to confirm that the ampicillin supplementation did not generate any false-positive signals for the *P. aeruginosa* PAO1 growth inhibition assay. Therefore, extracellular media (FM) collected post-growth of the wild-type ClearColi strain was supplemented with 100 µg/mL ampicillin or 2 µg/mL darobactin to test for their antimicrobial activity against *P. aeruginosa* PAO1. Supplementation with 100 µg/mL of ampicillin did not affect the growth of the pathogenic strain, whereas 2 µg/mL of darobactin significantly inhibited the growth of *P. aeruginosa* PAO1 (**Figure 9E**). In addition, there was no significant synergistic effect observed for the combination of 100 µg/mL ampicillin and 2 µg/mL darobactin against *P. aeruginosa* PAO1, compared to darobactin supplementation alone. Therefore, the antimicrobial activity in the extracellular media could be solely attributed to darobactin and not to the residual ampicillin concentrations. As expected, none of the pUC-Tlp-DarA ClearColi cell-free media samples were able to inhibit the growth of *P. aeruginosa* PAO1 (**Figure 9F**). This observation confirmed that the darobactin concentration present in the extracellular media was insufficient to exert significant antimicrobial activity.

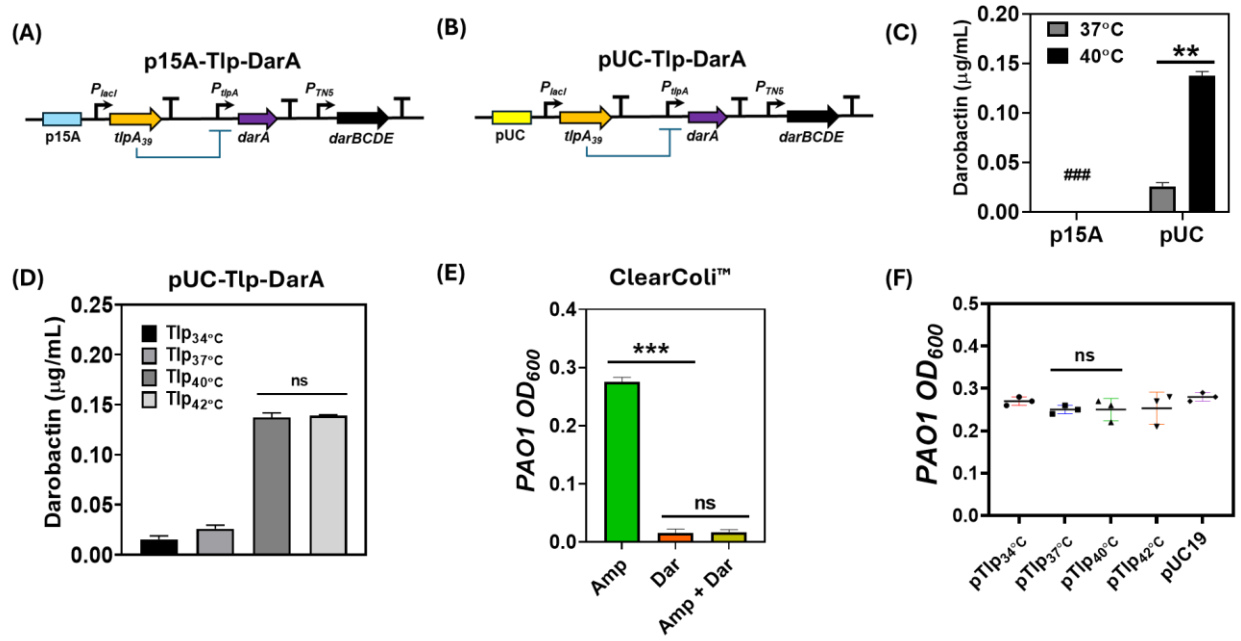

Figure 9. (A) Schematic diagram of the p15A-Tlp-DarA genetic circuit (B) Schematic diagram of the pUC-Tlp-DarA genetic circuit (C) Darobactin concentration in the liquid medium (in µg/mL) for the p15A and pUC origin based Tlp-DarA genetic circuits from ClearColi BL21 (DE3) strains after 24 h incubation at 37°C and 40°C respectively. (###) represents darobactin concentration lower than the Limit of Detection (LOD) by ESI-MS. The pUC-Tlp-DarA circuit produced higher darobactin levels (~4 fold change) at 40°C

in comparison to 37°C. The error bars represent standard deviation based on three independent measurements (**p=0.0016 as calculated by paired t-test) (D) Darobactin concentration in the liquid medium (in µg/mL) for the pUC-Tlp-DarA construct in ClearColi BL21 (DE3) strain after 24 h of incubation at 34°C, 37°C, 40°C and 42°C respectively. The bacteria were cultivated in FM supplemented with 100 µg/mL ampicillin. The error bars represent standard deviation based on three independent measurements (^{ns}p= 0.6304 as calculated by paired t-test) (E) End-point absorbance (OD_{600}) of *P. aeruginosa* PAO1 after 18 h incubation at 37°C in filter-sterilized FM sustaining the growth of the wild type ClearColi™ strain. The extracellular media was supplemented with 100 µg/mL ampicillin, 2 µg/mL darobactin or a combination of both (100 µg/mL ampicillin + 2 µg/mL darobactin) before the assay to assess their respective antimicrobial activity. The error bars represent standard deviation based on three independent measurements (***p=0.0006, ^{ns}p=0.6460 as calculated by paired t-test) (F) End-point absorbance (OD_{600}) of *P. aeruginosa* PAO1 after 18 h incubation at 37°C in filter-sterilized FM (supplemented with 100 µg/mL ampicillin) sustaining the growth of the pUC-Tlp-DarA ClearColi BL21 (DE3) strain for 24 h at 34°C, 37°C, 40°C and 42°C incubation temperatures respectively. The pUC19 ClearColi strain (37°C, 24 h) was used as a negative control. The error bars represent standard deviation based on three independent measurements (^{ns}p>0.9999 as calculated by paired t-test).

Our previous observations indicated that the P_{T7} promoter driven *darA* gene transcription for the pNOSO-darABCDE ClearColi strain resulted in higher levels of darobactin accumulation in the extracellular media. I hypothesized that a genetic circuit that utilized the P_{T7} promoter for *darA* gene transcription and the thermal input to regulate the stability of the $TlpA_{39}$-P_{tlpA} repressor-promoter complex could be a better option for thermo-responsive darobactin production. When incubated at 37°C, $TlpA_{39}$ repressor protein would bind to the P_{tlpA} promoter and prevent *darA* gene transcription from the adjacent P_{T7} promoter. At higher temperatures (40°C), repression by $TlpA_{39}$ protein would be destabilized, allowing T7RNAP to bind to the P_{T7} promoter and initiate *darA* gene transcription. To test this hypothesis, I designed two genetic circuits, pT7-Tlp-DarA and pT7-spc-Tlp-DarA, based on the high-copy number replication origin (pUC) and established them in ClearColi. The gene circuit pT7-Tlp-DarA had the P_{T7} promoter placed immediately upstream (no spacer) of the P_{tlpA} promoter region (**Figure 10A**). In contrast, I introduced a spacer region (134 nucleotide base pairs) between the P_{T7} and P_{tlpA} promoters for the PT7-spc-Tlp-DarA gene circuit to avoid steric hindrance between the T7RNAP and σ70-RNAP protein complexes during their interaction with the respective promoter regions (**Figure 10B**) (Song and Su., 2014). Both pT7-Tlp-DarA and pT7-spc-Tlp-DarA ClearColi strains were grown in ampicillin-supplemented FM and incubated at 37°C and 40°C for 24 hours. However, none of the strains could exceed the darobactin concentration previously observed for the pUC-Tlp-DarA ClearColi strain incubated at 40°C. The pT7-spc-Tlp-darA Clearcoli strain demonstrated a ~2.8-fold increase in darobactin concentration at 40°C compared to the 37°C incubated samples (**Figure 10C**). On the other hand,

the pT7-Tlp-darA ClearColi strain resulted in a ~0.8-fold decrease in darobactin concentration for the samples incubated at 40°C compared to 37°C (**Figure 10C**). Due to the low darobactin concentrations, none of the cell-free media could inhibit the growth of *P. aeruginosa* PAO1 during the growth inhibition assay (**Figure 10D**). These results suggested that our previous genetic design (pUC-Tlp-DarA) had superior performance in terms of overall darobactin production (~0.14 ug/mL) and higher fold changes (~5 fold) compared to the pT7-Tlp-DarA and pT7-spc-Tlp-DarA genetic circuits.

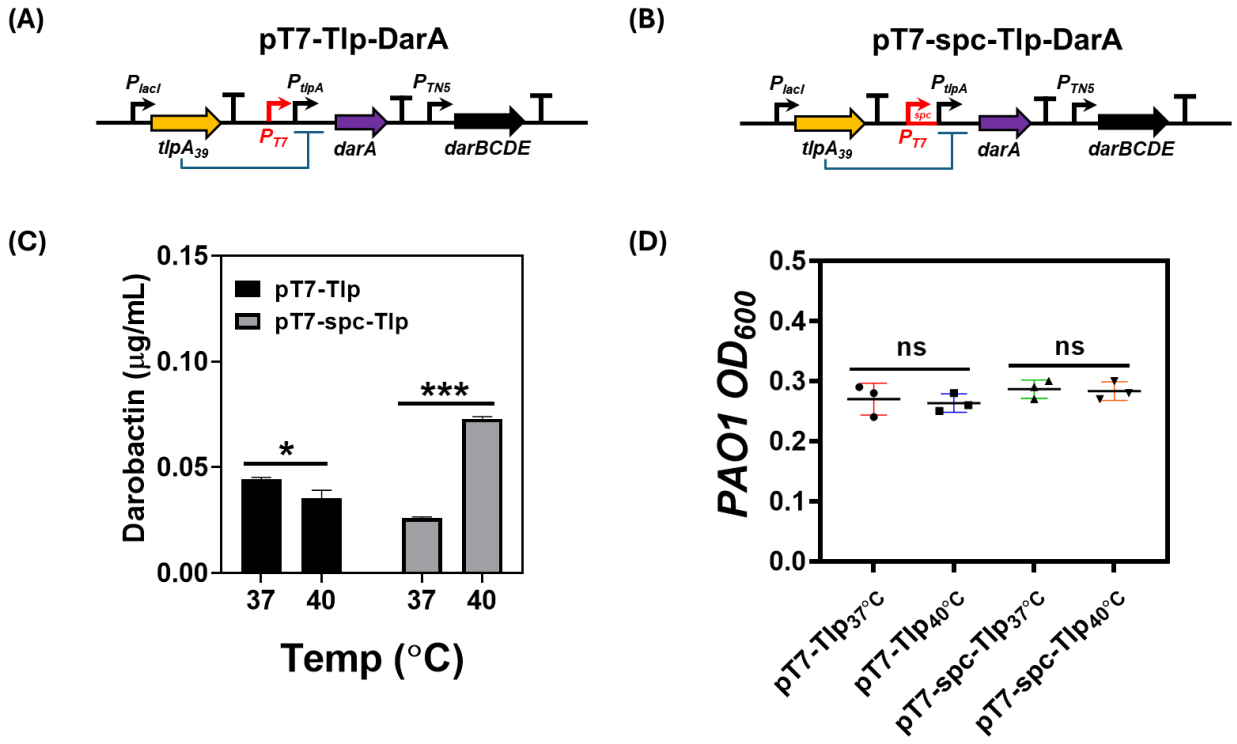

Figure 10. (A) Schematic diagram of the pT7-Tlp-DarA genetic circuit (B) Schematic diagram of the pT7-spc-Tlp-DarA genetic circuit (C) Darobactin concentration in the liquid medium (in µg/mL) for the pT7-Tlp-DarA and pT7-spc-Tlp-DarA ClearColi BL21 (DE3) strains after 24 h incubation in FM at 37°C and 40°C respectively. The error bars represent standard deviation based on three independent measurements (*p=0.0373, ***p=0.0002 as calculated by paired t-test) (D) End-point absorbance (OD_{600}) of *P. aeruginosa* PAO1 after 18 h incubation at 37°C in filter-sterilized FM (supplemented with 100 µg/mL ampicillin) sustaining the growth of the pT7-Tlp-DarA and pT7-spc-Tlp-DarA ClearColi BL21 (DE3) strains for 24 h at 37°C and 40°C incubation temperatures respectively. The error bars represent standard deviation based on three independent measurements (^{ns}p=0.6349, ^{ns}p=0.4226 as calculated by paired t-test).

3.3.4. Designing antibiotic-free plasmid retention strategies for thermo-responsive darobactin production

Before proceeding with testing further strategies to improve thermos-responsive darobactin production, I addressed the issue of antibiotic-based plasmid retention needed in the current constructs. Although the addition of antibiotics (ampicillin and kanamycin) to the growth media (FM) did not affect darobactin-mediated inhibition of *P. aeruginosa* PAO1, antibiotic selection pressure-based plasmid retention is not suitable for engineered live biotherapeutic product (eLBP) development. To avoid the need for antibiotic supplementation during darobactin production, I tested two strategies for retaining the recombinant plasmids: nutrient auxotrophy and toxin-antitoxin-dependent post-segregational killing. First, using the Cre-loxP-based recombination strategy, the essential alanine racemase genes (*alr* and *dadX*) responsible for D-alanine biosynthesis were deleted from the ClearColi genome. The inability of the Δ*alr* Δ*dadX* ClearColi strain to synthesize D-alanine, a critical component required for bacterial cell wall synthesis, resulted in its dependence on the external supplementation of D-alanine in the growth media (Hwang et al., 2017). For plasmid retention in the absence of D-alanine, I inserted the *alr* gene (amplified from the *E. coli* K-12 bacterial genome) into the pUC-Tlp-DarA vector, creating the pTlp-DarA-alr plasmid, and established it in the Δ*alr* Δ*dadX* ClearColi strain (**Figure 11A**). The microbial chassis would then ensure retention of the recombinant plasmid over several generations to facilitate D-alanine synthesis using the alanine racemase enzyme. For toxin-antitoxin (TA) based plasmid retention, the type II TA gene pair, *txe-axe*, was amplified from the pUC-GFP AT plasmid (Addgene #133306) and cloned into the pUC-Tlp-DarA vector backbone, creating the pTlp-DarA-AT plasmid, and maintained in the ClearColi strain (**Figure 11B**). The *txe* gene encodes for the Txe endoribonuclease enzyme responsible for depleting the mRNA transcript pool of the microbial chassis. The Axe antitoxin protein actively sequesters the Txe enzyme and prevents it from degrading the mRNA transcripts. Due to its low stability, losing the recombinant plasmid would cause a drastic decrease in Axe antitoxin protein levels and halt its production. Without the Axe antitoxin, the relatively stable Txe enzyme would start degrading the mRNA population and prevent protein translation, thereby eliminating the bacterial population that has lost the recombinant plasmid (Fedorec et al., 2019).

The pTlp-DarA-alr Δ*alr* Δ*dadX* ClearColi and pTlp-DarA-AT ClearColi strains were cultivated in FM, both with and without antibiotic supplementation at 37°C and 40°C for 24 hours. No significant difference in darobactin concentration was observed for either strain when cultivated at 40°C without antibiotic supplementation (**Figure 11C, Figure 11D**). In addition, incorporating these genetic modules did not affect the overall thermo-responsive fold change (~5 fold), as observed previously for the pUC-Tlp-DarA ClearColi strain-based darobactin production. All the cell-free media samples were tested for their respective antimicrobial activity against *P. aeruginosa* PAO1 in the growth inhibition assay. None of the samples could inhibit the growth of *P. aeruginosa* PAO1, suggesting that neither of the plasmid retention gene modules interfered with nor boosted the antimicrobial activity of darobactin (**Figure 11E**). As both strategies were comparable in performance, I decided to incorporate the *txe-axe* TA system in all the genetic designs made for further optimization of thermo-responsive darobactin production, since it did not require additional genomic modification of the host strain.

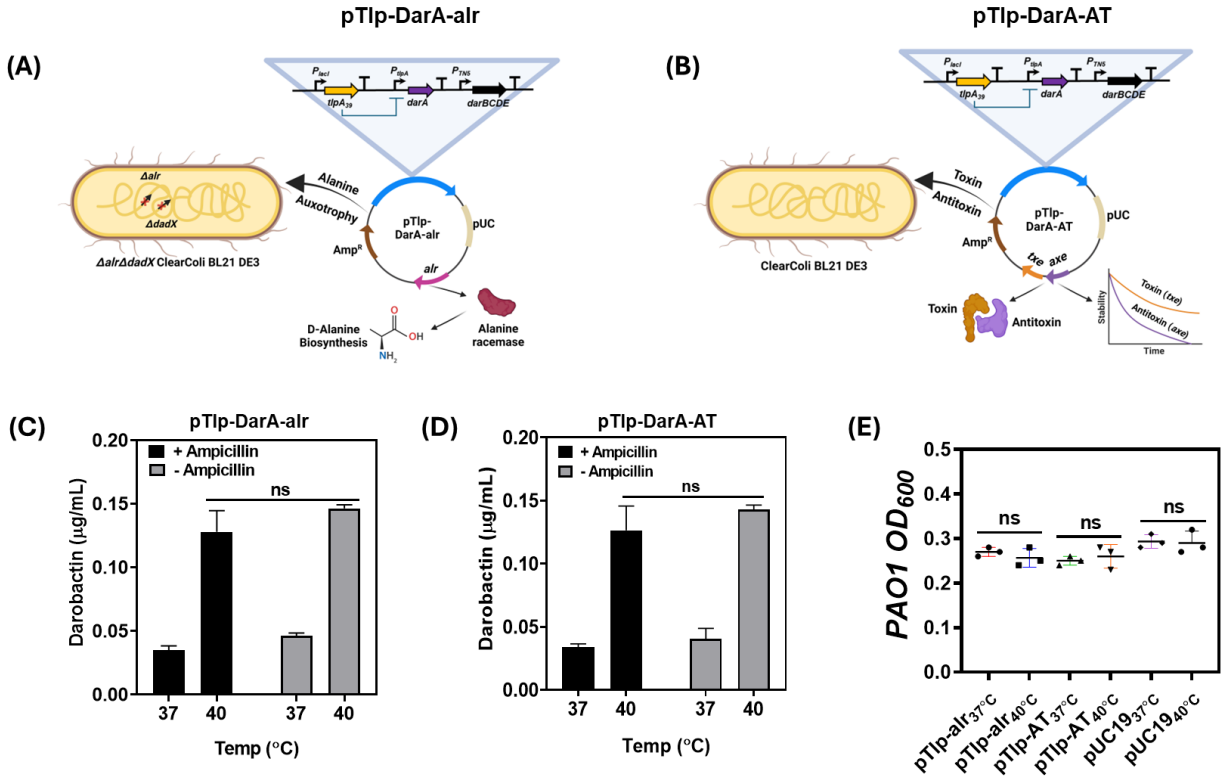

Figure 11. (A) Schematic representation of the pTlp-DarA-alr construct transformed in Δ*alr* Δ*dadX* ClearColi BL21 DE3 strain. The integration of the alanine racemase (*alr*) gene in the pUC-Tlp-DarA vector backbone facilitates alr enzyme mediated conversion of L-alanine to D-alanine, which is responsible for bacterial cell wall synthesis in the auxotrophic strain (B) Schematic representation of the pTlp-DarA-AT construct transformed in ClearColi BL21 (DE3). The integration of the *txe* toxin - *axe* antitoxin (TA) gene

pair in the pUC-Tlp-DarA vector backbone mediates plasmid retention by its controlled endoribonuclease activity and differential protein stability rates (C) Darobactin concentration in the liquid medium (in µg/mL) for the pTlp-DarA-alr construct after 24 h of incubation at 37°C and 40°C, both with and without 100 µg/mL ampicillin supplementation in FM. The error bars represent standard deviation based on three independent measurements (^{ns}p =0.2428 as calculated by paired t-test) (D) Darobactin concentration in the liquid medium (in µg/mL) for the pTlp-DarA-AT construct after 24 h of incubation at 37°C and 40°C, both with and without 100 µg/mL ampicillin supplementation in FM. The error bars represent standard deviation based on three independent measurements (^{ns}p =0.2135 as calculated by paired t-test) (E) End-point absorbance (OD_{600}) of *P. aeruginosa* PAO1 after 18 h incubation at 37°C in filter-sterilized FM (no ampicillin supplementation) sustaining the growth of the pTlp-DarA-alr and pTlp-DarA-AT ClearColi BL21 (DE3) strains for 24 h at 37°C and 40°C incubation temperatures respectively. The pUC19 ClearColi strain was used as a negative control. The error bars represent standard deviation based on three independent measurements (^{ns}p=0.2697, ^{ns}p=0.6784, ^{ns}p=0.7418 as calculated by paired t-test).

3.3.5. Evaluation of thermo-responsive darobactin production in *E. coli* Nissle 1917 (EcN)

Based on my previous experiments, I concluded that the P_{T7} promoter was more effective (**Figure 6C**) for darobactin production in ClearColi compared to the P_{tlpA} promoter (**Figure 9C**). I hypothesized that if the T7RNAP production could be regulated in response to thermal trigger in the bacterial strain, which then facilitated P_{T7} promoter-based *darA* gene transcription, then the darobactin production from this thermo-amplifier circuit would significantly improve compared to the thermo-responsive genetic circuit (pTlp-DarA-AT). To enable this, I needed to design a genetic circuit where the $TlpA_{39}$ repressor protein regulated the P_{tlpA} promoter-driven transcription of the *t7-RNAP* gene in the microbial chassis. However, this genetic circuit could not be established in the ClearColi strain (being used this far in the experimental design) because constitutive expression of the genomically integrated *t7-RNAP* gene would then interfere with its performance. Therefore, I needed a microbial strain where orthogonal expression of the *t7-RNAP* gene could be facilitated, without any interference from the host strain itself.

To overcome the obstacle, I decided to use the *E. coli* Nissle 1917 (EcN) strain for conducting further analysis of the genetic circuits. EcN is a well-known probiotic bacteria isolated by Dr. Alfred Nissle in 1917 from the fecal matter of a German soldier who participated in the First World War (Sonnenborn, 2016). Early reports indicated that the EcN strain could prevent harmful enterobacteria infections in the gut and reduce the risk of diarrhea in humans. Due to its beneficial properties, Ardeypharm GmbH in Germany acquired a license to manufacture and market the EcN strain commercially under the trade name Mutaflor®. Several studies have confirmed the effectiveness of the EcN strain in positively modulating the human intestinal microflora, making

it an ideal candidate for eLBP development. To investigate whether high darobactin production could be sustained by the EcN microbial chassis, I decided to first test the performance of the pNOSO-darABCDE plasmid in the EcN-T7 strain (**Figure 12A**). In the EcN-T7 strain, the *t7-RNAP* gene has been integrated into the EcN genome, and its expression is constitutively driven by the P_{lacUV5} promoter (Fiege and Frankenberg-Dinkel., 2020) like the ClearColi strain. The constitutively expressed single-subunit protein T7RNAP (**Figure 12B**) would bind specifically to the P_{T7} promoter (Fuerst et al., 1987) to drive *darA* gene transcription without interference from the native RNAP of EcN. The pNOSO-darABCDE EcN-T7 strain was cultivated in FM supplemented with 50 µg/mL kanamycin at 37°C, both with and without IPTG supplementation, for 24 hours. After incubation, ~4.7 µg/mL and ~8.2 µg/mL of darobactin was detected in the uninduced and IPTG-induced pNOSO-darABCDE EcN-T7 samples respectively (**Figure 12C**). The darobactin concentrations were significantly higher than that observed previously for the pNOSO-darABCDE ClearColi strain (~2.5 µg/mL), suggesting that P_{T7} promoter-based darobactin expression was superior in the EcN-T7 strain when compared to ClearColi. Darobactin production was also approximately 2 to 3 times higher in the non-induced and IPTG-induced pNOSO-darABCDE EcN-T7 strain compared to the IPTG-induced pNOSO-darABCDE ClearColi strain. This difference in production levels may be due to the inherent ability of the EcN-based strains to better manage the intracellular toxicity caused by darobactin production, allowing for higher levels of darobactin to be released into the extracellular media. In addition, both the uninduced and IPTG-induced cell-free media significantly inhibited the growth of *P. aeruginosa* PAO1 strain compared to the control (**Figure 12D**). Despite significant darobactin production with IPTG supplementation, the pNOSO-darABCDE circuit still displayed high basal level expression in EcN-T7 even without IPTG. Although lacI-based regulation was inefficient to control darobactin production in EcN-T7, these observations confirmed that EcN could be a suitable microbial chassis for sustaining high levels of darobactin production.

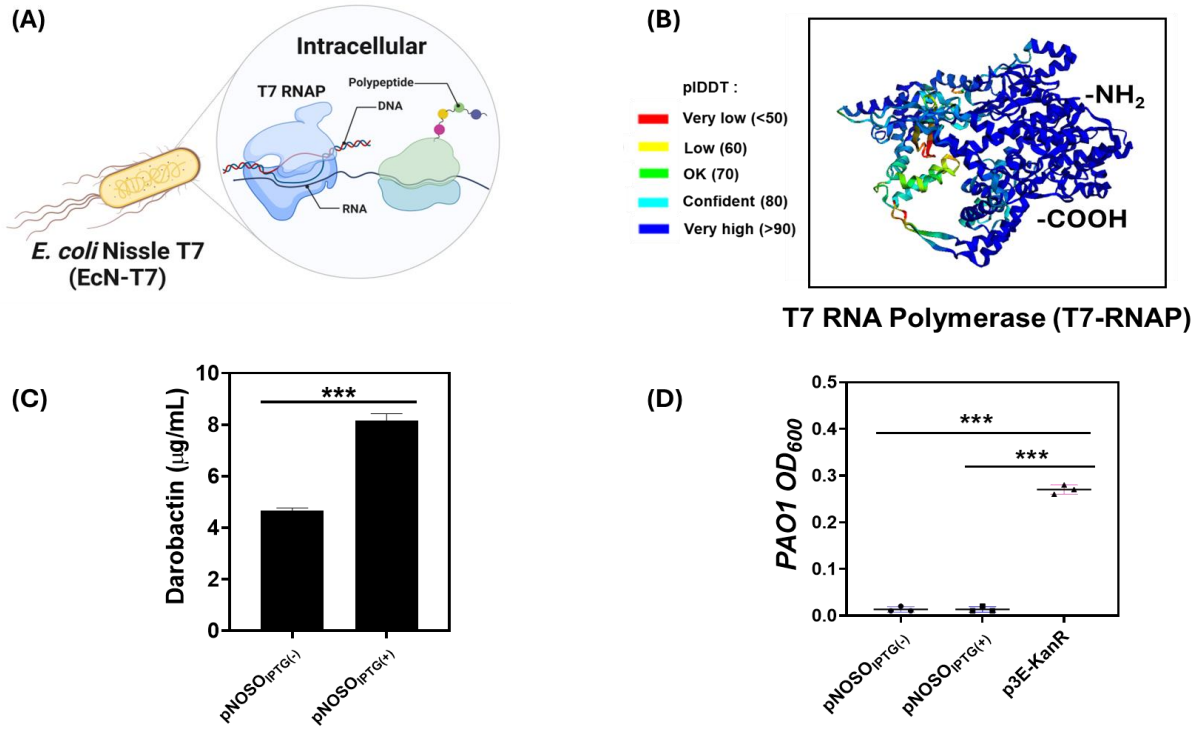

Figure 12. (A) Schematic diagram of the *E. coli* Nissle 1917 – T7 RNAP encoded (EcN-T7) strain (Fiege and Frankenberg-Dinkel, 2020). The inset highlights the orthogonal T7 RNA Polymerase (encoded in the bacterial genome) driving gene transcription from the P_{T7} promoter in the intracellular milieu (B) AlphaFold 3D structure prediction of the T7 RNA Polymerase (originally isolated from the T7 bacteriophage). The per-residue confidence metric (pLDDT) highlights the confidence in the predicted structure represented by the respective color codes (C) Darobactin concentration in the liquid medium (in µg/mL) for the pNOSO-darABCDE construct established in the EcN-T7 strain after 24 h incubation at 37°C. The strain was grown in FM (with 50 µg/mL kanamycin) both in the absence [$pNOSO_{IPTG(-)}$] and presence [$pNOSO_{IPTG(+)}$] of 500 µM IPTG supplementation (added at OD_{600} =0.4). The error bars represent standard deviation based on three independent measurements (***p= 0.0010 as calculated by paired t-test) (D) End-point absorbance (OD_{600}) of *P. aeruginosa* PAO1 after 18 h incubation at 37°C in filter-sterilized FM sustaining the growth of pNOSO-darABCDE EcN-T7 strain both with and without IPTG supplementation (37°C, 24 h). The p3E-KanR EcN-T7 strain was used as a negative control (FM, No IPTG, 37°C, 24 h). The error bars represent standard deviation based on three independent measurements (***p=0.0007 as calculated by paired t-test).

As with other *E. coli* strains, the process of gene transcription in the EcN strain also relies on the RNAP holoenzyme, which consists of five subunits - α (2 copies), ß and ß' (1 copy each), and ω (1 copy). Initiation proteins (σ factors) recruit the RNAP holoenzyme to specific regions on the DNA, called promoters, and drive gene transcription (**Figure 13A**). In *E. coli*, most of the gene transcription is initiated by the housekeeping sigma factor RpoD (σ70) protein (Tomatis et al., 2019). Previous studies have shown that the σ70-RNAP complex drives transcription from the P_{tlpA} promoter in the *E. coli* DH10B strain (Piraner et al., 2017). To determine if the P_{tlpA} promoter

incorporating genetic circuits functioned similarly in related *E. coli* strains, I established the pTlp-DarA-AT recombinant plasmid in the EcN strain (**Figure 13B**). The pTlp-DarA-AT EcN strain was incubated in FM without antibiotic supplementation for 24 hours at 37°C and 40°C. After incubation, I detected ~0.02 µg/mL and ~0.07 µg/mL of darobactin in the extracellular media of samples incubated at 37°C and 40°C, respectively with a net fold change of ~3 (**Figure 13C**). Although the concentrations and fold change of darobactin were slightly lower than its ClearColi-based counterparts, the experiment confirmed that P_{tlpA} promoter-driven *darA* gene transcription was possible in the EcN strain. As anticipated, none of the cell-free media could inhibit *P. aeruginosa* PAO1 growth compared to the wild-type control strains in the inhibition assay (**Figure 13D**). The non-inhibitory potential of the cell-free media further confirmed that the EcN secretome had no natural antimicrobial activity, making it orthogonal to the darobactin based *P. aeruginosa* PAO1 inhibition process.

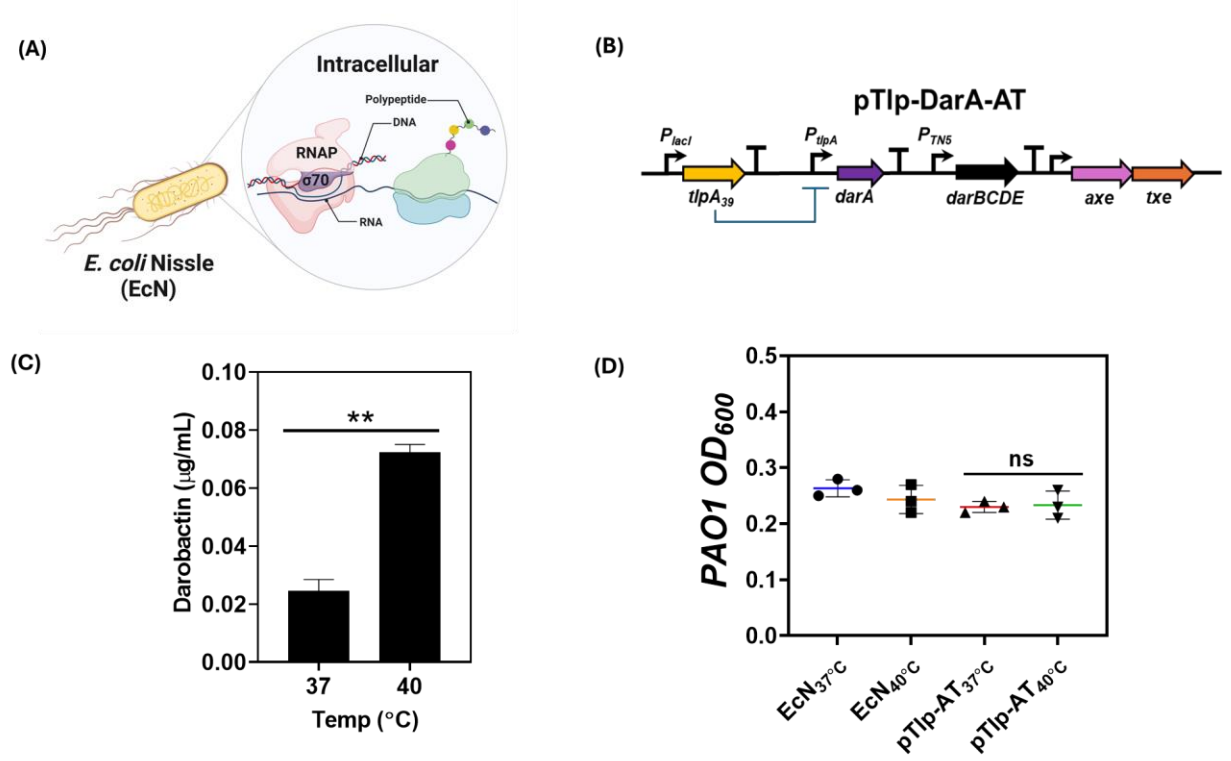

Figure 13. (A) Schematic diagram of the probiotic *E. coli* Nissle (EcN) 1917 (Mutaflor®) strain. The inset highlights the housekeeping σ70 RNA Polymerase responsible for transcribing the P_{tlpA} promoter encoded gene in the intracellular milieu (B) Schematic diagram of the pTlp-DarA-AT genetic circuit established in EcN (C) Darobactin concentration in the liquid medium (in µg/mL) for the pTlp-DarA-AT *E. coli* Nissle 1917 strain after 24 h incubation in FM (no ampicillin supplementation) at 37°C and 40°C respectively. The error bars represent standard deviation based on three independent measurements (**p=0.0058 as

calculated by paired t-test) (D) End-point absorbance (OD_{600}) of *P. aeruginosa* PAO1 after 18 h incubation at 37°C in filter-sterilized FM (no ampicillin supplementation) sustaining the growth of the wild type and pTlp-DarA-AT *E. coli* Nissle 1917 strains for 24 h at 37°C and 40°C incubation temperatures respectively. The error bars represent standard deviation based on three independent measurements ($^{ns}p=0.8845$ as calculated by paired t-test).

3.3.6. Genetic circuit modifications for thermo-responsive darobactin production in EcN

Despite the low levels of darobactin produced by the thermo-responsive genetic circuit, it was apparently clear that the EcN strain was suitable for testing the performance of a thermo-amplifier genetic circuit. To enable this, I amplified the *t7-RNAP* gene from the mBP-T7RNAP plasmid (Addgene # 74096) and placed it downstream of the P_{tlpA} promoter. Although at 37°C, the $TlpA_{39}$ repressor protein would prevent its expression, at elevated temperatures (like 40°C) the de-repression of the P_{tlpA} promoter would enable T7RNAP expression, resulting in P_{T7} promoter-based transcription of the *darA* gene. Translation of the *darA* mRNA transcript would then produce the DarA propeptide, leading to extracellular release of darobactin after post-translational modification. In addition, the *txe-axe* TA genes encoded in the plasmid would further allow antibiotic-free plasmid retention in the microbial chassis during darobactin production. Due to its ability to amplify the darobactin production in response to a thermal trigger (thermo-amplifier), the recombinant plasmid was named pTAMP-DarA-AT and established in EcN (**Figure 14A**). To test whether the thermo-amplifier circuit could lead to high darobactin production, I cultured the pTAMP-DarA-AT EcN strain in FM for 24 hours without antibiotic supplementation at both 37°C and 40°C incubation temperatures. Upon analyzing the extracellular media, I found that the concentration of darobactin was ~4.1 µg/mL at 40°C, while below the ESI-MS detection limit of 0.01 µg/mL at 37°C (**Figure 14B**). This result confirmed that T7RNAP production was strongly regulated at 37°C and could only be expressed at higher temperatures, such as 40°C, to drive *darA* gene transcription from the P_{T7} promoter and ensure darobactin production. Upon analyzing the cell-free media for their antimicrobial activity, only the samples collected from the pTAMP-DarA-AT EcN strain incubated at 40°C were observed to inhibit growth of the *P. aeruginosa* PAO1 strain (**Figure 14C**). In contrast, the 37°C incubated pTAMP-DarA-AT and wild-type EcN samples (at both 37°C and 40°C), did not exhibit any such inhibition (**Figure 14C**). To confirm our findings from the growth inhibition assay, I plated the *P. aeruginosa* PAO1 samples treated with cell-free media on MHI Agar (no antibiotic supplementation) and incubated them at 37°C. A

bacterial lawn of *P. aeruginosa* PAO1 was observed on MHI Agar for samples grown in the cell-free media of the 37°C-incubated pTAMP-DarA-AT EcN strain (**Figure 14D**). In contrast, only a few isolated colonies of *P. aeruginosa* PAO1 appeared for the samples treated with the cell-free media of pTAMP-DarA-AT EcN strain incubated at 40°C (**Figure 14D**). These experiments confirmed that darobactin, produced by the thermo-amplifier circuit, could show significant antimicrobial activity against *P. aeruginosa* PAO1 and drastically reduce its ability to regrow on fresh media.

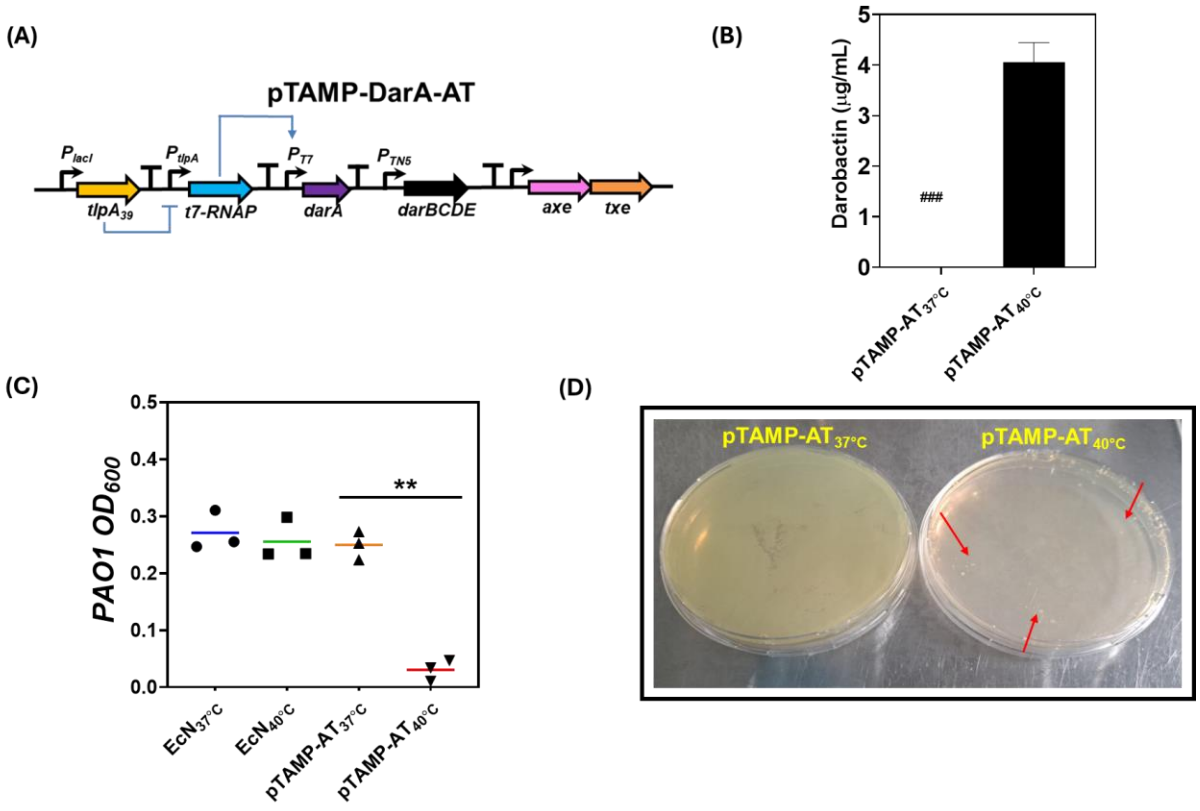

Figure 14. (A) Schematic diagram of the pTAMP-DarA-AT genetic circuit. The $TlpA_{39}$ repressor protein regulates the *t7-RNAP* gene expression at incubation temperatures <39°C, beyond which the system is de-repressed leading to *t7-TNAP* gene expression and P_{T7} promoter based DarA propeptide production (B) Darobactin concentration in the liquid medium (in µg/mL) for the pTAMP-DarA-AT EcN strain in FM (no ampicillin supplementation) after 24 h incubation at 37°C and 40°C respectively. (##) represents darobactin concentrations lower than the Limit of Detection (LOD) by ESI-MS. The error bars represent standard deviation based on three independent measurements (C) End-point absorbance (OD_{600}) of *P. aeruginosa* PAO1 after 18 h incubation at 37°C in filter-sterilized FM (no ampicillin supplementation) sustaining the growth of the wild type and pTAMP-DarA-AT EcN strains for 24 h at 37°C and 40°C incubation temperatures respectively. The error bars represent standard deviation based on three independent measurements (**p=0.0093 as calculated by paired t-test) (D) *P. aeruginosa* PAO1 cultivated on Mueller-Hinton (MHI) Agar post treatment with filter-sterilized FM (no ampicillin supplementation) sustaining the

growth of pTAMP-DarA-AT EcN strain for 24 h at 37°C and 40°C incubation temperature respectively (Figure 14C). The agar plates were placed in a static incubator at 37°C for 18 h before imaging. The pTAMP-DarA-AT (37°C) supernatant treated samples gave rise to a lawn of *P. aeruginosa* PAO1 bacteria (The plate appears green due to pyoverdine pigment produced naturally by the bacteria). The pTAMP-DarA-AT (40°C) supernatant treated samples only produced a few isolated colonies of *P. aeruginosa* PAO1 (The plate appears yellowish due to the natural color of the MHI Agar devoid of any pigment production). The red arrows highlight *P. aeruginosa* PAO1 colonies. The data was independently verified at least two times.

Both the thermo-responsive (pTlp-DarA-AT) and thermo-amplifier (pTAMP-DarA-AT) EcN strains were observed to produce darobactin after the 24-hour incubation period. However, it was essential to determine the maximum darobactin concentration that the recombinant EcN strains could tolerate before undergoing self-inhibition. MIC analysis revealed that ~1.6 µg/mL of darobactin could suppress the growth of the wild-type EcN strain cultivated in FM at both 37°C and 40°C incubation temperatures. However, higher concentrations of darobactin (>16 µg/mL) were required to inhibit the growth of the recombinant pTlp-DarA-AT and pTAMP-DarA-AT EcN strains cultivated in FM at similar incubation temperatures (37°C and 40°C). This increased darobactin tolerance capacity of the recombinant EcN strains could be due to the constitutive expression of the DarBCD tripartite efflux pump, which facilitates the extracellular export of darobactin to prevent its accumulation within the microbial chassis. The darobactin export machinery (DarBCD) facilitated the pNOSO-darABCDE EcN-T7 and pTAMP-DarA-AT EcN strains to previously sustain higher darobactin production and extracellular release without undergoing self-inhibition. To determine if darobactin production caused intracellular toxicity by interfering with the cell membrane formation of the production strain, I analyzed the growth kinetics (OD_{600}) of wild-type and recombinant EcN strains in FM (without antibiotic supplementation) for 24 hours at 37°C and 40°C using the UV-Vis Microplate Reader. Although all strains of EcN had a brief lag phase of approximately one hour, they exhibited a similar temporal pattern of attaining their exponential growth and stationary phases. By the end of the 24-hour incubation period, the wild-type EcN strain reached a slightly higher optical density (0.99±0.03 at 37°C, 0.94±0.03 at 40°C) than the pTlp-DarA-AT (0.94±0.01 at 37°C, 0.90±0.04 at 40°C) and pTAMP-DarA-AT EcN strains (0.90±0.01 at 37°C, 0.84±0.04 at 40°C) (**Figure 15A; Figure 15B**). To assess whether the reduction in optical density affected the overall bacterial biomass, I compared the pellet weight of the wild-type and recombinant EcN strains. The bacteria were grown in 25 mL FM cultures without antibiotic supplementation and incubated for 24 hours at 40°C. No

significant difference between the wild-type EcN biomass (539±7 mg), pTlp-DarA-AT EcN biomass (535±7 mg), and pTAMP-DarA-AT EcN biomass (527±3 mg) could be observed after 24 hours. This study confirmed that the production of darobactin by the recombinant pTlp-DarA-AT and pTAMP-DarA-AT plasmids did not significantly affect the growth or biomass formation of the EcN strain. Another interesting trend in the bacterial growth kinetics was that the 40°C incubated pTlp-DarA-AT and pTAMP-DarA-AT EcN strains showed the highest spike in growth rate within the 3 to 4-hour incubation period, accounting for a growth rate of 0.1 and 0.08-hour^{-1} and gradually tapering off to 0.04 and 0.05-hour^{-1} within the 4-to-6-hour period respectively (**Figure 15A; Figure 15B**). The high growth rates of the recombinant EcN strains during this brief incubation time piqued my curiosity about their impact on darobactin production. To determine if sufficient darobactin could be produced within the given time, the pTlp-DarA-AT and pTAMP-DarA-AT EcN strains were cultivated at 40°C for 4 and 6 hours, respectively. Post incubation, the cell-free media was checked for antimicrobial activity against *P. aeruginosa* PAO1 in the growth inhibition assay. None of the 4 and 6-hour-incubated cell-free media collected from the pTlp-DarA-AT EcN strain inhibited *P. aeruginosa* PAO1, as was previously observed for the 24-hour-incubated samples (**Figure 15C**). Both samples showed the formation of a bacterial lawn when plated on MHI agar after inoculating the cell-free media with *P. aeruginosa* PAO1 (**Figure 15D**). Although no antimicrobial activity was observed for the 4-hour incubated cell-free media collected from the pTAMP-DarA-AT EcN strain, significant growth inhibition of *P. aeruginosa* PAO1 was observed for the 6-hour incubated cell-free media samples (**Figure 15C**). Upon plating the 4-hour incubated samples, a bacterial lawn was observed, while only a few isolated colonies of *P. aeruginosa* PAO1 were seen on MHI Agar for the 6-hour incubated samples (**Figure 15D**). These observations suggested that the pTAMP-DarA-AT EcN strain could produce sufficient darobactin within the first 6-hour incubation at 40°C to inhibit the growth of the pathogenic *P. aeruginosa* PAO1 strain.

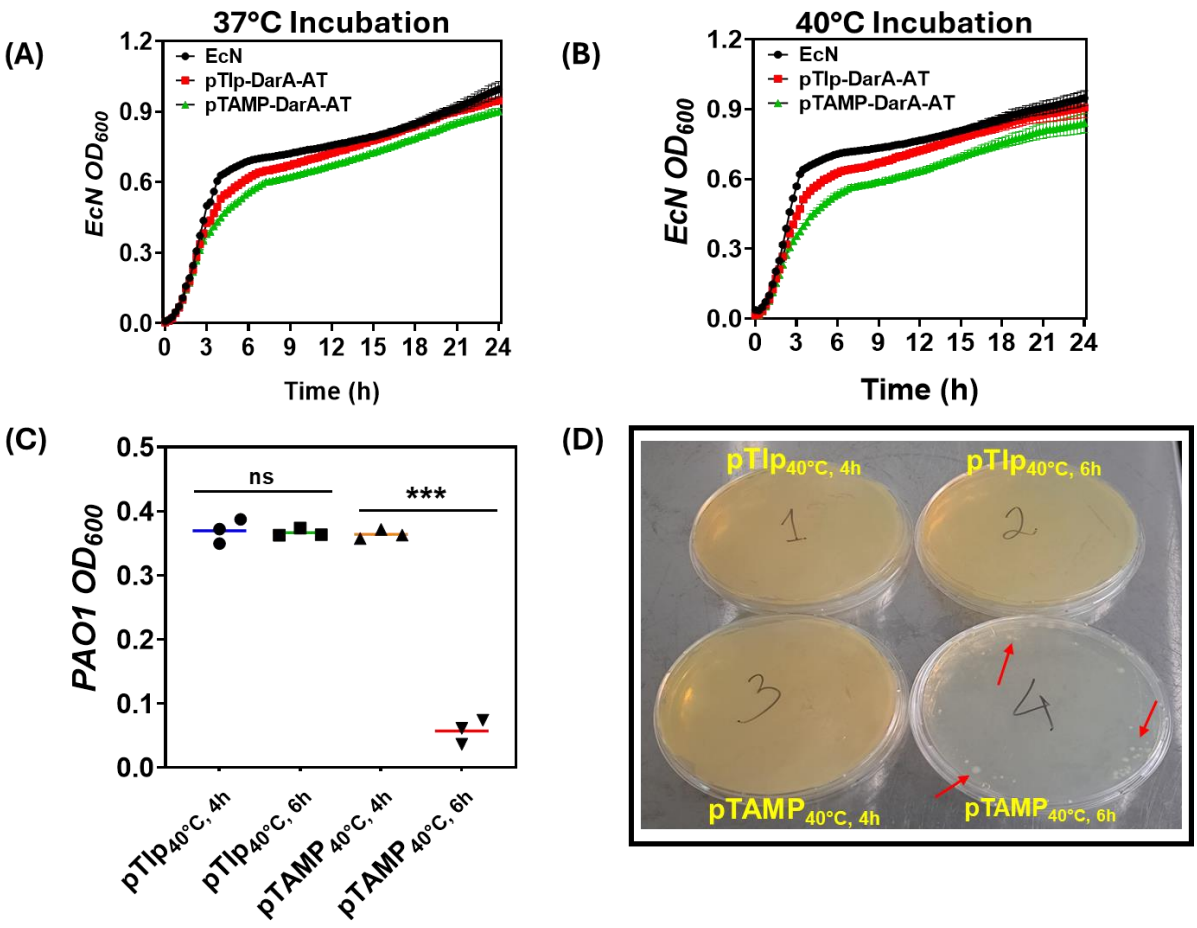

Figure 15. (A) Growth Kinetics of the wild type, pTlp-DarA-AT and pTAMP-DarA-AT EcN strains in FM (no antibiotic supplementation) at 37°C incubation temperature for a 24 h kinetic cycle. The samples were shaken continuously, and their Optical Density (OD_{600}) measured at equal time intervals. The error bars represent standard deviation based on three independent measurements (B) Growth Kinetics of the wild type, pTlp-DarA-AT and pTAMP-DarA-AT EcN strains in FM (no antibiotic supplementation) at 40°C incubation temperature for a 24 h kinetic cycle. The samples were shaken continuously, and their Optical Density (OD_{600}) measured at equal time intervals. The error bars represent standard deviation based on three independent measurements (C) End-point absorbance (OD_{600}) of *P. aeruginosa* PAO1 after 18 h incubation at 37°C in filter-sterilized FM (no ampicillin supplementation) sustaining the growth of the pTlp-DarA-AT and pTAMP-DarA-AT EcN strains at 40°C for 4 h and 6 h incubation periods respectively. The error bars represent standard deviation based on three independent measurements ($^{ns}p=0.8526$, $***p=0.0010$ as calculated by paired t-test) (D) *P. aeruginosa* PAO1 cultivated on Mueller-Hinton (MHI) Agar post treatment with filter-sterilized FM (no ampicillin supplementation) sustaining the growth of pTlp-DarA-AT and pTAMP-DarA-AT EcN strains at 40°C for 4 h and 6 h incubation periods respectively (Figure 15C). The agar plates were placed in a static incubator at 37°C for 18 h before imaging. The pTlp-DarA-AT (40°C, 4 h), pTlp-DarA-AT (40°C, 6 h) and pTAMP-DarA-AT (40°C, 4 h) supernatant treated samples gave rise to a lawn of *P. aeruginosa* PAO1 bacteria (The plate appears yellowish-green due to pyoverdine pigment produced naturally by the bacteria). The pTAMP-DarA-AT (40°C, 6 h) supernatant treated samples only produced a few isolated colonies of *P. aeruginosa* PAO1 (The plate appears light yellow due to the natural color of the MHI Agar devoid of any pigment production). The red arrows highlight *P. aeruginosa* PAO1 colonies. The data was independently verified at least two times.

Inspired by the antimicrobial activity of the extracellular media collected from the 6-hour incubated pTAMP-DarA-AT EcN strain, I decided to analyze its performance in further detail. The pTAMP-DarA-AT EcN strain was grown in 25 mL FM cultures for 6 hours at 37°C and 40°C without antibiotic supplementation. Post incubation, ~3.9 µg/mL of darobactin was detected in the extracellular media of the samples incubated at 40°C, whereas for the 37°C incubated samples, the darobactin concentration was below the ESI-MS detection limit of 0.01 µg/mL (**Figure 16A**). No significant increase in darobactin concentration was observed between the 6- and 24-hour incubated pTAMP-DarA-AT EcN samples, confirming that the majority of darobactin was produced by the recombinant strains within the first 6 hours of thermal induction. When assessed for their antimicrobial activity, only the 40°C incubated cell-free media inhibited the growth *of P. aeruginosa* PAO1, whereas the 37°C incubated cell-free media failed to demonstrate any such inhibition (**Figure 16B**). These observations confirmed that a significant proportion of the DarA propeptide underwent post-translational modification to form darobactin within six hours of thermal induction.

To further verify these findings, I conducted transcriptional analysis to evaluate gene expression differences for the recombinant EcN strains. I started by assessing the *darA* mRNA transcript levels for the thermo-responsive, pTlp-DarA-AT EcN strain. Quantitative reverse transcription polymerase chain reaction (RT-qPCR) analysis was performed on the *darA* mRNA transcripts collected from bacterial samples (pTlp-DarA-AT EcN) incubated at 37°C and 40°C for 6 hours. The ΔΔCt were obtained by normalizing the *darA* cycle threshold (Ct) values to their respective 16S rRNA Ct values, and the relative quantification ($2^{-\Delta\Delta Ct}$) was measured. No significant transcriptional upregulation of the *darA* gene was observed at 40°C compared to 37°C for the pTlp-DarA-AT EcN samples (**Figure 16C**). The low fold change (~2) in the P_{tlpA} promoter-driven expression of *darA* mRNA transcript could be a significant reason for the poor darobactin production ability of the pTlp-DarA-AT EcN strain after 6 hours of incubation at 40°C. I then conducted RT-qPCR analysis of the *t7-RNAP* and *darA* mRNA transcripts produced by the pTAMP-DarA-AT EcN strain after 6 hours of incubation at 37°C and 40°C. After incubation at 40°C, the pTAMP-DarA-AT EcN strain showed ~7 and ~20-fold increase in the *t7-RNAP* and *darA* mRNA levels, respectively, compared to the 37°C incubated samples, as highlighted by their relative quantification ($2^{-\Delta\Delta Ct}$) values (**Figure 16D; Figure 16E**). The *darA* mRNA levels for the

pTAMP-DarA-AT genetic circuit was ~10 times higher than that observed for the pTlp-DarA-AT genetic circuit when both were incubated at 40°C. This significant increase in the *darA* transcript levels for thermo-amplifier circuit could be attributed to the *darA* gene being transcribed from the P_{T7} promoter by T7RNAP, in contrast to the P_{tlpA} promoter-σ70-RNAP complex driven *darA* transcription in the thermo-responsive circuit. Decoupling *darA* transcription from σ70-RNAP and introducing an additional layer of thermally regulated *t7-RNAP* expression also led to a significant reduction of the basal level darobactin production by the thermo-amplifier circuit, pTAMP-DarA-AT. All these experiments provided further evidence for the superior performance of the thermo-amplifier circuit (pTAMP-DarA-AT) compared to the thermo-responsive circuit (pTlp-DarA-AT), both in terms of better thermal regulation as well as enhanced darobactin production. In addition to the superior performance of the genetic circuit, I needed to ensure whether the pTAMP-DarA-AT plasmid could be stably retained in EcN even after several bacterial generations in non-antibiotic supplemented growth media. To do so, the pTAMP-DarA-AT EcN strain was cultured in FM with and without ampicillin supplementation at 40°C for 50 consecutive generations. Quantitative Polymerase Chain Reaction (qPCR) was used to detect the pTAMP-DarA-AT plasmid DNA after the 10^{th} and 50^{th} generation, for non-ampicillin and ampicillin-supplemented samples. The results were then normalized to the chromosomally expressed 16S rRNA reference gene to obtain the double delta Ct (ΔΔCt) parameter and measure the respective relative quantification ($2^{-\Delta\Delta Ct}$) values. No significant difference was observed between the fold change of the relative quantification ($2^{-\Delta\Delta Ct}$) values for the non-ampicillin and ampicillin-supplemented samples between the 10^{th} and 50^{th} cell generation number (**Figure 16F**). This suggested that the *txe-axe* TA system could stabilize the recombinant plasmid in the EcN microbial chassis for at least 50 generations, even without antibiotic supplementation.

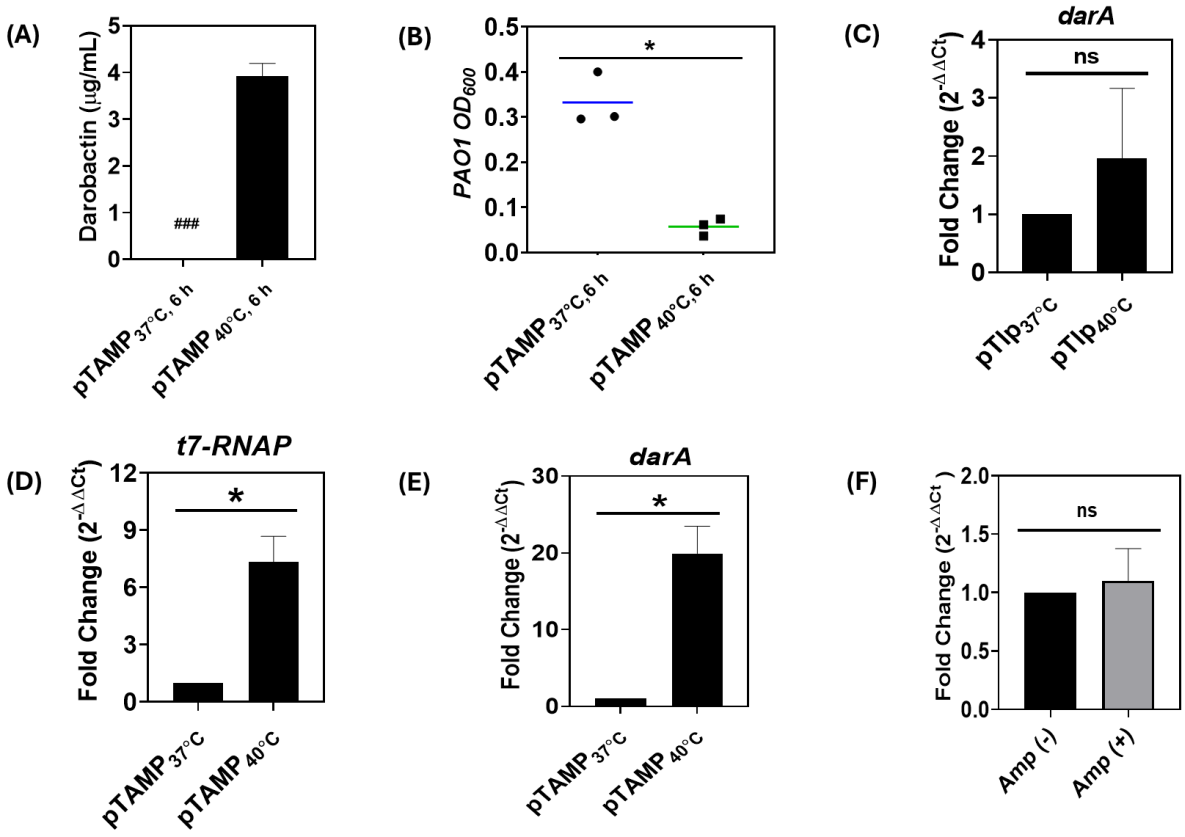

Figure 16. (A) Darobactin concentration in the liquid medium (in µg/mL) for the pTAMP-DarA-AT EcN strain in FM (no ampicillin supplementation) after 6 h incubation at 37°C and 40°C respectively. (##) represents darobactin concentrations lower than the Limit of Detection (LOD) by ESI-MS. The error bars represent standard deviation based on three independent measurements (B) End-point absorbance (OD_{600}) of *P. aeruginosa* PAO1 after 18 h incubation at 37°C in filter-sterilized FM (no ampicillin supplementation) sustaining the growth of the pTAMP-DarA-AT EcN strains for 6 h at 37°C and 40°C incubation temperatures respectively. The error bars represent standard deviation based on three independent measurements (*p=0.0253 as calculated by paired t-test) (C) Fold change between the relative quantification values ($2^{-\Delta\Delta Ct}$) of *darA* gene expression driven by the P_{tlpA} promoter of pTlp-DarA-AT construct in EcN after 6 h incubation at 37°C and 40°C respectively. The error bars represent standard deviation based on three independent measurements (^{ns}p =0.2981 as calculated by paired t-test) (D) Fold change between the relative quantification values ($2^{-\Delta\Delta Ct}$) of *t7-RNAP* gene expression driven by the P_{tlpA} promoter of pTAMP-DarA-AT construct in EcN after 6 h incubation at 37°C and 40°C respectively. The error bars represent standard deviation based on three independent measurements (*p=0.0146 as calculated by paired t-test) (E) Fold change between the relative quantification values ($2^{-\Delta\Delta Ct}$) of *darA* gene expression driven by the P_{T7} promoter of pTAMP-DarA-AT construct in EcN after 6 h incubation at 37°C and 40°C respectively. The error bars represent standard deviation based on three independent measurements (*p=0.0114 as calculated by paired t-test) (F) Fold change between the relative quantification values ($2^{-\Delta\Delta Ct}$) between the recombinant pTAMP-DarA-AT plasmid levels in EcN, with and without 100 µg/mL ampicillin supplementation at 40°C incubation temperature, compared over 10th and 50th cell generation number. The error bars represent standard deviation based on three independent measurements (^{ns}p=0.5852)

3.3.7. Analysis of the pTAMP-DarA-AT genetic circuit in colibactin deficient EcN

The previous experiments provided me with a comprehensive understanding of the transcriptional and translational capabilities of the pTAMP-DarA-AT genetic circuit as compared to the pTlp-DarA-AT genetic circuit in EcN. However, despite the high darobactin production capability of the pTAMP-DarA-AT genetic circuit, concerns regarding the biosafety of the EcN microbial chassis remained. Although EcN has beneficial attributes as a therapeutic production chassis, it is also responsible for producing colibactin, a polyketide peptide (Nougayrède et al., 2021). Colibactin is a highly potent genotoxin that can cause damage to eukaryotic DNA by alkylating adenine residues, which can lead to inter-strand crosslink formation that impedes the progression of the cell cycle (Nougayrède et al., 2006). Colibactin-induced damage to epithelial cells is also linked to colorectal cancer development in adults with ulcerative colitis (Pleguezuelos-Manzano et al., 2020; Mousa., 2022). Biotherapeutic EcN strains are primarily administered orally, increasing the probability of colibactin exposure in the gut lumen (Cevallos et al., 2019). This raises concerns about its safety and potential to cause adverse effects on the host. To address the issue, Bian and colleagues developed a colibactin mutant EcN strain called *Δclb* EcN by removing the polyketide synthase genomic island (*pks*) from the bacterial genome, which makes the resulting strain incapable of colibactin synthesis (**Bian et al., 2013**). The authors replaced the *pks* island, made up of 17 genes (from *clbA* to *clbQ*), with a zeocin resistance marker using the Red/ET gene recombination technique and confirmed the absence of colibactin in the cell-free media using the Ultra-Performance Liquid Chromatography-High-Resolution Mass Spectrometry (UPLC-HRMS) technique (**Figure 17A**). To improve the effectiveness of our biotherapeutic strain, I introduced the pTAMP-DarA-AT genetic circuit into the *Δclb* EcN strain. The pTAMP-DarA-AT *Δclb* EcN strain was then cultivated in FM (no antibiotic supplementation) for 6 hours at 37°C and 40°C incubation temperatures. Upon analyzing the extracellular media, darobactin was detected at a concentration of ~3.8 µg/mL for samples incubated at 40°C, while the concentration was below the ESI-MS detection limit of 0.01 µg/mL for samples incubated at 37°C (**Figure 17B**). The production pattern of darobactin for the pTAMP-DarA-AT *Δclb* EcN strain was consistent with previous observations for the pTAMP-DarA-AT EcN strain, incubated for 6 hours at 37°C and 40°C, respectively. In addition, only the 40°C incubated cell-free media collected from the pTAMP-DarA-AT *Δclb* EcN strain was able to inhibit the growth of *P. aeruginosa* PAO1 when compared to its 37°C incubated counterpart and the control strains (**Figure 17C**). A similar experiment was conducted where the

bacterial cultures were grown in FM (no antibiotic supplementation) for 24 hours instead of 6 hours at 37°C and 40°C incubation temperatures. After analyzing the extracellular media of the pTAMP-DarA-AT *Δclb* EcN that was incubated at 40°C, it was found to contain ~4.0 µg/mL darobactin, whereas the darobactin concentration was below the ESI-MS detection limit of 0.01 µg/mL for the samples that were incubated at 37°C (**Figure 17D**). The non-significant difference in the darobactin concentrations at 40°C between the 6-hour and 24-hour incubated pTAMP-DarA-AT *Δclb* EcN strain was in line with our previous observations (**Figure 14B, Figure 16A**). Upon analyzing the antimicrobial activity of the cell-free media, only the pTAMP-DarA-AT *Δclb* EcN samples incubated at 40°C (for 24 hours) showed significant inhibition of *P. aeruginosa* PAO1, as compared to the 37°C-incubated samples and control strains (**Figure 17E**). It was also observed that the optical density (OD_{600}) reached by *P. aeruginosa* PAO1 in the cell-free media samples collected after 6 hours of incubation (0.33 ± 0.06, 37°C) was higher than the 24 hour incubated samples (0.24 ± 0.03, 37°C) for the pTAMP-DarA-AT *Δclb* EcN strain. This optical density (OD_{600}) increase was due to the higher availability of nutrients in the cell-free media of the 6-hour incubated pTAMP-DarA-AT *Δclb* EcN samples. In contrast, the samples incubated for 24 hours would likely experience significant nutrient depletion to support the growth and metabolism of the darobactin production strains. This reduced nutrient pool would therefore restrict *P. aeruginosa* PAO1 from reaching higher OD_{600} values.

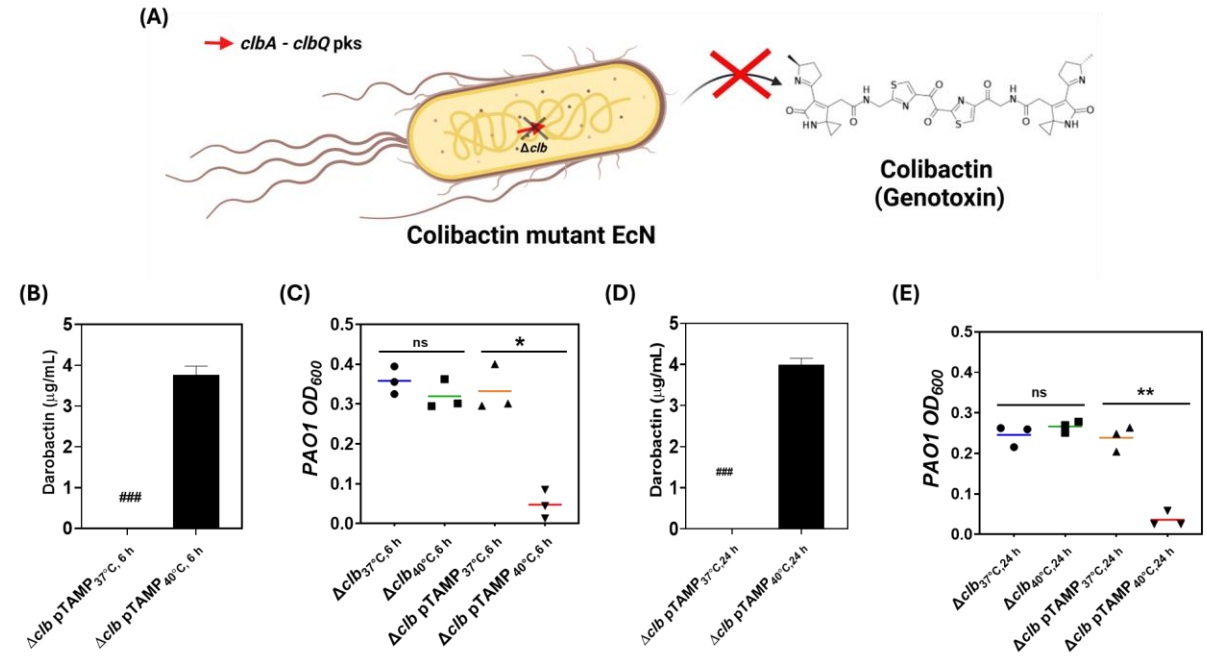

Figure 17. (A) Schematic diagram of the colibactin mutant *E. coli* Nissle (EcN) strain. The polyketide synthase (pks) cluster containing 17 genes (from *clbA* to *clbQ*) in the EcN genome has been replaced with a zeomycin resistance gene. This modification prevents the resultant Δ*clb* EcN strain from producing the genotoxin, colibactin (Bian et al., 2013) (B) Darobactin concentration in the liquid medium (in μg/mL) for the pTAMP-DarA-AT construct in Δ*clb* EcN strain (FM, no ampicillin supplementation) after 6 h incubation at 37°C and 40°C respectively. (##) represents darobactin concentrations lower than the Limit of Detection (LOD) by ESI-MS. The error bars represent standard deviation based on three independent measurements (C) End-point absorbance (OD_{600}) of *P. aeruginosa* PAO1 after 18 h incubation at 37°C in filter-sterilized FM (no ampicillin supplementation) sustaining the growth of the wild type and pTAMP-DarA-AT Δ*clb* EcN strains for 6 h at 37°C and 40°C incubation temperatures respectively. The error bars represent standard deviation based on three independent measurements (^{ns}p=0.0728, *p=0.0325 as calculated by paired t-test) (D) Darobactin concentration in the liquid medium (in μg/mL) for the pTAMP-DarA-AT construct in Δ*clb* EcN strain (FM, no ampicillin supplementation) after 24 h incubation at 37°C and 40°C respectively. (##) represents darobactin concentrations lower than the Limit of Detection (LOD) by ESI-MS. The error bars represent standard deviation based on three independent measurements (E) End-point absorbance (OD_{600}) of *P. aeruginosa* PAO1 after 18 h incubation at 37°C in filter-sterilized FM (no ampicillin supplementation) sustaining the growth of the wild type and pTAMP-DarA-AT Δ*clb* EcN strains for 24 h at 37°C and 40°C incubation temperatures respectively. The error bars represent standard deviation based on three independent measurements (^{ns}p=0.4437, **p=0.0040 as calculated by paired t-test).

The non-fastidious nature of *P. aeruginosa* PAO1 enables it to survive in environments with varying nutrient availability (LaBauve and Wargo, 2012). Apart from nutrient requirements, the growth and metabolism of *P. aeruginosa* PAO1 are influenced by other stress factors such as pH (Mozaheb et al., 2023), oxygen limitation (Arai, 2011), and osmolarity (Mittal et al., 2009). Recent evidence has also shown that the presence of bile can affect the virulence of *P. aeruginosa* PAO1 (Bayat et al., 2023). Bile is an aqueous solution produced by the liver, stored in the gallbladder, and composed of bile acids, organic matter, inorganic salts, and pigments (Reshetnyak., 2013). Bile is released from the gallbladder into the duodenum via the common bile duct to aid in the digestion and absorption of dietary fats. Bile not only aids digestion but also possesses antimicrobial properties against bacteria by disrupting cell membranes, damaging DNA, and generating oxidative stress (Begley et al., 2005). Despite its antimicrobial properties, some Gram-negative bacteria can still tolerate bile stress and survive in the host environment. A study by Reen and coworkers showed that exposure to bile upregulated efflux pump expression in *P. aeruginosa* PAO1, resulting in increased antibiotic tolerance (**Figure 18A**). Exposure to bile can also promote biofilm formation (**Figure 18A**), thereby selecting for highly adaptive and virulent bacterial subpopulations of *P. aeruginosa* PAO1 (Flynn et al., 2019). I wanted to investigate whether the darobactin antimicrobial activity would be affected if *P. aeruginosa* PAO1 was exposed to bile stress. First, I determined the maximum bile tolerance threshold of the *Δclb* EcN-based darobactin-producing strains. Both *Δclb*

EcN and pTAMP-DarA-AT *Δclb* EcN strains were incubated in bovine bile-supplemented FM at 37°C and 40°C, respectively. Both strains tolerated the presence of bovine bile and reached comparable growth up to 1.2% (w/v) at either temperature, beyond which the bacterial growth drastically plummeted. This experiment confirmed that *Δclb* EcN-based strains tolerated high bile concentrations and could be suitable for darobactin production in bile-enriched media. To test my hypothesis, I grew the pTAMP-DarA-AT *Δclb* EcN strain in FM (without antibiotics) and supplemented it with 0.3% (w/v) bovine bile. I opted for 0.3% (w/v) bovine bile since it was utilized in previous research studies that examined the effects of bile stress on *P. aeruginosa* PAO1 (Reen et al., 2016; Flynn et al., 2019). The bacterial cultures were then incubated at 37°C and 40°C for 24 hours. Upon analyzing the extracellular media, it was found that the samples incubated at 40°C showed a significant increase in the concentration of darobactin (~3.6 µg/mL) as compared to the samples incubated at 37°C (~0.1 µg/mL) (**Figure 18B**). Although darobactin was detectable at 37°C, its production was strongly temperature-dependent, as indicated by a ~32-fold increase in darobactin concentration at 40°C. While it is not entirely confirmed, evidence suggests that bile exposure can affect the carbon metabolism pathways of bacteria (De Paepe et al., 2011). The pTAMP-DarA-AT genetic circuit employs the P_{lacI} promoter to drive the expression of the $TlpA_{39}$ repressor protein. Interestingly, this promoter is also present in the bacterial genome of *Δclb* EcN and helps in regulating carbohydrate metabolism. It is possible that the adaptive metabolism of *Δclb* EcN in response to bile led to cross-reactivity between the P_{lacI} promoter-driven endogenous and recombinant gene ($tlpA_{39}$) expression. This could have impacted the regulation of T7RNAP, causing the leaky expression of darobactin even at 37°C. To examine the impact of bile supplementation on the antimicrobial properties of darobactin, *P. aeruginosa* PAO1 was inoculated in the cell-free media and incubated at 37°C. Significant growth inhibition of *P. aeruginosa* PAO1 was observed in the extracellular media of pTAMP-DarA-AT *Δclb* EcN samples incubated at 40°C, while no antimicrobial activity was observed for the samples incubated at 37°C (**Figure 18C**). This showed that the presence of bile did not affect the antimicrobial activity of darobactin present in the cell-free media. Upon recultivation on fresh MHI Agar plates, the 37°C incubated cell-free samples gave rise to a bacterial lawn, whereas the 40°C incubated samples gave rise to isolated colonies of *P. aeruginosa* PAO1 (**Figure 18D**). Despite the distinct difference between the re-emergence capability of *P. aeruginosa* PAO1 in bile-supplemented FM samples (**Figure 18D**), the number of colonies were visibly higher (qualitative) than those observed previously for the non-

bile supplemented samples incubated at 40°C (**Figure 14D**). This observation may be another indication that the presence of bile could lead to the generation of an antibiotic-tolerant *P. aeruginosa* PAO1 subpopulation over long-term exposure.

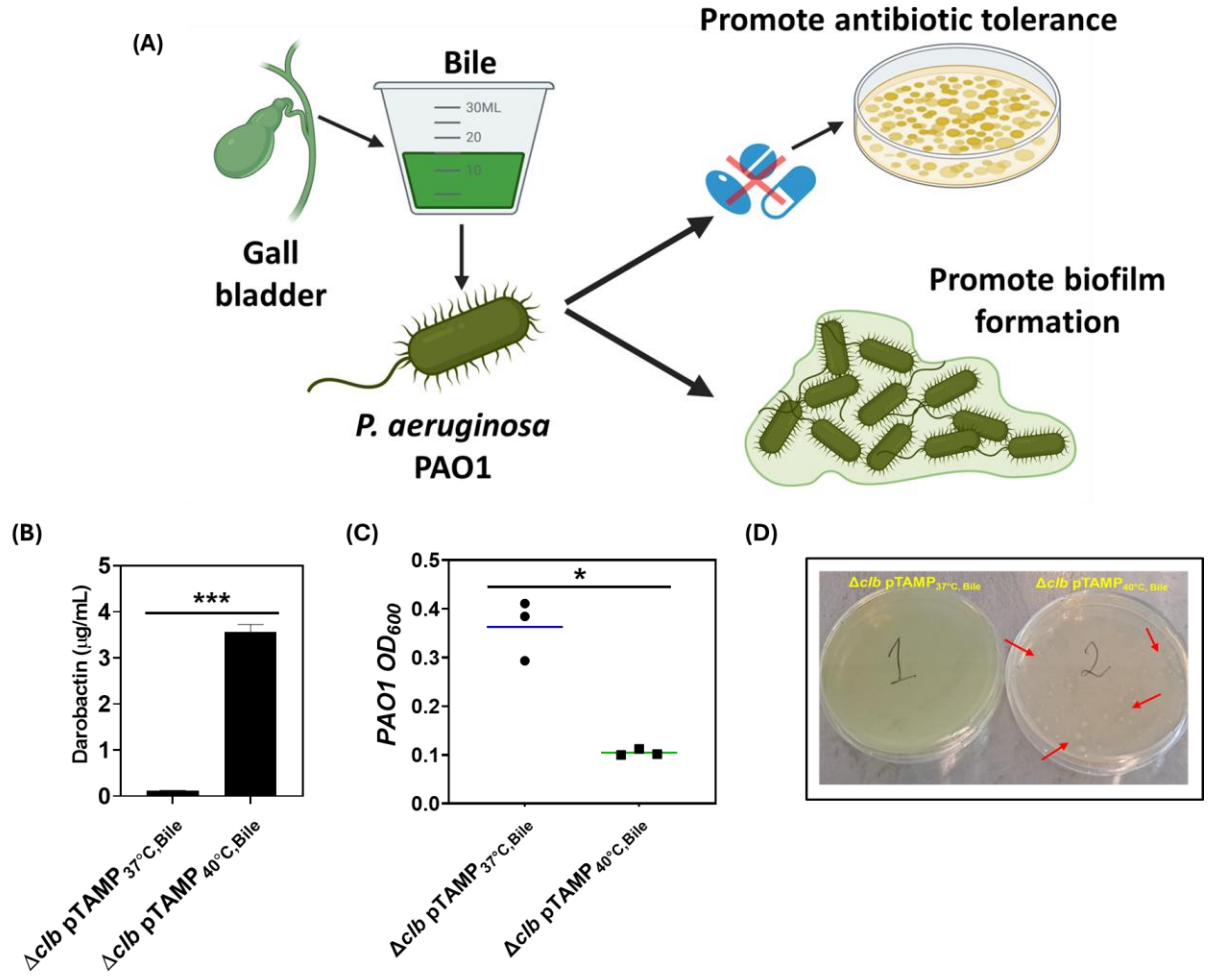

Figure 18. (A) Schematic diagram of the influence of bile on enhancing *P. aeruginosa* PAO1 virulence. Bile is known to promote antibiotic resistance (Reen et al., 2016) and trigger biofilm formation (Flynn et al., 2019) among *P. aeruginosa* PAO1 bacterial cultures (B) Darobactin concentration in the liquid medium (in µg/mL) for the pTAMP-DarA-AT Δ*clb* EcN strain in FM containing 0.3% (w/v) bovine bile (no ampicillin supplementation) after 24 h incubation at 37°C and 40°C respectively. The error bars represent standard deviation based on three independent measurements (***p=0.0008 as calculated by paired t-test) (C) End-point absorbance (OD_{600}) of *P. aeruginosa* PAO1 after 18 h incubation at 37°C in filter-sterilized FM containing 0.3% (w/v) bovine bile (no ampicillin supplementation) sustaining the growth of pTAMP-DarA-AT Δ*clb* EcN strains for 24 h at 37°C and 40°C incubation temperatures respectively. The error bars represent standard deviation based on three independent measurements (*p =0.0181 as calculated by paired t-test) (D) *P. aeruginosa* PAO1 cultivated on Mueller-Hinton (MHI) Agar post treatment with filter-sterilized FM containing 0.3% (w/v) bovine bile (no ampicillin supplementation) sustaining the growth of pTAMP-DarA-AT Δ*clb* EcN strains for 24 h at 37°C and 40°C incubation temperatures respectively (Figure 18C). The agar plates were placed in a static incubator at 37°C for 18 h before imaging. The pTAMP-DarA-AT Δ*clb* EcN

strain (37°C, 24 h) gave rise to a lawn of *P. aeruginosa* PAO1 bacteria (The plate appears green due to pyoverdine pigment produced naturally by the bacteria). The pTAMP-DarA-AT Δ*clb* EcN strain (40°C, 24 h) supernatant treated samples only produced a few isolated colonies of *P. aeruginosa* PAO1 (The plate appears light yellow due to the natural color of the MHI Agar devoid of any pigment production). The red arrows highlight *P. aeruginosa* PAO1 colonies. The data was independently verified at least two times.

3.3.8. Simulating the therapeutic efficacy of the pTAMP-DarA-AT *Δclb* EcN

Although our previous experiments highlighted the robustness of the pTAMP-DarA-AT *Δclb* EcN strain towards thermo-responsive darobactin production, all of them were conducted in a nutritionally enriched growth media (FM). This nutrient-rich media enabled better growth of the microbial chassis, increased the overall bacterial biomass, and facilitated high darobactin production when the thermal trigger was applied. Although the human intestine is reported to represent a nutrient-rich environment (Townsend et al., 2021), it was necessary to obtain further insights regarding the robustness of the pTAMP-DarA-AT *Δclb* EcN strain in nutrient-limited growth media. To do so, I cultivated the pTAMP-DarA-AT *Δclb* EcN strain in the nutritionally limited growth media (M9 Minimal Broth, no antibiotic supplementation) for 24 hours at 37°C and 40°C incubation temperatures. Post incubation, ~0.1 µg/mL of darobactin was detected in the extracellular media of the 40°C incubated samples, whereas for the 37°C incubated samples, the darobactin concentration was below the ESI-MS detection limit. In both cases, the bacterial biomass reached ~200 mg (per 25 mL), significantly less than the biomass previously observed for FM-based cultures (~530 mg per 25 mL). The low bacterial biomass directly correlated with the reduced darobactin concentration, indicating that direct cultivation of the bacteria in M9 Minimal Broth was inappropriate for thermo-responsive darobactin production. To address this issue, I looked into the method used by Ardeypharm GmbH to ensure maximum biological efficacy of the EcN strain post human consumption. The company's approach involves incorporating the lyophilized EcN strain at a concentration of 2.5 - 25 X 10^9 colony forming units (CFU) per mL into enteric-coated hard gelatin capsules (**Figure 19A**). The capsules are coated with methacrylic acid-methyl methacrylate copolymer (1:1), which enables them to dissolve specifically in the small intestine when triggered by the alkaline pH and release the EcN strain. Direct delivery of the precultivated, freeze-dried EcN strain to the small intestine increases its chances of colonizing and exhibiting its anti-inflammatory properties in the gut. Inspired by this approach, I decided to decouple the growth of the pTAMP-DarA-AT *Δclb* EcN strain from its thermo-responsive darobactin production capability. Instead of

directly culturing the recombinant strain in M9 Minimal Broth and screening for thermo-responsive darobactin production, I opted to precultivate the bacterial biomass at a lower temperature. The pTAMP-DarA-AT *Δclb* EcN strain was first cultured in FM (no antibiotic supplementation) at 30°C for 24 hours to allow it to reach higher biomass without inducing darobactin production. After 24 hours of incubation, the bacterial biomass reached ~500 mg, with an optical density (OD_{600}) of around 8 ± 0.5, which corresponded to 8 – 9 $X10^9$ CFU/mL of bacteria. After discarding the media, the bacterial pellet was resuspended in fresh M9 Minimal Broth (no antibiotic supplementation) and incubated at 37°C and 40°C for 24 hours (**Figure 19B**). After incubation, the bacterial biomass was removed, and the concentration of darobactin in the filter-sterilized extracellular media was measured. Upon analysis, ~1.7 µg/mL of darobactin was detected for the 40°C incubated samples, whereas ~0.2 µg/mL of darobactin was detected in the 37°C incubated samples (Figure 19C). Although there was an ~11-fold increase in darobactin concentration at 40°C, leaky production of darobactin was observed at 37°C. It is possible that the reason for the leaky production was the extended experimental timeframe. The previous experiments had a timeline of 24 hours, while this one involved 48 hours to cultivate the bacterial biomass and induce thermo-responsive darobactin production. This prolonged incubation may have resulted in basal-level T7RNAP expression, eventually producing darobactin from the biomass samples incubated at 37°C. In addition, due to reduced nutrient availability in M9 Minimal Broth, the darobactin concentration produced by the pTAMP-DarA-AT *Δclb* EcN strain at 40°C was lower than the FM-based cultures (~4.0 µg/mL, **Figure 17D**). Despite the relatively low darobactin concentration, I proceeded with testing the antimicrobial activity of the cell-free media against *P. aeruginosa* PAO1. It was observed that only the pregrown biomass samples of the pTAMP-DarA-AT *Δclb* EcN strain, which were incubated at 40°C, could inhibit the growth of *P. aeruginosa* PAO1 (**Figure 19D**). On the other hand, no antimicrobial activity was observed for the pregrown biomass samples incubated at 37°C and the control strains (**Figure 19D**). When grown on MHI Agar plates, cell-free media samples incubated at 37°C resulted in the formation of a bacterial lawn, while samples incubated at 40°C yielded only a few isolated colonies of *P. aeruginosa* PAO1 (**Figure 19E**). These experiments show that pre-cultivated biomass of the pTAMP-DarA-AT *Δclb* EcN strain is suitable for thermo-responsive darobactin production in nutrient-limited media, representative of the gut lumen's nutrient environment (Ferraris et al., 1990). Therefore, the pTAMP-DarA-AT *Δclb* EcN strain can be

progressed for further *in-vivo* characterization of thermally induced darobactin production in the gut to prevent *P. aeruginosa* PAO1 colonization.

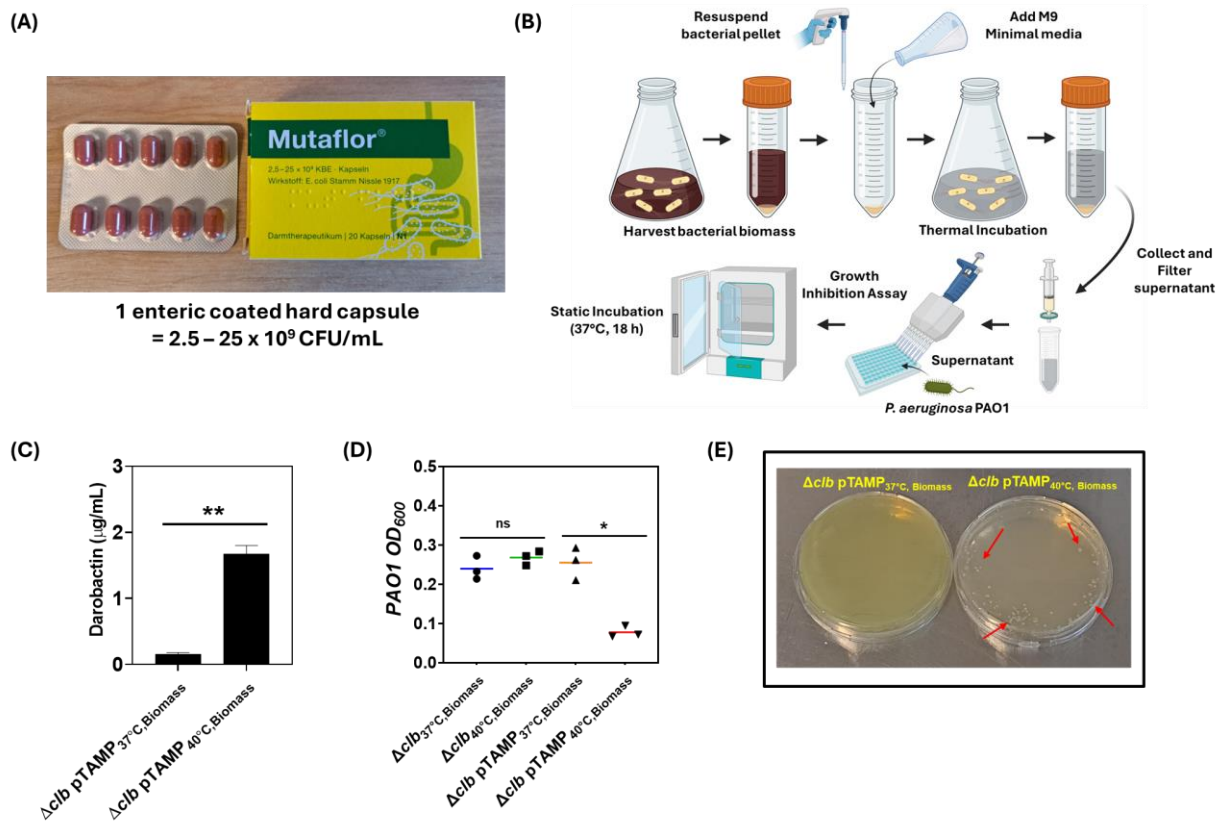

Figure 19. (A) Probiotic *E. coli* Nissle 1917 (EcN) commercially sold under the brandname Mutaflor® (Ardeypharm GmbH, Germany). Each enteric coated hard capsule contains 2.5 – 25 X 10^9 colony forming units (CFU/mL) of the lyophilized or freeze-dried *E. coli* Nissle 1917 strain (B) Schematic diagram of the steps taken to cultivate the bacterial biomass equivalent to a Mutaflor® capsule and test its darobactin production capability in a chemically defined media (M9 Minimal media) under different incubation temperatures. The growth inhibitory potential of the darobactin secreted into the extracellular media is then tested on the pathogenic strain *P. aeruginosa* PAO1 (C) Darobactin concentration in the M9 Minimal Media (in µg/mL) for the pre-cultivated biomass of pTAMP-DarA-AT Δ*clb* EcN strain (no ampicillin supplementation) after 24 h incubation at 37°C and 40°C respectively. The error bars represent standard deviation based on three independent measurements (**p=0.0015 as calculated by paired t-test) (C) End-point absorbance (OD_{600}) of *P. aeruginosa* PAO1 after 18 h incubation at 37°C in filter-sterilized M9 Minimal media (no ampicillin supplementation) sustaining the pre-cultivated biomass of the wild type and pTAMP-DarA-AT Δ*clb* EcN strains for 24 h at 37°C and 40°C incubation temperatures respectively. The error bars represent standard deviation based on three independent measurements (^{ns}p=0.2039, *p =0.0203 as calculated by paired t-test) (D) *P. aeruginosa* PAO1 cultivated on Mueller-Hinton (MHI) Agar post treatment with filter-sterilized M9 Minimal media (no ampicillin supplementation) sustaining the pre-cultivated biomass of pTAMP-DarA-AT Δ*clb* EcN strains for 24 h at 37°C and 40°C incubation temperatures respectively (Figure 18C). The agar plates were placed in a static incubator at 37°C for 18 h before imaging. The pTAMP-DarA-AT Δ*clb* EcN strain (37°C, 24 h, Biomass) gave rise to a lawn of *P. aeruginosa* PAO1 bacteria (The plate appears yellowish-green due to pyoverdine pigment produced naturally by the bacteria). The pTAMP-DarA-AT Δ*clb* EcN strain (40°C, 24 h, Biomass) supernatant treated samples only produced a

few isolated colonies of *P. aeruginosa* PAO1 (The plate appears light yellow due to the natural color of the MHI Agar devoid of any pigment production). The red arrows highlight *P. aeruginosa* PAO1 colonies. The data was independently verified at least two times.

3.4. Conclusion

In this chapter, I demonstrated that temperature elevation can be used as an effective trigger to induce antimicrobial production from a probiotic strain. I developed a thermo-amplifier circuit by combining the thermal regulation ability of the $TlpA_{39}$ repressor protein with the excellent transcriptional capability of the T7RNAP. Although previous studies have demonstrated the optogenetic regulation of T7RNAP in bacterial strains (Raghavan et al., 2020; Fernandez-Rodriguez et al., 2017), this study is the first to demonstrate the thermoregulation of T7RNAP to achieve significant production of a therapeutically relevant antimicrobial agent, darobactin at 40°C. In addition, the thermoamplifier circuit-based darobactin production showed effective antimicrobial activity against the Gram-negative *P. aeruginosa* PAO1 strain. Overall, the insights gained from this chapter can also be applied to darobactin derivatives with superior antimicrobial activity against pathogenic bacteria, such as *Salmonella typhimurium* and *Shigella sonnei*, which are closely associated with cases of gastroenteritis (Imai et al., 2019; Böhringer et al., 2021; Miller et al., 2022; Seyfert et al., 2023).

3.5. Current Limitations

Despite the robust nature of the thermo-amplifier system, there is room for further improvement in its performance. When tested in nutrient-limited media (M9), the pTAMP-DarA-AT Δ*clb* EcN strain showed a ~2-fold decrease in darobactin concentration compared to enriched media (FM). Although it was enough to inhibit the growth of *P. aeruginosa* PAO1, a higher darobactin concentration may be needed to inhibit bacterial strains more commonly associated with gastroenteritis. A recent study by Redenti and colleagues reported that deleting Lon and OmpT protease-encoding genes from the EcN bacterial genome resulted in an 80-fold increase in recombinant protein production (Redenti et al., 2023). Therefore, establishing the thermo-amplifier system in a *ΔlonΔompTΔclb* EcN strain may boost darobactin production in nutrient-limited media, making it more suitable for *in-vivo* applications. However, enhancing recombinant protein production may inadvertently increase

leaky expression of darobactin, as seen with the Lon and OmpT protease-deficient ClearColi strain. To address this issue, the expression of the T7 lysozyme (T7lysY), a natural inhibitor of T7RNAP, can be simultaneously expressed in the engineered strain. Low levels of T7lysY can efficiently reduce the leaky expression mediated by T7RNAP without severely compromising its transcriptional capability (Wagner et al., 2008). The expression of T7lysY can be regulated by either a weak constitutive promoter (Song et al., 2015) or the rhaBAD promoter, specifically induced by the presence of L-rhamnose, a common prebiotic used for gut health (Hirano et al., 2021).

In addition, the recombinant plasmid also contains an antibiotic resistance gene (ARG) as a selection marker. This gene produces the β-lactamase enzyme, which confers resistance to β-lactam antibiotics in the microbial host. Studies suggest that acquiring ARGs through horizontal gene transfer can lead to the development of antibiotic-resistant pathogens (Breidenstein et al., 2011; Pang et al., 2019). Therefore, removing ARGs from the engineered strain is crucial before using it for therapeutic purposes. In a recent study, Amrofell and colleagues developed a recombinant plasmid containing the essential thymidylate synthase (*thyA*) gene and established it in a thymidine auxotrophic EcN strain. This strategy allowed for the exclusion of ARG from their engineered strain while enabling plasmid retention for several days in mouse models. A recent study using *Bacteroides thetaiotaomicron* showed that an additional layer of Cas9-based regulation could prevent *thyA* gene acquisition from gut symbionts, thus ensuring plasmid retention in mouse models (Hayashi et al., 2024). Establishing the thermo-amplifier system in a suitable microbial chassis can be achieved without using ARGs through these two strategies.

Recombinant gene expression by engineered EcN strains reduces bacterial fitness and tends to be cleared earlier (<4 days) from the gut of mouse models compared to unmodified strain (Kan et al., 2021). However, stable EcN colonization and persistence have been observed in newborn infants and healthy human adults for over 1 week (Lodinová-Žádníková and Sonnenborn., 1997; Sonnenborn and Schulze., 2009). A detailed investigation has revealed that EcN incorporates itself into mixed biofilms formed in the mouse intestinal mucus to facilitate colonization. This association enables anaerobic bacteria to metabolize dietary fiber-based polysaccharides into mono- and disaccharides, which EcN can utilize to promote their growth (Conway and Cohen., 2015). Although this interaction is essential for EcN survival, horizontal transfer of recombinant plasmids to the human gut microbiota population can be a significant health concern. Even though, research

in mice models for bacterial enteropathogen infections has shown that engineered EcN has an innate tendency to be cleared from the mice gut compared to the wild type, probably due to reduced fitness imposed by recombinant gene expression (Kan et al., 2021), it might not necessarily be true for human hosts. Commensal strains of *E. coli* have been responsible for transferring ARG-containing plasmids to *Shigella sonnei*, causing fluoroquinolone-resistant *S. sonnei* infections in human hosts in Vietnam (Thanh Duy et al., 2020). Therefore, there is a possibility that the thermo-amplifier plasmid could get transferred to pathogenic bacteria present in the human gut. The recombinant plasmid encodes for the DarBCD efflux pump system, responsible for the extracellular export of darobactin. Pathogenic bacteria can acquire this plasmid, and the heterologous expression of the DarBCD efflux pump system would then contribute to their resistance toward darobactin. The best approach to prevent the emergence of darobactin-resistant pathogen populations would be to integrate the thermo-amplifier genetic circuit into the *Δclb* EcN genome. A recent report by Synlogic demonstrated that by integrating recombinant genetic modules into specific genomic loci of the EcN strain called "landing pads", the phenylalanine to trans-cinnamic acid conversion efficiency of the engineered strain was equivalent to its plasmid harboring counterpart (Triassi et al., 2023). In addition, deleting the dihydrodipicolinate synthase (*dapA*) gene responsible for diaminopimelic acid-based linkage formation in the bacterial cell wall ensured robust biocontainment and prevented the survival of the engineered strain in the environment. A similar strategy can be adopted for the thermo-amplifier darobactin production circuit to develop a “living therapeutic” strain capable of resolving bacterial gastroenteritis without any serious medical and environmental repercussions.

3.6. Supplementary Information

Table S1. Nucleotide Sequences of the recombinant genetic modules used in this chapter

NAME	SEQUENCE (5’ → 3’)
darA	atgcataataccttaaatgaaaccgttaaaactcaagaagcactcaattctcttgctgcatcattcaaagagac tgaactctcaattactgataaagcactaaacgaattaagcaataaacctaagatccctgagatcacggcctg

	gaactggtcaaaaagcttccaggaaatttaa
darB	atgaatgctattaacatctcagaatccatgaaacgtttcaatatattggtatcgatactctcagtatcaatagca atattagcaatttatttactttctactgccttctattcagatgctcgagttgataactattatcaagataatggcaac atttaccgggtggaaaccacctttaatttgcccaatggagaaaaagtgagatcggcaaaatcgccattgccg ctcatagacgagctagaaaaagataaaaggataaatcgtgcagactacttttttcaaacttaacacgacgatt gagttacaaggaaaaaagatcaccaaagttcccgtgtttgcagtcagtcatcaattcctgaataccctgtctc cctttaagaaaatcgataatatcctgggagcaaatgagatttacatcacaaaagagttcaataatcgctatctc ggcctggaaaatcccaaaggaaaatctattgttctggataatgaaacctatatcatcaaggatatcgtagaaa aacgtcatgattcgagtcttaatatgaatgctattatttcatttaagccaacacttatcaaaaactacaataaaga aatattcaattggtatgatacacatgcttatatttttataaaactctctgatgaaaaatcaatatccaatcgcgatg cgcttcttaatcatattattgcaaccaaagcccccaatcttccaggcgctccatttactgccagtgaatttattca cctatcattaaaaaaatcaaaagatattcattaccaagatggattgcctgatgaaatttctattggtttatcaaag gagataatttatagctcatatatcgcgttcgcatttatcttattttccacattaaccaactattataatttaacttctg ctgattcagcagaaaaaagggatatttatcagttaaagaaagcgctaggcgcttcaactttcaatattatttgc gattcactgccggccatgttgatcaaaataatcctttccacccttatctttttgttacttatcataactatatttaatg tctctctctatataaataatatatttaccctattagaagcagacagtttaatatatctagggatattttcagttgttat tgcctttatctttatttcatcaatacatttttcattctcattacgtttttatatttatcaaagaaacagaaaaatggata tgagatatgaatcaacccttgcctcttggtttaggaaatcatcattggctattcaattacttgtttccggaatatct atttatttagtcaccggattaaccaatcaatatattcaccttgttgatttacatactccttatgataatgccaagac aatatcaatagcaattaataacgataataataaaaaatcaactattgatgaattaagctatgagtttatcagaaa atacaatacttcaaaaataaccctcagtaattggcgaccatttgatatgtcaagagaaaatatcactattaatta ttccggccaacaaaacaggaataactatatctcttcaaatgttattactgcggatgaaaatttcactgatgtgtg gagaatgaagatattagccggtggtgataaacgagtatatcagagtgataatgctgatgtagtccatgcatta gtgacaaaagaatttttaaaacagaatggaattctcaaatatgatgatatttttaacaactactattggtacaca atggaggataaaaagatccaaatcagatttattcagattatagatgatttcaatttaggtgctgtagatgaacc attcaggccaatagttgttttcatcaaaaaagatcatggaaaatatgcttcgctgaatttaaacaatatgaaaaa cctttctccggtacttaacgaactatcaaaacagggttttgataataatgaaattgatttaaccagtcacttattta actcttattatgataattatttaaaagtaataaaattatcatctgccgtcgctattttctcggttctattattagtcatc gcctgctttactaccagcatgactgactttaacgcgatgaaaagggagttaagtataatggaatctattggtg gttctatttacaccaatctcattcacttttatcgaaaagtgtcatcccgataatcgcatcaattttcgtggcatat atatcaggaagaactattttagtttatctgcttgatgaatatagtgtgatttacaccgattcttttgtatacagtgct atcgccctatctgctacaatgatattcaccgttattataatgatgactacctatttggtgaattatagaaaattatc cgccactaaatttttgtga
darC	atggatatagaaatcagaaaaaaaggcatacataacagagagaaattactcattctcattttctttatcgctttt atttcatttgttgtatttattatctattatgtcgtttcggctaaagacgctttcgtgaatgaaaatgaagttacccag tttcaggtcagcagcaaagtagatagtgatattctgaaaaccagggcagttgtggttcctgataaaagtgtct ctatctcaaccgagataggggggaatcgttaccgatataatgaaaaaaccatcacaagatgttttaaagaatg aagaaatcgtgaaattatctaattttaatttcacattgaataattcttcgatgttagcggacgtgacagataaact caataatttaataaacataagaataaacttgcaatctgactatcgggatatcaataaccgattcttagaagccg ccaaagaactaaaagaagtagaagataaattaaagcgatatcacgatcttgtacataaaaattatatttctaaa gaaactatgtccgatttaaggattaaaagagattattggcacgatgtttatctattctacaaaaaattaaaaaat gataaagatcgtgatatatcaaaacagttaaaggaaatcgacgagtttgtcgaaaaacagagaaaactctct gacatcatcgaaaatggtttcgagcagctttcaataaaatcccctatcgccggtaatatcagttcattagattta

	attttaggacaacggttaaaacctggcgataaaatagctattgttgatgatttatcaaacttttattttgaatcaga aatcaacgaatactatttaaacaaaataacataccattcatctgccagtttaatctataacaatggaaaaatacc tttactggtgaaattaatttcatctgaagtgaataatggaacattcaaagtcagatttgaattggaagataaaaa aacaattaacttcaaacgggggcaatccgttgatgtcatgattaaacttgatgaagatcggaaaatattctcc gtaccttcatctatggtgttttctattgacaataaaaactatgtgtttgtttaccatccagataaaaaaattgcccg acgtattcaagtttccaccggccaagataatggttctgatattgagatcaaaagtggtgttactgaaggacaa acgctcgttagctttggtaagaataaattagttaataatgatacagtaaggattgaataa
darD	atgattagcatgatgaatatctgtaaatcatataaaacgaaattcattcaaacaaatgttttgaatgacataaatc tcaatatagataaaggcgaatttatttctataatgggagcgtcagggtcagggaaatcaacattactgaatgtc attggcatgtttgaaacaatcgatagcggtcaattaacactgaacaatagcaatattttaacaatgaaatattct gaaaaaatatcattcagacgagaatttattggttatatttttcaatcattcaatctgttacccaatttgacggtattt gaaaacatagagttaccgttaaaatacagaggttttcctaaaaaacagcggaaaagcaaagtatttgatgca ataaatagttttggattagaaaatcgggaaaatcataaaccgatacaattatctggtggacaacagcaacgtg ttgctatcgccagagcaatgatagcaaaccccaccattttattagctgatgaaccaacggggaacctggata gcgtaaatggtcagaatattttatcttcacttaaggagctgaatgaaaacggtacgacgattgttatggtaacc cattccgtagaagcggcagcgttttctgacagaatattaacgatgagggatggccacttgcttgtttga
darE	atggacacaataatccccataaaatatttagattcagacgaatcatcgattcttaagaaatcatctaaaattaa ctacaggcaattagcttgcagaattatcggtgaaatctccgccgaaaaaatattagatgatgatgaactggc tttatataataaagaaatcagtatacatttcagccctgaaattattaatgctaataaattagttgtggttgtgaaa gccaccaggctttgcaatttaagatgcacttattgtcactcctgggcagaaggaaaaggaaataccttaaca ttcttcaatttaatgcgttccattcaccgtttcttatccctaccgaatatcaagcgatttgaattcgtctggcatg gcggcgaagtaacgttgttgaatgttaattactttaagaaactcatctggttacaggaacaatttaaaaaacc ggatcaagttatcaccaattcggtacagacaaatgccgtcaatattcctgaagattggttagtgttcctcaaa ggtattggaatgggggtaggaataagcgttgatggtattccggaaatacacgatagcaggagattagatta cagaggaaggccaacatcccataaagtcgcggcaagtatgaaaaagttaagaagttatggcataccttac ggtgcgcttatcgtcgtcgaccgcgatgtttatgaatcaaatatagaaaaaatgctctcttatttttacgaaatc ggtttaacggatattgaatttctgaatattgtcccagataaccgatgccagccgggtgatgatcctggagga agttatataacttaccataactatattaatttccttctaaggttttccgtgtctggtggaatggttatcaaggcaa aatcaatattcgcttgtttgacggatttattgacagtatcaaatcgtcccaaaagaaaatgtcagattgttattg ggcgggtaactgttctcaggaaataatcacattagaacctaatggtacggtatcagcatgtgataaatatgtt ggtgctgaagggaataattatggttcgattattgataatgatcttgggaatttactatctaaatcaaatacaaat aaggatcatcttaaagaggaaatggaatcttatgaaaaaatgcatcaatgtaaatggtttcatttgtgtaatgg tggatgcccacacgatcgagtgaccaacaggaagcacaatccaaattatgatggttcatgttgtggaacc ggcggtttgttggagacaataaaacaaaccatcgcggcgtaa
***tlpA*$_{39}$ repressor**	atgcgtccggcgacatacgaaccagaacagattattgaagcagggctggccctgcaggctgaaggacg gaatatcaccgggttcgcactacgtaaccaggtgggtggcggcaatccgacacgtctccgccagatatg ggacgaataccaggcttcacagagcacggtcgtcactgaacccgttgccgagctgccagtggaagtgg ctgaagaagtgaaggccgtctccgccgcgctgtccgaacgcatcacccagctggcgacagaactgaat gacaaggcggtccgggctgcagaacgccgggttgcggaagtcacgcgtgctgccggtgaacagacc gcacaggcagagcgggagctggccgacgccgcgcagacagtcgacgacctggaagaaaaactggtt gaactgcaggacagatatgacagtttgacgctggcgctggagtcagaacgttcactgcgtcagcagcat gatgtggagatggcccagctgaaagagcgtcttgcggccgctgaagagaatacccgtcagcgagagg aacggtatcaggagcagaagacagtgctgcaggatgcgcttaatgcggagcaggcacagcacaaaaa cacgcgggaagacctgcagaaacgactggagcaaatttctgtcgaagctaatgcgcgtacagaagaact gaagtctgaacgcgataaagtcaatactttccttacccgccttgaatcgcaggaaaatgcgctggcctcag aacgtcagcagcatctggccacccgcgaaacgctgcagcaacgcctcgagcaggccatcgctgacac

	gcaggcgcgcgccggtgagattgcacttgaacgtgacagagtcagcagcctcaccgcaaggctggaat cgcaggaaaaggcctcctcggagcaactggtgcgtatgggcagtgaaatagccagtctgacagagcgtt gcacacagctggaaaaccagcgtgatgatgcccgtctggagacgatgggggagaaagaaacggtcgc ggcactgcgtggtgaggctgaagccctgaagcgtcagaaccagtcactgatggcggcgctttcaggca ataaacagaccggtggccagaatgcgtga
txe **toxin**	atgattaaggcttggtctgatgatgcttgggatgattatctttattggcatgagcaaggaaacaaaagcaata taaaaaagattaacaagttaataaaagatatcgatcgttccccctttgctggattaggaaaacctgagccatt aaagcatgatttatctggaaaatggtccagaagaattacagatgaacatagactgatatatagagttgaaaa tgaaacgatatttatttattctgcaaaagatcactattaa
axe **antitoxin**	atggaagcagtagcttattcaaatttccgccaaaatttacgtagttatatgaaacaagttaatgaggatgctg aaacacttattgtaacaagtaaagatgtagaagatacagttgttgtattatcaaaaagagattatgattctatg caagaaacgttgagaacactttctaataattacgtcatggaaaaaattcgtcgaggagatgaacaattctcc aaaggtgcatttaaaacacatgacttaatcgaggttgaatctgatgattaa
t7-RNAP	atgaacacgattaacatcgctaagaacgacttctctgacatcgaactggctgctatcccgttcaacactctg gctgaccattacggtgagcgtttagctcgcgaacagttggcccttgagcatgagtcttacgagatgggtga agcacgcttccgcaagatgtttgagcgtcaacttaaagctggtgaggttgcggataacgctgccgccaag cctctcatcactaccctactccctaagatgattgcacgcatcaacgactggtttgaggaagtgaaagctaag cgcggcaagcgcccgacagccttccagttcctgcaagaaatcaagccggaagccgtagcgtacatcac cattaagaccactctggcttgcctaaccagtgctgacaatacaaccgttcaggctgtagcaagcgcaatcg gtcgggccattgaggacgaggctcgcttcggtcgtatccgtgaccttgaagctaagcacttcaagaaaaa cgttgaggaacaactcaacaagcgcgtagggcacgtctacaagaaagcatttatgcaagttgtcgaggct gacatgctctctaagggtctactcggtggcgaggcgtggtcttcgtggcataaggaagactctattcatgta ggagtacgctgcatcgagatgctcattgagtcaaccggaatggttagcttacaccgccaaaatgctggcgt agtaggtcaagactctgagactatcgaactcgcacctgaatacgctgaggctatcgcaacccgtgcaggt gcgctggctggcatctctccgatgttccaaccttgcgtagttcctcctaagccgtggactggcattactggt ggtggctattgggctaacggtcgtcgtcctctggcgctggtgcgtactcacagtaagaaagcactgatgc gctacgaagacgtttacatgcctgaggtgtacaaagcgattaacattgcgcaaaacaccgcatggaaaat caacaagaaagtcctagcggtcgccaacgtaatcaccaagtggaagcattgtccggtcgaggacatccc tgcgattgagcgtgaagaactcccgatgaaaccggaagacatcgacatgaatcctgaggctctcaccgc gtggaaacgtgctgccgctgctgtgtaccgcaaggacaaggctcgcaagtctcgccgtatcagccttgag ttcatgcttgagcaagccaataagtttgctaaccataaggccatctggttcccttacaacatggactggcgc ggtcgtgtttacgctgtgtcaatgttcaacccgcaaggtaacgatatgaccaaaggactgcttacgctggc gaaaggtaaaccaatcggtaaggaaggttactactggctgaaaatccacggtgcaaactgtgcgggtgtc gataaggttccgttccctgagcgcatcaagttcattgaggaaaaccacgagaacatcatggcttgcgctaa gtctccactggagaacacttggtgggctgagcaagattctccgttctgcttccttgcgttctgctttgagtac gctggggtacagcaccacggcctgagctataactgctcccttccgctggcgtttgacgggtcttgctctgg catccagcacttctccgcgatgctccgagatgaggtaggtggtcgcgcggttaacttgcttcctagtgaaa ccgttcaggacatctacgggattgttgctaagaaagtcaacgagattctacaagcagacgcaatcaatgg gaccgataacgaagtagttaccgtgaccgatgagaacactggtgaaatctctgagaaagtcaagctggg cactaaggcactggctggtcaatggctggcttacggtgttactcgcagtgtgactaagcgttcagtcatgac gctggcttacgggtccaaagagttcggcttccgtcaacaagtgctggaagataccattcagccagctattg attccggcaagggtctgatgttcactcagccgaatcaggctgctggatacatggctaagctgatttgggaat ctgtgagcgtgacggtggtagctgcggttgaagcaatgaactggcttaagtctgctgctaagctgctggct gctgaggtcaaagataagaagactggagagattcttcgcaagcgttgcgctgtgcattgggtaactcctga tggtttccctgtgtggcaggaatacaagaagcctattcagacgcgcttgaacctgatgttcctcggtcagttc cgcttacagcctaccattaacaccaacaaagatagcgagattgatgcacacaaacaggagtctggtatcg

	ctcctaactttgtacacagccaagacggtagccaccttcgtaagactgtagtgtgggcacacgagaagtac ggaatcgaatcttttgcactgattcacgactccttcggtaccattccggctgacgctgcgaacctgttcaaag cagtgcgcgaaactatggttgacacatatgagtcttgtgatgtactggctgatttctacgaccagttcgctga ccagttgcacgagtctcaattggacaaaatgccagcacttccggctaaaggtaacttgaacctccgtgaca tcttagagtcggacttcgcgttcgcgtaa
alanine racemase (*alr*)	atgcaagcggcaactgttgtgattaaccgccgcgctctgcgacacaacctgcaacgtcttcgtgaactgg cccctgccagtaaaatggttgcggtggtgaaagcgaacgcttatggtcacggtcttcttgagaccgcgcg aacgctccccgatgctgacgcctttggcgtagcccgtctcgaagaagctctgcgactgcgtgcgggggg aatcaccaaacctgtactgttactcgaaggctttttgatgccagagatctgccgacgatttctgcgcaacatt ttcataccgccgtgcataacgaagaacagctggctgcgctggaagaggctagcctggacgagccggtta ccgtctggatgaaactcgataccggtatgcaccgtctgggcgtaaggccggaacaggctgaggcgtttta tcatcgcctgacccagtgcaaaaacgttcgtcagccggtgaatatcgtcagccattttgcgcgcgcggatg aaccaaaatgtggcgcaaccgagaaacaactcgctatctttaatacctttgcgaaggcaaacctggtcaa cgttccattgccgcgtcgggtggcattctgctgtggccacagtcgcattttgactgggtgcgcccgggcat cattctttatggcgtctcgccgctggaagatcgctccaccggtgccgattttggctgtcagccagtgatgtc actaacctccagcctgattgccgtgcgtgagcataaagccggagagcctgttggttatggtggaacctgg gtaagcgaacgtgatacccgtcttggcgtagtcgcgatgggctatggcgatggttatccgcgcgccgcgc cgtccggtacgccagtgctggtgaacggtcgcgaagtaccgattgtcgggcgcgtggcgatggatatga tctgcgtagacttaggtccacaggcgcaggacaaagccggggatccggtcattttatggggcgaaggttt gcccgtagaacgtatcgctgaaatgacgaaagtaagcgcttacgaacttattacgcgcctgacttcaagg gtcgcgatgaaatacgtggat

Table S2. List of primers and their corresponding sequences used for RT-qPCR and qPCR analysis

Primer Name	Sequence (5'→ 3')	Description	Reference
darA Fwd	GCACTCAATTCTCTTGCTGCAT	qRT-PCR forward primer for darA	This study
darA Rev	TTTTGACCAGTTCCAGGCCG	qRT-PCR reverse primer for darA	This study
T7RNAP Fwd	CGAGAACATCATGGCTTGCG	qRT-PCR forward primer for T7RNAP	This study
T7RNAP Rev	CCCAGCGTACTCAAAGCAGA	qRT-PCR reverse primer for T7RNAP	This study
pUC Fwd	TTGCCGGATCAAGAGCTACC	qPCR forward primer for pUC origin	This study
pUC Rev	GGCGGTGCTACAGAGTTCTT	qPCR reverse primer for pUC origin	This study
16S rRNA Fwd	CATGCCGCGTGTATGAAGAA	qRT-PCR forward primer for 16S rRNA	Smati et al., 2013
16S rRNA Rev	CGGGTAACGTCAATGAGCAAA	qRT-PCR reverse primer for 16S rRNA	Smati et al., 2013

3.7. Acknowledgement

I thank Till F. Schäberle for providing the pZW-ADC7 and pZW-ADC9 recombinant plasmids. I also thank Sanjana Balaji Kuttae for her help in recombinant plasmid construction. This work was supported by the Leibniz Science Campus on Living Therapeutic Materials [LifeMat].

3.7. Conflict of Interest

Rolf Müller and Carsten E. Seyfert are inventors of patent application WO2022175443A1, titled "Novel darobactin derivatives".

3.8. References

1. Ikuta, K.S., Swetschinski, L.R., Aguilar, G.R., Sharara, F., Mestrovic, T., Gray, A.P., Weaver, N.D., Wool, E.E., Han, C., Hayoon, A.G. and Aali, A., 2022. Global mortality associated with 33 bacterial pathogens in 2019: a systematic analysis for the Global Burden of Disease Study 2019. *The Lancet*, *400*(10369), pp.2221-2248.
2. Årdal, C., Balasegaram, M., Laxminarayan, R., McAdams, D., Outterson, K., Rex, J.H. and Sumpradit, N., 2020. Antibiotic development—economic, regulatory and societal challenges. *Nature Reviews Microbiology*, *18*(5), pp.267-274.
3. Payne, D.J., Gwynn, M.N., Holmes, D.J. and Pompliano, D.L., 2007. Drugs for bad bugs: confronting the challenges of antibacterial discovery. *Nature reviews Drug discovery*, *6*(1), pp.29-40.
4. Holmes, A.H., Moore, L.S., Sundsfjord, A., Steinbakk, M., Regmi, S., Karkey, A., Guerin, P.J. and Piddock, L.J., 2016. Understanding the mechanisms and drivers of antimicrobial resistance. *The Lancet*, *387*(10014), pp.176-187.
5. Ling, L.L., Schneider, T., Peoples, A.J., Spoering, A.L., Engels, I., Conlon, B.P., Mueller, A., Schäberle, T.F., Hughes, D.E., Epstein, S. and Jones, M., 2015. A new antibiotic kills pathogens without detectable resistance. *Nature*, *517*(7535), pp.455-459.
6. Imai Y, Meyer KJ, Iinishi A, Favre-Godal Q, Green R, Manuse S, Caboni M, Mori M, Niles S, Ghiglieri M, Honrao C. A new antibiotic selectively kills Gram-negative pathogens. Nature. 2019 Dec 19;576(7787):459-64.
7. Kaur, H., Jakob, R.P., Marzinek, J.K., Green, R., Imai, Y., Bolla, J.R., Agustoni, E., Robinson, C.V., Bond, P.J., Lewis, K. and Maier, T., 2021. The antibiotic darobactin mimics a β-strand to inhibit outer membrane insertase. *Nature*, *593*(7857), pp.125-129.

8. Knowles, T.J., Scott-Tucker, A., Overduin, M. and Henderson, I.R., 2009. Membrane protein architects: the role of the BAM complex in outer membrane protein assembly. *Nature Reviews Microbiology*, *7*(3), pp.206-214.
9. Nesic, M., Ryffel, D.B., Maturano, J., Shevlin, M., Pollack, S.R., Gauthier Jr, D.R., Trigo-Mouriño, P., Zhang, L.K., Schultz, D.M., McCabe Dunn, J.M. and Campeau, L.C., 2022. Total synthesis of Darobactin A. *Journal of the American Chemical Society*, *144*(31), pp.14026-14030.
10. Lin, Y.C., Schneider, F., Eberle, K.J., Chiodi, D., Nakamura, H., Reisberg, S.H., Chen, J., Saito, M. and Baran, P.S., 2022. Atroposelective total synthesis of darobactin A. *Journal of the American Chemical Society*, *144*(32), pp.14458-14462.
11. Wuisan ZG, Kresna ID, Böhringer N, Lewis K, Schäberle TF. Optimization of heterologous Darobactin A expression and identification of the minimal biosynthetic gene cluster. Metabolic Engineering. 2021 Jul 1;66:123-36.
12. Groß S, Panter F, Pogorevc D, Seyfert CE, Deckarm S, Bader CD, Herrmann J, Müller R. Improved broad-spectrum antibiotics against Gram-negative pathogens via darobactin biosynthetic pathway engineering. Chemical science. 2021;12(35):11882-93.
13. Fleckenstein, J.M., Kuhlmann, F.M. and Sheikh, A., 2021. Acute bacterial gastroenteritis. *Gastroenterology Clinics*, *50*(2), pp.283-304.
14. Hennessy, T.W., Hedberg, C.W., Slutsker, L., White, K.E., Besser-Wiek, J.M., Moen, M.E., Feldman, J., Coleman, W.W., Edmonson, L.M., MacDonald, K.L. and Osterholm, M.T., 1996. A national outbreak of Salmonella enteritidis infections from ice cream. *New England Journal of Medicine*, *334*(20), pp.1281-1286.
15. Khaghani, S., Shamsizadeh, A., Nikfar, R. and Hesami, A., 2014. Shigella flexneri: a three-year antimicrobial resistance monitoring of isolates in a Children Hospital, Ahvaz, Iran. *Iranian Journal of Microbiology*, *6*(4), p.225.
16. Igwaran, A. and Okoh, A.I., 2019. Human campylobacteriosis: A public health concern of global importance. *Heliyon*, *5*(11).
17. Chuang, C.H., Wang, Y.H., Chang, H.J., Chen, H.L., Huang, Y.C., Lin, T.Y., Ozer, E.A., Allen, J.P., Hauser, A.R. and Chiu, C.H., 2014. Shanghai fever: a distinct Pseudomonas aeruginosa enteric disease. *Gut*, *63*(5), pp.736-743.
18. Regalado, N.G., Martin, G. and Antony, S.J., 2009. Acinetobacter lwoffii: bacteremia associated with acute gastroenteritis. *Travel medicine and infectious disease*, *7*(5), pp.316-317.
19. Sattar SBA, Singh S. Bacterial Gastroenteritis. [Updated 2023 Aug 8]. In: StatPearls [Internet]. Treasure Island (FL): StatPearls Publishing; 2024 Jan-. Available from: https://www.ncbi.nlm.nih.gov/books/NBK513295/
20. Authority, E.F.S., 2022. The European Union Summary Report on Antimicrobial Resistance in zoonotic and indicator bacteria from humans, animals and food in 2019–2020. *EFSA Journal*, *20*(3).
21. Walker, S.S. and Black, T.A., 2021. Are outer-membrane targets the solution for MDR Gram-negative bacteria?. *Drug discovery today*, *26*(9), pp.2152-2158.

22. Hwang IY, Koh E, Wong A, March JC, Bentley WE, Lee YS, Chang MW. Engineered probiotic Escherichia coli can eliminate and prevent Pseudomonas aeruginosa gut infection in animal models. Nature communications. 2017 Apr 11;8(1):15028.
23. Koh, E., Hwang, I.Y., Lee, H.L., De Sotto, R., Lee, J.W.J., Lee, Y.S., March, J.C. and Chang, M.W., 2022. Engineering probiotics to inhibit Clostridioides difficile infection by dynamic regulation of intestinal metabolism. *Nature Communications*, *13*(1), p.3834.
24. Achaiah, N.C., Bhutta, B.S. and AK, A.K., 2021. Fever in the intensive care patient.
25. Balli, S., Shumway, K.R. and Sharan, S., 2022. Physiology, fever. In *StatPearls [Internet]*. StatPearls Publishing.
26. Cole, L. and Kramer, P.R., 2016. Bacteria, virus, fungi, and infectious diseases. *Human Physiology, Biochemistry and Basic Medicine*, p.193.
27. Carsons, S.E., 1996. Fever in rheumatic and autoimmune disease. *Infectious Disease Clinics*, *10*(1), pp.67-84.
28. Casadevall, A., 2016. Thermal restriction as an antimicrobial function of fever. *PLoS pathogens*, *12*(5), p.e1005577.
29. El-Radhi, A.S., 2018. Fever in common infectious diseases. *Clinical Manual of Fever in Children*, pp.85-140.
30. Dennehy, P.H., 2019. Infectious Gastroenteritis: diarrhea with fever. *Introduction to Clinical Infectious Diseases: A Problem-Based Approach*, pp.157-168.
31. D'Aoust, J.Y. and Doyle, M.P., 1989. Foodborne bacterial pathogens. *Marel Dekker Inc., New York, New York*.
32. Zaika, L.L., Engel, L.S., Kim, A.H. and Palumbo, S.A., 1989. Effect of sodium chloride, pH and temperature on growth of Shigella flexneri. *Journal of food protection*, *52*(5), pp.356-359.
33. Doyle, M.P. and Roman, D.J., 1981. Growth and survival of Campylobacter fetus subsp. jejuni as a function of temperature and pH. *Journal of Food Protection*, *44*(8), pp.596-601.
34. Wei, Y., Murphy, E.R., Larramendy, M. and Soloneski, S., 2016. Temperature-dependent regulation of bacterial gene expression by RNA thermometers. *Nucleic Acids—from Basic Aspects to Laboratory Tools Specific. IntechOpen, London*, pp.157-181.
35. Piraner DI, Abedi MH, Moser BA, Lee-Gosselin A, Shapiro MG. Tunable thermal bioswitches for in vivo control of microbial therapeutics. Nature chemical biology. 2017 Jan;13(1):75-80.
36. Fedorec AJ, Ozdemir T, Doshi A, Ho YK, Rosa L, Rutter J, Velazquez O, Pinheiro VB, Danino T, Barnes CP. Two new plasmid post-segregational killing mechanisms for the implementation of synthetic gene networks in Escherichia coli. Iscience. 2019 Apr 26;14:323-34.
37. Moore, S.J., Lai, H.E., Kelwick, R.J., Chee, S.M., Bell, D.J., Polizzi, K.M. and Freemont, P.S., 2016. EcoFlex: a multifunctional MoClo kit for E. coli synthetic biology. *ACS Synthetic Biology*, *5*(10), pp.1059-1069.
38. Fowler, D.K., Stewart, S., Seredick, S., Eisen, J.S., Stankunas, K. and Washbourne, P., 2016. A MultiSite Gateway toolkit for rapid cloning of vertebrate expression constructs with diverse research applications. *PloS one*, *11*(8), p.e0159277.

39. Basaran, S., Dey, S., Bhusari, S., Sankaran, S. and Kraus, T., 2023. Plasmonic stimulation of gold nanorods for the photothermal control of engineered living materials. *Biomaterials Advances*, *147*, p.213332.
40. Škulj M, Okršlar V, Jalen Š, Jevševar S, Slanc P, Štrukelj B, Menart V. Improved determination of plasmid copy number using quantitative real-time PCR for monitoring fermentation processes. Microbial cell factories. 2008 Jul;7:1-2.
41. Smati M, Clermont O, Le Gal F, Schichmanoff O, Jauréguy F, Eddi A, Denamur E, Picard B, Coliville Group. Real-time PCR for quantitative analysis of human commensal Escherichia coli populations reveals a high frequency of subdominant phylogroups. Applied and environmental microbiology. 2013 Aug 15;79(16):5005-12.
42. Nguyen H, Made Kresna ID, Böhringer N, Ruel J, Mora ED, Kramer JC, Lewis K, Nicolet Y, Schäberle TF, Yokoyama K. Characterization of a radical SAM oxygenase for the ether crosslinking in darobactin biosynthesis. Journal of the American Chemical Society. 2022 Oct 4;144(41):18876-86.
43. Mamat U, Wilke K, Bramhill D, Schromm AB, Lindner B, Kohl TA, Corchero JL, Villaverde A, Schaffer L, Head SR, Souvignier C. Detoxifying Escherichia coli for endotoxin-free production of recombinant proteins. Microbial cell factories. 2015 Dec;14:1-5.
44. Singha TK, Gulati P, Mohanty A, Khasa YP, Kapoor RK, Kumar S. Efficient genetic approaches for improvement of plasmid based expression of recombinant protein in Escherichia coli: A review. Process Biochemistry. 2017 Apr 1;55:17-31.
45. Xu J, Banerjee A, Pan SH, Li ZJ. Galactose can be an inducer for production of therapeutic proteins by auto-induction using E. coli BL21 strains. Protein expression and purification. 2012 May 1;83(1):30-6.
46. Song, H.Y. and Su, X., 2014. Spacer effect of cooperative binding of estrogen receptor α and specificity protein 1 to composite DNA: a surface plasmon resonance study. *Sensors and Actuators B: Chemical*, *195*, pp.635-642.
47. Sonnenborn, U., 2016. Escherichia coli strain Nissle 1917—from bench to bedside and back: history of a special Escherichia coli strain with probiotic properties. *FEMS microbiology letters*, *363*(19), p.fnw212.
48. Fiege K, Frankenberg-Dinkel N. Construction of a new T7 promoter compatible Escherichia coli Nissle 1917 strain for recombinant production of heme-dependent proteins. Microbial Cell Factories. 2020 Oct 6;19(1):190.
49. Fuerst, T.R., Earl, P.L. and Moss, B., 1987. Use of a hybrid vaccinia virus-T7 RNA polymerase system for expression of target genes. *Molecular and Cellular Biology*.
50. Tomatis, P.E., Schütz, M., Umudumov, E. and Plückthun, A., 2019. Mutations in sigma 70 transcription factor improves expression of functional eukaryotic membrane proteins in Escherichia coli. *Scientific reports*, *9*(1), p.2483.
51. Nougayrède JP, Chagneau CV, Motta JP, Bossuet-Greif N, Belloy M, Taieb F, Gratadoux JJ, Thomas M, Langella P, Oswald E. A toxic friend: genotoxic and mutagenic activity of the probiotic strain Escherichia coli Nissle 1917. MSphere. 2021 Aug 25;6(4):10-128.

52. Nougayrède, J.P., Homburg, S., Taieb, F., Boury, M., Brzuszkiewicz, E., Gottschalk, G., Buchrieser, C., Hacker, J., Dobrindt, U. and Oswald, E., 2006. Escherichia coli induces DNA double-strand breaks in eukaryotic cells. *Science*, *313*(5788), pp.848-851.
53. Pleguezuelos-Manzano, C., Puschhof, J., Rosendahl Huber, A., van Hoeck, A., Wood, H.M., Nomburg, J., Gurjao, C., Manders, F., Dalmasso, G., Stege, P.B. and Paganelli, F.L., 2020. Mutational signature in colorectal cancer caused by genotoxic pks+ E. coli. *Nature*, *580*(7802), pp.269-273.
54. Mousa, W.K., 2022. The microbiome-product colibactin hits unique cellular targets mediating host–microbe interaction. *Frontiers in Pharmacology*, *13*, p.958012.
55. Cevallos, S.A., Lee, J.Y., Tiffany, C.R., Byndloss, A.J., Johnston, L., Byndloss, M.X. and Bäumler, A.J., 2019. Increased epithelial oxygenation links colitis to an expansion of tumorigenic bacteria. *MBio*, *10*(5), pp.10-1128.
56. Bian X, Fu J, Plaza A, Herrmann J, Pistorius D, Stewart AF, Zhang Y, Müller R. In vivo evidence for a prodrug activation mechanism during colibactin maturation. ChemBioChem. 2013 Jul 8;14(10):1194-7.
57. LaBauve, A.E. and Wargo, M.J., 2012. Growth and laboratory maintenance of Pseudomonas aeruginosa. *Current protocols in microbiology*, *25*(1), pp.6E-1.
58. Mozaheb, N., Rasouli, P., Kaur, M., Van Der Smissen, P., Larrouy-Maumus, G. and Mingeot-Leclercq, M.P., 2023. A mildly acidic environment alters Pseudomonas aeruginosa virulence and causes remodeling of the bacterial surface. *Microbiology Spectrum*, *11*(4), pp.e04832-22.
59. Arai, H., 2011. Regulation and function of versatile aerobic and anaerobic respiratory metabolism in Pseudomonas aeruginosa. *Frontiers in microbiology*, *2*, p.103.
60. Mittal, R., Aggarwal, S., Sharma, S., Chhibber, S. and Harjai, K., 2009. Urinary tract infections caused by Pseudomonas aeruginosa: a minireview. *Journal of infection and public health*, *2*(3), pp.101-111.
61. Bayat, M., Nahand, J.S., Farsad-Akhatr, N. and Memar, M.Y., 2023. Bile effects on the Pseudomonas aeruginosa pathogenesis in cystic fibrosis patients with gastroesophageal reflux. *Heliyon*.
62. Reshetnyak, V.I., 2013. Physiological and molecular biochemical mechanisms of bile formation. *World journal of gastroenterology: WJG*, *19*(42), p.7341.
63. Begley, M., Gahan, C.G. and Hill, C., 2005. The interaction between bacteria and bile. *FEMS microbiology reviews*, *29*(4), pp.625-651.
64. Reen FJ, Flynn S, Woods DF, Dunphy N, Chróinín MN, Mullane D, Stick S, Adams C, O'Gara F. Bile signalling promotes chronic respiratory infections and antibiotic tolerance. Scientific reports. 2016 Jul 19;6(1):29768.
65. Flynn S, Reen FJ, O'Gara F. Exposure to bile leads to the emergence of adaptive signaling variants in the opportunistic pathogen Pseudomonas aeruginosa. Frontiers in microbiology. 2019 Aug 29;10:456279.

66. De Paepe, M., Gaboriau-Routhiau, V., Rainteau, D., Rakotobe, S., Taddei, F. and Cerf-Bensussan, N., 2011. Trade-off between bile resistance and nutritional competence drives Escherichia coli diversification in the mouse gut. *PLoS genetics*, *7*(6), p.e1002107.
67. Townsend, E.M., Kelly, L., Muscatt, G., Box, J.D., Hargraves, N., Lilley, D. and Jameson, E., 2021. The human gut phageome: origins and roles in the human gut microbiome. *Frontiers in cellular and infection microbiology*, *11*, p.643214.
68. Ferraris, R.P., Yasharpour, S.A.S.A.N., Lloyd, K.C., Mirzayan, R.A.F.F.Y. and Diamond, J.M., 1990. Luminal glucose concentrations in the gut under normal conditions. *American Journal of Physiology-Gastrointestinal and Liver Physiology*, *259*(5), pp.G822-G837.
69. Raghavan, A.R., Salim, K. and Yadav, V.G., 2020. Optogenetic control of heterologous metabolism in E. coli. *ACS synthetic biology*, *9*(9), pp.2291-2300.
70. Fernandez-Rodriguez, J., Moser, F., Song, M. and Voigt, C.A., 2017. Engineering RGB color vision into Escherichia coli. *Nature chemical biology*, *13*(7), pp.706-708.
71. Böhringer, N., Green, R., Liu, Y., Mettal, U., Marner, M., Modaresi, S.M., Jakob, R.P., Wuisan, Z.G., Maier, T., Iinishi, A. and Hiller, S., 2021. Mutasynthetic production and antimicrobial characterization of darobactin analogs. *Microbiology spectrum*, *9*(3), pp.e01535-21.
72. Miller, R.D., Iinishi, A., Modaresi, S.M., Yoo, B.K., Curtis, T.D., Lariviere, P.J., Liang, L., Son, S., Nicolau, S., Bargabos, R. and Morrissette, M., 2022. Computational identification of a systemic antibiotic for gram-negative bacteria. *Nature microbiology*, *7*(10), pp.1661-1672.
73. Seyfert, C.E., Müller, A.V., Walsh, D.J., Birkelbach, J., Kany, A.M., Porten, C., Yuan, B., Krug, D., Herrmann, J., Marlovits, T.C. and Hirsch, A.K., 2023. New Genetically Engineered Derivatives of Antibacterial Darobactins Underpin Their Potential for Antibiotic Development. *Journal of Medicinal Chemistry*, *66*(23), pp.16330-16341.
74. Redenti, A., Im, J., Redenti, B., Li, F., Rouanne, M., Sheng, Z., Sun, W., Gurbatri, C.R., Huang, S., Komaranchath, M. and Jang, Y., 2023. Probiotic neoantigen delivery vectors for precision cancer immunotherapy. *bioRxiv*, pp.2023-09.
75. Wagner, S., Klepsch, M.M., Schlegel, S., Appel, A., Draheim, R., Tarry, M., Högbom, M., Van Wijk, K.J., Slotboom, D.J., Persson, J.O. and De Gier, J.W., 2008. Tuning Escherichia coli for membrane protein overexpression. *Proceedings of the National Academy of Sciences*, *105*(38), pp.14371-14376.
76. Song, C.W., Lee, J., Ko, Y.S. and Lee, S.Y., 2015. Metabolic engineering of Escherichia coli for the production of 3-aminopropionic acid. *Metabolic engineering*, *30*, pp.121-129.
77. Hirano, R., Sakanaka, M., Yoshimi, K., Sugimoto, N., Eguchi, S., Yamauchi, Y., Nara, M., Maeda, S., Ami, Y., Gotoh, A. and Katayama, T., 2021. Next-generation prebiotic promotes selective growth of bifidobacteria, suppressing Clostridioides difficile. *Gut Microbes*, *13*(1), p.1973835.
78. Breidenstein, E.B., de la Fuente-Núñez, C. and Hancock, R.E., 2011. Pseudomonas aeruginosa: all roads lead to resistance. *Trends in microbiology*, *19*(8), pp.419-426.
79. Pang, Z., Raudonis, R., Glick, B.R., Lin, T.J. and Cheng, Z., 2019. Antibiotic resistance in Pseudomonas aeruginosa: mechanisms and alternative therapeutic strategies. *Biotechnology advances*, *37*(1), pp.177-192.

80. Amrofell, M.B., Rengarajan, S., Vo, S.T., Tovar, E.S.R., LoBello, L., Dantas, G. and Moon, T.S., 2023. Engineering E. coli strains using antibiotic-resistance-gene-free plasmids. *Cell Reports Methods*, *3*(12).
81. Hayashi, N., Lai, Y., Fuerte-Stone, J., Mimee, M. and Lu, T.K., 2024. Cas9-assisted biological containment of a genetically engineered human commensal bacterium and genetic elements. *Nature Communications*, *15*(1), p.2096.
82. Kan, A., Gelfat, I., Emani, S., Praveschotinunt, P. and Joshi, N.S., 2020. Plasmid vectors for in vivo selection-free use with the probiotic E. coli Nissle 1917. *ACS synthetic biology*, *10*(1), pp.94-106.
83. Lodinová-Žádníková, R. and Sonnenborn, U., 1997. Effect of preventive administration of a nonpathogenic Escherichia coli strain on the colonization of the intestine with microbial pathogens in newborn infants. *Neonatology*, *71*(4), pp.224-232.
84. Sonnenborn, U. and Schulze, J., 2009. The non-pathogenic Escherichia coli strain Nissle 1917–features of a versatile probiotic. *Microbial Ecology in Health and Disease*, *21*(3-4), pp.122-158.
85. Conway, T. and Cohen, P.S., 2015. Commensal and pathogenic Escherichia coli metabolism in the gut. *Metabolism and bacterial pathogenesis*, pp.343-362.
86. Thanh Duy, P., Thi Nguyen, T.N., Vu Thuy, D., Chung The, H., Alcock, F., Boinett, C., Dan Thanh, H.N., Thanh Tuyen, H., Thwaites, G.E., Rabaa, M.A. and Baker, S., 2020. Commensal Escherichia coli are a reservoir for the transfer of XDR plasmids into epidemic fluoroquinolone-resistant Shigella sonnei. *Nature microbiology*, *5*(2), pp.256-264.
87. Triassi, A.J., Fields, B.D., Monahan, C.E., Means, J.M., Park, Y., Doosthosseini, H., Padmakumar, J.P., Isabella, V.M. and Voigt, C.A., 2023. Redesign of an Escherichia coli Nissle treatment for phenylketonuria using insulated genomic landing pads and genetic circuits to reduce burden. *Cell Systems*, *14*(6), pp.512-524.

This chapter is in large part a reformatted version of the manuscript entitled **"Novel genetic modules encoding high-level antibiotic-free protein expression in probiotic lactobacilli"** published in the Microbial Biotechnology journal (Wiley Publishing Group). To avoid self-plagiarism and excessive citation, I am providing this note as a general citation without further citation in the body of the chapter.

Citation – Sourik Dey[+], Marc Blanch-Asensio[+], Sanjana Balaji Kuttae and Shrikrishnan Sankaran (2023) Novel genetic modules encoding high-level antibiotic-free protein expression in probiotic lactobacilli. *Microbial Biotechnology*, *16*(6), pp.1264-1276. ([+]equal contribution)

Contribution Report

Sourik Dey conceived the overall idea of the project and constructed the mCherry expressing recombinant plasmids with the aid of a student assistant, Sanjana Balaji Kuttae. Sourik Dey performed all the fluorescent protein expression experiments and analyzed the bacterial growth profile. Sourik Dey and Marc Blanch-Asensio jointly constructed the toxin-antitoxin expressing recombinant plasmids and analyzed the plasmid retention profile. Sourik Dey and Marc Blanch-Asensio wrote the manuscript and Shrikrishnan Sankaran edited it.

Chapter 4

NOVEL GENETIC MODULES ENCODING HIGH-LEVEL ANTIBIOTIC-FREE PROTEIN EXPRESSION IN PROBIOTIC LACTOBACILLI

Abstract

Lactobacilli are ubiquitous in nature, often beneficially associated with animals as commensals and probiotics, and are extensively used in food fermentation. Due to this close-knit association, there is considerable interest to engineer them for healthcare applications in both humans and animals, for which high-performance and versatile genetic parts are greatly desired. For the first time, we describe two genetic modules in *Lactiplantibacillus plantarum* that achieve high-level gene expression using plasmids that can be retained without antibiotics, bacteriocins or genomic manipulations. These include (i) a promoter, P_{tlpA}, from a phylogenetically distant bacterium, *Salmonella typhimurium*, that drives up to 5-fold higher level of gene expression compared to previously reported promoters and (ii) multiple toxin-antitoxin systems as a self-contained and easy-to-implement plasmid retention strategy that facilitates the engineering of tunable transient Genetically Modified Organisms. These modules and the fundamental factors underlying their functionality that are described in this work will greatly contribute to expanding the genetic programmability of lactobacilli for healthcare applications.

4.1. Introduction

Lactobacilli are Gram-positive rod-shaped lactic acid bacteria (LAB), typically found in humans and animals as commensals. Their stress tolerant phenotypic traits allow them to colonize a wide range of host microenvironments, like the gut, skin, vagina, nasal and oropharyngeal cavity (Ma *et al.,* 2012; Turroni *et al.,* 2014) often providing health benefits in the form of anti-inflammatory, anti-pathogenic and immunomodulatory activities (Darby and Jones, 2017; Bibalan *et al.,* 2017). Due to this, they are one of the largest classes of probiotics and several species are being clinically

tested for treating a variety of diseases like ulcerative colitis (Zocco *et al.,* 2006), mastitis (Jiménez *et al.,* 2008), atopic dermatitis (Rosenfeldt *et al.,* 2003), bacterial vaginosis (Mastromarino *et al.,* 2009) and periodontitis (Teughels *et al.,* 2013). Apart from their health benefits, lactobacilli are also vital for numerous fermentation processes in the food industry, for example in the production of yogurt (Ashraf and Shah, 2011), cheese (Kasımoğlu *et al.,* 2004), sourdough bread (Plessas *et al.,* 2008), beer (Chan *et al.,* 2019) and wine (du Toit *et al.,* 2011). Due to this ubiquity in our lives, there is considerable interest to genetically enhance and expand the capabilities of these bacteria for healthcare applications (Pedrolli *et al.,* 2019). For instance, lactobacilli are being engineered as live biotherapeutic products (LBPs) that produce and deliver drugs right at the site of diseases like ulcerative colitis (de Vos, 2011), Human Immunodeficiency Virus (HIV) infection (Watterlot *et al.,* 2010) and respiratory infections (Janahi *et al.,* 2018). They are also prominent candidates for the development of mucosal vaccines in which they are engineered to either display heterologous antigens on their surface or to secrete them (LeCureux and Dean, 2018). These food-grade *Lactobacillus* vaccine vectors would be cheap to produce and can be easily administered orally or intranasally, improving the ability to deploy them both in humans and animals. Examples of infectious diseases against which such vaccines are under development include anthrax, infantile diarrhea, pneumonia and viral infections like, HIV, HPV, influenza and coronavirus (LeCureux and Dean, 2018; Wang *et al.,* 2020). Finally, to track these therapeutic bacteria within the body and study their colonization and clearance profiles, there is considerable interest to make them express reporter proteins that can be imaged *in situ* (Landete *et al.,* 2015; Salomé-Desnoulez *et al.,* 2021).

Despite such potential, the main limitations for engineering lactobacilli are the scarcity of well-characterized genetic parts and insufficient understanding of biochemical pathways required to build the type of genetic circuits that have been demonstrated in *E. coli* (Elowitz and Leibler, 2000; Wang *et al.,* 2011) and *B. subtilis* (Courbet *et al.,* 2015; Castillo-Hair *et al.,* 2019) . Over two decades of painstaking investigation and screening across phylogenetically close bacteria have generated a handful of reliable parts for use in lactobacilli such as constitutive and inducible promoters, operators, replicons, retention-modules, signal peptides etc. Most of these have been developed in a few species that were found to be amenable to genetic modification, among which *Lactiplantibacillus plantarum* (Zheng *et al.,* 2020) is widely reported (Siezen and van Hylckama Vlieg, 2011). While genomic integration of genes has been demonstrated in these bacteria, the greatest versatility of functions has been achieved using plasmids. Excellent progress has been

made in establishing plasmid backbones with low, medium and high copy number replicons (Tauer *et al.,* 2014) , constitutive promoters with a wide range of expression strengths (Rud *et al.,* 2006), a few inducible promoters that can be triggered by peptides (Halbmayr *et al.,* 2008) or sugars (Heiss *et al.,* 2016), signal peptides sequences enabling protein secretion (Mathiesen *et al.,* 2009) or surface display (Mathiesen *et al.,* 2020) and food-grade plasmid retention systems based on resistance to external stressors (e.g. bacteriocins) (Takala and Saris, 2002; Allison and Klaenhammer, 1996) or auxotrophy complementation requiring genomic knockout of a metabolic gene and providing it in the plasmid (Nguyen *et al.,* 2011; Chen *et al.,* 2018). However, the available set of well-characterized genetic parts is still minuscule compared to the toolbox of *E. coli* and needs to be expanded in order to improve the performance and versatility of *Lactobacillus* engineering for healthcare applications.

In this work, we introduce 2 new versatile and powerful genetic parts to expand the capabilities of *Lactobacillus* engineering - (i) a novel constitutive promoter from a phylogenetically distant *Salmonella* species that drive protein expression at levels considerably higher than previously reported strong *L. plantarum* promoters and (ii) toxin-antitoxin systems as an alternative strategy for plasmid retention that does not require manipulating the bacterial genome. Unique features of the novel promoter sequence are discussed, which can lead to new design criteria for improving promoter strengths in lactobacilli. The toxin-antitoxin systems introduce a thus-far unexplored modality of plasmid retention in lactobacilli that enables the generation of temporary Genetically Engineered Microorganisms (GEMs), desirable for medical and food-grade applications. These parts and the fundamental insights gained in their characterization will strongly aid in expanding the genetic programmability of lactobacilli.

4.2. Materials and Methods

Strain, Media and Plasmids

L. plantarum WCFS1 was used as the parent strain for promoter strength and plasmid retention characterization. The strain was maintained in the De Man, Rogosa and Sharpe (MRS) media. The culture media, antibiotics and complementary reagents were purchased from Carl Roth Gmbh, Germany. Growth media was supplemented with 10 μg/mL of erythromycin to culture engineered

L. plantarum WCFS1 strains. The plasmids pSIP403 and pLp_3050sNuc used in this study were a kind gift from Prof. Lars Axelsson (Addgene plasmid # 122028) (Sørvig *et al.,* 2005a) and Prof. Geir Mathiesen (Addgene plasmid # 122030) (Mathiesen *et al.,* 2009) respectively. The plasmid pTlpA39-Wasabi was a kind gift from Prof. Mikhail Shapiro (Addgene plasmid # 86116) (Piraner *et al.,* 2017). The plasmid pUC-GFP-AT was a kind gift from Prof. Chris Barnes (Addgene plasmid # 133306) (Fedorec *et al.,* 2019). The sequence verified genetic constructs created in this study have been maintained in *E. coli* DH5α.

Molecular Biology

The genetic constructs developed in this study are based on the pLp3050sNuc/ pSIP403 vector backbone. The HiFi Assembly Master Mix, Quick Blunting Kit and the T4 DNA Ligase enyzme were purchased from New England BioLabs (NEB, Germany). PCR was performed using Q5 High Fidelity 2X Master Mix (NEB) with primers purchased from Integrated DNA Technologies (IDT) (Leuven, Belgium). Oligonucleotide gene fragments were purchased as eBlocks from IDT (Coralville, USA). These were codon optimized for maximal expression in the host strain using the IDT Codon Optimization Tool (Coralville, USA). Plasmid extraction and DNA purification were performed using kits purchased from Qiagen GmbH (Hilden, Germany) and Promega GmbH (Walldorf, Germany) respectively. The general schematic of plasmid construction for this study has been shown in **Supplementary Figure S1**. The promoter sequences used in this study are provided in **Supplementary Table S1** and the nucleotide sequences of the toxin-antitoxin modules have been highlighted in **Supplementary Table S2**.

***L. plantarum* WCFS1 Competent Cell Preparation and DNA Transformation**

A single colony of *L. plantarum* WCFS1 was inoculated in 5 mL of MRS media and cultured overnight at 37°C with shaking (250 rpm). The primary culture was diluted in a 1:50 (v/v) ratio in a 25 mL secondary culture composed of MRS media and 1% (w/v) glycine premixed in a 4:1 ratio. The secondary culture was incubated at 37°C, 250 rpm until OD_{600} reached 0.8, following which the cells were pelleted down by centrifuging at 4000 rpm (3363 × g) for 10 min at 4°C. The pellet was washed twice with 5 mL of ice-cold 10 mM $MgCl_2$ and then washed twice with 5 mL and 1 mL of ice-cold Sac/Gly solution [10% (v/v) glycerol and 1 M sucrose mixed in a 1:1 (v/v) ratio] respectively. Finally, the residual supernatant was discarded, and the pellet resuspended in 500 µL

of Sac/Gly solution. The competent cells were then dispensed in 60 µL aliquots for DNA transformation. For all transformations, 1 µg of dsDNA were added to the competent cells and then transferred to chilled 2 mm gap electroporation cuvettes (Bio-Rad Laboratories GmbH, Germany). Electroporation transformation was done with a single pulse at 1.8 kV, after which 1 mL of lukewarm MRS media was immediately added. The mixture was kept for incubation at 37°C, 250 rpm for a recovery period of 3 h. Following the recovery phase, the cells were centrifuged at 4000 rpm (3363 × g) for 5 min, 800 µL of the supernatant discarded, and 200 µL of the resuspended pellet was plated on MRS Agar supplemented with 10 µg/mL of Erythromycin. The plates were incubated at 37°C for 48 h to allow the growth of distinct single colonies.

Direct cloning in *L. plantarum* WCFS1

To obtain sufficient plasmid quantities (~1 µg) for transformation in *L. plantarum* WCFS1, a modified direct cloning method (Spath *et al.,* 2012) involving PCR-based amplification and circularization of recombinant plasmids was used. Plasmids were constructed and transformed directly in *L. plantarum* WCFS1 strain using a DNA assembly method. Complementary overhangs for HiFi Assembly were either created using PCR primers or synthesized as custom designed eBlocks. Purified overlapping DNA fragments were mixed with the HiFi DNA Assembly Master Mix and assembled as recommended in the standard reaction protocol from the manufacturer. The assembled DNA product was then exponentially amplified by another round of PCR using a pair of primers annealing specifically to the insert segment. 5 µL of the HiFi assembly reaction was used as a template for this PCR amplification of the assembled product (100 µL final volume). The purified PCR product was then subjected to phosphorylation using the Quick Blunting Kit. 2000 ng of the purified PCR product was mixed with 2.5 µL of 10X Quick blunting buffer and 1 µL of Enzyme Mix (Milli-Q water was added up to 25 µL). The reaction was incubated first at 25°C for 30 min and then at 70°C for 10 min for enzyme inactivation. Next, phosphorylated products were ligated using the T4 ligase enzyme. 6 µL of the phosphorylated DNA was mixed with 2.5 µL of 10X T4 Ligase Buffer and 1.5 µL of T4 Ligase enzyme (Milli-Q water was added up to 25 µL). Two ligation reactions were performed per cloning (25 µL each). The respective reactions were incubated at 25°C for 2 h and then at 70°C for 30 min for enzyme inactivation. The ligated reactions were mixed together and purified. In order to concentrate the final purified product, three elution rounds were performed instead of one. Each elution was based on 10 µL of Milli-Q water. The

concentration of the ligated purified product was measured using the NanoDrop Microvolume UV-Vis Spectrophotometer (ThermoFisher Scientific GmbH, Germany). Finally, 1000 ng of the ligated product were transformed into *L. plantarum* WCFS1 electrocompetent cells, resulting in a transformation efficiency of 2 – 3 x 10^2 cfu/µg.

Notably, since *L. plantarum* harbors 3 endogenous plasmids (Van Kranenburg *et al.,* 2005), sequencing was performed on PCR amplified sections. In detail, colonies of interest were inoculated in MRS supplemented with 10 µg/mL of Erythromycin and grown overnight at 37°C. The following day, 1 mL of the culture was pelleted down, and the supernatant was discarded. Next, a tip was used to collect a tiny part of the pellet, which was used as a template for PCR (100 µL final volume). Finally, PCR products were purified and sent for Sanger sequencing to Eurofins Genomics GmbH (Ebersberg, Germany) by opting for the additional DNA purification step.

Microplate reader Setup for Thermal Gradient Analysis

Bacterial cultures were cultivated in 5 mL of MRS media (supplemented with 10 µg/mL erythromycin) at 30°C with continuous shaking (250 rpm). The following day, cultures were diluted to 0.1 OD_{600} in 3 mL of antibiotic supplemented fresh MRS media and propagated at 30°C, 250 rpm. At OD_{600} = 0.3, the cultures were dispensed into Fisherbrand™ 0.2 mL PCR Tube Strips with Flat Caps (Thermo Electron LED GmbH, Germany) and placed in the Biometra Thermocycler (Analytik Jena. GmbH, Germany). For the P_{spp}-mCherry construct, 25 ng/mL of the 19 amino acid Sakacin P inducer peptide (SppIp) with the sequence NH_2- MAGNSSNFIHKIKQIFTHR-COOH (GeneCust, France) was added to the culture and thoroughly vortexed before preparing the aliquots. The thermal assay was set at a temperature gradient from 31°C to 41°C with regular increment of 2°C. The lid temperature was set at 50°C to prevent the evaporation of the liquid and maintain a homogeneous temperature in the spatially allocated PCR tubes. After a time interval of 18 h, the PCR strips were centrifuged in a tabletop minicentrifuge (Biozym GmbH, Germany) to pellet down the cells and discard the supernatant. The cells were then resuspended in 200 µL of 1X PBS and added to the clear bottom 96-well microtiter plate (Corning® 96 well clear bottom black plate, USA). The samples were then analyzed in the Microplate Reader Infinite 200 Pro (Tecan Deutschland GmbH, Germany) and both the absorbance (600 nm wavelength) and mCherry fluorescence intensity (Ex_λ / Em_λ = 587 nm/625 nm) were measured. The z-position and gain settings for recording the mCherry fluorescent intensity were set to 19442 µm and 136 respectively.

Fluorescence values were normalized with the optical density of the bacterial cells to calculate the Relative Fluorescence Units (RFU) using the formula RFU = Fluorescence/OD_{600}.

Fluorescence Microscopy Analysis

Bacterial cultures were grown overnight in 5 mL of MRS media (supplemented with 10 µg/mL erythromycin) at 37°C with continuous shaking (250 rpm). The following day, the OD_{600} of the P_{spp}-mCherry construct was measured and subcultured at OD_{600} = 0.01. When the P_{spp}-mCherry bacterial culture reached OD_{600} =0.3, it was induced with 25 ng/mL of SppIp and the remaining constructs were subcultured in fresh media at 0.01 OD_{600}. All the cultures were then allowed to grow for 18 h under the same growth conditions (37°C, 250 rpm) to prevent any heterogeneity in promoter strength expression due to differential growth parameters. Later, 1 mL of the cultures were harvested by centrifugation (15700 × g, 5 min, 4°C), washed twice with Dulbecco's 1X PBS (Phosphate Buffer Saline) and finally resuspended in 1 mL of 1X PBS. 10 µL of the suspensions were placed on glass slides of 1.5 mm thickness (Paul Marienfeld GmbH, Germany) and 1.5H glass coverslips (Carl Roth GmbH, Germany) were placed on top of it. The samples were then observed under the Plan Apochromat 100X oil immersion lens (BZ-PA100, NA 1.45, WD 0.13 mm) of the Fluorescence Microscope BZ-X800 (Keyence Corporation, Illinois, USA). The mCherry signal were captured in the BZ-X TRITC filter (model OP-87764) at excitation wavelength of 545/25 nm and emission wavelength of 605/70 nm with a dichroic mirror wavelength of 565 nm. The images were adjusted for identical brightness and contrast settings and were processed with the FiJi ImageJ2 software.

Flow Cytometry Analysis

Quantification of fluorescent protein expression levels of the strains were performed using Guava easyCyte BG flow-cytometer (Luminex, USA). Bacterial cultures subjected to the same treatment conditions mentioned above were used for Flow Cytometry analysis. 1 mL of the bacterial suspensions were harvested by centrifugation at 13000 rpm (15700 × g). The supernatant was discarded and the pellet was resuspended in 1 mL of sterile Dulbecco's 1X PBS. The samples were then serially diluted by a 10^4 Dilution Factor (DF) and 5,000 bacteria events were recorded for analysis. Experiments were performed in triplicates on three different days. During each analysis, the non-fluorescent strain carrying the empty vector was kept as the negative control. A predesigned

gate based on forward side scatter (FSC) and side scatter (SSC) thresholding was used to remove debris and doublets during event collection and analysis. mCherry fluorescence intensity was measured using excitation by a green laser at 532 nm (100 mW) and the Orange-G detection channel 620/52 nm filter was used for signal analysis. The gain settings used for the data recording were, Forward Scatter (FSC) – 11.8; Side Scatter (SSC) - 4, and Orange-G Fluorescence – 1.68. The compensation control for fluorescence recording was set at 0.01 with an acquisition rate of 5 decades. Data analysis and representation were done using the Luminex GuavaSoft 4.0 software for EasyCyte.

Toxin/Antitoxin Module based Plasmid Construction

Similar to previous reports in *E. coli* (Fedorec *et al.,* 2019), the effect of Txe/Axe (toxin/antitoxin) module from *E. faecium* (Grady and Hayes, 2003) was tested in *L. plantarum* WCFS1 to test its capability for antibiotic-free plasmid retention. TA Finder version 2.0 tool (Xie *et al.,* 2018) was used to select further type-II TA (Toxin/Antitoxin) systems present in *Lactobacillus* genomes. *L. acidophilus*, *L. crispatus*, *L. casei*, *L. reuteri*, and *L. plantarum* WCFS1 genomes were retrieved from NCBI Genome. TA systems harbored within these genomes were mined using the default parameters of TA Finder. Only TA systems annotated by NCBI BlastP were selected as test candidates. The TA systems YafQ/DinJ, HicA/HicB, HigB/HigA, MazF/MazE from *L. casei, L. acidophilus and L. plantarum* WCFS1 were selected for further testing and analysis.

Txe/Axe system was amplified by PCR from the plasmid pUC-GFP-AT (Fedorec *et al.,* 2019). DinJ/YafQ and HicA/HicB systems were synthesized as custom-designed eBlocks. HigA/HigB and MazE/MazF were amplified from the genome of *L. plantarum* WCFS1. TA systems were inserted into the P_{tlpA}-mCherry plasmid, generating the plasmids P_{tlpA}-mCherry-Txe/Axe, P_{tlpA}-mCherry-YafQ/DinJ, P_{tlpA}-mCherry-HicA/HicB, P_{tlpA}-mCherry-HigB/HigA, P_{tlpA}-mCherry-MazF/MazE. For constructing the combinatorial TA module (P_{tlpA}-mCherry Combo), the best performing endogenous and non-endogenous TA systems recorded after 100 generations (MazF/MazE and YafQ/DinJ) were subcloned and integrated into the same plasmid in reverse orientations.

TA Mediated Plasmid Retention Analysis

The TA module containing constructs were inoculated in 5 mL cultures of 10 µg/mL erythromycin supplemented MRS media and incubated overnight at 37°C with continuous shaking (250 rpm).

The following day, the constructs were subcultured at an initial OD_{600} = 0.01 in fresh MRS media (both with and without antibiotic supplementation). The bacterial cultures were incubated for 12 consecutive days with a daily growth period of 24 h ensuring an average of ~8 generations per day, until crossing the final threshold of 100 generations. Sample preparation for flow cytometry analysis was conducted according to the protocol mentioned before. The mCherry positive cell population directly correlated to the bacterial population retaining the engineered plasmid. The entire experiment was repeated in biological triplicates.

To cross-check the flow cytometry analysis, the bacterial cultures grown for 100 generations without antibiotic supplementation were centrifuged and resuspended in 1 mL of sterile Dulbecco's 1X PBS. The resuspended bacterial solutions were diluted ($DF=10^{6}$) and plated on MRS Agar plates supplemented without antibiotic and incubated in a static incubator for 48 h. The plates were then imaged using the GelDocumentation System Fluorchem Q (Alpha Innotech Biozym Gmbh, Germany) both in the Ethidium Bromide channel ($Ex_{\lambda}/Em_{\lambda}$ = 300 nm/600 nm) and Cy3 channel ($Ex_{\lambda}/Em_{\lambda}$ = 554 nm/568 nm) to visualize the cell population producing mCherry fluorescence. The fluorescent bacterial subpopulation on the non-selective MRS agar medium correlated to the plasmid retention frequency of the respective TA systems in the absence of selection pressure.

Growth Rate Measurements

For studying the influence of the heterologous protein production and toxin-antitoxin modules on the bacterial growth rate, bacterial cultures were cultivated overnight in antibiotic supplemented MRS media at 37°C with continuous shaking (250 rpm). Following day, the bacterial cultures were subcultured in secondary cultures at an initial OD_{600} = 0.01. After 4 h incubation at 37°C, the OD_{600} of the cultures reached 0.1 and 200 µL of the cultures were distributed in UV STAR Flat Bottom 96 well microtiter plates (Greiner BioOne GmbH, Germany). The 96 well assay plate was placed in the Microplate Reader with constant shaking conditions at an incubation temperature of 37°C. The kinetic assay was set to record the absorbance of the bacterial cultures at 600 nm wavelength with an interval of 10 min for an 18 h time duration. The experiment was conducted in triplicates on three independent days.

Bioinformatic analysis

All genome sequence included in the phylogenetic analysis were retrieved from NCBI Genome. The phylogenetic tree was built using the web server for genome-based prokaryote taxonomy "Type (Strain) Genome Server" (TYGS), restricting the analysis only to the sequences provided (Meier-Kolthoff and Göker, 2019). The Genome BLAST Distance Phylogeny (GBDP) tree, based on 16S rDNA gene sequences, was obtained. The Interactive Tree of Life (iTOL) tool was used for the display, annotation, and management of the phylogenetic tree (Letunic and Bork, 2007).

For the multiple sequence alignment, protein sequences of the σ70 subunits from *L. plantarum*, *E. coli* and *S. typhimurium* RNA polymerases were first retrieved from Uniprot. Sequences were aligned using the tool MUSCLE (Edgar, 2004). Jalview was used to visualize and edit the multiple sequence alignment (Waterhouse *et al.,* 2009).

SnapGene was used to identify DNA sequences similar to P_{tlpA} within the genome of *L. plantarum* WCFS1 using the feature "Find Similar DNA Sequences". The search allowed a mismatch or gap/insertion every 4 bases. BPROM, an online tool for predicting bacterial promoters, was used to identify the -35 and -10 boxes within this promoter (Madeira *et al.,* 2022). BlastP was used to identify the protein encoded by the gene driven by this promoter. Promoter alignment was performed using MUSCLE (Edgar, 2004).

4.3. Results and Discussions

4.3.1. P_{tlpA} Promoter from Salmonella drives high-level constitutive expression

The strongest promoters in lactobacilli have been found by either screening the genome of the host strain (Rud *et al.,* 2006; Bron *et al.,* 2004) or adapting those driving high-level protein expression in phylogenetically close lactic acid bacteria (Russo *et al.,* 2015) (**Figure 1A**). In the few reports where promoters from phylogenetically distant species like *P. megaterium* (P_{xylA}) or *E. coli* (P_{T7} from lambda phage) (Heiss *et al.,* 2016) have been tested, expression levels were found to be comparatively low. Contrary to this trend, we serendipitously stumbled upon a promoter (P_{tlpA}) from the phylogenetically distant gram-negative *Salmonella typhimurium* (**Figure 1A**) capable of driving protein expression at levels higher than previously reported strong promoters in *L. plantarum* WCFS1. In Salmonella, P_{tlpA} along with its repressor is capable of thermo-responsively regulating

gene expression and this functionality had been previously transferred to *E. coli* for therapeutic purposes (Piraner *et al.,* 2017; Hurme *et al.,* 1997). To test whether the P_{tlpA} promoter would be a suitable candidate for driving transcription in *L. plantarum*, a fluorescent reporter protein (mCherry) was cloned downstream of this promoter. The promoter surprisingly seemed to constitutively drive a high-level of protein expression with a mild degree of thermal regulation (<5-fold increase from 31°C to 39°C) (**Figure 1B**). Next the repressor based thermo-responsive functionality was tested in *L. plantarum*, by creating the pTlpA39 plasmid, with the P_{tlpA} promoter driving expression of mCherry and the codon optimized TlpA repressor being expressed constitutively by the P_{48} promoter (Rud *et al.,* 2006). However, the pTlpA39 plasmid showed no significant repression of mCherry at lower temperature gradients in comparison to its repressor-free counterpart (**Supplementary Figure S2D**). Most remarkably, flow cytometry and fluorescence spectroscopy analysis revealed that mCherry expression levels driven by the P_{tlpA} promoter significantly exceeded the levels driven by some of the strongest promoters previously reported in *L. plantarum* - P_{23} (Meng *et al.,* 2021), P_{48} (Rud *et al.,* 2006), P_{spp} (Sørvig *et al.,* 2003) and P_{Tuf} (Spangler *et al.,* 2019) (**Figure 1C, Supplementary S3A**). At 31°C, mCherry expression levels were at least 2-fold higher than these other promoters, while this increased to 5-fold at 39°C (**Figure 1D, Supplementary Figure S3B**). All constitutive promoters (P_{23}, P_{48}, P_{Tuf}) were mildly thermo-responsive, while the inducible promoter (P_{spp}) was not (**Supplementary Figure S4A**). To check whether such high gene expression can be driven by other phylogenetically distant thermo-responsive promoters, we tested the well-known heat inducible *pR* and *pL* promoters from *E. coli* lambda phage. However, only low levels of mCherry expression were observed with these promoters (**Supplementary Figure S2A, Supplementary S2B**). Fluorescence spectroscopy revealed that the strength of the P_{tlpA} promoter at 37°C was 26- and 39-fold higher than the *pR* and *pL* promoter, respectively (**Supplementary Figure S2C**).

Another important factor for high-level gene expression driven by P_{tlpA} is that the spacer length between the ribosome binding site (RBS, 5'-AGGAGA-3') and the start codon needs to be different in *L. plantarum* compared to *E. coli*. In *E. coli* this spacer length of 6 bp has been previously reported (Piraner *et al.,* 2017; Kan et al., 2020; Chee et al., 2022; Rottinghaus et al., 2022), whereas in *L. plantarum* a 9 bp spacer improves expression levels by 25-fold compared to a 6 bp spacer (**Supplementary Figure S4B**), in accordance with previous reports (Tauer *et al.,* 2014). Despite the high level of protein expression driven by P_{tlpA} with a 9 bp spacer, the growth rate of this strain

at 37°C was similar to that of the empty vector control strain, suggesting that this protein overexpression did not metabolically overburden the cell (**Figure 1E**).

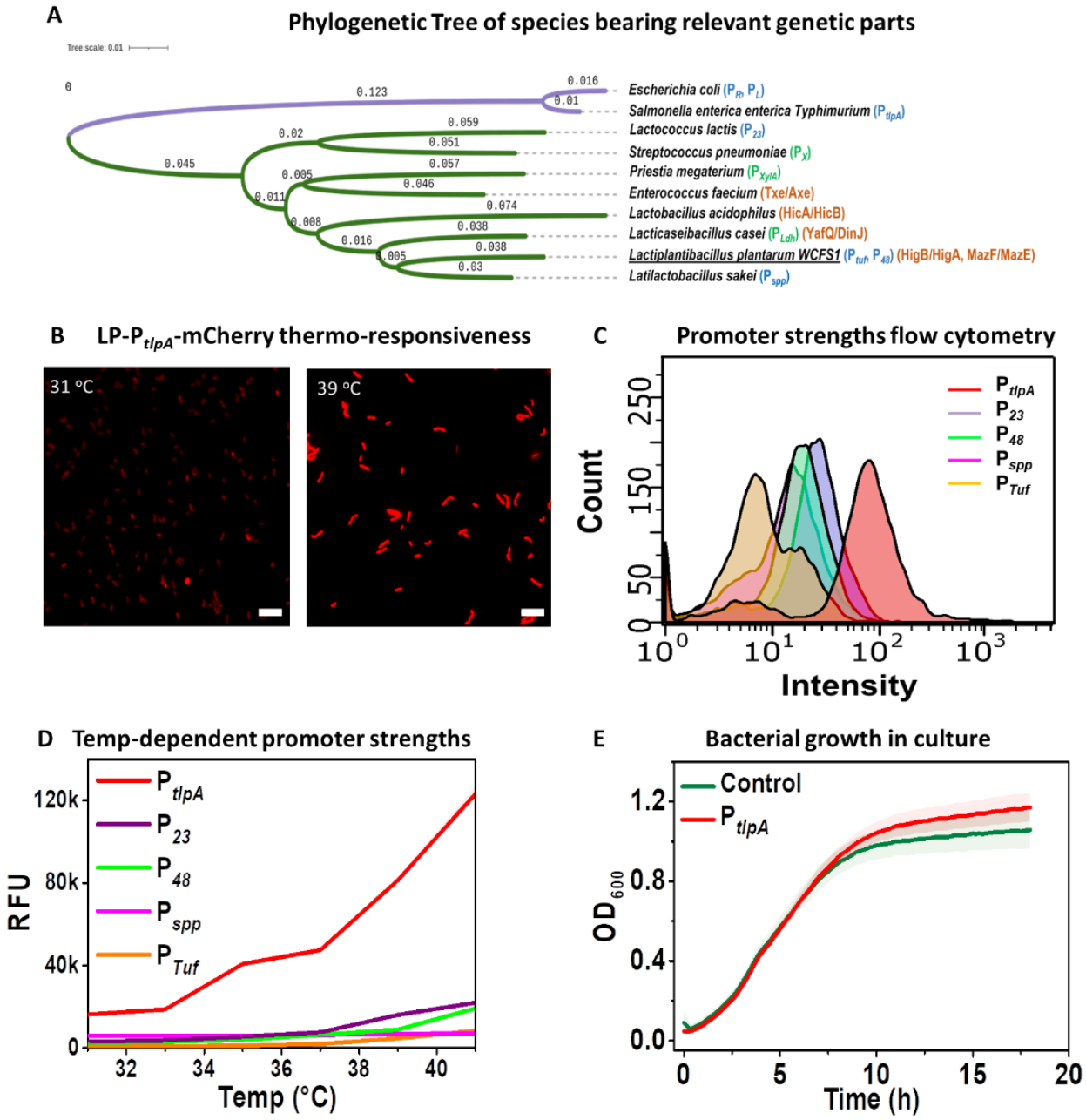

Figure 1. (A) Phylogenetic tree highlighting the distances between species from which various genetic parts have been tested in *L. plantarum*. Purple clade corresponds to Gram-negative bacteria. Green clade corresponds to Gram-positive bacteria. Promoters tested in this study are labelled in blue. Promoters tested by others in *L. plantarum* are labelled green. Orange labels correspond to the TA systems tested in this study. (B) Fluorescence microscopy of P_{tlpA} driven mCherry expression in *L. plantarum* WCFS1 cultivated at 31°C and 39°C for 18 h. Scale bar = 10 µm (C) Flow Cytometry analysis of P_{tlpA}, P_{23}, P_{48}, P_{spp} and P_{Tuf} driven mCherry expression in *L. plantarum* WCFS1 after 18 h incubation at 37°C. (D) Fluorescence spectroscopy

analysis of the P_{tlpA}, P_{23}, P_{48}, P_{spp} and P_{Tuf} driven mCherry expression after 18 h incubation at temperatures ranging from 31°C to 41°C. (E) Growth rate (OD_{600}) measurement of *L. plantarum* WCFS1 strains containing a control plasmid and P_{tlpA}-mCherry for 18 h at 37°C. In (C) and (D), the solid lines represent mean values, and the lighter bands represent standard deviations calculated from three independent biological replicates.

To understand why P_{tlpA} drives gene expression in *L. plantarum*, we looked into its function in Salmonella, where it is a promoter of the σ70 sigma factors. (Dawoud et al., 2017). This family of sigma factors is involved in regulating the expression of housekeeping genes in most prokaryotes, including lactobacilli (Todt *et al.,* 2012). Multiple Sequence Alignment (MSA) among the major RNA polymerase σ70 proteins (RpoD) of *E. coli*, *S. typhimurium*, and *L. plantarum* strains (**Figure 2A**) revealed significant similarity between the domain-2 and domain-4 regions, responsible for binding to the -10 and -35 regions of the promoter during transcription initiation. Interestingly, Gaida *et al.,* (2015) showed that, when expressed in *E. coli,* the *L. plantarum* RpoD can recruit *E. coli*'s RNA polymerase to initiate transcription from a wide variety of heterologous promoters. Compared to sigma factors from six other bacteria, they found that the *L. plantarum* RpoD was the most promiscuous and helped to enlarge the genomic space that can be sampled in *E. coli*. These analyses explain why the P_{tlpA} promoter from a phylogenetically distant species functions in *L. plantarum* but does not necessarily reveal how it drives such high expression levels compared to previously reported promoters.

To understand this, we investigated aspects of P_{tlpA}'s sequence (**Figure 2B**). One unique characteristic is that it harbors the σ70 consensus sequence at the -10 region (5′-TATAAT-3′) but not at the -35 region (5′-TTGACA-3′) (Todt et al., 2012). Based on previous reports in Gram-positive bacteria like *B. subtilis* (Helmann et al., 1995), it is possible that the deviation from the consensus –35 sequence can be compensated for the presence of the conserved dinucleotide "TG" sequence at the -14 and -15 position of the P_{tlpA} promoter. It has been shown that the presence of this sequence upstream of the –10 region in the promoter can mediate rapid promoter melting during transcription initiation and upregulate the transcription rate of corresponding genes. However, most of the promoters reported by Rud et al. (Rud et al., 2006) for *L. plantarum*, also have the conserved "TG" dinucleotide at the –15 position of the promoter. When the strength of the strongest promoter in that library (P_{48}) was compared to the P_{tlpA} promoter, the mCherry production rate by the P_{tlpA}

promoter was significantly higher. This suggests that the P_{tlpA} promoter must have additional reasons that contribute to its exceptional performance in *L. plantarum* WCFS1.

More interestingly, the whole promoter sequence contains no cytosine (C) bases, in contrast to previously reported in *L. plantarum* promoters, most of which contain 2 to 4 cytosine bases in the -35 to -10 region (Rud *et al.,* 2006; Meng *et al.,* 2021; Sørvig *et al.,* 2003; Spangler *et al.,* 2019). Additionally, the spacer between the -35 and -10 regions of the P_{tlpA} promoter contains no adenine (A) bases. Notably, A and C bases are susceptible to methylation in bacteria, which has been associated with epigenetic gene regulation (Beaulaurier *et al.,* 2019; Casadesús *et al.,* 2006). However, on analysis of 34 constitutive promoter sequences from the synthetic promoter library reported by Rud *et al.,* (2006) and those tested in this study (**Supplementary Table S3**), no correlation could be derived between promoter strengths and number of C bases within the -35 to -10 region (**Supplementary Figure S6A**) or the A bases in the spacer (**Supplementary Figure S6B**). If methylation could be influencing promoter strengths, it would be necessary to identify the methyltransferase recognition sequences in *L. plantarum* to derive meaningful correlations. We then searched for DNA sequences similar to P_{tlpA} within the genome of *L. plantarum* WCFS1. Out of 6 hits (**Supplementary Figure S7A**), only one of them was located upstream of a gene that encodes for a known protein (HAMP domain-containing histidine kinase - locus: lp_0282, complement: 255805..257181), with a percent identity score of 82.76 compared to P_{tlpA}. This sequence (G**TTTATG**TTGGTTATTTACGTAA**TAAAAT**) was identified as a promoter (referred to as P_{HAMP}) using BPROM, with -35 and -10 regions (in bold) diverging from P_{tlpA} by single bases each (**Supplementary Figure S7B**). Notably, P_{HAMP} also contains four A bases and one C base in the spacer. When the full promoter sequence (**Supplementary Table S1**) was cloned upstream of mCherry, only weak expression was observed (**Supplementary Figure S7C**), suggesting that one or more of these mismatches compared to P_{tlpA} are essential for driving high-level gene expression. These unique features of the P_{tlpA} promoter sequence provide interesting clues for understanding factors affecting promoter strengths in *L. plantarum*. To gain deeper insights into P_{tlpA}'s unprecedented strength, further studies analyzing mutant libraries of the promoter and/or measuring DNA methylation patterns are required.

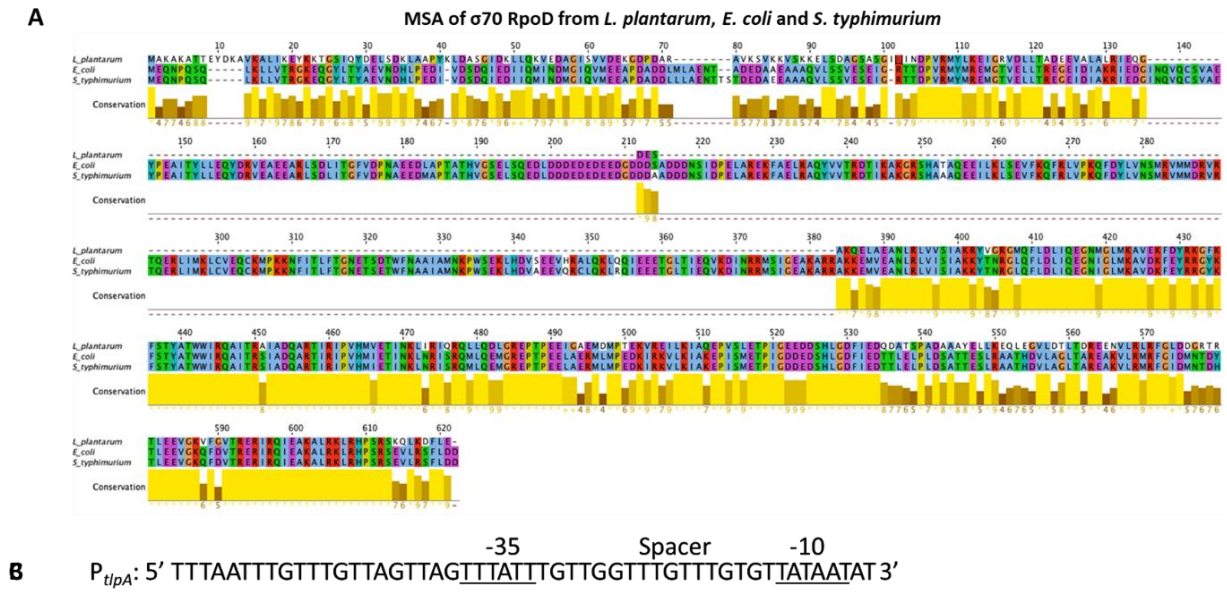

Figure 2. (A) Homology analysis of σ70 RpoD genes from *L. plantarum*, *E. coli*, and *S. typhirmurium*. Height and brightness of the yellow bars indicate the extent to which individual residues are conserved across all 3 bacteria. (B) P_{tlpA} promoter sequence with -35, spacer and -10 regions labelled.

4.3.2. Toxin/Antitoxin based plasmid retention and transient GEMs

Apart from high expression levels, use of lactobacilli for healthcare applications requires strategies to retain heterologous genes in the engineered bacteria in a cheap and compatible manner. TA systems ensure plasmid retention in a bacterial population through a post-segregation killing mechanism. They constitutively express long-lasting toxins and short-lived antitoxins. As long as the plasmid is present, sufficient antitoxin is produced to neutralize the corresponding toxin. On bacterial division, if a daughter cell does not receive any plasmid copies, the antitoxin rapidly degrades, and the active toxin kills the cell. While TA systems have been investigated in the past for bioremediation and biotechnology purposes, their applicability was limited by the fact that their plasmid retention efficiency did not match that of antibiotic or auxotrophy based retention systems (Stirling et al., 2020). However, interest in TA systems has reemerged for living therapeutic applications because of 2 reasons – (i) better understanding of TA systems leading to improved efficiencies (Fedorec *et al.,* 2019) and (ii) biosafety features they offer in reducing horizontal gene transfer (Wright *et al.,* 2013). Accordingly, reports have recently emerged where TA systems are showing greater promise for bacteria engineered as live vaccines or drug delivery vehicles (Kan et

al., 2020; Abedi *et al.,* 2022). While these demonstrations have been done in *E. coli*, the use of TA system in lactobacilli for plasmid retention has not yet been systematically investigated. From literature reports and using the TA finder bioinformatics tool, we identified and selected 5 different type II TA system (all named as toxin/antitoxin) – (i) Txe/Axe, from *Enterococcus faecium* that was shown to ensure long-term plasmid retention in *E. coli* (Fedorec *et al.,* 2019), (ii) YafQ/DinJ from *L. casei* (Levante *et al.,* 2019), (iii) HigB/HigA and (iv) MazF/MazE from *L. plantarum* WCFS1, and (v) HicA/HicB from *L. acidophilus* (Phylogeny in **Figure 1A**). In all these systems, the toxin is an endoribonuclease and the antitoxin is its corresponding inhibitory protein. These modules were added to the plasmid encoding P_{tlpA}-driven mCherry expression (**Figure 3A**) and the resultant strain was repeatedly sub-cultured for up to 100 generations. Plasmid retention was quantified by determining the proportion of the bacterial population expressing mCherry using flow cytometry and agar plate colony imaging analysis (**Supplementary Figure S5B**). Notably, the sensitivity of this analysis was greatly improved by the high-level of expression driven by the P_{tlpA} promoter, which enabled clear demarcation of plasmid-retained and plasmid-lost cells (**Figure 3B**). Such a clear demarcation was not possible with the other promoters, like P_{23} since the fluorescent signal seemed to partially overlap with background signal from non-fluorescent cells (**Supplementary Figure S5A**). In the absence of a TA system (P_{tlpA} mCherry plasmid), the proportion of plasmid-bearing bacteria steadily declined by about 1%/ generation, ending with ~15% of the population retaining the plasmid after 100 generations (**Figure 3C**). Compared to this, the Txe/Axe system initially supported better retention with a plasmid loss of about 0.5%/generation for 40 generations, after which this loss accelerated to ~1.2%/generation, ending in ~18% of the population retaining the plasmid after 100 generations. HigB/HigA and MazF/MazE systems performed similarly for the most part but provided slightly better retention after 100 generations (20% and 30% respectively). HicA/HicB slowed plasmid loss to 0.5%/generation for 50 generations and 0.8%/ generation, thereafter, resulting in retention level of ~35% after 100 generations. Finally, YafQ/DinJ was found to provide the best retention capabilities with plasmid loss of 0.5%/generation for 70 generations and 1%/ generation thereafter, resulting in a retention level of ~40% after 100 generations (**Figure 3C**).

Previous studies have shown that combining different TA systems can cumulatively offer better plasmid retention capabilities (Torres et al., 2003; Bardaji *et al.,* 2019), although this has not been tested in lactobacilli. So, we combined the best-performing TA system endogenous to *L. plantarum*

WCFS1 (MazF/MazE) with the best-performing non-endogenous system (YafQ/DinJ) and observed better plasmid retention capabilities with this combination, yielding a slow plasmid loss of 0.2%/generation for 50 generations and a gradual increase to 0.8%/generation thereafter, resulting in a considerably higher retention of 60% over 100 generations. Comparatively, plasmids maintained under antibiotic selection pressure were steadily retained at >90% through 100 generations, as expected. In all strains harboring TA modules, bacterial growth rates (**Figure 3D**) and mCherry expression levels (**Figure 3E**) were found to be minimally impacted compared to "No TA" or antibiotic-retention conditions over the first 10 generations. These results suggest that the toxins did not drastically impede the regular functioning of the cells. Fluorescence spectroscopy analysis of the liquid cultures after 10 generations (**Figure 3F**) reveals that the TA modules showing higher efficiency in retaining plasmids in the absence of selection pressure (YafQ/DinJ and combo), have significantly lower intensities of mCherry production in comparison to the other TA candidates. The greatest drop in protein expression (~23%) was observed in the strain harboring the TA combo and could be due to an increase in the plasmid size possibly burdening the cells and maybe even resulting in a minor drop in copy number. However, since the YafQ/DinJ construct also causes a drop of comparable magnitude (~20%), it is possible that the toxin in this system mildly interferes with protein expression, which becomes detectable with the overexpression of mCherry by P_{tlpA} but does not drastically affect growth. Further in depth investigation would be required to identify the specific cause of this effect. However, it must be noted that even with the drop in expression level caused by the combo TA system, P_{tlpA} driven mCherry expression was at least 4-fold higher than that of the next strongest promoter, P_{23}.

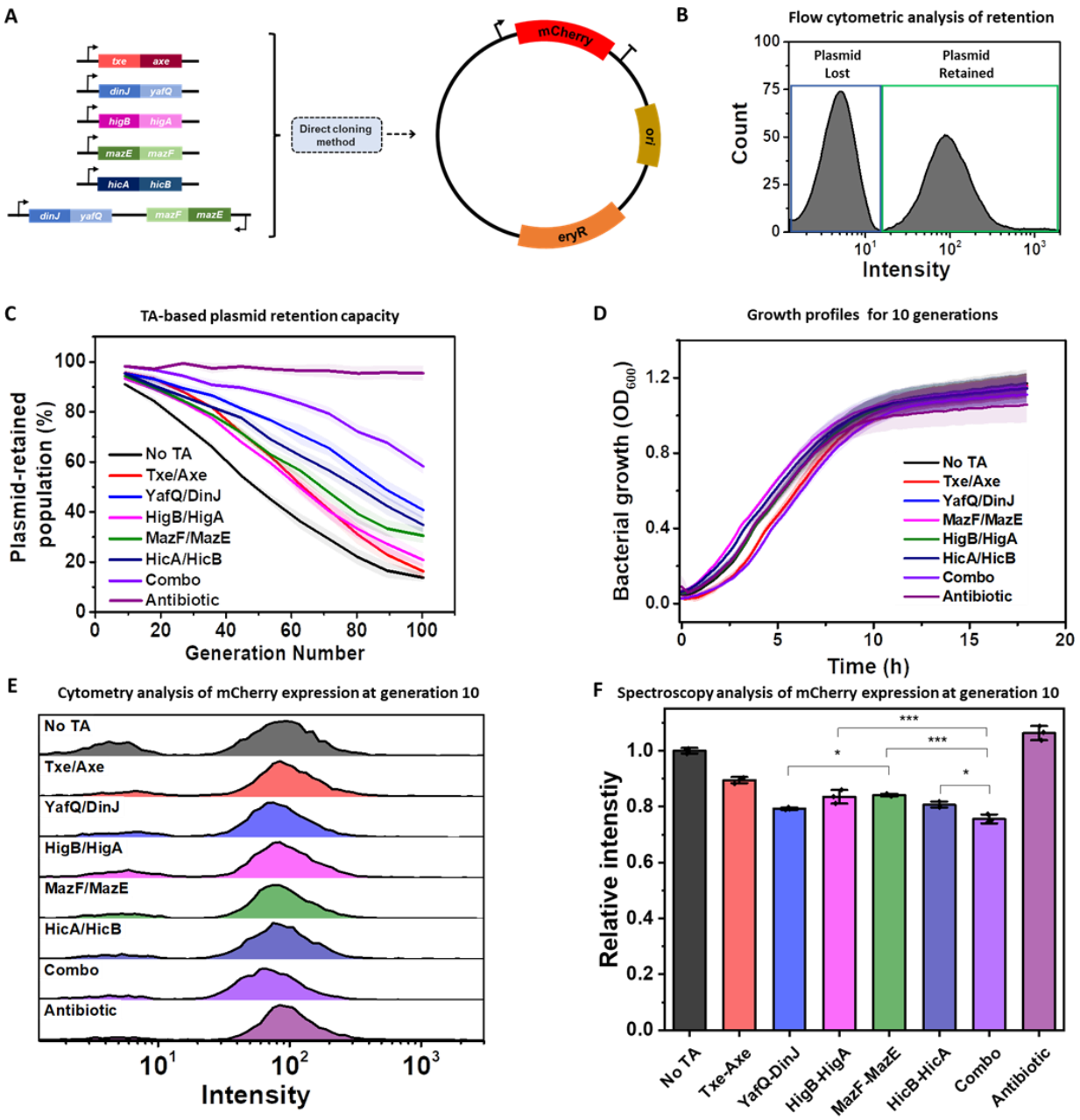

Figure 3. (A) Schematic Representation of cloning the different TA genetic modules into the P_{tlpA}-mCherry plasmid. (B) Sample flow Cytometry histogram plot of the P_{tlpA}-mCherry plasmid containing strain without any TA module or selection pressure after 50 generations of serial passaging in the absence of antibiotic. The green box corresponds to the bacterial population retaining the plasmid and the blue box represents the population devoid of the plasmid. (C) Plasmid retention analysis of the TA module containing strains for 100 generations without antibiotics along with no TA and antibiotic selection pressure conditions for comparison. (D) Growth rate (OD_{600}) of strains with the TA modules, no TA and antibiotic retention over 10 generations at 37°C. In (C) and (D), the solid lines represent mean values and the lighter bands represents SD calculated from three independent biological replicates. Combo = MazF/MazE + YafQ/DinJ . (E) Flow cytometry plots of strains containing TA modules, no TA and antibiotic retention after 10 generations. The Y-axis for each plot represents counts with plot heights in the range of 450 – 500 (F) Fluorescence Spectroscopy analysis of strains containing TA modules, no TA and antibiotic retention after 10 generations. The relative intensity has

been plotted for all the TA strains by normalizing their respective fluorescence values against the "No TA" strain. The data represents three independent biological replicates. p-values are calculated using one-way ANOVA with Tukey test on respective means (* $p<0.05$, *** $p<0.001$). The "No TA", "Txe-Axe" and "Antibiotic" conditions are significantly different from other candidates, so their p - values have not been explicitly highlighted.

It is important to note that a single generation corresponds to a bacterial duplication, so 10 generations = 2^{10} or ~10^3 bacteria and 100 generations = 2^{100} or ~10^{30} bacteria from a single cell. Potential applications of lactobacilli for living therapeutics or engineered living materials are not expected to reach such high generation numbers either due to short application time periods (Janahi *et al.,* 2018; LeCureux and Dean, 2018; Wang *et al.,* 2020) or external growth restrictions (Bhusari *et al.,* 2022). Thus, the >90% retention levels provided by the combo TA system for up to 40 generations should be more than sufficient for these applications. Furthermore, loss of the plasmid only reverts the bacteria to their non-GEM probiotic status, thus enabling the generation of transient GEMs that would be desirable for such applications. Accordingly, by varying the TA system used, the GEM lifetime of these organisms could be tuned. Based on this concept, we introduce a new metric, G_{50}, for characterizing such transient GEMs. The G_{50} value corresponds to the generation at which half the population of a strain has lost its plasmid. As shown in **Figure 4**, G_{50} can be tuned from 50 generations for the No TA condition up to 110 generations (extrapolated) for the combo system. Further exploration of additional TA systems in future studies will contribute to more fine tuning of retention lifetimes and possibly even lead to near-perfect retention as has been achieved in *E. coli* by the Txe/Axe system (Fedorec *et al.,* 2019). These G_{50} values are expected to depend on culture parameters and environmental factors, due to which it could also become a useful metric for assessing natural and industrial conditions in which lactobacilli grow and function.

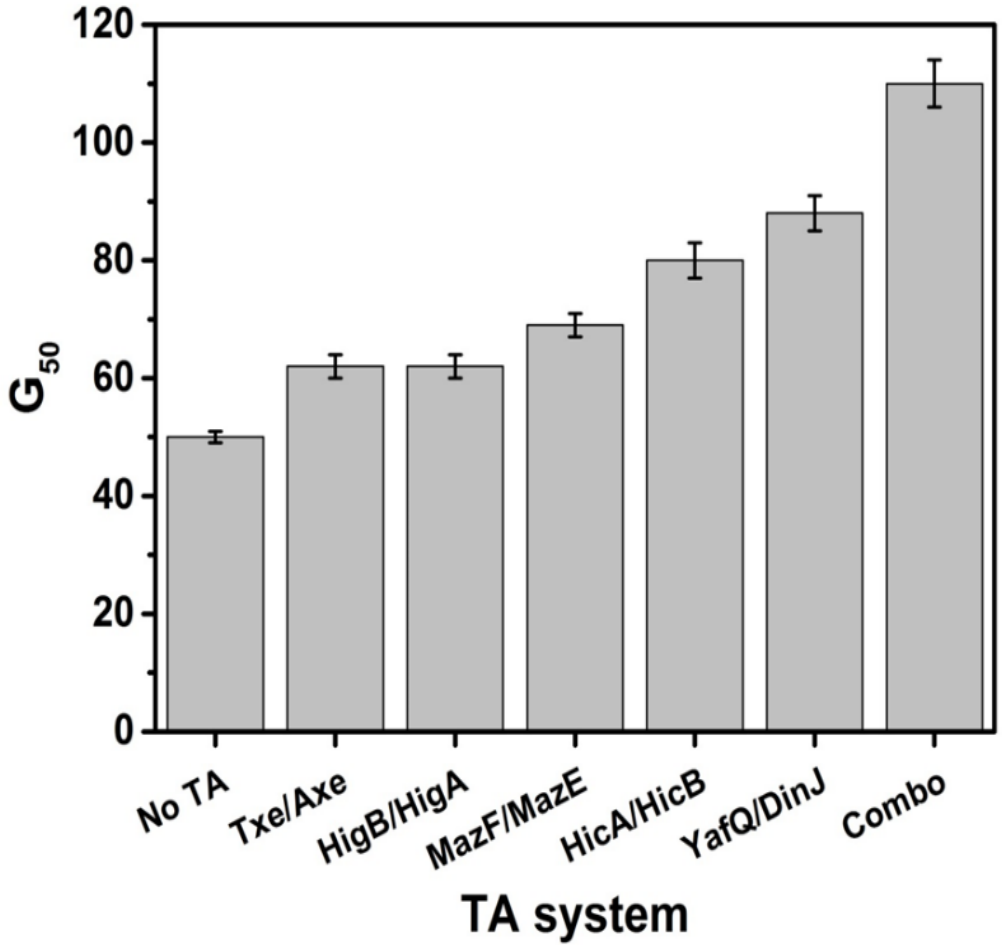

Figure 4. G_{50} values of the different TA systems tested in *L. plantarum.* Combo = MazF/MazE + YafQ/DinJ.

4.4. Conclusion

Lactobacilli as probiotics and commensals in humans and animals have immense potential to be developed for healthcare applications but as non-model organisms, have very poorly equipped genetic toolboxes. Addressing this limitation, this study describes two new genetic modules, characterized in probiotic *L. plantarum* – an ultra-strong constitutive promoter (P_{tlpA}) and TA plasmid retention systems. Our results demonstrate that the promoter drives gene expression at levels over 5-fold higher than the strongest promoters previously reported in *L. plantarum* and the TA systems decelerate plasmid loss in a tunable manner without the need for external selection pressures or genomic manipulations.

Apart from the impact these modules will have in expanding the programmability of lactobacilli, the unique conceptual insights gained from this work will aid in the further development of genetic parts. For one, the unique features of the P_{tlpA} promoter sequence that originate from phylogenetically distant Salmonella provide clues to understanding what drives promoter strength. Secondly, both homologous and heterologous toxin/antitoxin systems can be used in *L. plantarum* for plasmid retention without considerably affecting bacterial growth rates or protein production levels. More interestingly, the plasmid retention efficacy of these systems can be improved by combining two toxin-antitoxin systems, a phenomenon that has yet been tested only in *E. coli*. Finally, these systems provide the possibility to generate tunable transient GEMs since plasmid loss reverts the cells to their non-GEM probiotic status, characterized by the new G_{50} metric.

4.5. Supplementary Information

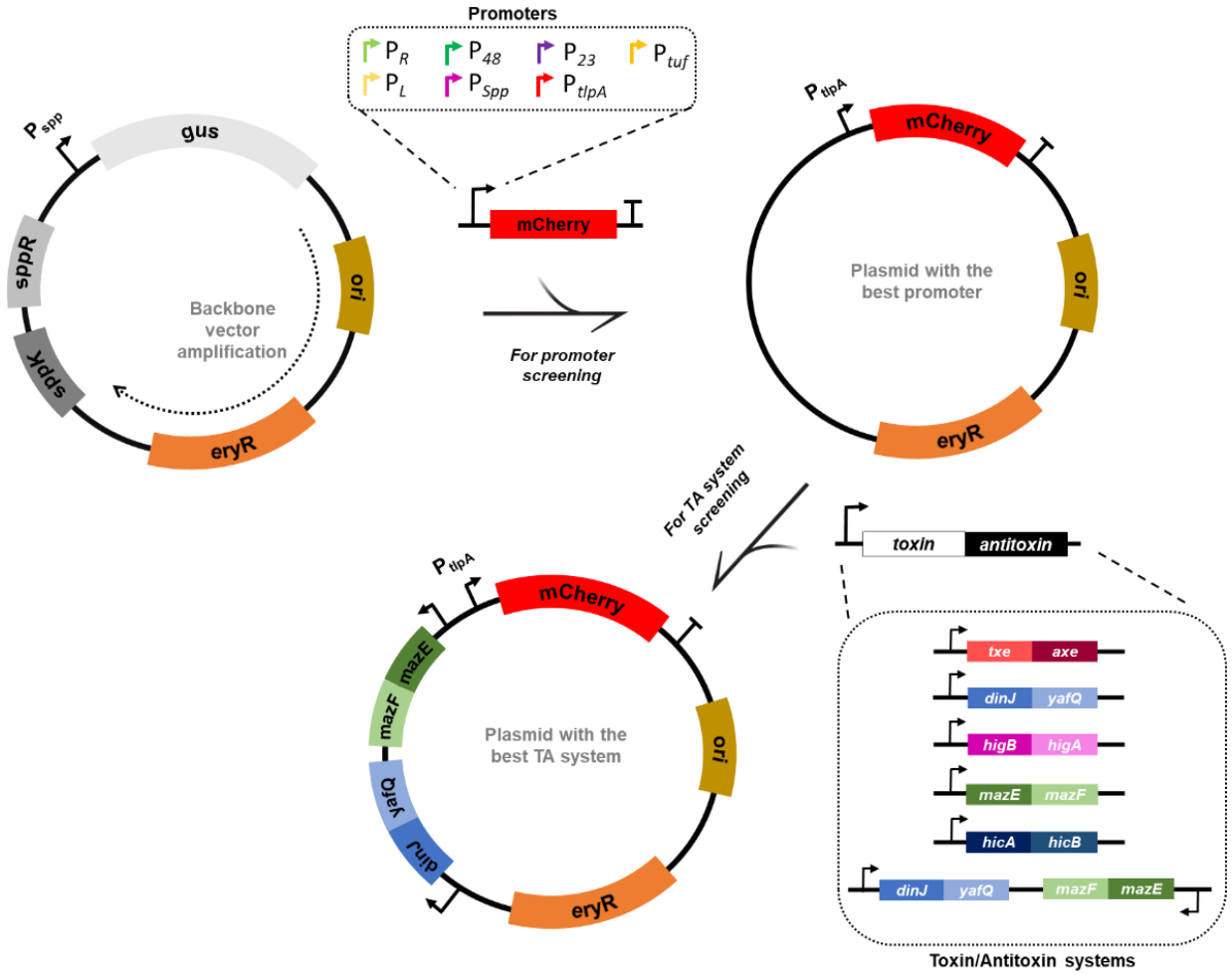

Supplementary Figure S1. Construction of plasmid variants using the direct cloning approach developed in this study. The p256 origin of replication and the erythromycin resistance marker has been amplified from the pSIP403 vector backbone. The interchangeable promoter sequences were upstream of the mCherry reporter gene with P_{tlpA} promotter showing the best performance (highlighted). The activity of the toxin/antitoxin modules were checked in the pTlpA mcherry plasmid with the combo TA system showing the best plasmid retention (higlighted).

Supplementary Table S1. Nucleotide Sequences of the common genetic parts and interchangeable promoter sequences tested in this study

NAME	GENETIC PART	COMMON FEATURE	ORIEN-TATION	SEQUENCE
Ori p256	**Replication Origin**	**Yes**	→	**ttgagatccttttttctgcgcgtaatctg ctgcttgcaaacaaaaaaaccaccgct accagcggtggtttgtttgccggatcaa gagctaccaactctttttccgaaggtaa ctggcttcagcagagcgcagataccaa atactgttcttctagtgtagccgtagtta ggccaccacttcaagaactctgtagca ccgcctacatacctcgctctgctaatcc tgttaccagtggctgctgccagtggcg ataagtcgtgtcttaccgggttggactc aagacgatagttaccggataaggcgc agcggtcgggctgaacgggggttcgt gcacacagcccagcttggagcgaacg acctacaccgaactgagatacctacag cgtgagctatgagaaagcgccacgctt cccgaagggagaaaggcggacaggt atccggtaagcggcagggtcggaaca ggagagcgcacgagggagcttccagg gggaaacgcctggtatctttatagtcct gtcgggtttcgccacctctgacttgagc gtcgatttttgtgatgctcgtcaggggg gcggagcctatggaaa**
				ttgaacaaaaatataaaatattctcaa aacttttaacgagtgaaaaagtactc aaccaaataataaaacaattgaattta aaagaaaccgataccgtttacgaaatt ggaacaggtaaagggcatttaacgac gaaactggctaaaataagtaaacagg taacgtctattgaattagacagtcatct attcaacttatcgtcagaaaaattaaa

eryR	**Antibiotic resistance**	**Yes**	→	**actgaatactcgtgtcactttaattcacc aagatattctacagtttcaattccctaa caaacagaggtataaaattgttgggaa tattccttacaatttaagcacacaaatt attaaaaaagtggtttttgaaagccgtg cgtctgacatctatctgactgttgaaga aggattctacaagcgtaccttggatatt caccgaacactagggttgctcttgcac actcaagtctcgattcagcaattgctta agctgccagcggaatgctttcatccta aaccaaaagtaaacagtgtcttaataa aacttacccgccataccacagatgttc cagataaatattggaagctatataagt actttgtttcaaaatgggtcaatcgaga atatcgtcaactgtttactaaaaatcag tttcgtcaagcaatgaaacacgccaaa gtaaacaatttaagtaccattacttatg agcaagtattgtctatttttaatagttat ctattatttaacgggaggaaataa**
mCherry	**Reporter gene**	**No**	→	**atggtttcaaagggtgaagaagataa catggctatcatcaaggaattcatgcg tttcaaggttcacatggaaggttcagtt aacggtcacgaattcgaaatcgaagg tgaaggtgaaggtcgtccatacgaag gtactcaaactgctaagttaaaggttac taagggtggtccattaccattcgcttgg gatatcttatcaccacaattcatgtacg gttcaaaggcttacgttaagcacccag ctgatatcccagattacttaaagttatc attcccagaaggtttcaagtgggaacg tgttatgaacttcgaagatggtggtgtt gttactgttactcaagattcatcattac aagatggtgaattcatctacaaggtta agttacgtggtactaacttcccatcaga tggtccagttatgcaaaagaagactat gggttgggaagcttcatcagaacgtat gtacccagaagatggtgctttaaaggg tgaaatcaagcaacgtttaaagttaaa ggatggtggtcactacgatgctgaagt taagactacttacaaggctaagaagcc agttcaattaccaggtgcttacaacgtt aacatcaagttagatatcacttcacac aacgaagattacactatcgttgaacaa tacgaacgtgctgaaggtcgtcactca actggtggtatggatgaattatacaag**

				taa
RBS	**Ribosome-binding site**	**No**	→	**tttgtttaactttaagaaggaga**
P*tlpA*	**Promoter**	**No**	→	**tttaatttgtttgttagttagtttatttgttggtttgtttgtgttataatat**
P*spp*	**Promoter**	**No**	→	**gcccatattaacgtttaaccgataaagttgaacgttaatatttttttt**
P*48*	**Promoter**	**No**	→	**tcgtaagttgttgacatggaacgaggaatgtgataatctgtgagt**
P*23*	**Promoter**	**No**	→	**ctgatgacaaaaagagaaaattttgataaaatagtcttagaattaaattaaaaa**
P*Tuf*	**Promoter**	**No**	→	**tctgtttacaaatcagattaggctatatataatatttaagga**
P*L*	**Promoter**	**No**	→	**ttgacataaataccactggcggtgatact**
P*R*	**Promoter**	**No**	→	**ttgactattttacctctggcggtgataa**
P*HAMP*	**Promoter**	**No**	→	**caaaatgtcgttgacgtttatgttggttatttacgtaataaaatcacgac**
T7 term	**Terminator**	**No**	→	**ctagcataacccctttggggcctctaaacgggtcttgaggggttttttg**

Supplementary Table S2. Nucleotide Sequences of the toxin/antitoxin modules tested in this study

NAME	GENETIC PART	COMMON FEATURE	ORIENTATION	SEQUENCE
YafQ/DinJ	Toxin-Antitoxin operon	No	→	agatggcagttacgcttccatttgtg cgaagaaaaagccagaaatccggt tgaattcatctcacatgatgttatccc actgtgtttacattgggataattcgtg atataattaggttgttagataggaag gagtggttagcaatggcagccacaa agaaagaaactcgcttgaatattcg tgttgatccggaattaaaaagtgctg ctcaaatcgtagcaaatgatatggg catcgacttgaccgcagctgttacta tgttcatgacgaaaatggtgaaaga tcacgccctcccgtttaccccaacaa gtctaccagttgaaaccttacaggc gctgaaagaagcaaagcacccaga gctgctcaaaaaatacagcacgcct gatgacatgtggagagacttgaatg tatagtctggttccgacgcctacattt aagcgcgatctaaaacgactctcca agaagcattggccgatggacgaac taaagacggctgttaatctcctagct gctggtacaaatgctgaactattaa gcaaaaagtatgcagatcatgcctt gtcttcaagcagcgagtggaaagg atatcgtgaactacatgttgacggcc ctcgtggcgactggttgctaatctat aaaattaagcagcaagatctcatttt gaccctggttagaactggatctcatc ataacctttgggtaaatagaactac gaaaggccgtccaaaaaaggcggc ttttgtgttgtggtcaaccagcagatt cattcgtcaatatacacgtgacttaa cgccaatcttcaatcagagattaga aaccgcgaactcgtcggcccagtaa aaatgttcagctatcgagatgagttg ggtgatctggggaagtgagcatcaa taagatgccaatctttatcatgcagg gttggaacgaaaatttaacccaatg

MazF/MazE	**Toxin-Antitoxin operon**	**No**	←	**gaaggatttacggtcaacgagtgtct ttcggacacgtccgttgatattgttat ttgactcgtggtcttactccaatcaat tatactgacaagcatcgcaaatata aaaccgccctacctaacctgagtaa gttacagggcgaagtagtgctgatt agaatggaaagtcgaagttgtaata caccgtttgcgcgacgtgataaaaa tcggcactgcgcatggtttcgatgta tgtgatactccgtcctgctctgggggt cgcatcaaacgaataaatttgggca gcagcaatttgtccgtgggtattgta accattaagactaaagtagccgggc aaatcacgcattgtagacgtaattg gtgaaacaattacaaacccggtgtt ctgagtgtagagattactactaaga actacagctggccgacgtttctttatt tcgcggccacgttgtgggtcaaaat caatccagatgatgtctttttgtttag gtaaataagtcattactcgacctcat tccagtcgacatcggaccatgcttca gtcattggccgtttcggcttggagcc ggcataaggattctcgatacgtggt acgagtgtatatgactcaccatcact tgatgggatgagtaaccatcgttgtc ctttcttaaaacgaccgtctttaggta gacttaatgccaatgaattaccacg actaactgtctttacctcaatcatatc aaggcctcctcgtattaataaacac actatttatgcaacgagtataacac gtattacgaaataagacagctaaag caatcgcgataactaattgataagc acacggtttttagtaattcatcaata aaggaagagactaattaatgtcgcc gtaactcagtgttatcaagttggatg gcccgctttagtattttccacctttag cctctt**
				tactgatgatgaacatgccccagcct gttgtagctctttgcgcaataaatcat ttattttgtctggattgaatagagctt gagcaaaatctttggtaaaatcattc atgaaggagttcttctttctgtatgtg ttttttgttcaaaccaatcatacgag aaaggaactccttttctaatgtttaa

HicA/HicB	**Toxin-Antitoxin operon**	**No**	→	**agaaataaatttaaggaatcattca tccttacacaaactattttacagtctc attcttcataaaccacatcctagaaa agaactattaccatatcaaatcaaa caaattcaagataaaatcaaagag atgaataaagatgaaaaaaactaa tcaatatatgaagtataagggttatg aaggttcaattgaatatactttggag gataagattctttttggtaaggttcag gggattaagagtcttatttcttacga aggtaatacaatagatgaattggag aaggattttcaaggagccattgatg attatctaatgagctgtaaggaagat ggagttataccagagaaacctttaa aggtaattttaatgtgcgcattgatc cttcattacatgaaaaattggctaat tatgctgcaacgaagcaccaatcat tgaatgctagtgtagaagaagctat aaaaagatttttggcttaggtgaaa gacgcttggaatttttcaagcgttttt ttcatgaaaacaattgctaaattcat tgaatgagtgtactattttagtataa caatagttgaacgggtgatgtcggc gatatagg**
HigB/HigA	**Toxin-Antitoxin operon**	**No**	→	**tactgatgatgaacatgcccactctg gttggttcctagctaaaataggggtc gtactagtcgggtaatcagatgaatt ggatatttgggtgtggtcagctaata ataggagcaagagtcggatggatt gagatatacacgtgatacgggtata atcgattaagaattttgcagataag gaaactcacaaggtttaccaacaaa aattctctaaacaattgccaccaacc attcagcaattagcattgcgaaaatt actaatgattgatcatgcggaaaca attaatgatttgagcctaccgcctgc caatcacttggaaaaattaagtcat gatcgccaagggcaatatagcatca ggattaataatcagtatcggatatgt tttgcaattcgaaatggtaatgagtt ttatgatgttgaaatagtcgattatc atcatggttaggagaccaaaaaatg aatgaaatcccaacacctaaaatta gtgaaattcttgaagaagagtttatg gctcccttgcatatctctgcatattttt**

				tggctcaacagattggggtacccac gtcacggattcaagacttactacatg atcgtcgacaggtgacggttgatac atcgctgcggctaggacgattctttg gagtgtcggatcgttatttcttggaac ttcaaaatgatattgaaattcgtaatt tgaaacagatacatggtgctgaata tgcacagataaaaaagtatcaagtc agttaaataaggacgtagaccgtag ttgcttggtagcgtactacggttttg caaatataacctaaactgataagca gcagatcttaaattttaaggttatca acaggtggataaagcagtggcgttt gtattatccacctgttgataatcattg agttggttaattgtactttcactactg ggttaactggtcgtgagaaaaatgg tcaagcattagtttcgtggtgatgtc ggcgatatagg
Txe/Axe	Toxin-Antitoxin operon	No	←	acgcgtaacaaacacattcattaat aacaatcaacactaagctatattag ctttttaaatgactagggtaaataaa ataaggatcaaaaacttttaagtttc tgacccttccttacttccgattggtta atagtgatcttttgcagaataaataa atatcgtttcattttcaactctatatat cagtctatgttcatctgtaattcttctg gaccattttccagataaatcatgcttt aatggctcaggttttcctaatccagc aaaggggaacgatcgatatctttt attaacttgttaatctttttatattgct ttgtttccttgctcatgccaataaag ataatcatcccaagcatcatcagac caagccttaatcatcagattcaacct cgattaagtcatgtgttttaaatgca cctttggagaattgttcatctcctcga cgaatttttccatgacgtaattatta gaaagtgttctcaacgtttcttgcata gaatcataatctctttttgataataca acaactgtatcttctacatctttacttg ttacaataagtgtttcagcatcctcat taacttgtttcatataactacgtaaat tttggcggaaatttgaataagctact gcttccattccctttcacccccttatttat ttctataaaacaattgtacattatatt gtacaattaagcaaatgattaatatt ctaacttcttataattaaaagtgctat

				cacttttagtttttaggataaaaggt gacgtcacttttgagtgctggtacct caaatcctgctttt

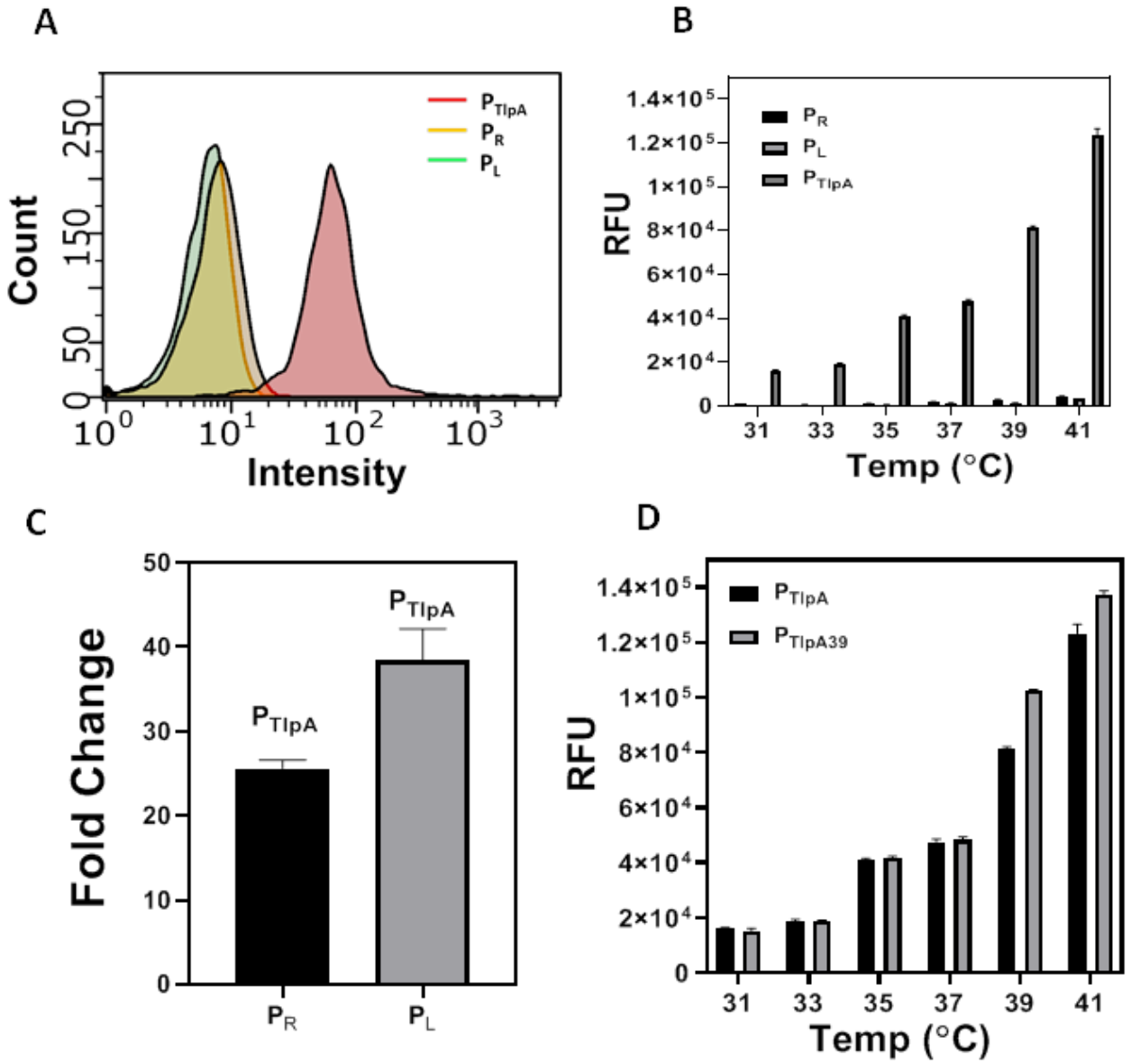

Supplementary Figure S2. (A) Flow Cytometry analysis of P_R, P_L and P_{tlpA} driven mCherry expression in *L. plantarum* WCFS1 after 18 h incubation at 37°C. (B) Fluorescence Spectroscopy analysis of the P_R, P_L and P_{tlpA} driven mCherry expression after 18 h incubation in the Thermocycler setup at thermal gradients ranging from 31°C to 41°C (See Materials and Methods section "Microplate reader Setup for Thermal Gradient Analysis"**)**. (C) Fold Change of P_{tlpA} driven mCherry expression in comparison to P_R and P_L promoters at 37°C (D) RFU Plot of mcherry production by plasmids pTlpA and pTlpA$_{39}$ after 18 h incubation at thermal gradients ranging from 31°C to 41°C. The pTlpA$_{39}$ plasmid encodes for an additional P_{48} promoter-driven codon-optimized TlpA$_{39}$ repressor. The data in B, C and D corresponds to three independently conducted biological replicates with column heights representing means and whiskers representing SD.

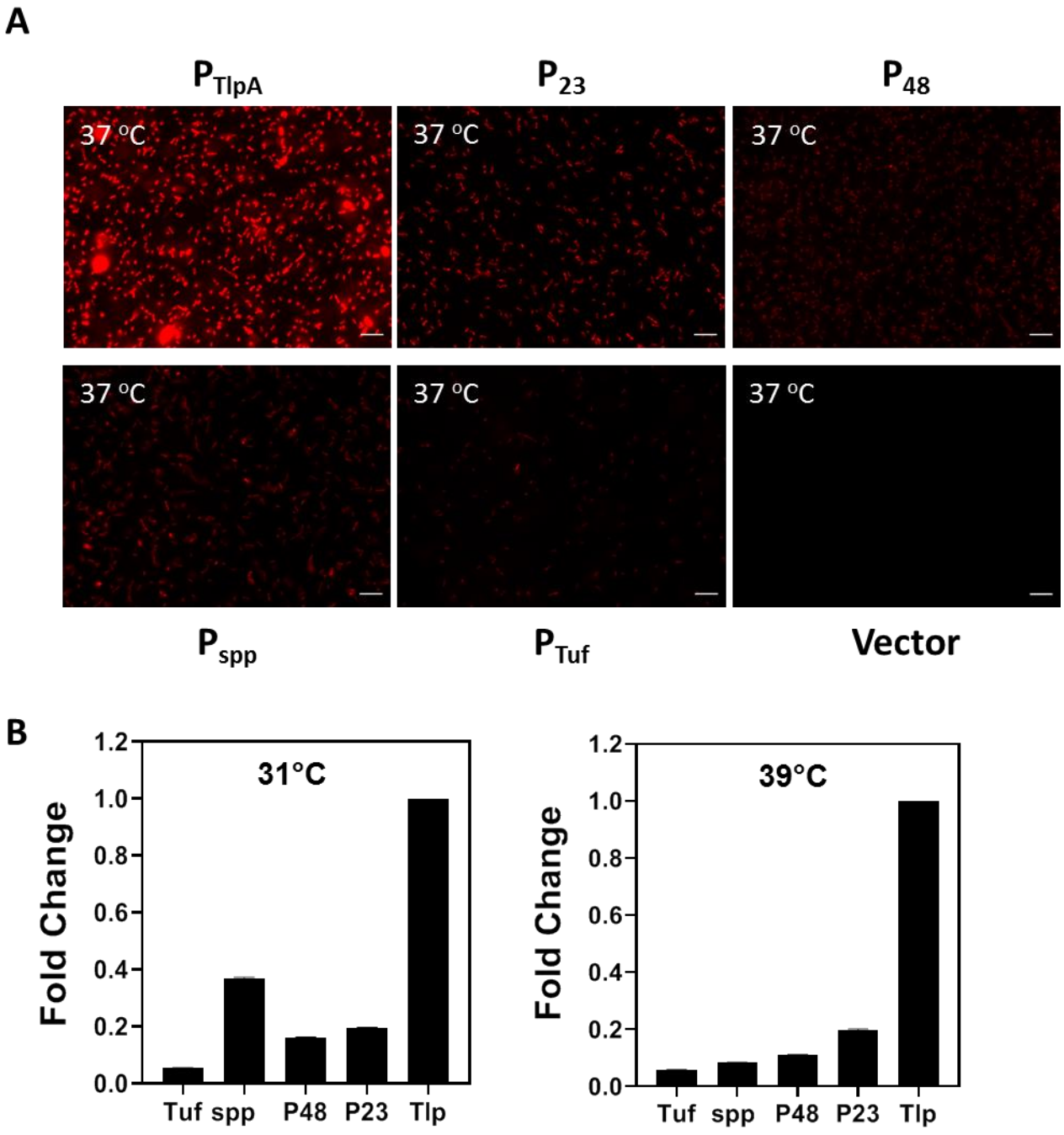

Supplementary Figure S3. (A) Fluorescence microscopy images of P_{tlpA}, P_{23}, P_{48}, $P_{spp,}$ P_{tuf} driven mCherry expression and Empty Vector constructs in *L. plantarum* WCFS1 cultivated at 37°C for 18 h (Scale = 10µm). (B) Fold Change of the P_{tuf}, P_{23}, P_{48}, $P_{spp,}$ driven mCherry expression normalized to the expression level of the P_{tlpA} promoter at 31°C and 39°C respectively. The data corresponds to three independently conducted biological replicates with whiskers as SD.

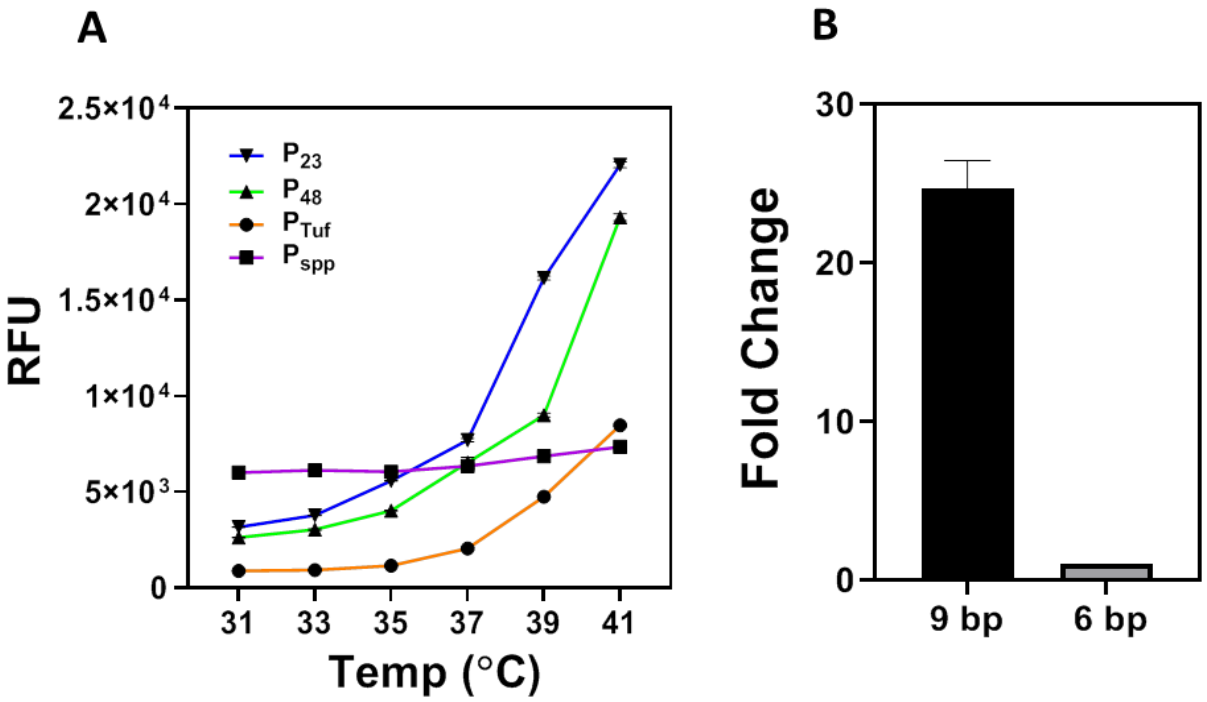

Supplementary Figure S4. (A) RFU Plot of P_{23}, P_{48} and P_{tuf} driven mCherry expression showing enhanced fluorescence expression in contrast to P_{spp} within the thermal gradients ranging from 31°C to 41°C. The data corresponds to three independently conducted biological replicates with whiskers as SD. (B) Fold Change of the P_{tlpA} promoter driven mCherry expression with 9 bp spacer (between the RBS and the start codon) in comparison to the P_{tlpA}-6 bp spacer construct.

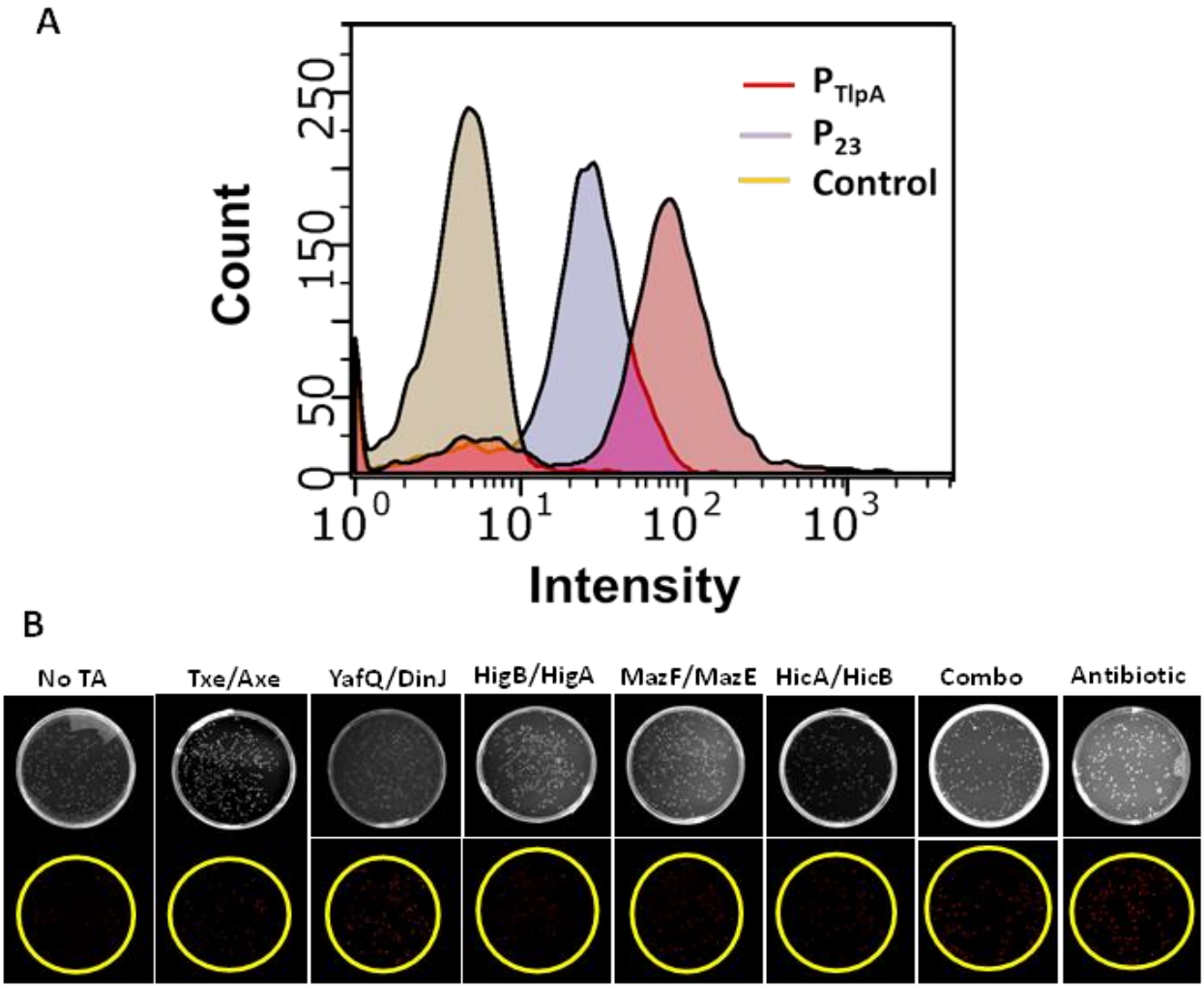

Supplementary Figure S5. (A) Flow cytometry plots showing that strains with P_{23}-driven mCherry expression produces relatively low intensities with part of the population overlapping with the signal gained from bacteria that do not express any fluorescent proteins (control). In comparison, the signal from P_{tlpA} is clearly demarcated from that of control. (B) Agar-plate based analysis of plasmid retention provided by the different TA systems. The total number of colonies can be determined from the brightfield images and the red colonies visible in the fluorescent images represent the plasmid-retaining bacteria.

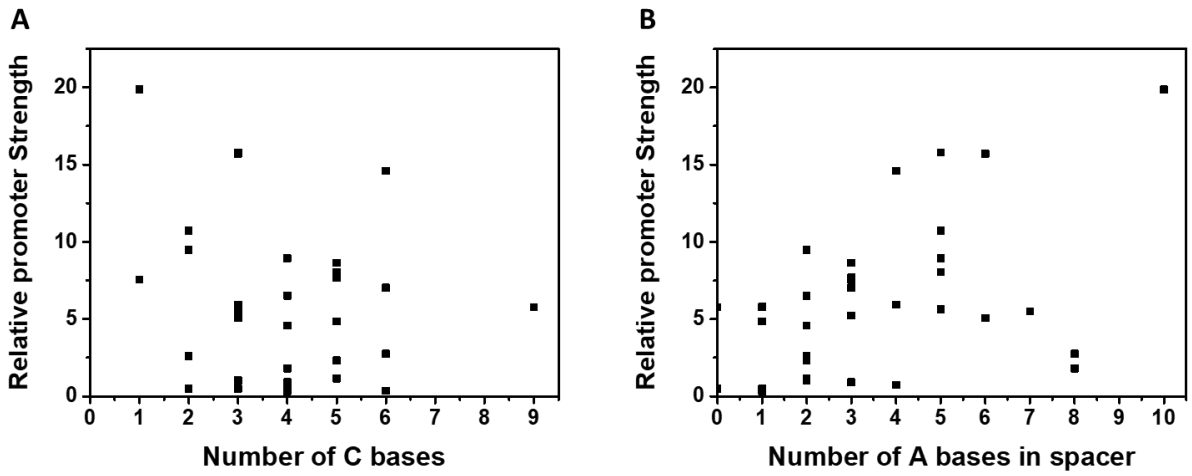

Supplementary Figure S6. Plots representing relative promoter strengths of 34 promoters in Table S3 vs (A) number of C bases in the -35 to -10 region and (B) number of A bases in the spacer between the -35 and -10 region (non-bold region in Table S3).

Supplementary Table S3. Promoter sequences included in Figure S7 and their relative strengths. Sequences and strengths derived from reference "Rud, I., et al., *A synthetic promoter library for constitutive gene expression in Lactobacillus plantarum.* Microbiology, 2006. **152**(4): p. 1011-1019." The relative strengths of P_{23} and P_{Tuf} from this study were estimated based on expression levels we determined in relation to P_{48}.

Promoter	Sequence	Relative strength
P_{20}	**-35 TTGACA**ACCTGTGGGCGGTTTGA**TTTGTT -10**	0.33
P_{17}	**-35 TTGACA**CTGATCCCGGCTGGTGG**TAAATT -10**	0.35
P_{13}	**-35 TTGACA**GCGTGGGTTGGTGCTGG**TAATTT -10**	0.48
P_{41}	**-35 -TGACA**GGGCTGTGATGGTGTGG**TATTGT -10**	0.50
P_{43}	**-35 TTGACA**GGATAAAGGTCGCCTGG**TATGGT -10**	0.74
P_{40}	**-35 TCAACA**TACATGGATCG---TGG**TATGTT -10**	0.91
P_{44}	**-35 TTGACA**CTTGGAGGGTTTGATGG**TAATCT -10**	1.02
P_{10}	**-35 TTGACA**TTGTTAATGGCCCCTGA**TATATT -10**	1.15
P_{34}	**-35 TTGACA**GACAAACATAAGGATGA**TATGCT -10**	1.80
P_{9}	**-35 TTGACA**GGGCTGAGCTGACCTGG**TATGGT -10**	2.33
P_{42}	**-35 TTGACA** GAGTTGTCTGGTATTGA**TATTGT -10**	2.60
P_{5}	**-35 TTGACA**CACAAAACCAGACATGG**TATTAT -10**	2.75
P_{33}	**-35 TTGACA**TGTGACCCGTTTTATGG**TATTAT -10**	4.58
P_{21}	**-35 TTGACA**TTCGGGGCATCTCGTGG**TATAAT -10**	4.84
P_{26}	**-35 TGGACA**AGTGATAAAACGGGTGA**TATGAT -10**	5.06
P_{22}	**-35 TTGACA**GATTAGGGCGGTCATGG**TAAAAT -10**	5.23
P_{18}	**-35 TTGACA**GGGAGGCTTCGTTGTGA**TAAGAT -10**	5.79
P_{47}	**-35 TTGACA**GACGCGGGAGAATATGG**TAAAGT -10**	5.65

P_{16}	**-35 TTGACA**TCCCCCTCTCTTTCTGG**TATAAT -10**	5.76
P_{3}	**-35 TTGACA**AAGAAGCCGGGTTTTGG**TATAAT -10**	5.93
P_{29}	**-35 TTGACA**GTTCTGGCTGGATATGG**TAAACT -10**	6.51
P_{6}	**-35 TTGACA**GGCAGCCATCTCTATGG**TAAAAT -10**	7.04
P_{38}	**-35 TTGACA**GAATGTTTTTGTAGTGG**TATAAT -10**	7.56
P_{30}	**-35 TTGACA**GCCGAGGTACCATGTGG**TATAAT -10**	7.69
P_{31}	**-35 TTGACA**AAAGTCCCAGGGTATGA**TATACT -10**	8.04
P_{8}	**-35 TTGACA**AATTCCGGTGTCTATGG**TATTCT -10**	8.64
P_{25}	**-35 TTGACA**TTAAGGCACATCATTGA**TATGGT -10**	8.94
P_{35}	**-35 TTGACA**TGCAGGGAGTTTGTTGG**TATAAT -10**	9.49
P_{1}	**-35 TTGACA**GGGATATTAGAGTATGG**TATGCT -10**	10.74
P_{4}	**-35 TTGACA**CGCGCAGCAAGGCATGA**TATAAT -10**	14.60
P_{11}	**-35 TTGACA**GAATGGACATACTATGA**TATATT -10**	15.70
P_{48}	**-35 TTGACA**TGGAACGAGGAATGTGA**TAATCT -10**	15.79
P_{23}	**-35 ATGACA**AAAAGAGAAAATTTTGA**TAAAAT -10**	19.86
P_{Tuf}	**-35 TTTACA**AATCAGATTAGGCTATA**TATAAT -10**	5.49

A

Hit	Upstream a gene	Position	Sequence	Sequence length	Identity Matrix
Hit 1	Yes	257,256..257,284	GTTTATGTTGGTTATTTACGTAATAAAAT	29	82.76
Hit 2	No	1,292,083..1,292,110	ATTTTTAAAACAACTAACAAAAATGAAC	28	69.23
Hit 3	No	1,541,627..1,541,653	GTTATTTTTTAGTTTGTTGTGAAATTT	27	77.78
Hit 4	No	2,772,508..2,772,536	ATACTTAAACACAACAAAAAACACTTAAC	29	32.82
Hit 5	No	3,129,614..3,129,645	ATATGGTCAGTCAATGAAATCAACAAATAAAC	32	60.00
Hit 6	No	3,209,426..3,209,455	ATAGTAACCACCAGCACACCACAAGTAAAC	30	71.43

B

P_{HAMP} GTTTA--TGTTGG-TTATTTACGTAATAAAAT
P_{TlpA} -TTTATTTGTTGGTTTGTTTGTGTTATAATAT
**** ****** ** *** ** **** **

C

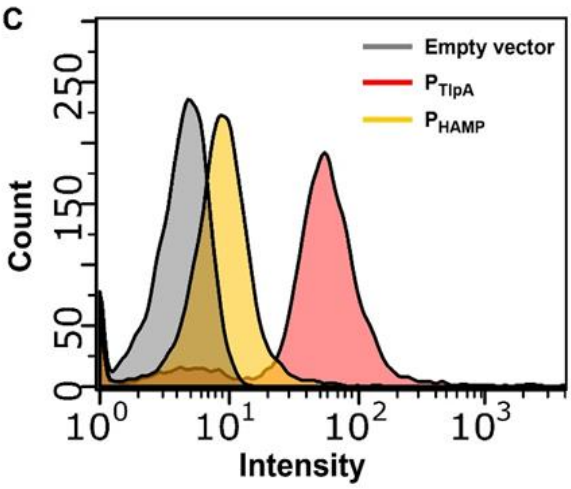

Supplementary Figure S7. (A) Results obtained after screening the entire genome of *L. plantarum* WCFS1 for a Pt_{lpA}-like sequence. (B) Sequence alignment of P_{HAMP} and P_{tlpA} promoters. (C) Flow Cytometry analysis of P_{tlpA} and P_{HAMP} driven mCherry expression in *L. plantarum* WCFS1 after 18 h incubation at 37°C.

4.6. Acknowledgement

The *L. plantarum* WCFS1 strain was a kind gift from Prof. Gregor Fuhrmann (Helmholtz Institute for Pharmaceutical Research, Saarland). The plasmids pSIP403 and pLp_3050sNuc were a kind gift from Prof. Lars Axelsson (Addgene plasmid # 122028) and Prof. Geir Mathiesen (Addgene plasmid # 122030) respectively. The plasmid pTlpA39-Wasabi was a kind gift from Prof. Mikhail Shapiro (Addgene plasmid # 86116). The plasmid pUC-GFP-AT was a kind gift from Prof. Chris Barnes (Addgene plasmid # 133306). The authors thank Dr. Samuel Pearson at the INM – Leibniz Institute for New Materials for discussions that led to the G_{50} concept. All the schematic figures were generated using Biorender.

4.7. Funding

This work was supported by the Deutsche Forschungsgemeinschaft's Research grant [Project # 455063657], Collaborative Research Centre, SFB 1027 [Project # 200049484] and the Leibniz Science Campus on Living Therapeutic Materials [LifeMat].

4.8. Conflict of Interest

A patent application has been filed based on the results of this work (Application No. is DE 10 2022 119 024.2).

4.9. References

1. Abedi, M.H., Yao, M.S., Mittelstein, D.R., Bar-Zion, A., Swift, M.B., Lee-Gosselin, A., et al. (2022) Ultrasound-controllable engineered bacteria for cancer immunotherapy. Nat. Commun., 13, 1-11.
2. Allison, G.E. and Klaenhammer, T.R. (1996) Functional analysis of the gene encoding immunity to lactacin F, lafI, and its use as a Lactobacillus-specific, food-grade genetic marker. Appl. Environ. Microbiol., 62, 4450-4460.
3. Ashraf, R. and Shah, N.P. (2011) Selective and differential enumerations of Lactobacillus delbrueckii subsp. bulgaricus, Streptococcus thermophilus, Lactobacillus acidophilus, Lactobacillus casei and Bifidobacterium spp. in yoghurt--A review. Int. J. Food Microbiol., 149, 194-208.
4. Bardaji, L., Añorga, M., Echeverría, M., Ramos, C. and Murillo, J. (2019) The toxic guardians—multiple toxin-antitoxin systems provide stability, avoid deletions and maintain virulence genes of Pseudomonas syringae virulence plasmids. Mobile DNA., 10, 1-17.
5. Beaulaurier, J., Schadt, E.E. and Fang, G. (2019) Deciphering bacterial epigenomes using modern sequencing technologies. Nat. Rev. Genet., 20,157-172.
6. Bhusari, S., Sankaran, S. and Del Campo, A. (2022) Regulating bacterial behavior within hydrogels of tunable viscoelasticity. Adv. Sci., 9, p2106026.
7. Bibalan, M.H., Eshaghi, M., Rohani, M., Esghaei, M., Darban-Sarokhalil, D., Pourshafie, M.R., et al. (2017) Isolates of Lactobacillus plantarum and L. reuteri display greater antiproliferative and antipathogenic activity than other Lactobacillus isolates. J. Med. Microbiol., 66, 1416-1420.

8. Bron, P.A., Hoffer, S.M., Van Swam, I.I., De Vos, W.M. and Kleerebezem, M. (2004) Selection and characterization of conditionally active promoters in Lactobacillus plantarum, using alanine racemase as a promoter probe. Appl. Environ. Microbiol., 70, 310-317.
9. Casadesús, J. and Low, D. (2006) Epigenetic gene regulation in the bacterial world. Microbiol. Mol. Biol. Rev., 70, 830-856.
10. Castillo-Hair, S.M., Baerman, E.A., Fujita, M., Igoshin, O.A. and Tabor, J.J. (2019) Optogenetic control of Bacillus subtilis gene expression. Nat. Commun., 10, 1-11.
11. Chan, M.Z.A., Chua, J.Y., Toh, M. and Liu, S.Q. (2019) Survival of probiotic strain Lactobacillus paracasei L26 during co-fermentation with S. cerevisiae for the development of a novel beer beverage. Food Microbiol., 82, 541-550.
12. Chee, W.K.D., Yeoh, J.W., Dao, V.L. and Poh, C.L. (2022) Highly reversible tunable thermal-repressible split-t7 RNA polymerases (thermal-T7RNAPs) for dynamic gene regulation. ACS Synthetic Biology, 11(2), pp.921-937.
13. Chen, Y., Qi, M., Xu, M., Huan, H., Shao, W. and Yang, Y. (2018) Food-grade gene transformation system constructed in Lactobacillus plantarum using a GlmS-encoding selection marker. FEMS Microbiol. Lett., 365, fny254.
14. Courbet, A., Endy, D., Renard, E., Molina, F. and Bonnet, J. (2015) Detection of pathological biomarkers in human clinical samples via amplifying genetic switches and logic gates. Sci. Transl. Med., 7, 289ra83-289ra83.
15. Darby, T.M., and Jones, R.M. (2017) Beneficial influences of Lactobacillus plantarum on human health and disease. In Floch, M., Ringel, Y., Walker,W.A. (ed.), The microbiota in gastrointestinal pathophysiology. Academic Press, Vol. I, pp. 109-117.
16. Davis, M.C., Kesthely, C.A., Franklin, E.A. and MacLellan, S.R. (2017) The essential activities of the bacterial sigma factor. Can. J. Microbiol., 63, 89-99.
17. Dawoud, T.M., Davis, M.L., Park, S.H., Kim, S.A., Kwon, Y.M., Jarvis, N., O'Bryan, C.A., Shi, Z., Crandall, P.G. and Ricke, S.C. (2017) The potential link between thermal resistance and virulence in Salmonella: a review. Frontiers in veterinary science, 4, p.93.
18. de Vos, W.M. (2011) Systems solutions by lactic acid bacteria: from paradigms to practice. Microb. Cell Fact., 10, 1-13.
19. du Toit, M., Engelbrecht, L., Lerm, E. and Krieger-Weber, S. (2011) Lactobacillus: the next generation of malolactic fermentation starter cultures—an overview. Food Bioprocess Technol., 4, 876-906.
20. Edgar, R.C. (2004) MUSCLE: a multiple sequence alignment method with reduced time and space complexity. BMC Bioinf., 5, 1-19.
21. Elowitz, M.B. and Leibler, S. (2000) A synthetic oscillatory network of transcriptional regulators. Nature., 403, 335-338.
22. Fedorec, A.J., Ozdemir, T., Doshi, A., Ho, Y.K., Rosa, L., Rutter, J., et al. (2019) Two new plasmid post-segregational killing mechanisms for the implementation of synthetic gene networks in Escherichia coli. iscience., 14, 323-334.

23. Gaida, S.M., Sandoval, N.R., Nicolaou, S.A., Chen, Y., Venkataramanan, K.P. and Papoutsakis, E.T. (2015) Expression of heterologous sigma factors enables functional screening of metagenomic and heterologous genomic libraries. Nat. Commun., 6, 1-10.
24. Grady, R. and Hayes, F. (2003) Axe–Txe, a broad-spectrum proteic toxin–antitoxin system specified by a multidrug-resistant, clinical isolate of Enterococcus faecium. Mol. Microbiol., 47, 1419-1432.
25. Halbmayr, E., Mathiesen, G., Nguyen, T.H., Maischberger, T., Peterbauer, C.K., Eijsink, V.G., et al. (2008) High-level expression of recombinant β-galactosidases in Lactobacillus plantarum and Lactobacillus sakei using a sakacin P-based expression system. J. Agric. Food Chem., 56, 4710-4719.
26. Heiss, S., Hörmann, A., Tauer, C., Sonnleitner, M., Egger, E., Grabherr, R. et al. (2016) Evaluation of novel inducible promoter/repressor systems for recombinant protein expression in Lactobacillus plantarum. Microb. Cell Factories., 15, 1-17.
27. Helmann, J.D. (1995) Compilation and analysus of Bacillus Subtilis σ A-dependent promoter sequences: evidence for extended contact between RNA polymerse and upstream promoter DNA. Nucleic Acids Res. 23, 2351-2360.
28. Hurme, R., Berndt, K.D., Normark, S.J. and Rhen, M. (1997) A proteinaceous gene regulatory thermometer in Salmonella. Cell., 90, 55-64.
29. Janahi, E.M.A., Haque, S., Akhter, N., Wahid, M., Jawed, A., Mandal, R.K., et al. (2018) Bioengineered intravaginal isolate of Lactobacillus plantarum expresses algal lectin scytovirin demonstrating anti-HIV-1 activity. Microb. Pathog., 122, 1-6.
30. Jiménez, E., Fernández, L., Maldonado, A., Martín, R., Olivares, M., Xaus, J., et al. (2008) Oral administration of Lactobacillus strains isolated from breast milk as an alternative for the treatment of infectious mastitis during lactation. Appl. Environ. Microbiol., 74, 4650–4655
31. Kasımoğlu, A., Göncüoğlu, M. and Akgün, S. (2004) Probiotic white cheese with Lactobacillus acidophilus. Int. Dairy J., 14, 1067-1073.
32. Kan, A., Gelfat, I., Emani, S., Praveschotinunt, P. and Joshi, N.S. (2020) Plasmid vectors for in vivo selection-free use with the probiotic E. coli Nissle 1917. ACS synthetic biology, 10(1), pp.94-106.
33. Landete, J.M., Langa, S., Revilla, C., Margolles, A., Medina, M. and Arqués, J.L. (2015) Use of anaerobic green fluorescent protein versus green fluorescent protein as reporter in lactic acid bacteria. Appl. Microbiol. Biotechnol., 99, 6865-6877.
34. LeCureux, J.S. and Dean, G.A. (2018) Lactobacillus mucosal vaccine vectors: immune responses against bacterial and viral antigens. mSphere., 3, e00061-18.
35. Letunic, I. and Bork, P. (2007) Interactive Tree Of Life (iTOL): an online tool for phylogenetic tree display and annotation. Bioinformatics., 23, 127-128.
36. Levante, A., Folli, C., Montanini, B., Ferrari, A., Neviani, E. and Lazzi, C. (2019) Expression of DinJ-YafQ System of Lactobacillus casei group strains in response to food processing stresses. Microorganisms., 7, 438.

37. Ma, B., Forney, L.J. and Ravel, J. (2012) The vaginal microbiome: rethinking health and diseases. Annu. Rev. Microbiol., 66, 371.
38. Mastromarino, P., Macchia, S., Meggiorini, L., Trinchieri, V., Mosca, L., Perluigi, M., et al. (2009) Effectiveness of Lactobacillus-containing vaginal tablets in the treatment of symptomatic bacterial vaginosis. Clin. Microbiol. Infect., 15, 67-74.
39. Mathiesen, G., Øverland, L., Kuczkowska, K. and Eijsink, V.G. (2020) Anchoring of heterologous proteins in multiple Lactobacillus species using anchors derived from Lactobacillus plantarum. Sci. Rep., 10, 1-10.
40. Mathiesen, G., Sveen, A., Brurberg, M.B., Fredriksen, L., Axelsson, L. and Eijsink, V.G. (2009) Genome-wide analysis of signal peptide functionality in Lactobacillus plantarum WCFS1. BMC genomics., 10, 1-13.
41. Madeira, F., Pearce, M., Tivey, A., Basutkar, P., Lee, J., Edbali, O., et al. (2022) Search and sequence analysis tools services from EMBL-EBI in 2022. Nucleic Acids Res.
42. Meier-Kolthoff, J.P. and Göker, M. (2019) TYGS is an automated high-throughput platform for state-of-the-art genome-based taxonomy. Nat. Commun., 10, 1-10.
43. Meng, Q., Yuan, Y., Li, Y., Wu, S., Shi, K. and Liu, S. (2021) Optimization of electrotransformation parameters and engineered promoters for Lactobacillus plantarum from wine. ACS Synth. Biol., 10, 1728-1738.
44. Nguyen, T.T., Mathiesen, G., Fredriksen, L., Kittl, R., Nguyen, T.H., Eijsink, V.G., et al. (2011) A food-grade system for inducible gene expression in Lactobacillus plantarum using an alanine racemase-encoding selection marker. J. Agric. Food Chem., 59, 5617-5624.
45. Nguyen, H.M., Pham, M.L., Stelzer, E.M., Plattner, E., Grabherr, R., Mathiesen, G., Peterbauer, C.K., Haltrich, D. and Nguyen, T.H. (2019) Constitutive expression and cell-surface display of a bacterial β-mannanase in Lactobacillus plantarum Microb. Cell Factories, 18,1-12.
46. Paget, M.S. and Helmann, J.D. (2003) The σ70family of sigma factors. Genome Biol., 4, 1-6.
47. Pedrolli, D.B., Ribeiro, N.V., Squizato, P.N., de Jesus, V.N., Cozetto, D.A., Tuma, R.B., et al. (2019) Engineering microbial living therapeutics: the synthetic biology toolbox. Trends Biotechnol., 37, 100-115.
48. Piraner, D.I., Abedi, M.H., Moser, B.A., Lee-Gosselin, A. and Shapiro, M.G. (2017) Tunable thermal bioswitches for in vivo control of microbial therapeutics. Nat. Chem. Biol., 13, 75-80.
49. Plessas, S., Fisher, A., Koureta, K., Psarianos, C., Nigam, P. and Koutinas, A.A. (2008) Application of Kluyveromyces marxianus, Lactobacillus delbrueckii ssp. bulgaricus and L. helveticus for sourdough bread making. Food Chem., 106, 985-990.
50. Rosenfeldt, V., Benfeldt, E., Nielsen, S.D., Michaelsen, K.F., Jeppesen, D.L., Valerius, N.H., et al. (2003) Effect of probiotic Lactobacillus strains in children with atopic dermatitis. J. Allergy Clin. Immunol., 111, 389-395.
51. Rottinghaus, A.G., Ferreiro, A., Fishbein, S.R., Dantas, G. and Moon, T.S. (2022) Genetically stable CRISPR-based kill switches for engineered microbes. Nature communications, 13(1), pp.1-17.

52. Rud, I., Jensen, P.R., Naterstad, K. and Axelsson, L. (2006) A synthetic promoter library for constitutive gene expression in Lactobacillus plantarum. Microbiology., 152, 1011-1019.
53. Russo, P., Iturria, I., Mohedano, M.L., Caggianiello, G., Rainieri, S., Fiocco, D., et al. (2015) Zebrafish gut colonization by mCherry-labelled lactic acid bacteria. Appl. Microbiol. Biotechnol., 99, 3479-3490.
54. Salomé-Desnoulez, S., Poiret, S., Foligné, B., Muharram, G., Peucelle, V., Lafont, F., et al. (2021) Persistence and dynamics of fluorescent Lactobacillus plantarum in the healthy versus inflamed gut. Gut Microbes., 13, 1897374.
55. Siezen, R.J. and van Hylckama Vlieg, J.E. (2011) Genomic diversity and versatility of Lactobacillus plantarum, a natural metabolic engineer. Microb. Cell Factories., 10, 1-13.
56. Stirling, F. and Silver, P.A.(2020) Controlling the implementation of transgenic microbes: are we ready for what synthetic biology has to offer? Molecular cell, 78(4), pp.614-623.
57. Sørvig, E., Grönqvist, S., Naterstad, K., Mathiesen, G., Eijsink, V.G. and Axelsson, L. (2003) Construction of vectors for inducible gene expression in Lactobacillus sakei and L. plantarum. FEMS Microbiol. Lett., 229, 119-126.
58. Sørvig, E., Mathiesen, G., Naterstad, K., Eijsink, V.G. and Axelsson, L. (2005a) High-level, inducible gene expression in Lactobacillus sakei and Lactobacillus plantarum using versatile expression vectors. Microbiology., 151, 2439-2449.
59. Sørvig, E., Skaugen, M., Naterstad, K., Eijsink, V.G. and Axelsson, L. (2005b) Plasmid p256 from Lactobacillus plantarum represents a new type of replicon in lactic acid bacteria, and contains a toxin–antitoxin-like plasmid maintenance system. Microbiology, 151, 421-431.
60. Spangler, J.R., Caruana, J.C., Phillips, D.A. and Walper, S.A. (2019) Broad range shuttle vector construction and promoter evaluation for the use of Lactobacillus plantarum WCFS1 as a microbial engineering platform. Synth. Biol., 4, ysz012.
61. Spath, K., Heinl, S. and Grabherr, R. (2012) Direct cloning in Lactobacillus plantarum: electroporation with non-methylated plasmid DNA enhances transformation efficiency and makes shuttle vectors obsolete. Microb. Cell Factories., 11, 1-8.
62. Takala, T. and Saris, P. (2002) A food-grade cloning vector for lactic acid bacteria based on the nisin immunity gene nisI. Appl. Microbiol. Biotechnol., 59, 467-471.
63. Tauer, C., Heinl, S., Egger, E., Heiss, S. and Grabherr, R. (2014) Tuning constitutive recombinant gene expression in Lactobacillus plantarum. Microb. Cell Factories., 13, 1-11.
64. Teughels, W., Durukan, A., Ozcelik, O., Pauwels, M., Quirynen, M. and Haytac, M.C. (2013) Clinical and microbiological effects of Lactobacillus reuteri probiotics in the treatment of chronic periodontitis: a randomized placebo-controlled study. J. Clin. Periodontol., 40, 1025-1035.
65. Todt, T.J., Wels, M., Bongers, R.S., Siezen, R.S., Van Hijum, S.A. and Kleerebezem, M. (2012) Genome-wide prediction and validation of sigma70 promoters in Lactobacillus plantarum WCFS1. PLoS One., 7, e45097
66. Tran, A.M., Unban, K., Kanpiengjai, A., Khanongnuch, C., Mathiesen, G., Haltrich, D. and Nguyen, T.H. (2021) Efficient secretion and recombinant production of a lactobacillal α-amylase

in Lactiplantibacillus plantarum WCFS1: analysis and comparison of the secretion using different signal peptides. Front. Microbiol., 12, 689413.
67. Turroni, F., Ventura, M., Buttó, L.F., Duranti, S., O'Toole, P.W., Motherway, M.O.C., et al. (2014) Molecular dialogue between the human gut microbiota and the host: a Lactobacillus and Bifidobacterium perspective. Cell. Mol. Life Sci., 71,183-203.
68. Van Kranenburg, R., Golic, N., Bongers, R., Leer, R.J., De Vos, W.M., Siezen, R.J., et al. (2005) Functional analysis of three plasmids from Lactobacillus plantarum. Appl. Environ. Microbiol., 71, 1223-1230.
69. Wang, M., Fu, T., Hao, J., Li, L., Tian, M., Jin, N., et al. (2020) A recombinant Lactobacillus plantarum strain expressing the spike protein of SARS-CoV-2. Int. J. Biol. Macromol., 160, 736-740.
70. Wang, B., Kitney, R.I., Joly, N. and Buck, M. (2011) Engineering modular and orthogonal genetic logic gates for robust digital-like synthetic biology. Nat. Commun., 2, 1-9.
71. Waterhouse, A.M., Procter, J.B., Martin, D.M., Clamp, M. and Barton, G.J. (2009) Jalview Version 2—a multiple sequence alignment editor and analysis workbench. Bioinformatics., 25, 1189-1191.
72. Watterlot, L., Rochat, T., Sokol, H., Cherbuy, C., Bouloufa, I., Lefèvre, F., et al. (2010) Intragastric administration of a superoxide dismutase-producing recombinant Lactobacillus casei BL23 strain attenuates DSS colitis in mice. Int. J. Food Microbiol., 144, 35-41.
73. Wright, O., Stan, G.B. and Ellis, T.(2013) Building-in biosafety for synthetic biology. Microbiology, 159(Pt_7), pp.1221-1235.
74. Xie, Y., Wei, Y., Shen, Y., Li, X., Zhou, H., Tai, C et al. (2018) TADB 2.0: an updated database of bacterial type II toxin–antitoxin loci. Nucleic Acids Res., 46, D749-D753.
75. Yamaguchi, Y. and Inouye, M. (2011) Regulation of growth and death in Escherichia coli by toxin–antitoxin systems. Nat. Rev. Microbiol., 9, 779-790.
76. Zheng, J., Wittouck, S., Salvetti, E., Franz, C.M., Harris, H.M., Mattarelli, P., et al. (2020) A taxonomic note on the genus Lactobacillus: Description of 23 novel genera, emended description of the genus Lactobacillus Beijerinck 1901, and union of Lactobacillaceae and Leuconostocaceae. Int. J. Syst. Evol. Microbiol., 70, 2782-2858.
77. Zocco, M. A., Verme L. Z.D., Cremonini, F., Piscaglia, A.C., Nista, E.C., Candelli, M., et al. (2006) Efficacy of Lactobacillus GG in maintaining remission of ulcerative colitis. Aliment. Pharmacol. Ther., 23, 1567-1574.

C h a p t e r 5

RECOMBINANT PROTEIN EXPRESSION AND SECRETION FROM *Lactiplantibacillus plantarum*

5.1. Introduction

Lactic Acid Bacteria (LAB) are an essential constituent of the human microbiome and facilitate host well-being (Tian et al., 2023; Stamper et al., 2016). Due to their natural propensity to colonize the host microenvironment, LABs can be ideal candidates for target-specific delivery of therapeutic macromolecules in the human body (Debnath et al., 2024). Over the past two decades, several LAB candidates have been genetically modified to facilitate recombinant expression of metabolic enzymes, cytokines, and receptor antagonists for treating different disease conditions (Singh et al., 2017). However, the limited efficacy of these engineered strains in achieving disease alleviation has hindered their progress in human clinical trials. Inefficient target site colonization, inadequate protein secretion, and poor pharmacokinetic profile are vital factors responsible for the underwhelming performance of these engineered bacterial therapeutic strains (Charbonneau et al., 2020). In addition to these factors, the low transcriptional strength of promoters driving therapeutic protein-encoding genes can severely restrict the performance of bacterial therapeutics. *L. plantarum* WCFS1 (isolated from human saliva) is a prominent LAB strain extensively modified for its ability to drive heterologous protein production and secretion (Rud et al., 2006; Mathiesen et al., 2009). Notably, the strain does not encode any harmful virulence factors and is well tolerated by the host, making it an ideal candidate for bacterial therapeutic development (Kleerebezem et al., 2003). Significant progress has been made in the last three decades to improve the ability of *L. plantarum* WCFS1 to secrete heterologous proteins (Karlskås et al., 2014). However, the lack of efficient promoters to drive protein expression is a bottleneck to achieving optimal protein secretion titers without overburdening the microbial chassis (Tran et al., 2021). My recent study showed that the P_{tlpA} promoter isolated from *S. typhimurium* could exhibit strong expression of the mCherry reporter protein in *L. plantarum* WCFS1 (Dey et al., 2023). Although higher mCherry expression can facilitate live imaging of bacteria under *in-vitro* and *in-vivo* conditions (Russo et al., 2015; Berlec et al., 2015),

it does not provide any therapeutic benefit to the host. However, within the physiological temperature range (36 - 38°C), the P_{tlpA} promoter was highly effective at driving heterologous protein (mCherry) production. The human body has a consistent temperature ranging from 36.8°C in the mouth to 37.6°C in the gut and 37.5°C in the vagino-rectal tract. As a human commensal, *L. plantarum* WCFS1 is naturally adapted to colonize and grow within the host at the physiological temperature of ~37 °C. Therefore, the ambient temperature of the host would allow for the P_{tlpA} promoter-based production and secretion of therapeutic proteins at the target site. In addition to protein secretion, ensuring recombinant plasmid retention without depending on external antibiotic supplementation is crucial for determining the therapeutic efficacy of the recombinant strain. Auxotrophic methods, such as alanine auxotrophy, have enabled researchers to eliminate the need for antibiotic selection pressure-based plasmid retention in *L. plantarum* WCFS1 (Nguyen et al., 2011). However, a recent study found that the secretion efficiency of the recombinant enzymes β-mannanase and chitosanase significantly decreased in alanine auxotrophic *L. plantarum* strains compared to non-auxotrophic antibiotic-supplemented bacterial cultures. The overall protein secretion efficiency of β-mannanase was reduced from 83.7% to 78.2%, while that of chitosanase decreased from 63.7% to 45.1%, even though the overall levels of intracellular protein production stayed the same (Sak-Ubol et al., 2016). Therefore, it is necessary to test alternative strategies for plasmid retention that do not compromise heterologous protein secretion efficiency. The "Combo" toxin-antitoxin module previously exhibited plasmid retention in 60% of the bacterial population after 100 generations of consecutive culturing without external antibiotic supplementation (Dey et al., 2023). Despite retaining the plasmid, strains harboring the "Combo" module showed a 23% decrease in mCherry production compared to strains not harboring it (after ~10 generations). Although the reason for the decrease in intracellular mCherry levels was unclear, it was imperative to study how the presence of the "Combo" module could affect protein secretion efficiency in the engineered *L. plantarum* strains.

I selected the Staphylococcal nuclease (sNucA) protein to study its P_{tlpA}-promoter-based production and secretion from *L. plantarum* WCFS1 and to investigate the influence of the "Combo" toxin-antitoxin module on its overall secretion efficiency. sNucA is a thermonuclease protein naturally secreted by *S. aureus* that possesses an exo-endonuclease activity to degrade both single-stranded (ss) and double-stranded (ds) DNA existing in a linear topology like

eukaryotic DNA (Shortle, 1995). The bacterial host is immune to sNucA activity because it cannot degrade its circular DNA, which is the natural form of the bacterial genome. The sNucA protein has been extensively characterized, including in the famous Anfinsen experiments that proved the correlation between the 3D structure of the protein (**Figure 1A**) and its constituent amino acid sequence (**Table 1**) (Taniuchi and Anfinsen, 1969). Coordination of calcium ions (Ca^{2+}) with specific amino acid residues in sNucA (Aspartate 19, Aspartate 38, and Threonine 39) is necessary for the protein's catalytic activity (**Figure 1B, Figure 1C**). Apart from that, the interaction between the basic (Arginine 33 and Arginine 85) and acidic (Glutamate 41) amino acids play a key role in stabilizing the transition state of the sNucA protein during its catalytic degradation of linear DNA (**Figure 1B, Figure 1C**).

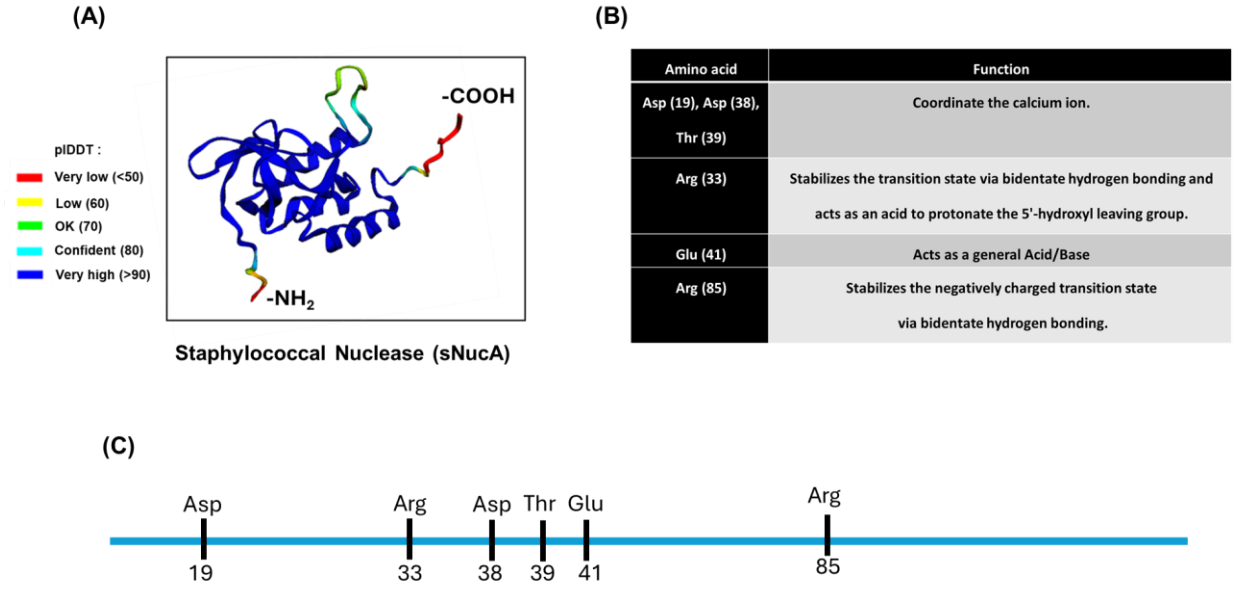

Figure 1. (A) AlphaFold 3D structure prediction of the Staphylococcal nuclease (sNucA) protein. The per-residue confidence metric (pLDDT) highlights the confidence in the predicted structure represented by the respective color codes (B) The critical amino acids (with their sequential position) of sNucA and their respective functions (C) Schematic illustrating the key amino acid positions in the sNucA protein sequence responsible for its DNA degradation activity.

Table 1: - Primary amino acid sequence of the Staphylococcal nuclease (sNucA) protein. The catalytic amino acid residues of the protein mentioned in Figure 1B and Figure 1C are highlighted in red.

Protein	Sequence
Staphylococcal nuclease (sNucA)	**NH2 -** STKKLHKEPATLIKAIDGDTVKLMYKGQPMTFRLLLVDTPETKHPKKGVEKYG PEASAFTKKMVENAKKIEVEFDKGQRTDKYGRGLAYIYADGKMVNEALVRQGLAK VAYVYKPNNTHEQHLRKSEAQAKKEKLNIWSEDNADSGQ – **COOH**

In this chapter, I will present the experimental results pertaining to sNucA secretion from *L. plantarum* WCFS1 and estimation of its bioactivity. Firstly, I will demonstrate the ability of the P_{tlpA} promoter to drive the production and subsequent secretion of sNucA into the extracellular media. Secondly, I will highlight an assay developed specifically for the quantitative estimation of the secreted sNucA protein. Thirdly, I will demonstrate how the "Combo" toxin-antitoxin genetic module influences sNucA protein secretion in the absence of antibiotic supplementation. Fourthly, I will elaborate on the parameters required for optimizing protein purification from *L. plantarum* WCFS1 using mCherry and sNucA proteins as examples. Lastly, I will demonstrate the growth pattern of engineered *L. plantarum* WCFS1 strains in different cell culture media formulations and its effect on sNucA protein secretion ability.

5.2. Materials and Methods

Media, strain, and plasmids

L. plantarum WCFS1 was the parent strain used for recombinant plasmid transformation and bioactivity screening. The strain was maintained in the De Man, Rogosa and Sharpe (MRS) media. The culture media, antibiotics and complementary reagents were purchased from Carl Roth Gmbh, Germany. Growth media was supplemented with 10 µg/mL of erythromycin to culture engineered *L. plantarum* WCFS1 strains. The plasmid pLp_3050sNuc (Mathiesen et al., 2009) was used as the vector backbone for developing the recombinant constructs tested in this chapter. Micrococcal nuclease (recombinant sNucA) was procured from Sigma Aldrich GmbH, Germany and was dissolved in 1X sterile Dulbecco's Phosphate Buffer Saline (PBS)

(ThermoFisher Scientific GmbH, Germany) to prepare the stock solution according to recommended guidelines. DNAse broth was prepared from the commercially procured DNAse Agar (Altmann Analytik GmbH, Germany) by precipitating the agar and collecting the supernatant (no additional filter-sterilization was required). The final formulation of the DNAse broth comprised of Tryptose (20 g/L), Sodium Chloride (5 g/L), Calf Thymus DNA (2 g/L) and Methyl Green (0.05 g/L) respectively.

Molecular biology

HiFi Assembly Master Mix, Quick Blunting Kit and T4 DNA Ligase were purchased from New England BioLabs (NEB, Germany). PCR was performed using Q5 High Fidelity 2X Master Mix (NEB) with primers purchased from Integrated DNA Technologies (IDT) (Leuven, Belgium). Oligonucleotide gene fragments were purchased as eBlocks from IDT (Coralville, USA) and codon optimized using the IDT Codon Optimization Tool (Coralville, USA). *Lactobacillus acidophilus* was selected as the host strain for codon optimization because of its genus similarity with *L. plantarum* WCFS1. Plasmid extraction and DNA purification were performed using kits purchased from Qiagen GmbH (Hilden, Germany) and Promega GmbH (Walldorf, Germany) respectively. The competent cell preparation and recombinant plasmid construction protocols were followed according to my previously published reports (Dey et al., 2023; Blanch-Asensio et al., 2023).

DNAse agar assay

To visualize nuclease secretion from the recombinant strains, the bacterial strains (glycerol stock) were inoculated in MRS media supplemented with 10 µg/mL erythromycin and kept for overnight incubation at 37°C with 250 rpm orbital shaking. The following day, the samples were sub-cultured in 3 mL of fresh MRS media (antibiotic supplemented) at an initial OD_{600} of 0.01 and incubated at 37°C until it reached an OD_{600} of 0.8. For **Figure 2B**, 100 µL of the bacterial cultures were plated on DNAse agar (Altmann Analytik GmbH, Germany) supplemented with 10 µg/mL of erythromycin using a sterile spreader and incubated at 37°C for 18 h. For **Figure 3E**, 10 µL of the bacterial cultures were spotted on the antibiotic supplemented DNAse agar and incubated at 37°C for 18 h. The discoloration zone surrounding the bacterial colonies was then imaged using

the ChemiDoc MP Imaging system (Biorad GmbH, Germany) in the Cy5 channel ($Ex_{\lambda}/Em_{\lambda}$ = 651 nm/670 nm).

Silver staining protocol

Samples were denatured and loaded on 15% SDS PAGE gels run at constant voltage (100 V) for 1 h, along with the respective controls and protein ladder. Following that, the gel was incubated in the Fixer solution (50% (v/v) methanol, 12% (v/v) acetic acid, 38% (v/v) H_2O and 50 µL of 37% formaldehyde) for 1 h [All incubation steps were conducted at room temperature on a rotary shaker]. The gel was then washed with 50% ethanol solution for 10 min, followed by a second step of washing with 30% ethanol solution. The gel was then sensitized in 0.02% (w/v) sodium thiosulfate (0.04 g $Na_2S_2O_3$, 200 ml H_2O) for only 1 min to prevent loss in peptide recovery. The gel was then washed thrice with Milli-Q water for 20 sec in each washing step. The gel was then incubated for 20 min in 4°C cold 0.1% (w/v) silver nitrate solution (0.1 g $AgNO_3$, 100 ml H_2O and 75 µL of 37% formaldehyde (added immediately before use). The gel was again washed twice with Milli-Q water for 20 sec in each washing step. The gel was then placed in a fresh glass tray to prevent background staining from the residual $AgNO_3$ on the gel surface. The gel was then incubated in the developer solution containing 6% (w/v) sodium carbonate and 4 X 10^{-5} % (w/v) sodium thiosulphate (with 50 µl of 37% formaldehyde added just before use). The developer solution was changed immediately when it turned yellow and sufficient staining was achieved. Further staining was terminated by incubating the gel in the stop solution (5% (v/v) acetic acid in Milli-Q water) for 20 min. The gel was again washed twice with Milli-Q water for 10 min in each washing step. The gel was then imaged using the silver stain detection channel of the ChemiDoc MP Imaging system (Biorad GmbH, Germany) for protein visualization.

Quantitative estimation of secreted nuclease

Bacterial cultures were grown overnight at 37°C and then subcultured the next day in fresh MRS media supplemented with 10 µg/mL erythromycin. Post growth (OD_{600}=0.8), 10 µL of the cultures were further inoculated in 1 mL of autoclaved DNAse broth (sterile 2.5 mL Eppendorf tubes) and incubated at 37°C, with constant shaking (250 rpm) for 18 h. After 18 h, bacterial cultures were centrifuged at 13,000 rpm (15700 × g) for 10 min, and 200 µL of the respective supernatants (bacteria-free) were added to the clear bottom 96-well microtiter plate (Corning®

96 well transparent bottom black plate, USA). The Microplate Reader Infinite 200 Pro (Tecan Deutschland GmbH, Germany) was used to analyze the methyl green-calf thymus DNA complex-based fluorescent intensity (Ex_{λ} / Em_{λ} = 633 nm/668 nm). The z-position and gain settings for fluorescence recording were set to 19442 µm and 140, respectively. For standard curve preparation, serial dilutions of the commercial micrococcal nuclease (0-270 nM) were made in the samples inoculated with the Empty Vector harboring *L. plantarum* strain. After incubation (37°C, 18 h) the fluorescence of the bacteria free supernatants was plotted against the respective nuclease concentrations. The nuclease concentration (nM) secreted by the recombinant *L. plantarum* strains were then determined from the exponential decay curve equation $y = A_1*\exp(-x/t_1) + A_2*\exp(-x/t_2) + A_3*\exp(-x/t_3) + y0$, where $A_1 = 7914.55$, $t_1 = 2.16$, $A_2 = 22601.12$, $t_2 = 36.11$, $A_3 = 16784.16$, $t_3 = 963.89$, $y_0 = -8136.39$ using their respective fluorescence quenching metrics.

Antibiotic free plasmid retention for nuclease-secreting *L. plantarum*

To facilitate antibiotic-free plasmid retention, the "Combo" toxin-antitoxin (TA) module was cloned in the pTlp-3050-His_{6X}-sNucA plasmid to create the pTlp-3050-His_{6X}-sNucA-Combo plasmid. The recombinant strains were cultured overnight in MRS media supplemented with 10 µg/mL erythromycin at 37°C with 250 rpm shaking. The following day, the strains were subcultured in fresh MRS media (antibiotic supplemented) and grown until they reached an OD_{600} of 0.8. 12.5 µL of the bacterial cultures were transferred in 1 mL of autoclaved DNAse Broth (with and without antibiotic supplementation) to bring the final OD_{600} to 0.01 and incubated at 37°C with 250 rpm shaking conditions for 24 h. Post 24 h incubation, the OD_{600} was measured in a NanoDrop Microvolume UV–Vis Spectrophotometer (ThermoFisher Scientific GmbH, Germany) and the bacteria were further subcultured in fresh DNAse Broth (starting inoculum of 0.01 OD_{600}). The remaining culture were then centrifuged at 13,000 rpm (15700 × g) for 10 min, and fluorescence was recorded (200 µL of respective bacteria-free supernatants) to quantify the concentration of the secreted nuclease using the exponential decay curve equation. This protocol was repeated for approximately 80 consecutive bacterial generations.

Growth rate measurements

Bacterial strains were cultivated overnight in MRS media supplemented with 10 µg/mL erythromycin at 37°C with continuous shaking (250 rpm). The following day, bacterial strains

were subcultured in the respective growth media supplemented with 10 µg/mL erythromycin at 1:25 (v/v) ratio. 200 µL of these subcultured bacteria were dispensed in Greiner UV-Star® 96 well plate (Greiner BioOne GmbH, Germany) and placed in the Microplate Reader Infinite 200 Pro (Tecan Deutschland GmbH, Germany). The absorbance (600 nm) was recorded at equal intervals of 30 min for a 24 h kinetic cycle. The incubation temperature was maintained at 37°C with intermediate orbital shaking of 15 min.

His_{6X}-mCherry protein purification from ClearColi BL21 DE3

ClearColi BL21 strain harboring the pT7-lacO-mCherry plasmid was used for mCherry protein overexpression and subsequent purification. The recombinant strain was inoculated in LB media supplemented with 2% (w/v) sodium chloride (LB-NaCl media) and 50 µg/mL kanamycin and incubated at 37°C with constant shaking (250 rpm). The strain was then subcultured in 100 mL of fresh LB-NaCl media (supplemented with 50 µg/mL kanamycin) in 1:50 (v/v) ratio in a 250 mL baffled flask. The secondary culture was grown at 37°C, 250 rpm until it reached early log-phase (OD_{600} =0.4), and then 500 µM of Isopropyl-ß-D-thiogalactopyranoside (IPTG) was added for inducing mCherry expression. Post induction, the culture was incubated at 30°C, with constant shaking at 180 rpm for 18 h to facilitate higher mCherry production. Post incubation, the bacterial biomass was harvested by centrifugation (3363 × g, 12 min, 4°C) and the pellet was resuspended in 10 mL of Lysis Buffer (Tris-HCl 20 mM, NaCl 500 mM, Imidazole 20 mM, pH 8) containing 1 mM of phenylmethylsulfonyl fluoride (PMSF). Branson Sonifier® ultrasonic cell disrupter (Branson Ultrasonics Corporation, USA) was used to disrupt the bacterial biomass. The Microtip 101-148-062 cell homogenization probe was used for 6 min with 3 sec "ON" and 8 sec "OFF" pulse at 30% power, with the sample being placed on ice to avoid excessive heat generation. The homogenized mixture was centrifuged at 15700 × g for 20 min at 4°C to remove the cell debris, and the soluble fraction was collected and filter-sterilized using a 0.22 µm pore-size PVDF filter. The filter-sterilized bacterial lysate was mixed with 4 mL of ROTI®Garose-His/Ni Beads (Carl Roth GmbH, Germany) equilibrated in the Lysis buffer for 1 h. The beads were then allowed to settle down in 10 mL columns with 10 µm filter pore size (MoBiTec GmbH, Germany) and washed with 60 mL of Wash Buffer (Tris-HCl 20 mM, NaCl 500 mM, Imidazole 30 mM, pH 8) to remove any non-specific proteins trapped in the matrix. The protein of interest was then eluted in 10 mL of Elution Buffer (Tris-HCl 20 mM, NaCl 500 mM, Imidazole 500 mM, pH 8). For

buffer exchange, the proteins were washed with 30 mL of sterile 1X Dulbecco PBS solution (ThermoFisher Scientific GmbH, Germany) in Amicon® Ultra-15 Centrifugal Filter Units with 10 kDa cutoff threshold (Merck GmbH, Germany) and maintained in ~ 1000 µL of PBS at -80°C. Absorbance was measured at 587 nm using the NanoDrop Microvolume UV–Vis Spectrophotometer (ThermoFisher Scientific GmbH, Germany) and His_{6X}-mCherry concentration was determined using Beer-Lambert law. The purity of the recombinant proteins was assessed on a 15% SDS-PAGE gel.

mCherry standard curve preparation

The purified mCherry protein was serially diluted in Lysis Buffer containing 1 mM PMSF in the range of 0 – 4 µM. 200 µL of the diluted protein samples were transferred to the transparent bottom 96-well plate (Corning® 96 well clear bottom black plate, USA). mCherry fluorescence intensity of the respective samples was analyzed in the Microplate Reader Infinite 200 Pro (Tecan Deutschland GmbH, Germany) at an excitation and emission wavelength of 587 nm and 625 nm, respectively. The *z*-position and gain settings were set to 19,442 µm and 136, respectively. The mCherry fluorescence values were plotted against their respective concentrations and a linear curve fitting was obtained with an equation of Y=11267*X, where y = mCherry fluorescence value (in arbitrary units) and x = mCherry concentration (in µM).

Cell homogenization parameter optimization for recombinant *L. plantarum* strain

Recombinant *L. plantarum* strain harboring the pTlp-mCherry-His_{6X} plasmid was inoculated in MRS media supplemented with 10 µg/mL erythromycin and incubated overnight at 37°C with 250 rpm shaking. The strain was subcultured in 200 mL of fresh MRS media (supplemented with 10 µg/mL erythromycin) in a 500 mL glass conical flask and incubated at 37°C, 250 rpm shaking for 18 h. Following day, the bacterial biomass was harvested by centrifugation (3363 × g, 12 min, 4°C) and the pellets (from an individual volume of 100 mL) were resuspended in 10 mL of Lysis Buffer containing 1 mM PMSF in a sterile 15 mL falcon (Greiner Bio-One GmbH, Germany). The resuspended bacterial pellets were subjected to mild and harsh sonication conditions using the ultrasonic cell disrupter. For mild sonication, the Microtip 101-148-062 was active for 10 min with 3 sec “ON” and 5 sec “OFF” pulse at 30% power, whereas for harsh sonication the probe was used for 10 min with 5 sec “ON” and 8 sec “OFF” pulse at 40% power. For mechanical

homogenization, 4.5 g of lysing matrix B (MP Biomedicals GmbH, Germany) was added to 10 mL of the resuspended bacterial pellet (in Lysis Buffer containing 1 mM PMSF) in a sterile 15 mL plug-seal cap falcon (Biologix GmbH, Germany). Mechanical disruption of the bacterial cells was conducted by 6 consecutive lysis cycles of 1 min each using the TeenPrep option of the FastPrep-24™ 5G bead beating grinder system (MP Biomedicals GmbH, Germany) set at a speed of 6.5 m/sec with an intermediate pause of 1 min after each lysis cycle. The Empty Vector harboring *L. plantarum* strain was used as a control for the mechanical homogenization protocol.

Recombinant protein purification from engineered *L. plantarum* strains

L. plantarum WCFS1 harboring the recombinant plasmids were grown overnight and subcultured in 100 mL MRS cultures supplemented with 10 µg/ml erythromycin at a 1:100 (v/v) ratio in a 250 mL glass conical flask. The cultures were incubated at 37°C with 250 rpm shaking for 18 h. The bacterial biomass was then harvested by centrifugation (3363 × g, 12 min, 4°C), resuspended in 10 mL of Lysis Buffer containing 1 mM PMSF and thoroughly disrupted by mechanical homogenization. The resultant solution was centrifuged (3363 × g, 12 min, 4°C) to remove the beads, and the lysate was collected. The lysate was again subjected to centrifugation at 15700 × g for 10 min at 4°C to remove the cell debris, and the supernatant was filter-sterilized with a 0.22 µm pore-size PVDF filter. The His_{6X} tag affinity chromatography-based protein purification steps proceeded as mentioned before. Absorbance of the purified protein was measured at 280 nm using the NanoDrop Microvolume UV–Vis Spectrophotometer (ThermoFisher Scientific GmbH, Germany) and the concentration was determined using the Beer-Lambert law.

Optimized cell culture media for bacterial growth

RPMI-1640, No phenol red (ThermoFisher Scientific GmbH, Germany) was used as the primary cell culture media for cultivating engineered *L. plantarum* strains. RPMI-Opti media was formulated by adding OPI Media Supplement (Sigma Aldrich GmbH, Germany) and MEM Non-Essential Amino Acids Solution (100X) (ThermoFisher Scientific GmbH, Germany) to RPMI 1640 media in 1:90 (v/v) and 1:90 (v/v) ratio respectively. RPMI-Opti-FBS media was formulated by adding 10% (v/v) Fetal Bovine Serum [FBS] (Pan Biotech, USA) to RPMI-Opti Media.

Standard curve preparation of purified His_{6X}-sNucA protein in optimized cell culture media

L. plantarum harboring the Empty Vector was grown overnight in MRS media supplemented with 10 µg/mL erythromycin at 37°C with 250 rpm shaking conditions. The following day, the strain was subcultured into 5 mL of RPMI-Opti and RPMI-Opti-FBS media in a 1:25 ratio (v/v) with antibiotic supplementation and incubated at 37°C, 250 rpm shaking conditions for 24 h. Post incubation, the bacterial cultures were centrifuged at 4000 rpm (3363 × g) for 15 min, and the supernatant was collected and filter-sterilized using a 0.22 µm PVDF filter. His_{6X}-sNucA protein (purified from *L. plantarum*) was serially diluted in a 100 µL mixture containing 50 µL of the filter-sterilized cell culture media supernatants (RPMI-Opti and RPMI-Opti-FBS) and 50 µL of sterile DNAse broth, in a concentration range starting from 0 nM to 85 nM. The final mixture (100 µL) was incubated at 37°C for 18 h under static conditions. After incubation, the entire 100 µL solution was transferred to a transparent bottom 96-well plate (Corning® 96 well clear bottom black plate, USA). The Microplate Reader Infinite 200 Pro (Tecan Deutschland GmbH, Germany) was used for sample analysis. The methyl green-DNA complex-based fluorescent intensity was recorded at $Ex_{\lambda}/Em_{\lambda}$ = 633 nm/668 nm for RPMI-Opti Media (z-position=18133 µm, gain=200) and RPMI-Opti-FBS Media (z-position=17806 µm, gain=195), respectively. The residual fluorescence of the mixture was plotted against the respective His_{6X}-sNucA concentrations, and an exponential decay curve equation was determined for both the cell culture formulations. The exponential decay curve equation for the RPMI-Opti based cell culture was:- $y = y_0 + A_1*\exp(-(x-x_0)/t_1) + A_2*\exp(-(x-x_0)/t_2) + A_3*\exp(-(x-x_0)/t_3)$, where $y_0 = 4623.23$, $x_0 = 0.35$, $t_1 = 4.55$, $A_2 = 4592.47$, $t_2 = 27.04$, $A_3 = 10709.35$, $t_3 = 27.05$. The exponential decay curve equation for the RPMI-Opti-FBS based cell culture was:- $y = y_0 + A_1*\exp(-(x-x_0)/t_1) + A_2*\exp(-(x-x_0)/t_2) + A_3*\exp(-(x-x_0)/t_3)$, where $y_0 = 342.81$, $x_0 = 1.36$, $t_1 = 6.95$, $A_2 = 7245.48$, $t_2 = 70.69$, $A_3 = 11254.13$, $t_3 = 70.38$.

Quantitative estimation of secreted His_{6X}-sNucA protein in optimized cell culture media

Bacterial strains were grown overnight in MRS media supplemented with 10 µg/mL erythromycin at 37°C with 250 rpm shaking conditions. The following day, the strains were subcultured into 5 mL of RPMI-Opti and RPMI-Opti-FBS media in a 1:25 ratio (v/v) with or without antibiotic supplementation. These cultures were further incubated at 37°C, 250 rpm shaking conditions for 24 h. Post incubation, the bacterial cultures were centrifuged at 4000 rpm (3363 × g) for 15 min, the supernatant was collected and filter-sterilized using a 0.22 µm PVDF filter. 50 µL of the

respective filter-sterilized supernatants were added to 50 µL of sterile DNAse broth and incubated at 37°C for 18 h under static conditions. The residual fluorescence of the samples was measured according to the above-mentioned protocol.

Statistical and bioinformatics analysis

GraphPad Prism 7.0 software was used to derive the linear regression (**Figure 5C**) and exponential decay equation (**Figure 4B, Figure 10A, Figure 10B**). Student t-test was used for estimating significant differences between the mean values of different samples. GRAVY Calculator was used to generate the grand average of hydropathy (GRAVY) value for the secreted Staphylococcal nuclease protein. AlphaFold2 GitHub code (ColabFold v1.5.5) was used to predict the 3D structure of the Staphylococcal nuclease (sNucA) protein. All the schematic figures were generated using Biorender.

5.3. Results and Discussions

5.3.1. Constitutive production and extracellular secretion of Staphylococcal nuclease

To facilitate constitutive secretion of Staphylococcal nuclease (sNucA) from *L. plantarum* WCFS1, the P_{spp} promoter was replaced with the P_{tlpA} promoter in the pLp_3050sNuc plasmid to create the pTlp-3050-sNucA plasmid. The P_{tlpA} promoter was cloned upstream of the sNucA gene, N-terminally fused to the signal peptide 3050 (Sp_{3050}), previously reported to drive maximum extracellular secretion of sNucA from the bacterial chassis compared to its counterparts (Mathiesen et al., 2009). The recombinant plasmid pTlp-3050-sNucA (**Figure 2A**) was transformed *into L. plantarum* WCFS1 and sequence-verified to eliminate mutant clones. To assess sNucA secretion, the pTlp-3050-sNucA plasmid harboring strain was plated on DNAse agar along with the control strain (Empty Vector). Post incubation, halo zones were created around the bacterial colonies (pTlp-3050-sNucA), indicating that the secreted sNucA protein degraded the calf thymus double-stranded DNA (dsDNA) present in the growth media (**Figure 2B**). The inability of the methyl green dye to intercalate with the degraded dsDNA led to a visible reduction in the fluorescence, that was not observed for the control strain. The Grand Average of Hydropathy (GRAVY) value (as determined by the GRAVY Calculator) for the secreted sNucA

protein was -0.84, indicating the overall hydrophilic nature of the protein and justifying its extracellular secretion. The recombinant strains were further grown in MRS media for 18 h, followed by harvesting of the bacterial biomass and extracellular media. The bacterial biomass was subjected to a "mild sonication" process and the soluble lysate (cellular debris free) was loaded on an SDS-PAGE gel, along with the extracellular media (supernatant). Silver staining confirmed the presence of the uncleaved sNucA protein in the intracellular fraction (**Figure 2C**), and the cleaved sNucA protein in the supernatant (**Figure 2D**) compared to the control (Empty Vector).

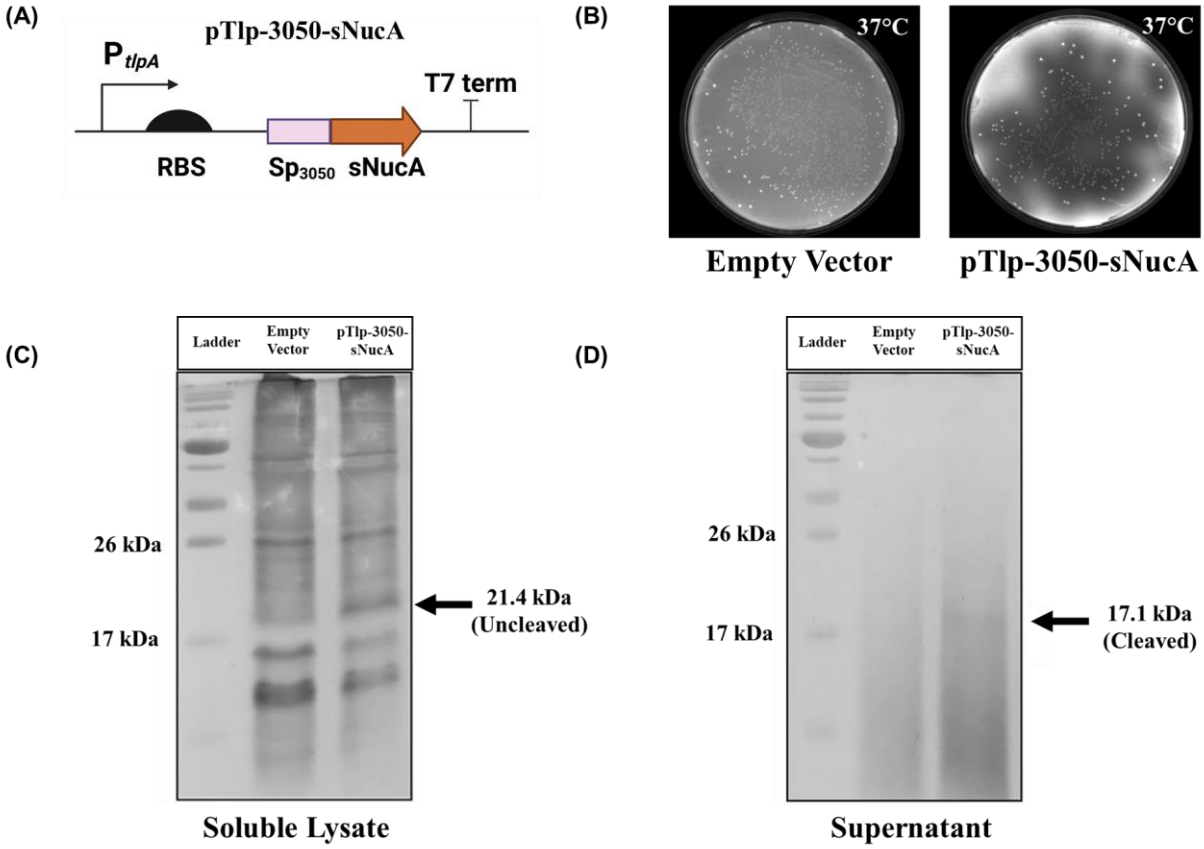

Figure 2. (A) Schematic representation of the pTlp-3050-sNucA genetic module (B) Cy5 ($Ex_{\lambda}/Em_{\lambda}$=587 nm/625 nm) channel imaging of the recombinant strains (Empty Vector and pTlp-3050-sNucA) cultivated on DNAse agar after 18 h incubation at 37°C. The halo around the bacterial colonies confirms extracellular sNucA secretion into the agar media (C) Silver staining of the soluble lysates collected after sonicating the recombinant strains (Empty Vector and pTlp-3050-sNucA). The arrow represents the uncleaved heterologous sNucA protein band (21.4 kDa) (D) Silver staining of the supernatants (MRS media) collected post incubation of the recombinant strains (Empty Vector and pTlp-3050-sNucA) at 37°C. The arrow represents the secreted sNucA protein band (17.1 kDa) into the extracellular media.

I further modified the pTlp-3050-sNucA plasmid by introducing a Histidine-6X (His_{6X}) tag between the Sp3050 cleavage site and the sNucA protein coding to create the pTlp-3050-His_{6X}-sNucA plasmid (**Figure 3A**). Incorporating the His_{6X} tag would provide the possibility to purify the secreted protein (if needed) from the supernatant as demonstrated in previous reports (Li et al., 2014). Following that, the "Combo" toxin-antitoxin module (DinJ-YafQ and MazF-MazE type II toxin-antitoxin system) was cloned in the pTlp-3050-His_{6X}-sNucA plasmid to create the pTlp-3050-His_{6X}-sNucA-Combo construct (**Figure 3B**). Growth kinetics of the recombinant strains were monitored in both MRS media and DNAse broth to determine the metabolic burden imposed by the genetic modules. Both the recombinant strains (pTlp-3050-His_{6X}-sNucA and pTlp-3050-His_{6X}-sNucA-Combo) showed a prolonged lag phase (~2 h) and a drop in the final biomass compared to the control strain (Empty Vector) in MRS media (**Figure 3C**). This growth pattern in the enriched media (MRS) confirmed that heterologous production of His_{6X}-sNucA protein imposed a metabolic burden on the recombinant strains. However, no significant difference in the lag phase period and final biomass was observed for the recombinant strains when grown in DNAse broth (**Figure 3D**). The nutrient-limiting conditions of the DNAse broth might be responsible for preventing the control strain from experiencing a significant growth advantage compared to the recombinant strains. To confirm whether the His_{6X}-sNucA protein was properly cleaved and secreted into the extracellular media, both the recombinant strains (pTlp-3050-His_{6X}-sNucA and pTlp-3050-His_{6X}-sNucA-Combo) were grown on DNAse agar and DNAse broth. Post-incubation (37°C), a uniform halo was observed for both the recombinant strains on DNAse agar without any noticeable difference (**Figure 3E**). Silver staining analysis of the DNAse broth supernatant of the control strain (Empty Vector) collected after 18 h of bacterial growth exhibited a uniform dsDNA smear (of different molecular weights). The dsDNA staining further confirmed that the natural secretome of the bacterial chassis had no intrinsic nuclease activity (Beidler et al., 1982). However, in contrast no smear was observed in the DNAse Broth supernatants collected from the pTlp-3050-His_{6X}-sNucA and pTlp-3050-His_{6X}-sNucA-Combo recombinant strains, confirming that the secreted His_{6X}-sNucA protein was functionally active and could degrade the dsDNA present in the media (**Figure 3F**).

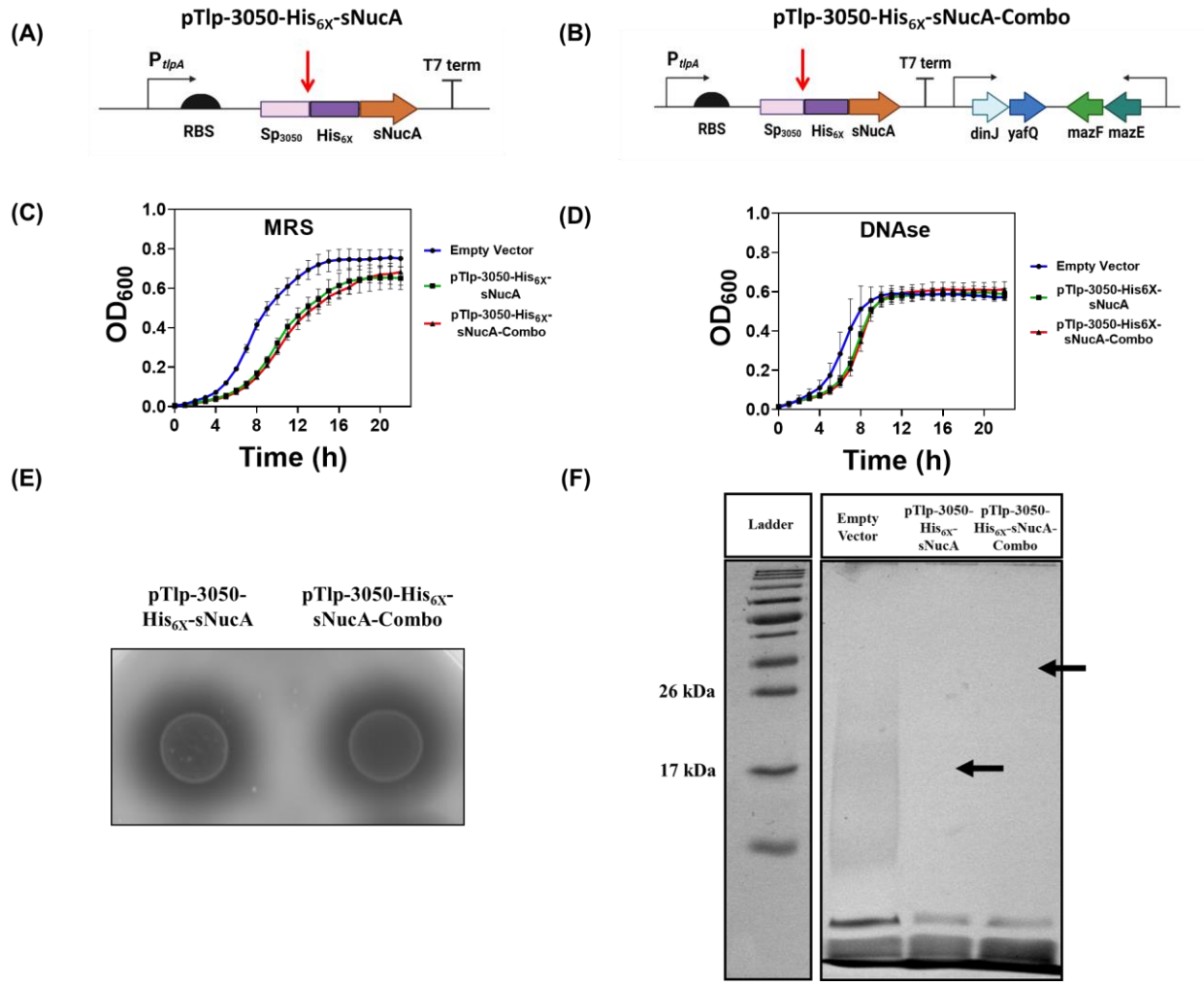

Figure 3. (A) Schematic representation of the pTlp-3050-His$_{6X}$-sNucA genetic module (B) Schematic representation of the pTlp-3050-His$_{6X}$-sNucA-Combo genetic module (C) Growth kinetics of Empty Vector, pTlp-3050-His$_{6X}$-sNucA and pTlp-3050-His$_{6X}$-sNucA-Combo *L. plantarum* WCFS1 strains in MRS media supplemented with 10 µg/mL erythromycin incubated at 37°C for 22 h. The error bars represent standard deviation based on three independent measurements (D) Growth kinetics of Empty Vector, pTlp-3050-His$_{6X}$-sNucA and pTlp-3050-His$_{6X}$-sNucA-Combo *L. plantarum* WCFS1 strains in DNAse Broth supplemented with 10 µg/mL erythromycin incubated at 37°C for 22 h. The error bars represent standard deviation based on three independent measurements (E) Cy5 ($Ex_{\lambda}/Em_{\lambda}$=587 nm/625 nm) channel imaging of the recombinant strains (pTlp-3050-His$_{6X}$-sNucA and pTlp-3050-His$_{6X}$-sNucA-Combo) cultivated on DNAse agar after 18 h incubation at 37°C. The halo around the bacterial colonies confirms extracellular sNucA secretion into the agar media (F) Silver staining of the DNAse broth supernatants collected after 18 h incubation of the recombinant strains (Empty Vector, pTlp-3050-His$_{6X}$-sNucA and pTlp-3050-His$_{6X}$-sNucA-Combo). The arrows highlight the absence of the smear due to the degraded dsDNA caused by the secreted His$_{6X}$-sNucA protein.

5.3.2. Antibiotic free plasmid retention for extracellular secretion of His_{6X}-sNucA

Qualitative analysis confirmed that the P_{tlpA} promoter was able to drive the production and subsequent extracellular secretion of His_{6X}-sNucA protein from the pTlp-3050-His_{6X}-sNucA and pTlp-3050-His_{6X}-sNucA-Combo plasmid harboring *L. plantarum* strains. However, a quantitative estimation of the secreted His_{6X}-sNucA protein was also needed to reliably compare the protein secretion performance of the different recombinant constructs. In addition, the quantitative analysis would also provide key insights regarding how the "Combo" toxin-antitoxin module would influence the secretion of the His_{6X}-sNucA protein over several generations. Commercial micrococcal nuclease (**Figure 4A**) was chosen to develop the quantitative assay because of its high sequence similarity (>95%) with the secreted sNucA protein. Increasing concentrations of the micrococcal nuclease in the DNAse broth (containing the control strain) led to decreased fluorescence intensity of the media. On plotting the fluorescence values of the DNAse broth against the respective nuclease concentrations, an exponential decay function of $y = A_1*\exp(-x/t_1) + A_2*\exp(-x/t_2) + A_3*\exp(-x/t_3) + y0$, where $A_1 = 7914.55$, $t_1 = 2.16$, $A_2 = 22601.12$, $t_2 = 36.11$, $A_3 = 16784.16$, $t_3 = 963.89$, $y_0 = -8136.39$, was obtained (**Figure 4B**). Nine independent measurements showed that the pTlp-3050-His_{6X}-sNucA and pTlp-3050-His_{6X}-sNucA-Combo recombinant strains secreted ~ 39 ± 2.77 nM and ~41 ± 0.11 nM of His_{6X}-sNucA protein into the DNAse broth, respectively (**Figure 4C**). There was no significant difference observed between the nuclease concentrations secreted by the pTlp-3050-His_{6X}-sNucA and pTlp-3050-His_{6X}-sNucA-Combo recombinant strains. This highlighted that inclusion of the "Combo" toxin-antitoxin module did not impose an additional burden on the protein secretion capability of the bacterial chassis. To assess whether the "Combo" toxin-antitoxin module could sustain plasmid retention and extracellular protein secretion over several generations, the pTlp-3050-His_{6X}-sNucA and pTlp-3050-His_{6X}-sNucA-Combo recombinant strains were subcultured in DNAse broth for ~13-15 consecutive days. The temporal period is mentioned as a range because the growth rates of the recombinant strains in DNAse broth were slightly different across the bacterial samples. No significant difference in the secreted nuclease concentrations was observed between the pTlp-3050-His_{6X}-sNucA and pTlp-3050-His_{6X}-sNucA-Combo strains when grown in antibiotic (erythromycin) supplemented DNAse broth within the tested period. However, in the absence of antibiotic (erythromycin) supplementation for the pTlp-3050-His_{6X}-sNucA strain,

nuclease secretion dropped gradually after ~40 generations and rapidly after ~65 generations. In contrast, for the pTlp-3050-His$_{6X}$-sNucA-Combo strain, the concentration of secreted nuclease remained constant across ~80 bacterial generations that surpassed within the tested period, even without antibiotic supplementation (**Figure 4D**). The difference in the secreted nuclease concentrations confirmed that incorporating the "Combo" toxin-antitoxin genetic module in the plasmid could significantly increase the plasmid retention rate over several cell generations without compromising the extracellular protein secretion levels. Additionally, this experiment suggested that the performance of the "Combo" toxin-antitoxin module is not restricted to fluorescent reporter proteins alone (Dey et al., 2023) and is able to retain recombinant plasmids expressing a heterologous protein like sNucA.

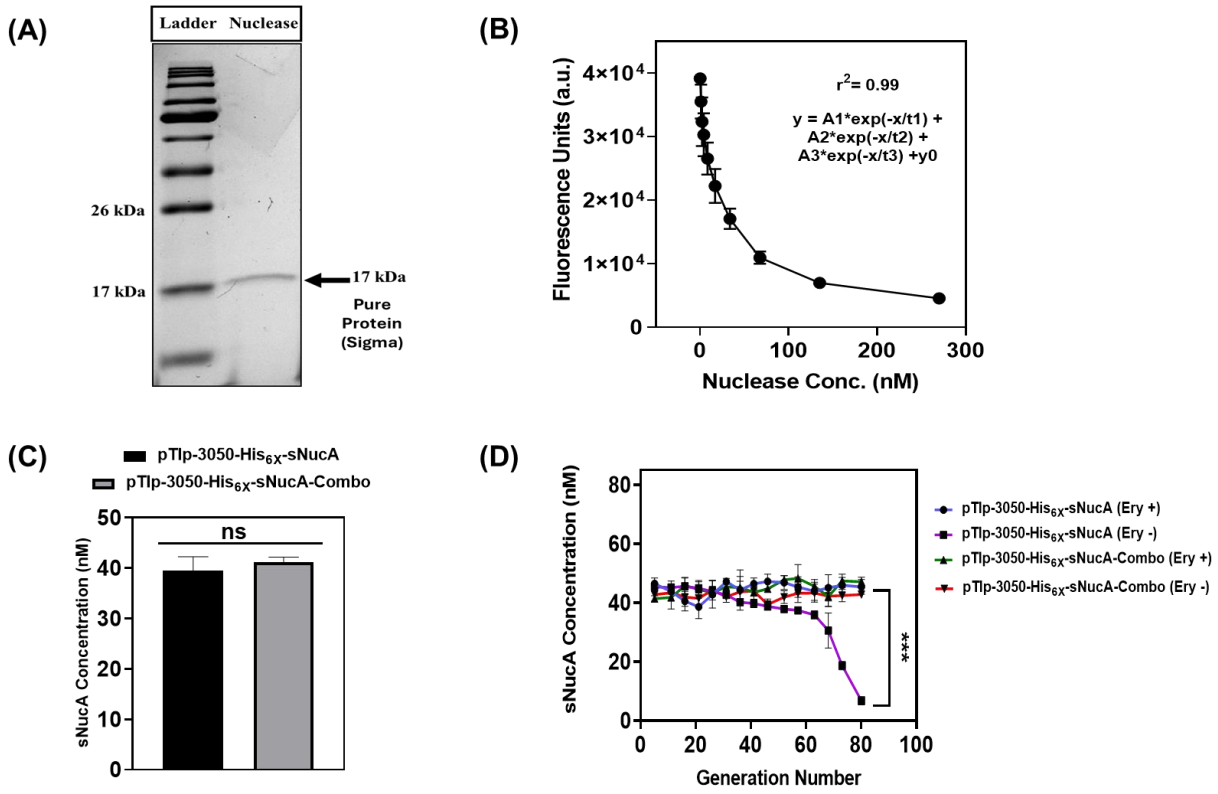

Figure 4. (A) SDS PAGE Image of commercial micrococcal nuclease (Sigma N3755-50UN) after Coomassie staining. The arrow highlights the protein band with a molecular weight of 17 kDa (B) Exponential Decay curve representing the micrococcal nuclease concentration (in nM) on x-axis against the respective fluorescence values (arbitrary units) of the DNAse broth (37°C, 18 h incubation) containing the control strain (Empty Vector, 10 µg/mL Erythromycin) on y-axis. The error bars represent standard deviation based on three independent measurements. The equation is $y = A_1*\exp(-x/t_1) + A_2*\exp(-x/t_2) + A_3*\exp(-x/t_3) + y0$, where $A_1 = 7914.55$, $t_1 = 2.16$, $A_2 = 22601.12$, $t_2 = 36.11$, $A_3 = 16784.16$, $t_3 = 963.89$, $y_0 = -8136.39$ (C) Secreted nuclease concentrations (in nM) from the pTlp-3050-His$_{6X}$-sNucA and pTlp-

3050-His_{6X}-sNucA-Combo recombinant strains in DNAse broth (37°C, 18 h incubation) determined by the standard curve depicted in Figure 4B. The error bars represent standard deviation based on nine independent measurements ($^{ns}p=0.1433$ as calculated by paired t-test) (D) Secreted nuclease concentrations (in nM) from the pTlp-3050-His_{6X}-sNucA and pTlp-3050-His_{6X}-sNucA-Combo recombinant strains in DNAse broth (37°C, 18 h incubation) both in the presence (Ery +) and absence (Ery -) of erythromycin over several generations. The respective nuclease concentrations were determined by the standard curve depicted in Figure 4B. The error bars represent standard deviation based on three independent measurements (***p=0.0004 as calculated by paired t-test).

5.3.3. Optimization of recombinant protein extraction from engineered *L. plantarum* strains

Although the commercial micrococcal nuclease protein was suitable for preliminary estimation of the secreted nuclease concentration, its amino acid sequence partially deviated (~5%) from that of the secreted His_{6X}-sNucA protein. Therefore, I decided to purify the His_{6X}-sNucA protein from the recombinant *L. plantarum* strain for plotting the standard curve, which could provide a more accurate estimation of the His_{6X}-sNucA protein concentration secreted by the bacterial strains into the extracellular media. However, before purifying the His_{6X}-sNucA protein, I needed to optimize the recombinant protein extraction parameters from *L. plantarum* WCFS1. This was because robust extraction of recombinant proteins from Gram-positive bacterial strains, such as *L. plantarum* is known to be relatively more difficult than that of *E. coli* BL21 DE3, a Gram-negative strain commonly used for protein overexpression experiments. Although both bacterial strains possess a cell-wall composed of peptidoglycan encapsulating the inner cytoplasmic membrane, Gram-positive bacteria have a thicker peptidoglycan layer than that of Gram-negative bacteria (Auer and Weibel., 2017). Although this rigid cell wall could be disrupted by using higher lysis energy, it can also negatively impact the stability of the cytosolic proteins and lead to degradation of the recombinant protein. To avoid that, I used the relatively stable mCherry reporter protein (Shaner et al., 2004) for optimizing the cellular lysis parameters and qualitative as well as quantitative detection of the process efficiency across bacterial samples. To obtain purified mCherry, I cloned the His_{6X}-mCherry reporter protein-encoding gene into the pET28 vector backbone and transformed the recombinant pT7-lacO-mCherry plasmid in the ClearColi BL21 strain (**Figure 5A**). Post IPTG induction, the recombinant His_{6X}-mCherry protein (31.1 kDa) was purified from ClearColi using His_{6X}-tag affinity chromatography technique (**Figure 5B**). The purified His_{6X}-mCherry protein was serially diluted in sterile Lysis Buffer containing 1 mM PMSF, and the respective fluorescence values were measured by fluorescence

spectrophotometry. The fluorescence values were plotted against their respective His_{6X}-mCherry protein concentrations (in µM) to plot a standard curve with a linear fitting equation of Y=11267*X (**Figure 5C**).

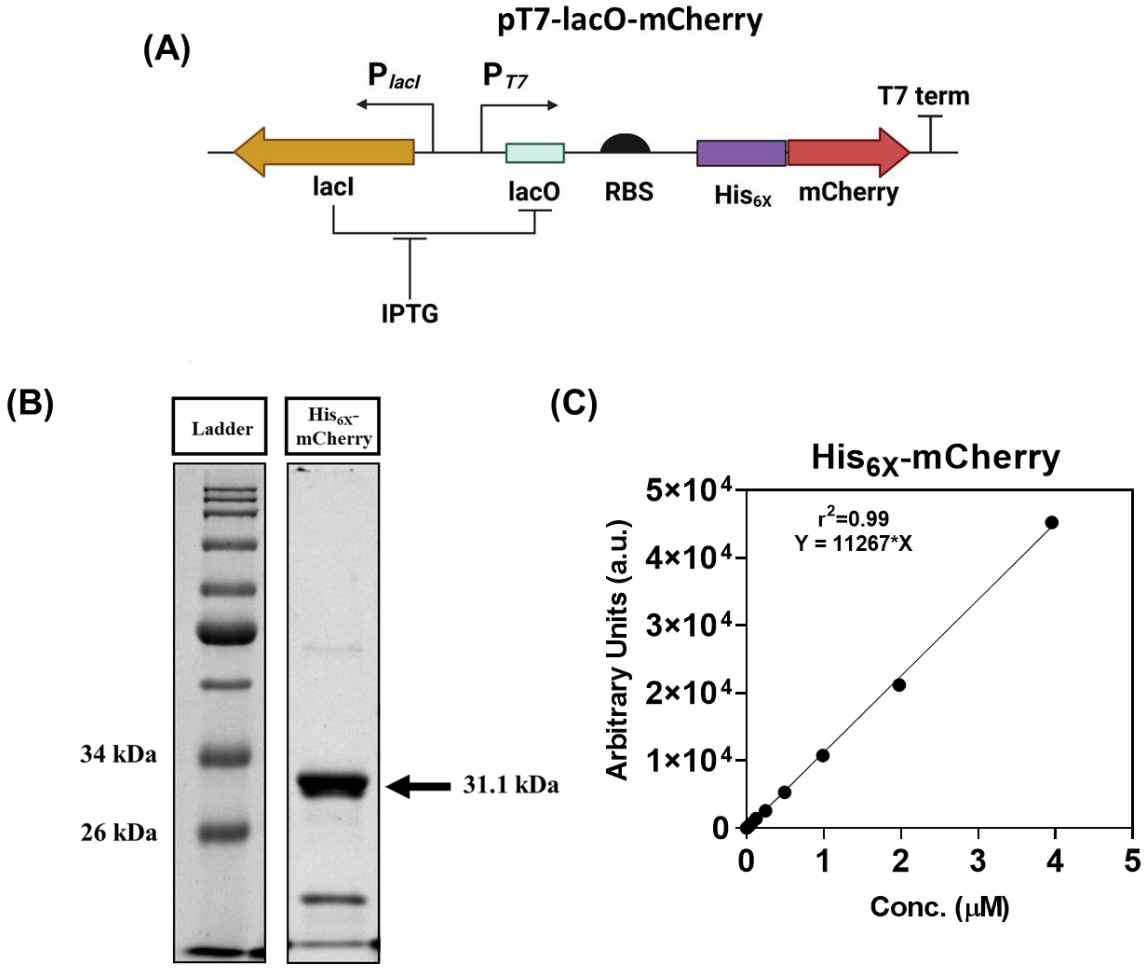

Figure 5. (A) Schematic representation of the pT7-lacO-mCherry genetic module. The mCherry reporter protein is repressed by the lacI protein, and the system is derepressed upon IPTG addition, allowing mCherry production (B) SDS PAGE Image of purified His_{6X}-mCherry protein from ClearColi BL21 using His_{6X}-tag affinity chromatography after Coomassie staining. The arrow highlights the protein band with a molecular weight of 31.1 kDa (C) Standard curve representing the fluorescence values (arbitrary units) against the serially diluted His_{6X}-mCherry protein concentrations (in µM). The linear fitting equation of the curve is Y = 11267*X. The symbols and error bars are merged due to low standard deviation values obtained from three independent measurements.

With the standard curve, the concentration of mCherry reporter protein being released into the lysates after cell homogenization processing could now be determined. Like the previous genetic

design, the pTlp-mCherry-His_{6X} recombinant plasmid was constructed and established in *L. plantarum* WCFS1 (**Figure 6A**). The P_{tlpA} promoter constitutively drove high levels of intracellular mCherry-His_{6X} reporter protein expression that could be visually detected (**Figure 6B**). Initially, I subjected the bacterial biomass to ultrasonic frequency-based cellular homogenization and categorized the sonication process as either "mild sonication" (MS) and "harsh sonication" (HS) [Exact parameters mentioned in the Materials and Methods section]. Both homogenization techniques achieved partial extraction of the recombinant proteins in the cellular lysate (**Figure 6C**). 0.9 µM and 1.8 µM of mCherry protein could be detected in the cellular lysates for the MS and HS cell homogenization techniques respectively. However, a significant amount of the mCherry-His_{6X} protein remained in the bacterial pellet after sonication and could not be released into the soluble lysate fraction (**Figure 6D**). The cellular lysates were further analyzed on SDS-PAGE, and as expected the mCherry-His_{6X} protein band was relatively more prominent for the HS cell homogenization technique in comparison to the bacterial samples subjected to MS (**Figure 6E**).

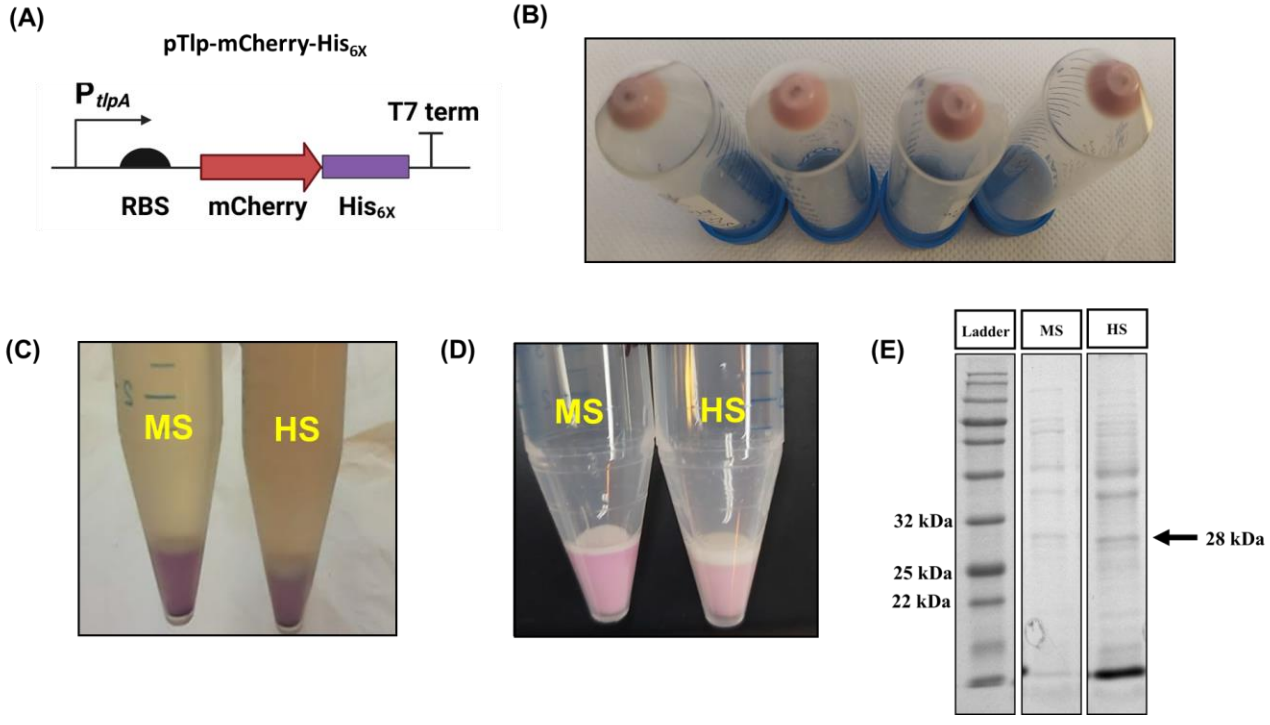

Figure 6. (A) Schematic representation of the pTlp-mCherry-His_{6X} plasmid (B) pTlp-mCherry-His_{6X} plasmid harboring bacterial pellets harvested after 24 h incubation at 37°C. Each 50 mL falcon tube shows

the bacterial pellet harvested from 50 mL of bacterial culture (C) The cellular lysates imaged after subjecting the bacterial pellets (harvested from 100 mL) to "mild sonication" (MS) and "harsh sonication" (HS) ultrasonication based cell homogenization techniques (D) The bacterial pellets imaged after subjecting them to "mild sonication" (MS) and "harsh sonication" (HS) based cell homogenization techniques (E) SDS PAGE image of the soluble lysates after Coomassie staining. The samples are depicted in the following order – Ladder, soluble lysate post Mild Sonication (MS) and soluble lysate post Harsh Sonication (HS) of the pTlp-mCherry-His_{6X} *L. plantarum* WCFS1 strain. The arrow highlights the mCherry-His_{6X} protein band with a molecular weight of 28 kDa.

However, even with harsh ultrasonication technique mCherry-His_{6X} protein could not be efficiently extracted into the soluble cellular lysate fraction. Therefore, I opted for a mechanical shearing-based cellular homogenization method called "bead beating" to extract the mCherry-His_{6X} protein from *L. plantarum*. In previous reports, this method has successfully homogenized similar Gram-positive bacterial strains without causing protein denaturation (Li et al., 2020). Both the Empty Vector and pTlp-mCherry-His_{6X} plasmid harboring *L. plantarum* strains were cultivated (**Figure 7A**) and subjected to "bead beating". Mechanical homogenization of the bacterial biomass was able to extract the mCherry-His_{6X} protein into the soluble fraction (**Figure 7B**) with high efficiency as highlighted by the minimal fluorescence of the pTlp-mCherry-His_{6X} bacterial pellet (**Figure 7C**). Significant amount of the mCherry-His_{6X} protein could be detected in the soluble lysate (3.2 µM) in addition to prominent visualization on the SDS PAGE (**Figure 7D**). These results confirmed that the mechanical disruption was a suitable format to extract recombinant proteins from engineered *L. plantarum* strains with good efficiency. Following cellular homogenization, His_{6X} tag affinity chromatography further facilitated the purification of the recombinant mCherry-His_{6X} protein from the soluble lysate (**Figure 7E**).

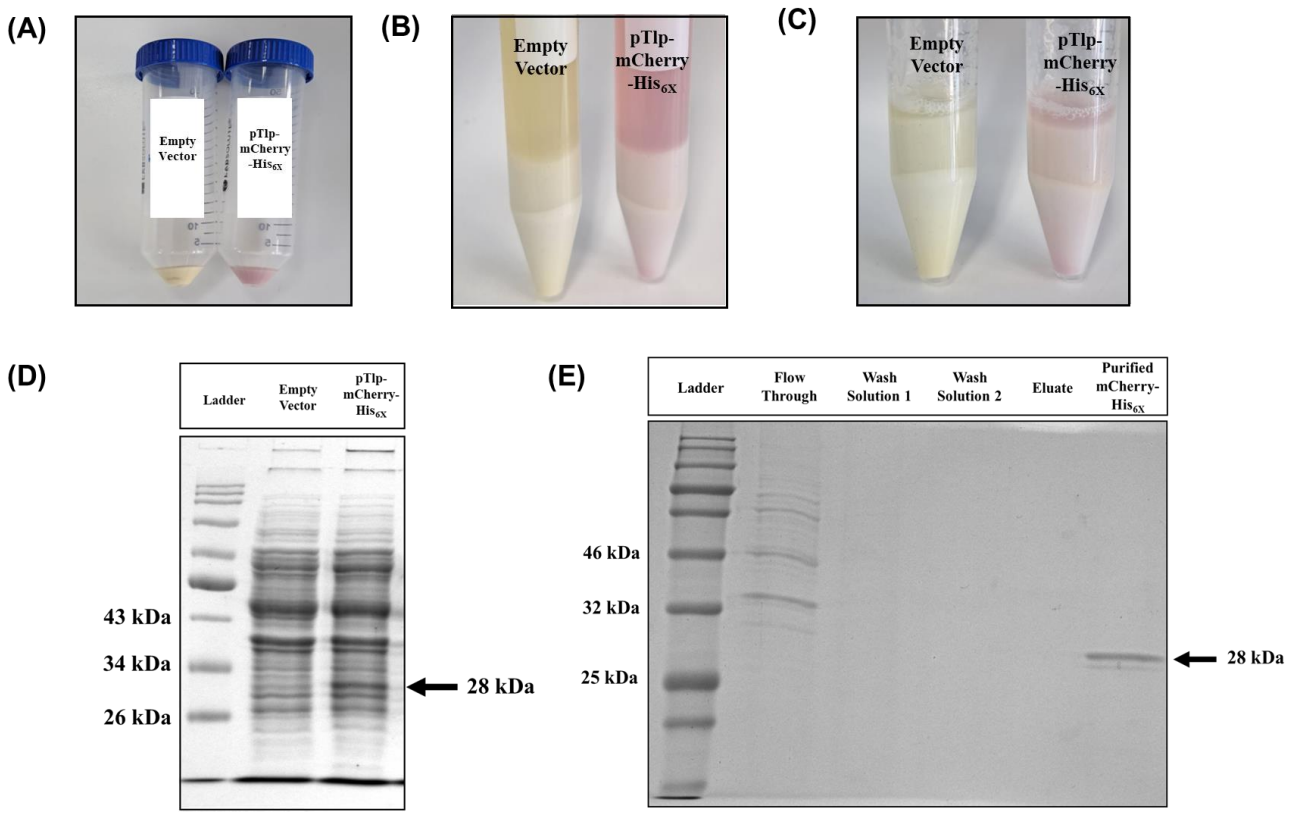

Figure 7. (A) Empty Vector and pTlp-mCherry-His_{6X} plasmid harboring *L. plantarum* WCFS1 bacterial pellets harvested after 24 h incubation at 37°C. Each 50 mL falcon tube shows the bacterial pellet harvested from 100 mL of bacterial culture (B) The cellular lysates (Empty Vector and pTlp-mCherry-His_{6X}) imaged after subjecting the bacterial pellets to mechanical shearing-based cell homogenization – "bead beating" technique (C) The bacterial pellets (Empty Vector and pTlp-mCherry-His_{6X}) imaged after subjecting them to "bead beating" (D) SDS PAGE image of the soluble lysates after Coomassie staining. The samples are depicted in the following order – Ladder, Empty Vector and pTlp-mCherry-His_{6X}. The arrow highlights the mCherry-His_{6X} protein band with a molecular weight of 28 kDa (E) SDS PAGE image of the different fractions collected during His_{6X} tag affinity chromatography-based purification of the mCherry-His_{6X} protein after Coomassie staining. The samples are loaded in the following order – Ladder, Flowthrough, Wash solution 1, Wash solution 2, Eluate and the pure mCherry-His_{6X} protein. The arrow highlights the purified mCherry-His_{6X} protein band with a molecular weight of 28 kDa.

Having optimized the recombinant protein extraction parameters, I proceeded with constructing the pTlp-His_{6X}-sNucA plasmid and established it in *L. plantarum*. This engineered strain allowed the constitutive expression of the His_{6X}-sNucA protein and its intracellular accumulation due to the absence of the signal peptide (Sp_{3050}). Post "bead beating", the recombinant His_{6X}-sNucA protein could be successfully extracted into the soluble lysate and purified by His_{6X} tag affinity chromatography (**Figure 8A**). In addition, the purified His_{6X}-sNucA protein was functionally

active as confirmed by its ability to degrade dsDNA in the DNAse agar (indicated by the halo formation) in comparison to the control buffer PBS (**Figure 8B**).

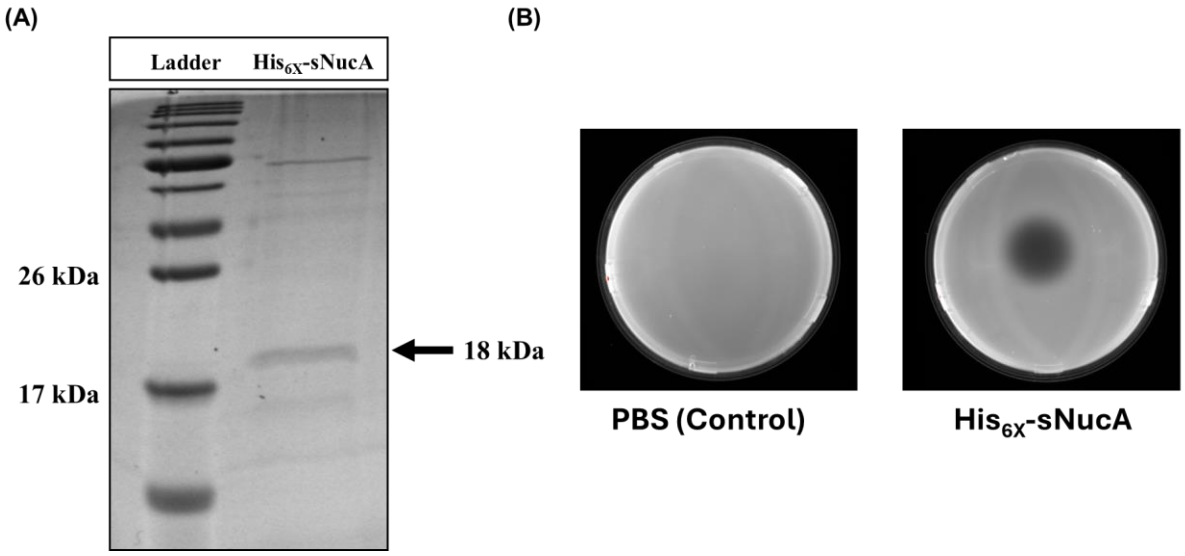

Figure 8. (A) SDS PAGE image of the purified His_{6X}-sNucA protein after Coomassie staining. The arrow highlights the His_{6X}-sNucA protein band with a molecular weight of 18 kDa (B) Cy5 ($Ex_{\lambda}/Em_{\lambda}$=587 nm/625 nm) channel imaging of the control buffer (PBS) and purified recombinant His_{6X}-sNucA protein spotted (10 µL) on DNAse agar after 18 h incubation at 37°C. The halo created by dsDNA degradation present in the agar media confirms that the purified His_{6X}-sNucA protein is functionally active.

5.3.4. Quantitative estimation of His_{6X}-sNucA in optimized cell culture media

My previous experiments confirmed that recombinant *L. plantarum* strains could facilitate His_{6X}-sNucA secretion into bacterial growth media (DNAse Broth). However, for therapeutic applications, the protein secretion capability must be validated in growth media suitable for culturing eukaryotic cell lines. Therefore, I decided to culture the bacterial strains in RPMI-1640 cell culture media, which has been used to assess *Lactobacillus* viability in previous reports (Sun et al., 2013). However, no bacterial growth was observed in the RPMI-1640 media, highlighting that although RPMI media may maintain bacterial viability, it does not support growth efficiently (**Figure 9A, 9B, 9C**). Therefore, it was critical to optimize the nutrient composition of the RPMI-1640 media, so that it could allow bacterial growth as well as be used for culturing mammalian cell lines. To compensate for the nutrient limitation, I modified the RPMI-1640 growth media composition in line with previous reports (Von Feldt et al., 1994). I

created the RPMI-Opti (RPMI-1640 + OPI supplement + MEM non-essential amino acids) and RPMI-Opti-FBS (RPMI-1640 + OPI supplement + MEM non-essential amino acids + Fetal Bovine Serum) formulations by enhancing the RPMI media with supplements that naturally promote eukaryotic cell viability and proliferation. Even though the bacterial growth in RPMI-Opti and RPMI-Opti-FBS media could not surpass MRS growth media, there was significant improvement in their growth pattern in comparison to the unmodified RPMI-1640 media alone (**Figure 9A, 9B, 9C**). In addition to more prominent growth in the RPMI-Opti-FBS media, there was a gradual decrease in bacterial growth for the RPMI-Opti media beyond 12 hours. It is possible that the nutrient content of RPMI-Opti media becomes depleted as the bacteria grow, which can cause a decrease in bacterial metabolism and a transition towards a phase of low cellular viability commonly observed for Gram-negative bacteria (Navarro Llorens et al., 2010). However, this behavior was not observed in the RPMI-Opti-FBS media, suggesting that FBS supplementation significantly enhanced bacterial growth and sustained their viability for more than 20 hours. This may be because FBS contains a wide range of amino acids and vitamins that could support bacterial growth (Gstraunthaler., 2003) as well as proteinaceous growth factors that could be metabolized by *L. plantarum* (Raveschot et al., 2018) to sustain their viability in the nutrient-limiting conditions of the RPMI media.

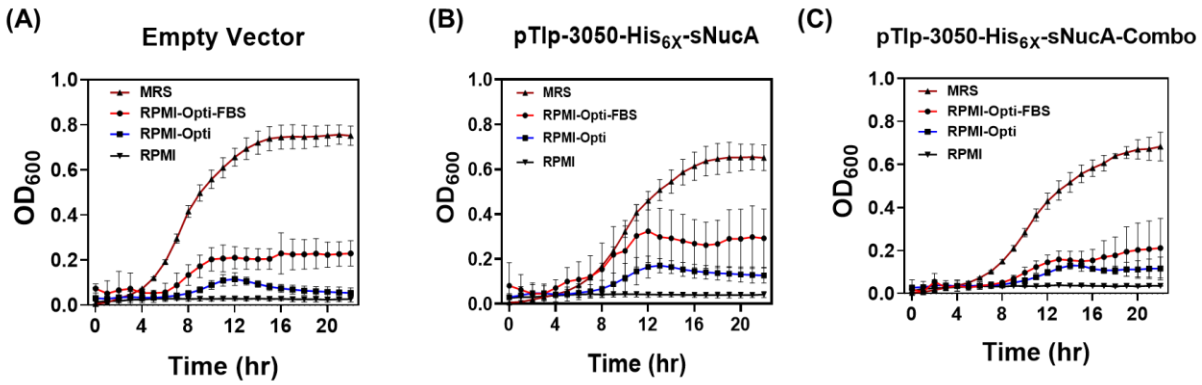

Figure 9. (A) Growth kinetics of Empty Vector plasmid harboring *L. plantarum* WCFS1 strain in MRS media, RPMI-Opti-FBS media, RPMI-Opti media and RPMI Media at 37°C for 22 h. The error bars represent standard deviation based on three independent measurements (B) Growth kinetics of pTlp-3050-His_{6X}-sNucA plasmid harboring *L. plantarum* WCFS1 strain in MRS media, RPMI-Opti-FBS media, RPMI-Opti media and RPMI Media at 37°C for 22 h. The error bars represent standard deviation based on three independent measurements (C) Growth kinetics of pTlp-3050-His_{6X}-sNucA-Combo plasmid harboring *L. plantarum* WCFS1 strain in MRS media, RPMI-Opti-FBS media, RPMI-Opti media

and RPMI Media at 37°C for 22 h. The error bars represent standard deviation based on three independent measurements.

Although bacterial growth was confirmed in RPMI-Opti and RPMI-Opti-FBS media, I still needed to determine the concentration of His_{6X}-sNucA protein secreted by the bacteria in these media. Therefore, an optimized nuclease detection standard curve was plotted by assessing the functional activity of the purified recombinant His_{6X}-sNucA protein in both RPMI-Opti (**Figure 10A**) and RPMI-Opti-FBS (**Figure 10B**) media mixed in a 1:1 ratio with DNAse broth. Like **Figure 4B**, both the standard curves followed an exponential decay function, with decreasing fluorescence values (~$4X10^4$ – $1X10^4$ arbitrary units) of the DNAse broth being observed for increasing concentrations of the His_{6X}-sNucA protein (~0 – 85 nM) and vice versa.

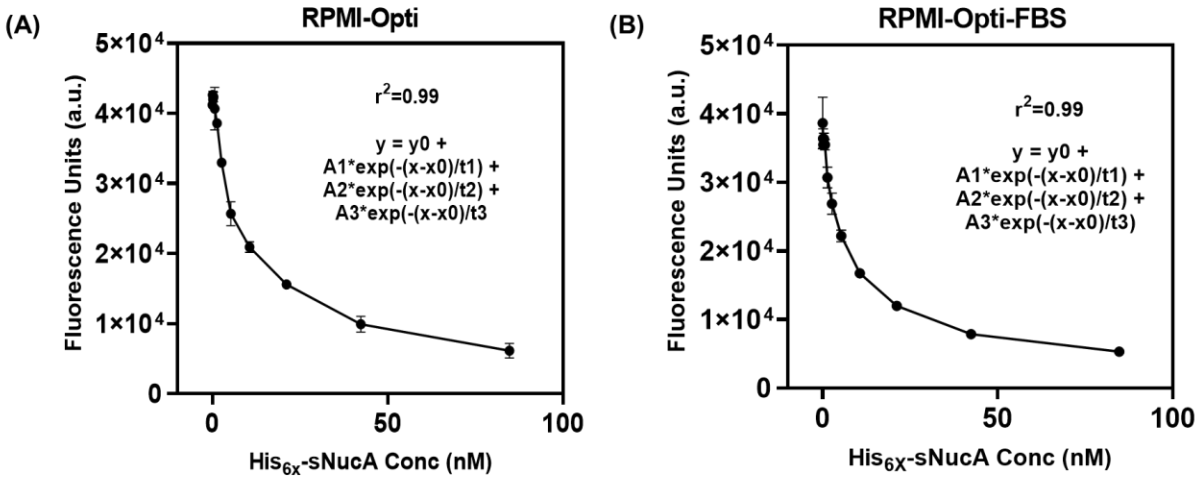

Figure 10. (A) Exponential decay standard curve representing the purified His_{6X}-sNucA protein concentration (in nM) against the respective fluorescence values (arbitrary units) of the RPMI-Opti media + DNAse broth combination (37°C, 18 h incubation), where the cell culture media was initially inoculated with the control strain (Empty Vector, 10 µg/mL Erythromycin). The error bars represent standard deviation based on three independent measurements. The equation is $y = y_0 + A_1*\exp(-(x-x_0)/t_1) + A_2*\exp(-(x-x_0)/t_2) + A_3*\exp(-(x-x_0)/t_3)$, where $y_0 = 4623.23$, $x_0 = 0.35$, $t_1 = 4.55$, $A_2 = 4592.47$, $t_2 = 27.04$, $A_3 = 10709.35$, $t_3 = 27.05$ (B) Exponential decay standard curve representing the purified His_{6X}-sNucA protein concentration (in nM) against the respective fluorescence values (arbitrary units) of the RPMI-Opti-FBS media + DNAse broth combination (37°C, 18 h incubation), where the cell culture media was initially inoculated with the control strain (Empty Vector, 10 µg/mL Erythromycin). The error bars represent standard deviation based on three independent measurements. The equation is $y = y_0 + A_1*\exp(-(x-x_0)/t_1) + A_2*\exp(-(x-x_0)/t_2) + A_3*\exp(-(x-x_0)/t_3)$, where $y_0 = 342.81$, $x_0 = 1.36$, $t_1 = 6.95$, $A_2 = 7245.48$, $t_2 = 70.69$, $A_3 = 11254.13$, $t_3 = 70.38$.

Secreted His_{6X}-sNucA protein concentrations from the engineered *L. plantarum* strains harboring the pTlp-3050-His_{6X}-sNucA and pTlp-3050-His_{6X}-sNucA-Combo plasmids were assessed with the optimized nuclease quantification assay. Using the standard curve equation; $y = y_0 + A_1*\exp(-(x-x_0)/t_1) + A_2*\exp(-(x-x_0)/t_2) + A_3*\exp(-(x-x_0)/t_3)$, where $y_0 = 4623.23$, $x_0 = 0.35$, $t_1 = 4.55$, $A_2 = 4592.47$, $t_2 = 27.04$, $A_3 = 10709.35$, $t_3 = 27.05$, I estimated that the **pTlp-3050-His_{6X}-sNucA** and **pTlp-3050-His_{6X}-sNucA-Combo** strain secreted **~4.2 ± 0.1 nM** and **~2.9 ± 0.2 nM** of His_{6X}-sNucA protein into the **RPMI-Opti media** (**Figure 11A; Figure 11B**). However, when cultivated in **RPMI-Opti-FBS media** and determined using the standard curve equation; $y = y_0 + A_1*\exp(-(x-x_0)/t_1) + A_2*\exp(-(x-x_0)/t_2) + A_3*\exp(-(x-x_0)/t_3)$, where $y_0 = 342.81$, $x_0 = 1.36$, $t_1 = 6.95$, $A_2 = 7245.48$, $t_2 = 70.69$, $A_3 = 11254.13$, $t_3 = 70.38$, both **pTlp-3050-His_{6X}-sNucA** and **pTlp-3050-His_{6X}-sNucA-Combo** strains secreted **~75.8 ± 1.9 nM** and **~72.8 ± 2.3 nM** of His_{6X}-sNucA protein in the extracellular media (**Figure 11A; Figure 11B**). The results confirmed that in addition to supporting bacterial growth and viability, FBS-supplemented growth media could significantly enhance protein secretion levels from the recombinant strains. Next, I assessed whether the absence of antibiotic supplementation in the growth media (RPMI-Opti-FBS) would decrease the concentration of secreted His_{6X}-sNucA protein compared to antibiotic presence. No significant difference in the secreted His_{6X}-sNucA protein concentration was observed for the pTlp-3050-His_{6X}-sNucA and pTlp-3050-His_{6X}-sNucA-Combo strains in either condition (with and without antibiotic supplementation) within the 24 hour growth period, representing ~6-8 bacterial generations (**Figure 11C; Figure 11D**). This result further validated my previous observation (**Figure 4D**), where a significant difference in the secreted protein concentrations could only be observed after several generations of the recombinant strains (pTlp-3050-His_{6X}-sNucA and pTlp-3050-His_{6X}-sNucA-Combo).

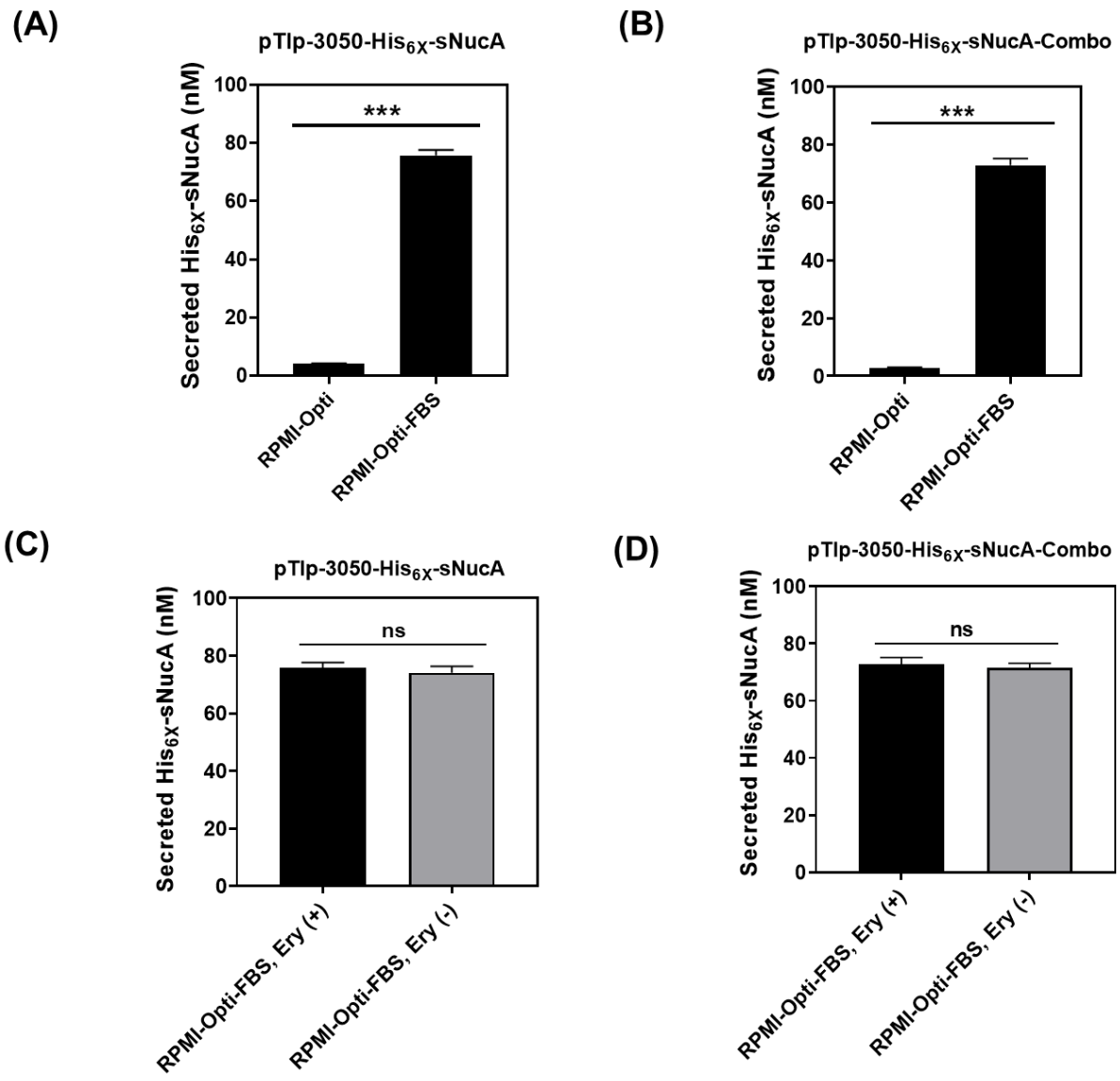

Figure 11. (A) Concentration of secreted His_{6X}-sNucA protein (in nM) by the pTlp-3050-His_{6X}-sNucA plasmid harboring *L. plantarum* strain in RPMI-Opti and RPMI-Opti-FBS media. The error bars represent standard deviation based on three independent measurements (***p=0.0002 as calculated by paired t-test) (B) Concentration of secreted His_{6X}-sNucA protein (in nM) by the pTlp-3050-His_{6X}-sNucA-Combo plasmid harboring *L. plantarum* strain in RPMI-Opti and RPMI-Opti-FBS media. The error bars represent standard deviation based on three independent measurements (***p=0.0003 as calculated by paired t-test) (C) Concentration of secreted His_{6X}-sNucA protein (in nM) by the pTlp-3050-His_{6X}-sNucA plasmid harboring *L. plantarum* strain in RPMI-Opti-FBS media both with (Ery +) and without (Ery -) antibiotic supplementation. The error bars represent standard deviation based on three independent measurements (^{ns}p=0.4163 as calculated by paired t-test) (D) Concentration of secreted His_{6X}-sNucA protein (in nM) by the pTlp-3050-His_{6X}-sNucA-Combo plasmid harboring *L. plantarum* strain in RPMI-Opti-FBS media both with (Ery +) and without (Ery -) antibiotic supplementation. The error bars represent standard deviation based on three independent measurements (^{ns}p=0.4341 as calculated by paired t-test).

5.4. Conclusion

In this chapter, I demonstrated the P_{tlpA} promoter-based expression and extracellular secretion of the Staphylococcal nuclease (sNucA) protein from *L. plantarum* WCFS1. In addition, the quantitative detection of the secreted nuclease showed that the "Combo" toxin-antitoxin genetic module could enable the retention of the recombinant plasmid for >80 generations without the need for antibiotic supplementation. Finally, the optimized nuclease bioactivity assay helped to assess the secreted sNucA titers in media formulations suitable for mammalian cell culture studies. Overall, the insights presented in this study confirm that the recently discovered genetic parts (P_{tlpA} promoter and "Combo" toxin-antitoxin genetic module) can facilitate both sustained protein production and stable plasmid retention in engineered *L. plantarum* WCFS1 strains.

5.5. References

1. Tian, L., Zhao, R., Xu, X., Zhou, Z., Xu, X., Luo, D., Zhou, Z., Liu, Y., Kushmaro, A., Marks, R.S. and Dinnyés, A., 2023. Modulatory effects of Lactiplantibacillus plantarum on chronic metabolic diseases. *Food Science and Human Wellness*, *12*(4), pp.959-974.
2. Stamper, C.E., Hoisington, A.J., Gomez, O.M., Halweg-Edwards, A.L., Smith, D.G., Bates, K.L., Kinney, K.A., Postolache, T.T., Brenner, L.A., Rook, G.A.W. and Lowry, C.A., 2016. The microbiome of the built environment and human behavior: implications for emotional health and well-being in postmodern western societies. *International Review of Neurobiology*, *131*, pp.289-323.
3. Debnath, N., Yadav, P., Mehta, P.K., Gupta, P., Kumar, D., Kumar, A., Gautam, V. and Yadav, A.K., 2024. Designer probiotics: Opening the new horizon in diagnosis and prevention of human diseases. *Biotechnology and Bioengineering*, *121*(1), pp.100-117.
4. Singh, B., Mal, G. and Marotta, F., 2017. Designer probiotics: paving the way to living therapeutics. *Trends in Biotechnology*, *35*(8), pp.679-682.
5. Charbonneau, M.R., Isabella, V.M., Li, N. and Kurtz, C.B., 2020. Developing a new class of engineered live bacterial therapeutics to treat human diseases. Nature Communications, 11(1), p.1738.
6. Rud, I., Jensen, P.R., Naterstad, K. and Axelsson, L., 2006. A synthetic promoter library for constitutive gene expression in Lactobacillus plantarum. *Microbiology*, *152*(4), pp.1011-1019.
7. Mathiesen, G., Sveen, A., Brurberg, M.B., Fredriksen, L., Axelsson, L. and Eijsink, V.G., 2009. Genome-wide analysis of signal peptide functionality in Lactobacillus plantarum WCFS1. *BMC genomics*, *10*, pp.1-13.
8. Kleerebezem, M., Boekhorst, J., Van Kranenburg, R., Molenaar, D., Kuipers, O.P., Leer, R., Tarchini, R., Peters, S.A., Sandbrink, H.M., Fiers, M.W. and Stiekema, W., 2003. Complete

genome sequence of Lactobacillus plantarum WCFS1. *Proceedings of the National Academy of Sciences*, *100*(4), pp.1990-1995.

9. Karlskås, I.L., Maudal, K., Axelsson, L., Rud, I., Eijsink, V.G. and Mathiesen, G., 2014. Heterologous protein secretion in lactobacilli with modified pSIP vectors. *PLOS one*, *9*(3), p.e91125.
10. Tran, A.M., Unban, K., Kanpiengjai, A., Khanongnuch, C., Mathiesen, G., Haltrich, D. and Nguyen, T.H., 2021. Efficient secretion and recombinant production of a lactobacillal α-amylase in Lactiplantibacillus plantarum WCFS1: analysis and comparison of the secretion using different signal peptides. *Frontiers in Microbiology*, *12*, p.689413.
11. Dey, S., Blanch-Asensio, M., Balaji Kuttae, S. and Sankaran, S., 2023. Novel genetic modules encoding high-level antibiotic-free protein expression in probiotic lactobacilli. *Microbial Biotechnology*, *16*(6), pp.1264-1276.
12. Russo, P., Iturria, I., Mohedano, M.L., Caggianiello, G., Rainieri, S., Fiocco, D., Angel Pardo, M., López, P. and Spano, G., 2015. Zebrafish gut colonization by mCherry-labelled lactic acid bacteria. *Applied microbiology and biotechnology*, *99*, pp.3479-3490.
13. Berlec, A., Završnik, J., Butinar, M., Turk, B. and Štrukelj, B., 2015. In vivo imaging of Lactococcus lactis, Lactobacillus plantarum and Escherichia coli expressing infrared fluorescent protein in mice. *Microbial cell factories*, *14*, pp.1-14.
14. Nguyen, T.T., Mathiesen, G., Fredriksen, L., Kittl, R., Nguyen, T.H., Eijsink, V.G., Haltrich, D. and Peterbauer, C.K., 2011. A food-grade system for inducible gene expression in Lactobacillus plantarum using an alanine racemase-encoding selection marker. *Journal of agricultural and food chemistry*, *59*(10), pp.5617-5624.
15. Sak-Ubol, S., Namvijitr, P., Pechsrichuang, P., Haltrich, D., Nguyen, T.H., Mathiesen, G., Eijsink, V.G. and Yamabhai, M., 2016. Secretory production of a beta-mannanase and a chitosanase using a Lactobacillus plantarum expression system. *Microbial Cell Factories*, *15*, pp.1-12.
16. Shortle, D., 1995. Staphylococcal nuclease: a showcase of m-value effects. *Advances in protein chemistry*, *46*, pp.217-247.
17. Taniuchi, H.I.R.O.S.I.I. and Anfinsen, C.B., 1969. An experimental approach to the study of the folding of staphylococcal nuclease. *Journal of Biological Chemistry*, *244*(14), pp.3864-3875.
18. Blanch-Asensio, M., Dey, S. and Sankaran, S., 2023. In vitro assembly of plasmid DNA for direct cloning in Lactiplantibacillus plantarum WCSF1. *PLOS one*, *18*(2), p.e0281625.
19. Li, X., Xing, Y., Guo, L., Lv, X., Song, H. and Xi, T., 2014. Oral immunization with recombinant Lactococcus lactis delivering a multi-epitope antigen CTB-UE attenuates Helicobacter pylori infection in mice. *Pathogens and disease*, *72*(1), pp.78-86.
20. Beidler, J.L., Hilliard, P.R. and Rill, R.L., 1982. Ultrasensitive staining of nucleic acids with silver. *Analytical biochemistry*, *126*(2), pp.374-380.
21. Auer, G.K. and Weibel, D.B., 2017. Bacterial cell mechanics. *Biochemistry*, *56*(29), pp.3710-3724.

22. Shaner, N.C., Campbell, R.E., Steinbach, P.A., Giepmans, B.N., Palmer, A.E. and Tsien, R.Y., 2004. Improved monomeric red, orange and yellow fluorescent proteins derived from Discosoma sp. red fluorescent protein. *Nature biotechnology*, *22*(12), pp.1567-1572.
23. Li, X., Bosch-Tijhof, C.J., Wei, X., de Soet, J.J., Crielaard, W., Loveren, C.V. and Deng, D.M., 2020. Efficiency of chemical versus mechanical disruption methods of DNA extraction for the identification of oral Gram-positive and Gram-negative bacteria. *Journal of International Medical Research*, *48*(5), p.0300060520925594.
24. Sun, K., Xie, C., Xu, D., Yang, X., Tang, J. and Ji, X., 2013. Lactobacillus isolates from healthy volunteers exert immunomodulatory effects on activated peripheral blood mononuclear cells. *Journal of biomedical research*, *27*(2), p.116.
25. Von Feldt, J.M., Monfardini, C., Kieber-Emmons, T., Voel, D., Weiner, D.B. and Williams, W.V., 1994. Granulocyte-macrophage colony-stimulating factor mimicry and receptor interactions. *Immunologic research*, *13*, pp.96-109.
26. Navarro Llorens, J.M., Tormo, A. and Martínez-García, E., 2010. Stationary phase in gram-negative bacteria. *FEMS microbiology reviews*, *34*(4), pp.476-495.
27. Gstraunthaler, G., 2003. Alternatives to the use of fetal bovine serum: serum-free cell culture. *ALTEX-Alternatives to animal experimentation*, *20*(4), pp.275-281.
28. Raveschot, C., Cudennec, B., Coutte, F., Flahaut, C., Fremont, M., Drider, D. and Dhulster, P., 2018. Production of bioactive peptides by Lactobacillus species: from gene to application. *Frontiers in Microbiology*, *9*, p.409606.

CONCLUSION AND OUTLOOK

This doctoral thesis discusses advancements toward improving the functionality of bacterial species as therapeutic agents. Two well-characterized probiotic bacteria, *E. coli* Nissle 1917 and *L. plantarum* WCFS1, were chosen as promising candidates for developing genetic circuits compatible with therapeutic production. The main outcomes of this thesis are: 1) A genetic circuit enabling stringent control over the production of the post-translationally modified peptide antibiotic, darobactin in *E. coli* Nissle 1917, and 2) Expansion of the genetic toolbox for recombinant protein expression and secretion in *L. plantarum* WCFS1.

Valuable insights from the first outcome are:

1. *E. coli* Nissle 1917 can facilitate the production and release of darobactin without observably experiencing its antimicrobial activity.
2. The temperature-responsive repressor $TlpA_{39}$ offers better regulation of recombinant protein expression with lower leaky expression compared to the IPTG-LacI-based system.
3. The thermo-amplifier genetic circuit results in minimal expression of darobactin at 37°C but can produce darobactin concentrations of up to ~4 µg/mL when incubated at 40°C.
4. Incubating the thermo-amplifier strain for 6 hours at 40°C can produce enough darobactin to inhibit the Gram-negative opportunistic pathogen, *P. aeruginosa* PAO1.
5. The type II toxin-antitoxin module, Txe-Axe, allows for stable plasmid retention for over 50 bacterial generations without antibiotic selection pressure.
6. Darobactin production by the thermo-amplifier strain can be sustained under harsh conditions, such as bile supplementation, and with limited nutrient composition, such as minimal media.

The thermo-amplifier genetic circuit provides precise control over the expression of recombinant proteins, overcoming a major limitation of "stimuli-responsive" bacterial therapeutics. The genetic circuit repressed darobactin production at 37°C and activated darobactin production at 40°C, representing the physiological and fever-associated temperatures in humans, respectively. Although *in-vitro* testing cannot predict the behavior of bacterial therapeutics in disease-related conditions, it provides evidence that the engineered strain could respond to a real-time increase in temperature associated to severe infections

caused by gastrointestinal pathogens (**Figure 1**). Upon host administration, the thermo-amplifier *E. coli* Nissle 1917 strain can sense the increased temperature and activate darobactin production. Darobactin, when released at the site of infection, can selectively eliminate fever-inducing gastrointestinal pathogens without considerably compromising the natural host microbiome. Once the infection subsides, the body temperature will return to normal, stopping further production of darobactin. Such a platform can be further adapted to control the production of potent antimicrobials targeting a wide range of pathogens and to mitigate chronic infectious disease in the body.

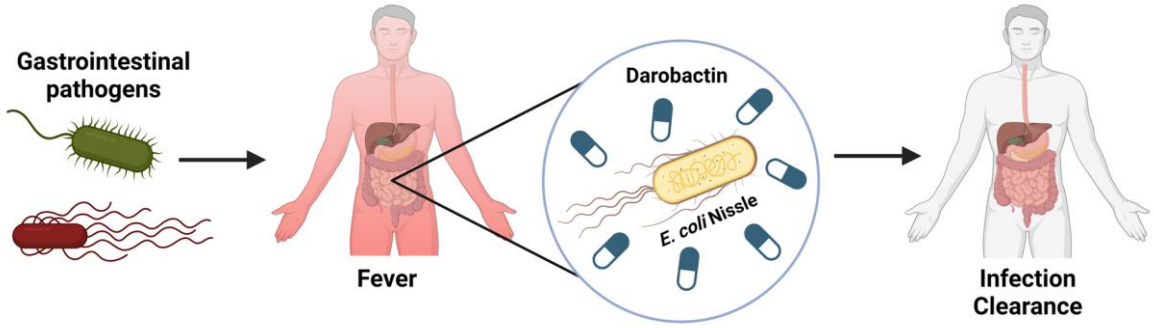

Figure 1. Schematic of the potential application for the thermo-amplifier circuit-based bacterial therapeutic: Gastrointestinal pathogens trigger fever-like conditions in the host, activating the engineered strain to release darobactin at the target site. Darobactin eliminates bacterial pathogens, helps clear infections, and facilitates thermal homeostasis in the host.

Valuable insights from the second outcome are:-

1. The *S. typhimurium* promoter, P_{tlpA}, has high transcriptional strength for recombinant protein expression in *L. plantarum* WCFS1.
2. Combining type II toxin-antitoxin (TA) modules - MazF/MazE and YafQ/DinJ created the "Combo" module. This combination promoted stable plasmid retention and protein production (mCherry) in *L. plantarum* WCFS1 for over 60 bacterial generations, without antibiotic selection pressure.
3. Extracellular secretion of Staphylococcal nuclease (sNucA) could be sustained from *L. plantarum* WCFS1 for over 80 generations using the "Combo" toxin-antitoxin module without antibiotic selection pressure.

4. In vitro characterization of secreted sNucA in mammalian cell culture media indicates that the protein is functionally active in degrading eukaryotic double-stranded DNA (dsDNA).

Cystic fibrosis (CF) patients typically experience the build-up of thick mucus that blocks their respiratory airways, leading to breathing difficulties and severe inflammation. Inflammatory cascade leads to active recruitment of circulating neutrophils in the respiratory tract, resulting in a significant upregulation of NETosis. During NETosis, neutrophils release dense chromatin fiber meshworks, known as neutrophil extracellular traps (NETs), into the surrounding microenvironment (**Figure 2A**) (Martínez-Alemán et al., 2017). These NETs further support the structural integrity of the mucosal layer in the respiratory tract, worsening the disease. One strategy that has shown clinical success in degrading these NETs in the purulent sputum of cystic fibrosis patients involves using the recombinant human DNase I enzyme. This recombinant enzyme (Pulmozyme®) significantly improved the lung function of pediatric and adult cystic fibrosis patients and is currently marketed by Genentech, USA, as an inhalation solution.

Recent reports demonstrate that sNucA can also aid in the efficient degradation of NETs under *in-vivo* conditions. *L. lactis* strains engineered to secrete sNucA were able to disrupt NET formation in the gut of Type I diabetes mouse models, reduce immune cell infiltration in pancreatic islets, and regulate the overall blood glucose level after oral delivery (Lang et al., 2017; Liang et al., 2019). In an independent study, an engineered strain of *L. plantarum* WCFS1 secreted the nanoluciferase reporter protein into the mice's respiratory tract without showing any adverse effects or signs of respiratory infection (Brasino et al., 2023). These studies suggest that a genetically modified *L. plantarum* strain that drives constitutive sNucA secretion could facilitate NET degradation and eventual mucus clearance from the respiratory tract (**Figure 2B**). Although sNucA-based NET degradation may not be as efficient as Pulmozyme® (Human DNAse-I), such an approach can be cost-effective and adjusted according to disease severity. Despite limitations, the constitutive expression of proteins from non-model microbes holds potential for therapeutic applications.

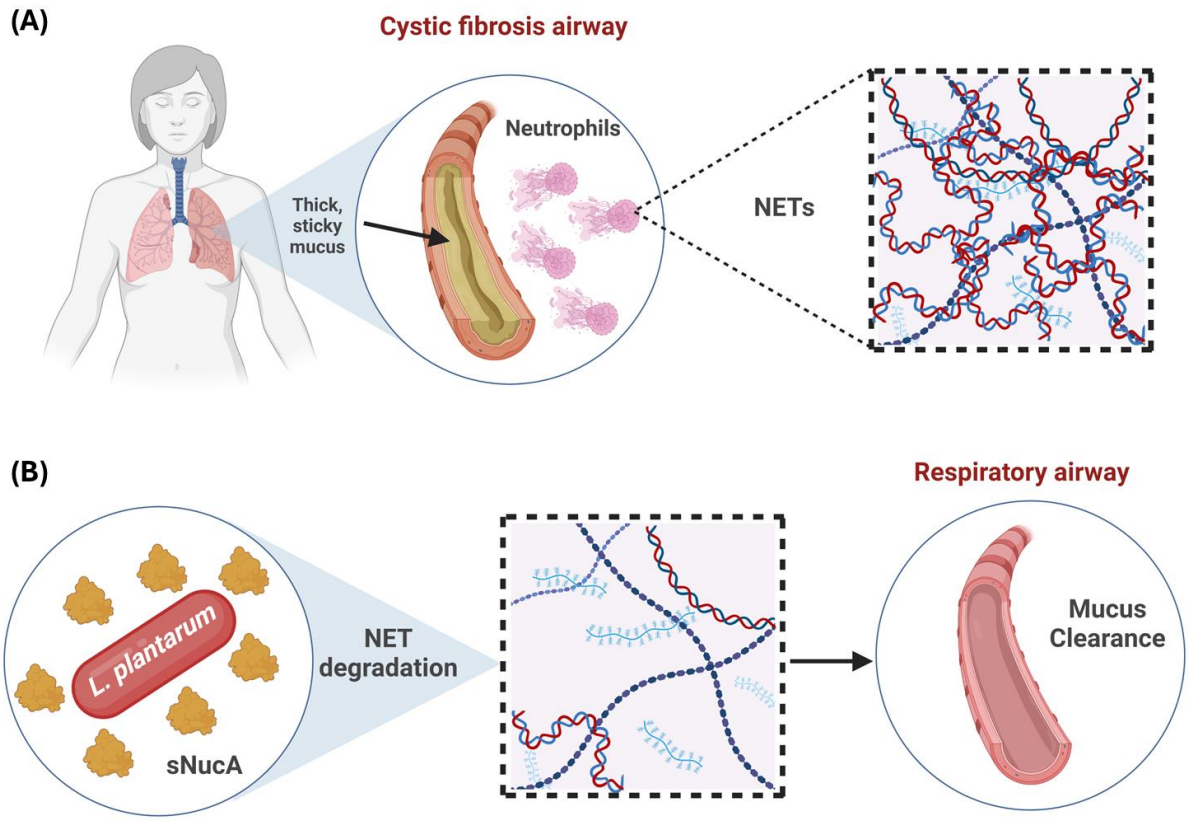

Figure 2. (A) Cystic fibrosis (CF) is characterized by the overproduction of thick mucus, which blocks the respiratory airway and causes severe breathing problems in the patient. Circulating neutrophils are recruited to the respiratory tract and undergo NETosis. The release of free DNA leads to the accumulation of Neutrophil Extracellular Traps (NETs) in the mucus, exacerbating respiratory difficulties (B) Schematic illustrating the potential use of the *Lactiplantibacillus plantarum* strain engineered for constitutive secretion of the Staphylococcal nuclease (sNucA) protein. sNucA degrades free DNA, disrupts NETs, and assists in mucus clearance from the respiratory airway to improve breathing in cystic fibrosis patients.

References

1. Martínez-Alemán, S.R., Campos-García, L., Palma-Nicolas, J.P., Hernández-Bello, R., González, G.M. and Sánchez-González, A., 2017. Understanding the entanglement: neutrophil extracellular traps (NETs) in cystic fibrosis. *Frontiers in cellular and infection microbiology*, *7*, p.104.
2. Lang, J., Wang, X., Liu, K., He, D., Niu, P., Cao, R., Jin, L. and Wu, J., 2017. Oral delivery of staphylococcal nuclease by Lactococcus lactis prevents type 1 diabetes mellitus in NOD mice. *Applied microbiology and biotechnology*, *101*, pp.7653-7662.
3. Liang, Y., Wang, X., He, D., You, Q., Zhang, T., Dong, W., Fei, J., Xing, Y. and Wu, J., 2019. Ameliorating gut microenvironment through staphylococcal nuclease-mediated intestinal NETs degradation for prevention of type 1 diabetes in NOD mice. *Life sciences*, *221*, pp.301-310.
4. Brasino, M., Wagnell, E., Manalo, E.C., Drennan, S., Fischer, J.M. and Merritt, J., 2023. Engineered Lactiplantibacillus plantarum as a Biosensor Probe for the Lungs. *bioRxiv*, pp.2023-09.

LIST OF SCIENTIFIC CONTRIBUTIONS

ARTICLES

1. **Sourik Dey** and Shrikrishnan Sankaran., 2024. Engineered bacterial therapeutics with material solutions. (Manuscript accepted for publication in *Trends in Biotechnology*)

2. **Sourik Dey** and Shrikrishnan Sankaran., 2024. Sustainable protein regeneration in encapsulated materials. *Cell Systems*, *15*(3), pp.211-212.

3. **Sourik Dey**., Carsten E. Seyfert., Claudia Fink-Straube., Andreas M. Kany., Rolf Müller and Shrikrishnan Sankaran., 2024. Thermally activated antibiotic production by probiotic bacteria for pathogen elimination. *bioRxiv*, pp.2024-02.

4. Marc Blanch-Asensio., **Sourik Dey**., Varun Sai Tadimarri and Shrikrishnan Sankaran., 2024. Expanding the genetic programmability of Lactiplantibacillus plantarum. *Microbial Biotechnology*, *17*(1), p.e14335.

5. Selim Basaran., **Sourik Dey**., Shardul Bhusari., Shrikrishnan Sankaran and Tobias Kraus., 2023. Plasmonic stimulation of gold nanorods for the photothermal control of engineered living materials. *Biomaterials Advances*, *147*, p.213332.

6. Marc Blanch-Asensio*., **Sourik Dey*** and Shrikrishnan Sankaran., 2023. In vitro assembly of plasmid DNA for direct cloning in Lactiplantibacillus plantarum WCSF1. *PLOS one*, *18*(2), p.e0281625. **(*equal contribution)**

7. **Sourik Dey*.,** Marc Blanch-Asensio*., Sanjana Balaji Kuttae and Shrikrishnan Sankaran., 2023. Novel genetic modules encoding high-level antibiotic-free protein expression in probiotic lactobacilli. *Microbial Biotechnology*, *16*(6), pp.1264-1276. **(*equal contribution)**

PATENT APPLICATION

1. **Sourik Dey*.,** Marc Blanch-Asensio* and Shrikrishnan Sankaran*. **"Novel genetic tools for Lactobacillus" / "Neuartige genetische Werkzeuge"** – Patent Application No. PCT/EP2023/068901– International Registration Date - July 7, 2023 (Status - Patent Filed, *equal entitlement as co-inventors)

SCIENTIFIC TALKS

1. **Sourik Dey**, Carsten E. Seyfert, Selim Basaran, Rolf Müller, Tobias Kraus, Shrikrishnan Sankaran (2023) **Thermoresponsive Living Therapeutic Materials** - International Synthetic Biology Workshop, Sense-Compute-Response Paradigm - 21.03.2023, Darmstadt, Germany
2. Marc Blanch-Asensio*, **Sourik Dey***, and Shrikrishnan Sankaran (2022) **Novel genetic modules encoding high-level antibiotic-free protein expression in probiotic Lactobacillus -** Symposium on Synthetic and Systems Biology (BioSynSys) **–** 14.09.2022, Paris, France (*co-presentors)
3. Christoph Porten*, **Sourik Dey***, and Selim Basaran* (2022) **Opto-thermally regulated release of novel antibiotics from ELMs -** 3rd International Conference on Engineered Living Materials **–** 23.06.2022, Saarbrücken, Germany (*co-presentors)
4. **Sourik Dey**, Carsten E. Seyfert, Rolf Müller, Shrikrishnan Sankaran (2021) **Thermoresponsive living therapeutic materials – Darobactin releasing bacterial hydrogels for treating chronic pathogenic infections (Flash Talk)** - German Conference on Synthetic Biology – Engineering Living Systems **-** 13.09.2021, Virtual

POSTER PRESENTATIONS

1. **Sourik Dey**, Varun Sai Tadimarri, Ketaki Deshpande, Sara Trujillo Muñoz, Shrikrishnan Sankaran (2023) **Engineering *Lactiplantibacillus plantarum* for mediating anti-inflammatory responses** - 14th International Symposium on Lactic Acid Bacteria – 28.08.2023, Egmond aan Zee, The Netherlands **(Received the GradUS Global Funding Support of 800 Euros)**
2. **Sourik Dey**, Carsten E. Seyfert, Selim Basaran, Rolf Müller, Tobias Kraus, Shrikrishnan Sankaran (2023) **Remote controlled Living Therapeutic Materials for pathogen elimination** - LSC Summer School on Engineered Living Materials – 03.07.2023, Nonnweiler, Germany
3. **Sourik Dey**, Carsten E. Seyfert, Selim Basaran, Rolf Müller, Tobias Kraus, Shrikrishnan Sankaran (2023) **Thermoresponsive Living Therapeutic Materials - Darobactin-Releasing Bacterial Hydrogels for Treating Chronic Pathogenic Infections** - Synthetic Biology: Engineering, Evolution & Design (SEED) Conference – 01.06.2023, Los Angeles, USA **(Received the AICHE Funding Travel Grant of 1,000 USD)**

4. **Sourik Dey**, Carsten E. Seyfert, Rolf Müller and Shrikrishnan Sankaran (2022) **Thermoresponsive living therapeutic materials –Darobactin releasing bacterial hydrogels for treating chronic pathogen infections -** 3rd International Conference on Engineered Living Materials **–** 21.06.2022 **-** 23.06.2022, Saarbrücken, Germany
5. **Sourik Dey** and Shrikrishnan Sankaran (2021) T**hermoresponsive living therapeutic materials – Darobactin releasing bacterial hydrogels for treating chronic pathogenic infections** - German Conference on Synthetic Biology – Engineering Living Systems – 13.09.2021 – 17.09.2021 (Virtual)

MASTER THESIS SUPERVISION

1. Postgraduate Dissertation of Ms. Sanjana Balaji Kuttae, M.Sc. Bioinformatics, Saarland University (2023) **Computational and Experimental Characterization of Optogenetic Systems in *E. coli*** (DOI: 10.13140/RG.2.2.11461.46562)

PARTICIPATION IN WORKSHOPS

1. **Sourik Dey***, Lea Duttenhofer and Shrikrishnan Sankaran (2023) **Business Model Pitch on the topic "Cervo-HEALTH – An innovative model to prevent cervical cancer"** - Ryon Summer School of the Rhine-Main Universities – 04.09.2023 - 08.09.2023, Gernsheim, Germany (*co-presentors)
2. **Sourik Dey** (2022) **Business Model Pitch on the topic "A Live Biotherapeutic Product based strategy for cervical cancer prevention using the patented *LactoBio* Platform"** - International Summer School on Technology Transfer in Life Sciences **–** 26.09.2022 – 30.09.2022, Dresden, Germany

PARTICIPATION IN SOFT SKILL SEMINARS

1. Conceptualizing and formulating grant idea – 07.05.2024 – 08.05.2024, Saarland University, Germany
2. Agile Project Management using the Scrum method - 27.09.2023 – 28.09.2023, INM, Saarbrücken, Germany